01 Nov 1975

Inelastic reserve capacity of cold-formed beams with stiffened compression elements

Hans Peter Reck

George Winter

Teoman Peköz

CCFSS LIBRARY
22 1 * 443
c1

Hans Peter Reck, Temoan Pekoz,
George Winter INELASTIC RESERVE
CAPACITY OF COLD-FORMED BEAMS
WITH STIFFENED COMPRESSION
ELEMENTS

DATE	ISSUED TO

Department of Structural Engineering
School of Civil and Environmental Engineering
Cornell University

Report No. 356

INELASTIC RESERVE CAPACITY OF COLD-FORMED BEAMS WITH STIFFENED COMPRESSION ELEMENTS

by

Hans Peter Reck

Teoman Peköz and George Winter
Project Directors

A Research Project Sponsored by the
American Iron and Steel Institute

Ithaca, New York November 1975

PREFACE

The present Report No. 356 deals with the inelastic reserve strength of cold-formed beams with stiffened compression flanges. The usual elastic design criterion regards the initiation of yielding in the outer fibers as defining failure. This criterion is used in Part I of the A.I.S.C. Specification and in the A.I.S.I. Specification for the design of steel structures. On the other hand, for so-called compact sections, as defined in the A.I.S.C. Specification, it is known that the actual maximum moment of a cross-section exceeds the initial yield moment and is reached only when yielding spreads over the entire section (complete plastification). It is also known that the carrying capacity of continuous compact beams and frames exceeds that calculated from the initial yield criterion, because of (a) the higher carrying capacity of the cross-section and (b) plastic moment redistribution subsequent to plastic hinge formation.

Cold-formed sections generally do not fall into the category of compact sections, which should make their inelastic reserve strength smaller than that of hot-rolled shapes. At the same time their neutral axis is frequently not located at mid-depth, which produces initial yielding in one flange only; also, because of constant thickness their web area is frequently relatively larger than in hot-rolled sections. Both these factors tend to increase the inelastic reserve strength as compared to that of doubly symmetrical hot-rolled shapes. It is this situation which necessitates developing an approach very different from that of conventional plastic design. To enable the economical utilization of this reserve strength in design, such an approach is developed and supported by tests in this report.

The report covers all phases of this investigation, regardless of whether one or the other particular phase is, at this time, ready for direct application to practical design problems. To enable a design-oriented reader to digest those parts which have the most direct practical implications, this preface attempts to guide such a reader to the relevant portions only.

For this purpose, at the end of this preface, those groups of pages are listed which contain the essential portions of the work, omitting subsidiary topics and necessary but complicating refinements of theory.

Most stiffened compression flanges with w/t significantly exceeding $(w/t)_{lim}$ as defined in the A.I.S.I. Specifications, do in fact fail when yielding initiates. These flanges, and therefore beams with such compression flanges, have no inelastic reserve capacity if yielding begins in the compression rather than the tension flange. However, flanges with w/t of the order of, or significantly smaller than $(w/t)_{lim}$ continue to carry their compression load after initial yielding is reached and when further yielding occurs. In this case yielding will spread into the web, causing significant inelastic reserve strength. Hence, Chapter II is devoted to the important determination of the amount of additional strain beyond initial yielding which can be sustained before failure by stiffened flanges of moderate or small w/t-ratios. The most important information is contained in Fig. 2-9 and in Eqs. 2.6 and 2.7 on p. 60.

As was mentioned before, the inelastic reserve strength of such sections depends not only on this inelastic strain capacity (denoted as critical strain) of the compression flange but also on the location of the neutral axis, i.e., whether yielding will occur first in tension or compression, and also on the relative magnitude of the web area as compared to the flange areas. Chapter III, therefore, determines the ultimate moment of cross-sections, depending on these three enumerated factors. For cross-sections of the general shape of Fig. 3.1 the most important information is contained in Figs. 3.2 through 3.6 which show that inelastic reserve strength, in terms of ultimate moments, of up to 30% and more are entirely realistic. The developed methodology is easily applied to other cross-sectional shapes. These experimentally confirmed reserve strengths can be applied directly to statically determinate beams, i.e., simple, single-span beams or cantilevers. On this basis it would be possible in the Specification to permit

conservative increases in allowable bending stresses for beams with stiffened compression flanges of low and moderate w/t-ratios. This may not be desirable at this time until similar information has been obtained for unstiffened compression flanges, which is being developed in a research project now under way at Cornell University.

For continuous beams, additional reserve strength can be developed through partial moment redistribution, somewhat similarly as in conventional plastic design of compact, hot-rolled continuous beams. However, the full development of plastic hinges, on which such plastic design is based, is generally not attainable in cold-formed sections with their thinner flanges. Therefore, the amount of moment redistribution that can be attained depends on the amount of rotation or curvature which such sections can develop, beyond initial yielding but prior to compression flange failure. This is the subject of Chapter IV.

Chapter V then develops a fairly involved analytical method for calculating the strength of continuous beams based on these plastic rotation capacities. The methodology is general and the most specific information is contained in Fig. 5.5a. It is seen that, for the investigated system, the preponderant portion of the inelastic load factors comes from the inelastic reserve strength of the cross-section (Ch. III), and only a small additional gain is obtained through inelastic moment redistribution. However, this purely analytical information is obtained for beams on idealized knife-edge supports, and it is shown that for realistic beams of finite width of support, significantly larger gains can be achieved (pp. 149-151). Methodology for this is given, but without graphical or otherwise directly usable information. Also, the entire treatment of continuous beams is purely analytical, without experimental confirmation. Therefore, at this time, it is not ready for practical use. It is hoped that time and funds in the previously mentioned research project at Cornell University will permit further work on this sub-topic.

With this exposition as a general guide, it is suggested that those readers who want to familiarize themselves only with the essential generalities and details of this report, while omitting information which is secondary either in general or at this time, concentrate on the following portions:

Introduction	pp. 1-3.
Summary	pp. 160-165.
Ch. I:	pp. 4 - 11, 16 - 19, 26 - 28.
Ch. II:	pp. 29 - 36, 39, 43 - 47, 51 - 66.
Ch. III:	pp. 67 - 70, 73 - 77, 80 - 86.
Ch. IV:	pp. 87 - 88, 94 bottom, 96 - 99, 101 - 103.
Ch. V:	pp. 104 - 109, 129 - 132, 149 - 151.
Ch. VI:	pp. 162 - 169.

This report was originally a thesis presented to the Faculty of the Graduate School of Cornell University for the degree of Doctor of Philosophy, for conferment in June 1974.

The research project covered by this report was sponsored by the American Iron and Steel Institute.

The valuable cooperation of the Sheet Committees of the American Iron and Steel Institute is gratefully acknowledged.

TABLE OF CONTENTS

NOTATIONS

(Indices that are used with consistent meaning in connection with different variables are listed separately at the end of the following list.)

A = Cross-sectional area

a = Position coordinate of partial hinge in span (see Fig. 5.2)

b = Width of compression flange, illustrated by Fig. 3.1

b_c = b

b_t = Width of tension flange, illustrated by Fig. 3.1

C = Elastic coefficient for residual moment, defined by Eq. 5.9

d = depth of cross-section, illustrated by Fig. 3.1

E = Young's modulus

H = Total hinge length of partial or full plastic hinge, see Fig. 4.2

h = Part of hinge length as defined by Fig. 4.2

$\bar{H}$ = Normalized hinge length, see Table 5.1

I = Moment of inertia

i = Normalized moment of inertia, see Table 5.1

L = Span length

ℓ = Normalized span length, see Table 5.1

M = Bending moment

M_p = Full plastic moment

m = Normalized bending moment, see Table 5.1

P = (i) Concentrated load

(ii) General load parameter

p_u = Inelastic load factor, defined by Eq. 4.26

p_S = Component of inelastic load factor due to inelastic strength reserves of section, see Eq. 4.26

p_R = Component of inelastic load factor due to moment redistribution, see Eq. 4.26

R = Inner radius of corner bents of coldformed sections

t = Thickness of sheet from which coldformed sections are formed

V = Shear force

v = Normalized shear force, see Table 5.1

w = (i) Uniformly distributed load

(ii) Width of compression flange between corner bents, defined by Eq. 2.1

$\bar{w}$ = Normalized uniformly distributed load, see Table 5.1

x = Coordinate of beam axis

y = Coordinate of cross-section in the direction of loading

y_p = Distance between neutral axis and elastic-plastic boundary in the stress distribution of the cross-section

α = Moment coefficient of elastic beam analysis, see Eq. 5.16d

β = Geometric section parameters, defined by Eq. 3.9 and 3.15

γ = Shear force coefficient of elastic beam analysis

δ = Flange out-of-plane deflection (also, column deflection)

ε = Strain

θ = Rotation of partial or full plastic hinge

κ = Normalized curvature, see Table 5.1

ξ = Normalized beam coordinate, see Table 5.1

ζ = Auxiliary function of rotation integral of partial hinge, see Eq. 4.22

ζ_{lin} = Same as ζ, for linear moment distribution

ζ_{par} = Same as ζ, for parabolic moment distribution

σ = Stress

Φ = Curvature

Indices

a = Position index, illustrated in Table 5.2

av = Average

b = Position index, illustrated in Table 5.2

c = Compression flange

cr = Critical (used in connection with Euler buckling)

el = Elastic, elastic component

f = At the occurrence of failure (used as superscript)

fl = Flange

ℓ = Left

p = (i) Plastic component (used in connection with curvature and rotation of partial hinge, as illustrated in Fig. 4.1)

(ii) Special meaning in connection with M_p and y_p as explained in the list of variables above

r = Right

res = Residual component

t = Tension flange

u = Ultimate

y = Initial yield

w = Web

* = Indicating a particular value of a function

ABSTRACT

Inelastic design of steel beams in the past was restricted to doubly symmetric beam sections capable of developing the full plastic moment (compact sections) and of providing sufficient rotation capacity for full moment redistribution required for mechanism-type failure of statically indeterminate beams. Research in the past was therefore directed at establishing the requirements for these compact symmetric sections in terms of width to thickness ratios of the compression flanges. This approach was adequate for hotrolled sections which are usually doubly symmetric and compact.

In the design with coldformed thin-walled beams it is of economical significance to consider the reserves of inelastic resistance of sections that cannot develop the full plastic moment, and do not provide sufficient rotation capacity for full moment redistribution. In addition, useful methods of strength design must include the effects of eccentricity of the centroidal axis in the plane of bending.

The present investigation, which is directed at inelastic reserves due to partial section plastification and partial moment redistribution, consists of two parts.

First, an experimental investigation of a failure criterion in terms of ultimate compressive strains is presented.

This investigation has been restricted to stiffened compression flanges which fail in the yield plateaus prior to reaching strainhardening. Failure occurs with incipient plastic buckling distortions of the flanges which, as they increase, cause a continuous loss of resistance of the section. The compressive strain failure criterion, therefore, is defined by the length of the compression flange yield plateau prior to failure.

Second, design methods for eccentric coldformed sections are presented for the failure criterion of ultimate compressive strain. This includes design methods to determine the ultimate moment of the section, and, for indeterminate beams, the additional inelastic reserves due to partial moment redistribution. The analysis of eccentric sections based on a compressive strain failure criterion requires a strict application of the equations of beam theory. Design aides in graphical form are given, based on rigorous treatment with respect to the section parameters. But, with respect to system parameters, approximations and/or restrictions become necessary to obtain a practical design approach.

INTRODUCTION

Fabrication methods and structural purpose create differences between coldformed and hotrolled structural steel members that have required separate investigations and design provisions. Specific research on coldformed sections over almost three decades has been addressed, among other problems, to postcritical behavior and reduced effective width of compression flanges, torsional-flexural buckling associated with asymmetric shapes, interaction of local and overall buckling of columns, structural effects of corner strain-hardening resulting from the forming process, problems of connection, etc.[1]

The present investigation addresses itself to the problem of reserves of inelastic resistance in the flexural behavior of coldformed steel beams. The investigation will be restricted to the simplest case of flexural response, bending about one principal axis, which requires symmetry at least about the plane of the acting loads. The general section considered will therefore be symmetric about one axis.

Flexural failure of coldformed beams is always determined by local failure of the compression flanges. This includes different modes of failure, whose ranges can essentially be defined in terms of the relative values of the ideal buckling

stress σ_{cr} and the yield stress σ_y. In addition, a distinction is necessary between stiffened flanges, where both longitudinal edges are supported by webs (e.g., hat and tubular sections), and unstiffened flanges, where one edge is free (e.g., I-sections). Within each of these two groups the critical stress can approximately be replaced as a characteristic parameter by the width to thickness ratio of the compression flange, w/t, which is more practical to use in design problems. For a physical interpretation of the behavior, however, the critical stress is a more suggestive quantity.

The inelastic response of unstiffened sections cannot strictly be reduced to simple bending unless the lateral bracing distance of the compression flange is so small that conditions of continuous lateral support are approached. Otherwise, the plastic failure strain in the compression flange will depend on the bracing distance and the parameters that define flexural-torsional displacements of the elastic-plastic section. No systematic experimental investigation of these additional problems has yet been undertaken.

The present experimental investigation was carried out for stiffened coldformed sections in simple bending. Experimental results and conclusions will be presented in Chapter 2. Chapters 3 to 5 will deal with analytical procedures with the principal objective to develop design methods for practical exploitation of inelastic reserve capacities of coldformed beams. Chapter 1 contains a discussion of established theories

of compression flange behavior with certain extensions necessary for the coldformed flange.

CHAPTER 1

BEHAVIOR OF COMPRESSION FLANGES: REVIEW AND DISCUSSION

As long as little was known about the inelastic behavior of a section on the one hand and postcritical strength of the compression flange on the other, beam design relied on linear elastic analysis. Consequently, the limiting conditions of linear elastic analysis, initial yielding of the second at $\sigma_{max} = \sigma_y$, or ideal buckling of the compression flange with $\sigma_{max} = \sigma_{cr}$, were thought of as failure conditions. This approach was too conservative for sections with additional inelastic or postcritical resistance, but unsafe in certain cases, e.g., if σ_{max} occurs in the compression flange and $\sigma_y \simeq \sigma_{cr}$.

The limiting conditions of linear elastic design have been replaced or supplemented, for two important modes of behavior, by more realistic failure conditions. (i) The critical stress has been eliminated as a failure criterion for mild structural steel and for some strainhardening materials like stainless steel by the development of postcritical theory with the limiting condition of initial yielding in the postcritical range. (ii) For very restrictive conditions of section geometry, which are usually not satisfied by cold-

formed sections, but frequently encountered in design with hotrolled sections, linear elastic or allowable stress design has been supplemented by "plastic design." In "plastic design" the local failure criterion of the section can be replaced by the structural failure criterion of an unstable mechanism produced by the necessary number of plastic hinges with sufficiently large capacity of plastic rotation.

Sections which do not fall within these two categories are designed according to linear elastic allowable stress design. It will be shown that it is in this range that significant reserves of inelastic resistance are neglected in the design of coldformed beams, reserves which are due to partial web plastification terminated by local instability of the compression flange. They are more significant for coldformed than for hotrolled sections due to the following properties of coldformed sections. (i) The amount of web area is relatively more substantial than in the case of hotrolled sections, since there are usually two webs of the same thickness as the flanges. (ii) Many coldformed sections are not doubly symmetric. Elastic design then makes poor use of potential material strength, the more, the larger the difference between the stress peaks in the two flanges. The economical gains from inelastic stress redistribution increase with this difference.

The engineering terminology is not always used consistently in the literature with respect to certain terms. The

word "compact" will here only be used in the sense of the AISC provisions[11] for hotrolled structural members, referring to sections that can develop the full plastic moment. The term "plastic design" as used in structural engineering convention is identical in theory with the term "limit analysis or design" in the literature of applied mechanics. The word "thinwalled" will be used in the sense of v. Kármán and Winter, to apply only to plates and flanges that are subject to postcritical behavior. As used by Vlasov the term has a much broader meaning and includes in fact hotrolled compact sections.

Following will be a review of research and theory on different modes of compression flange instability. We will begin with the postcritical behavior of compression flanges and particularly look into past research for an answer to the question whether we neglect any significant reserve of inelastic resistance in the postcritical range.

1.1 Elastic Critical Stress and Postcritical Behavior

It was in connection with ship and aeronautical structures that the ability of thin plates in compression to carry considerable loads beyond the classical stability limit was first recognized and that the concept of effective width was introduced, although at first in the form of rough estimates. This postcritical load carrying capacity of thin plates is physically explained by a membrane stress state generated as the plate deflections exceed values of the order of magnitude

of the plate thickness. These membrane stresses tend to counteract increasing plate deflections.

The foundations for a mechanically exact treatment of plates in this state of "large" deflections were laid by v. Kármán in 1912 with the well-known non-linear v. Kármán large deflection equations. However, only at a much later time were approximate analytical solutions obtained, often in combination with energy methods. An extensive list of references of the literature which sprang up after 1935 is given in Ref. 19. Based on the simplest assumptions of boundary conditions and with almost unmanageable numerical difficulties these solutions were of limited practical usefulness. Today's computer techniques have alleviated numerical problems but are in any case inappropriate for standardized design.

Preceding this line of analytical treatments and parallel to it is a continuous line of efforts to create reliable empirical design tools based on experimental results and new physical insights. These efforts are reflected today in the form of the effective width concept in the design specifications for hotrolled and coldformed sections in the USA.[10,11] The development was again initiated by v. Kármán who reports the observation that the ultimate load of thin plates in compression, stiffened along two edges, "showed to be independent of the width and length of the plate and approximately proportional to the square of the thickness."[14] From this observation and with an approximate assumption of the deflected

shape in the postcritical state, v. Kármán derived a simple design equation which can be written in the form

$$\frac{b_{eff}}{b} = \sqrt{\frac{\sigma_{cr}}{\sigma_y}} \qquad (1.1)$$

where b_{eff} is the reduced effective width at ultimate load, and b is the actual width. The simplicity of the approach comes mainly from two facts. (i) The effective width concept is introduced, which does not make any reference to the actual non-linear stress-distribution across the plate, but instead deals only with the average stress and the maximum stress. (ii) All variables refer to the axial behavior of the plate, eliminating such variables as plate out-of-plane deflections and bending moments that are of no direct interest.

However, v. Kármán's equation is based on the concept of bifurcation of equilibrium at σ_{cr}, assuming perfectly plane geometry below σ_{cr} and a deflected configuration above. The assumption of bifurcation is of little consequence if the plate fails in the advanced postcritical state, but is quite inaccurate for plates whose geometric proportions are such that they fail in the neighborhood, above or below, of σ_{cr}. This range is much more important for coldformed structural members than, e.g., in aeronautical structures which v. Kármán had in mind. These shortcomings were recognized by Winter[15,16] in working with coldformed sections. Winter's effective width formula can be written in the form

$$\frac{b_{eff}}{b} = \sqrt{\frac{\sigma_{cr}}{\sigma_y}}\left(1 - \xi\sqrt{\frac{\sigma_{cr}}{\sigma_y}}\right) \tag{1.2}$$

at failure, where ξ is an experimental constant. In this equation, σ_{cr} has lost its meaning as the actual lower limit of the postcritical range. The failure mode associated with postcritical behavior is now determined by a certain transition ratio $(\sigma_y/\sigma_{cr})_{lim} < 1$. This takes into account plate deflections at stress levels considerably below σ_{cr}, which are the result of small initial deflections magnified by the axial load. If the experimental values of the buckling coefficient k and the constant ξ are substituted into the Winter equation and if it is considered that at transition to postcritical behavior $b_{eff} = b$, the equation can be solved for the ratio $(\sigma_y/\sigma_{cr})_{lim}$, which can then be transformed into a parameter $(b/t)_{lim}$. In referring to design specifications b will be replaced by w which measures, more specifically, the flange width between the roots of the corner bents. The design formula for $(w/t)_{lim}$, as given in the AISI Specs.[10] for stiffened sections is

$$\left(\frac{w}{t}\right)_{lim} = \frac{221}{\sqrt{\sigma_y}} \tag{1.3}$$

For $\sigma_y = 36$ ksi we obtain $(w/t)_{lim} \simeq 37$. According to the AISC Specs.,[11]

$$\left(\frac{w}{t}\right)_{lim} = \frac{253}{\sqrt{\sigma_y}} \tag{1.4}$$

In this case, for σ_y = 36 ksi, $(w/t)_{lim}$ = 42. Failure occurs in the postcritical mode when $w/t > (w/t)_{lim}$.

It is now necessary to look into the postcritical failure mode more carefully, to determine the role of plasticity in connection with actual failure.

It has generally been observed that failure in the state of large deflections "occurs when the stress intensity at the edge reaches a value approximately equal to the compressive yield strength of the material."[4] Since the axial displacements of the flange at failure then correspond to the yield strain, no significant plastification of the section takes place. This conclusion was drawn from direct test observations by Winter[15] and Gerard[4,17] who also summarized all of the relevant research carried out in the Laboratories of the National Advisory Committee for Aeronautics.

Among the theoretical investigations only the recent work by Graves-Smith[18] shall be mentioned, whose results by computer analysis for certain types of square and rectangular columns are in good agreement with test results. Graves-Smith analyzes the spreading of plastic zones in the postcritical range. According to his analysis the yield stress is first reached in combined bending and compression at the center of the buckling wave. Thereafter the load can only increase by a small amount before the yield point is reached in pure axial compression at the edge. At this stage the ultimate load is practically obtained.

If, however, the compression flange in the postcritical range fails upon reaching axial displacements approximately corresponding to the yield strain, no web plastification on the compression side can be obtained. These conclusions are confirmed by the present experimental program, presented in Chapter 2. The possibility of reserves of inelastic resistance is then only existent in the case of web plastification from the tension side, prior to postcritical failure of the compression flange.

Since failure above the critical stress level is so closely connected with the occurrence of initial yielding in compression, the failure point can be considered as a limit to elastic behavior. Hence, it was concluded by Winter that equations 1.1 and 1.2 also describe approximately the elastic axial behavior before failure, if σ_y is replaced by σ_{max}, the maximum elastic compressive stress in the flange, at the junction with the webs. These equations can then be applied to define the stiffness and nonlinear-elastic load-deflection behavior of the beam.

1.2 General Discussion of the Failure Modes of Compression Flanges

To explain the discrepancies, apart from postcritical strength, between actual failure loads and the critical load level derived from the bifurcation concept, it is necessary to take into account the effects of small initial deflections together with initial plasticity. This approach will lead to

a distinction between three general failure modes. Some important conclusions can be drawn by analogy from the failure modes of linear members in axial compression. The following short discussion of linear members in axial compression is based on well established knowledge, to which v. Kármán has made an early contribution in 1909.[20] The subject was again pursued in a more general context by v. Kármán, L. G. Dunn and H. S. Tsien in 1940.[21] Drucker and Onat[22] have contributed the discussion of a simple spring-column model, where the spring is subject to an elastic-plastic stress strain law. In these investigations the bifurcation-stability analysis is treated merely as a mathematical bound to the maximum load carrying capacity of an initially imperfect column. The general results are illustrated by Figs. 1.1-a to 1.1-c in the form of load-deflection diagrams. The solid curves in the diagrams represent schematically the real behavior, based on initial imperfections. If we consider a column of unit area, σ_y will represent the yield load in the undeflected state, $\sigma_{cr,el}$ the Euler load. The behavior upon elastic bifurcation is represented by the line of neutral equilibrium at the load level $\sigma_{cr,el}$, assuming that the material is infinitely elastic. In addition, a curve is plotted, representing a column which is constrained to remain straight until it reaches the load level σ_y in uniform yielding. At this point the column is allowed to deflect. A reduced load value can now be computed for each deflection value, which will produce the

unstable curve. This curve is of interest, since it will be approached asymptotically by the unstable branch of the actual load-deflection curve based on initial imperfections.

Comparing the failure loads of the imperfect column (represented by the average stress with respect to the full flange area, $\sigma_{av,u}$) with the load level at bifurcation (represented by $\sigma_{cr,el}$), three cases can be distinguished.

Case 1: $\sigma_y >> \sigma_{cr,el}$ (Fig. 1.1-a)
The load-deflection curve based on small initial deflections closely approaches the elastic critical stress level asymptotically before the failure load is reached. Obviously, the critical stress is a good approximation to actual failure. Since the yield stress is much higher than the elastic critical stress, considerable bending stresses can be superimposed on the axial stress state before initial yielding leads to instability.

Case 2: $\sigma_y \simeq \sigma_{cr,el}$ (Fig. 1.1-b)
The superposition on the axial stress state of bending stresses, resulting from magnified initial deflections, leads to initial yielding at the extreme fiber where compressive stresses add, at an average axial stress significantly below the yield stress. Since initial yielding has a drastic effect on the load-deflection behavior, the failure stress level is practically reached at this point, i.e., $\sigma_{av,u} < \sigma_{cr,el}$ and $\sigma_{av,u} < \sigma_y$. This mode also applies to a certain range of σ_y

above or below $\sigma_{cr,el}$, but the maximum discrepancy between the failure stress level and both $\sigma_{cr,el}$ and σ_y is found for $\sigma_y = \sigma_{cr,el}$.

Case 3: $\sigma_y << \sigma_{cr,el}$ (Fig. 1.1-c)
The effects of small initial deflections on the maximum load are practically negligible in this case, because the bending stresses are negligible as the maximum mean stress approaches σ_y, i.e., $\sigma_{av,u} = \sigma_y$. In this limiting case, the capacity to carry axial load corresponds approximately to the yield stress intensity.

Analogy with Respect to the Strength of Compression Flanges ($\sigma_{av,u}$)

Fig. 1.1-a to 1.1-c show the effects of small imperfections in combination with initial plasticity on the maximum axial compressive load of a column. These effects are of general nature and have a correspondence in the case of the compression flange.

Fig. 1.1-a will have to be modified, since, in the case of the compression flange, elastic equilibrium after bifurcation at the Euler load would not be neutral, but stable because of the plate membrane stresses. The axial compressive load on the flange can increase in the deflected equilibrium configuration, i.e., the flange will be in the state of post-critical strength. This modification is shown in Fig. 1.1-d. A correspondence between Fig. 1.1-a and Fig. 1.1-d is found in the fact that in both cases the curves based on initial

imperfections approach their respective ideal postcritical curves asymptotically before initial yielding in the extreme fiber occurs. This means for the flange in the advanced postcritical range $\sigma_{av,u} > \sigma_{cr,el}$, but $\sigma_{av,u} < \sigma_y$. Failure of the flange in the postcritical range was discussed in Sec. 1.1. Its strength is computed according to Eq. 1.2. In the advanced postcritical range Eq. 1.1 is also valid (the results of both equations will be very close).

Case 2, Fig. 1.1-b can be interpreted for the compression flange as follows. The flange is in a state of small deflections as initial yielding is reached at the extreme fiber, where compressive stresses due to axial load and local bending add most unfavorably. At this instant, the average axial stress across the flange width and thickness is still significantly below the yield stress. However, after such incipient yielding at the extreme fiber, the flange loses its stiffness rapidly and fails without appreciable increase in average stress. Therefore, $\sigma_{av,u} < \sigma_{cr,el}$, as well as $\sigma_{av,u} < \sigma_y$. The reduced ultimate average stress of the flange, for this failure mode, has been incorporated in the Winter effective width equation (Eq. 1.2) which therefore governs both Case 1 and Case 2. Case 2 applies to flange dimensions such that $\sigma_{cr,el}$ is in the vicinity of σ_y (both below and above).

Finally, in Case 3, for $\sigma_y << \sigma_{cr,el}$, a flange will reach initial yielding in a state of negligible out-of-plane deflections. Hence, in the latter case, at failure, there will be a

state of practically uniform axial yield stress over the flange width and thickness.

According to Graves-Smith's analysis,[18] the load-deflection curve for Case 1, after initial extreme fiber yielding (point 1), has the form indicated in Fig. 1.1-d. Although the average stress cannot increase significantly, additional out-of-plane deflections beyond point 1 will not immediately cause a drop in average stress, due to the membrane stresses which are still elastic in large portions of the flange. In Cases 2 and 3, however, the flange deflections that follow point 1 represent the distortions of the flange in the state of elastic-plastic or plastic buckling. These distortions will cause a decrease in resistance to axial load. Hence, in Cases 2 and 3 the descending unstable branch of the load-deflection curve begins approximately with point 1, although the transition into unstable behavior will not be as sharp as indicated in the sketches of Fig. 1.1-b and 1.1-c.

Load-deflection curves are well suited to discuss the strength of flanges in connection with initial imperfections and incipient yielding. However, they cannot describe the flange behavior in another important structural aspect which will be discussed in the following section.

Inelastic Reserves of Resistance of Beam Cross-Sections

Inelastic reserves of resistance of the beam cross-section are gained from inelastic stress redistribution across

the depth of the section, associated with web plastification which occurs with continued axial flange compression at yield. Therefore, to calculate the ultimate moment of the section, it will not only be necessary to know the ultimate strength of the flanges, particularly of the compression flange, but also their capacity to undergo axial plastic deformations. Obviously, we will only be concerned about potential axial plastic deformations of the compression flange, since it is the critical element of the section.

The axial plastic deformations of the compression flange can be measured in terms of its axial strains at the corners, where the flange is in pure axial compression in the longitudinal direction. Curves where the average stress of the compression flange is plotted vs. the axial strain at the corners will represent the "stress-strain curve" of the compression flange.

For Case 1, i.e., for the flange with failure in the post-critical range, failure of the compression flange and failure of the cross-section were correlated in Sec. 1.1. It was concluded that the cross-section fails with sharp decrease in resistance approximately when the corner compressive strain reaches the yield strain of the material stress-strain curve ε_y.

In Case 2, the flange is in a state of small but not negligible out-of-plane deflections (due to small initial deflections) as incipient yielding occurs in the extreme fiber

of the flange. σ_{av} cannot appreciably increase beyond this point of loading, because the flange loses its bending stiffness rapidly after incipient plasticity. Therefore it must be expected that inelastic buckling distortions of the flange begin approximately as the compressive corner strains reach ε_y, followed by a decline of resistance, i.e., failure, of the cross-section.

It is verified by experimental research, and may be considered established knowledge, that in Cases 1 and 2 compressive corner strains of the magnitude of the material yield strain ε_y constitute the failure criterion of the cross-section. Hence, the stress-strain curves of these compression flanges will not show an appreciable yield plateau which could cause increased resistance of the section due to web plastification on the compression side. This concerns the range of flange dimensions where the strength is governed by the reduced effective width approach according to Eq. 1.2.

However, experiments show that compression flanges, discussed in connection with Case 3, which are practically plane as they reach $\sigma_{av} = \sigma_y$, sustain various amounts of axial compression beyond the yield strain without flange distortions, visible to the naked eye. In this case, the compression flange stress-strain curve can have a yield plateau of variable length. The yield plateau will end with incipient plastic buckling of the flange. As these distortions increase, the drop of load will become pronounced. The load (out-of-

plane)-deflection curve cannot indicate this yield plateau which can cause significant web plastification on the compression side and increase in section resistance.

For the compression flanges of "compact" sections, as defined by the AISC design provisions,[11] the yield plateau will always extend into the strain-hardening range. However, the flange dimensions of most coldformed sections, which are not governed by reduced effective width design (Eq. 1.2), will not satisfy the requirements of compact sections. In this case, the yield plateau will end prior to strain hardening by plastic buckling with a significant decline of the average stress. This case will be the main subject of the present investigation.

An analysis of the extension of the compression flange yield plateau (if it does not reach into the strain-hardening range) as a function of the yield stress, and flange and section dimensions, has not yet been undertaken, and is not possible by any of the classical methods. In the present investigation this problem will be investigated experimentally.

However, a theory for plastic flange buckling exists for compact sections, where the compression flange yield plateau extends into the strain-hardening range. This theory will be discussed in Sec. 1.3 and 1.4.

1.3 Theory of Local Instability of Hotrolled Sections for Plastic Design

Hotrolled symmetric shapes that qualify for plastic design are called compact and are determined by a limiting w/t-ratio for plastic design. The design of structural beams with flanges below this limiting w/t-ratio, is governed by the failure criterion of the structural mechanism, which replaces the criterion of local failure. Therefore, the research for plastic design was not concerned with local failure as a function of the w/t-ratio, but simply with a criterion for a limiting w/t-ratio for plastic design.

In the theoretical treatment, the limiting w/t-ratio is not directly derived from a rotation requirement for the plastic hinge of a failure mechanism, but from the condition of obtaining the buckling mode associated with the strainhardening range of the stress-strain curve of structural steel. The lowest critical stress level in the strainhardening portion is, of course, the yield stress. Hence, if the material constants in the strainhardening range are known, and if σ_y is chosen as the lowest and therefore most conservative critical stress level in that range, the conventional buckling problem can be solved for the w/t-ratio. The result is the limiting w/t-ratio for plastic design.

Physically, however, the strains have passed the yield plateau and it is necessary to justify why the yield plateau does not have to be taken into account in the mathematical analysis. In fact, the theory is based on a certain premise

with respect to material behavior. The arguments are that the yield process of structural steel is discontinuous, more specifically, that plastic deformations occur in a pattern of slip planes along which the displacements between the neighboring surfaces "jump" from their elastic state into the beginning strainhardening range. Hence, according to this theory, there are no static properties associated with the yield plateau. Strains in the range of the yield plateau are assumed to be obtained as an average between "complete" slip displacements along slip planes and elastic strains in the neighboring lamellas. Where slip planes accumulate over a "long enough portion of the flange so that at least one full wave length of the buckle can develop"[13] the condition of buckling in the strainhardening range is given. This implies, obviously, considerable hinge rotation.

In plastic design, theory is of course secondary to experimental experience. Theory has been adjusted to experimental results particularly through modification of the material constants in strainhardening.

Research on plastic design has been carried out in different places over a period of time. The plastic design theory of local flange buckling has been developed at Lehigh University. It is reflected in the AISC commentary on plastic design[13] where references can be found.

According to the AISI provisions, the w/t-ratio of box sections and cover plates for plastic design shall not exceed

$190/\sqrt{\sigma_y}$ (Ref. 11, Part 2, Sect. 2.7). I.e., the limiting w/t-ratio for plastic design for σ_y = 36 ksi is 31.7. Recent research,[25] however, suggests strongly that the value $190/\sqrt{\sigma_y}$ is too high, at least for coldformed box sections. A considerable number of tests on coldformed box sections has been reported in Ref. 25, from which a tentative value equal to $150/\sqrt{\sigma_y}$ has been derived as the limiting w/t-ratio for plastic design.

1.4 Plastic Deformations of Structural Steel with Yield Plateau

The theory of flange buckling of hotrolled sections for plastic design is interesting mainly with respect to its premise of material behavior. However, there is no unified way to describe the structural performance of steel in the plastic range, unless a theory would be built on the behavior on a scale not larger than the grain structure, which could only be of statistical nature. On the phenomenological level the process of plastic deformation in crystal and grain structure can express itself in different modes of structural behavior, requiring different mechanical theories. The following outline uses several arguments of Freudenthal.[2]

At the outset, Freudenthal shall be cited to recall the circumstances that led to slip initiation. "If a crystal grain is favorably oriented with regard to slip and is entirely surrounded by less favorably oriented grains, slip bands will develop only when the applied shear energy is sufficient

to force several neighboring grains to deform. Slip initiation thus consists of a series of localised catastrophic processes along planes of maximum shear." The effects can be observed in a tension coupon where the stress field is uniform and plastic deformations are not affected by external restraints. Initial plastic deformation in the tension coupon is associated with abrupt slip occurring in a rapid sequence in slip planes that coincide approximately with the principal shear trajectories. The formation of slip planes is usually delayed, leading to an upper yield point after which the load drops to a lower stress level where additional fluctuations can often be observed. At the end of this stage a fine pattern of narrowly spaced glide lamellas has developed. Hence, on the phenomenological level, plastic deformations in a tension coupon occur in an abrupt manner. This mode of plastic deformations seems to apply if, essentially, two conditions are satisfied. (1) The stress field has to be homogeneous (a field of constant stress). (2) The homogeneous stress field is not contained by neighboring elastic zones.

These conditions, according to experimental evidence, are satisfied in the compression flanges of hotrolled compact sections, which can be explained as follows. (1) The effects of initial imperfections have no influence on the stress field and on the process of slip plane formation, i.e., the stress field is homogeneous. (2) The webs are thin as compared to the flanges, and, therefore, do not seem to impose a signifi-

cant elastic restraint on the axial plastic deformations of the compression flange; instead, it seems more likely, that the slip planes of the flanges, after initial delay, propagate more or less deeply into the elastic webs. The inelastic buckling theory of hotrolled compact sections (Lehigh buckling theory) is based on this abrupt mode of plastic deformations (dynamic slip) in single slip planes that traverse the flange through its full depth.

On the other hand, if a stress field is (1) non-uniform and (2) contained by significant portions of material still in the elastic range, a different mode of plastic deformations on the phenomenological level must be expected. E.g., in fields of non-uniform bending moments, in torsion of solid bars, in problems of non-uniform plane stress, etc., the slip planes associated with initial anisotropic yielding extend gradually from the highly stressed into the less stressed portions of material. Hence, the anisotropy and heterogeneity of the deformation process on the microscopic level does not become apparent on the macroscopic level, as it does in the homogeneous stress fields with unrestricted propagation of slip planes. Accordingly, the theory of plastic flow, based on the assumptions of continuous, homogeneous and isotropic plastic deformations, has found considerable experimental support in connection with elastically contained plastic zones and non-homogeneous stress fields.

However, the theory of plastic flow (theory of plasticity

of elastic-perfectly plastic material) constitutes an analytical approach completely different from the Lehigh theory of inelastic buckling of compression flanges of compact sections.

This second mode of continuous, homogeneous and isotropic plastic behavior, to which the theory of plastic flow applies, seems to be better justified than the abrupt, anisotropic first mode, in the case of coldformed compression flanges, where one or more of the following conditions must be taken into account.

1) A coldformed stiffened section has two webs, each of the same thickness as the compression flange, which will impose a considerable elastic restraint on the flange, at least in the initial stage of web plastification.
2) In flanges whose w/t-ratios do not satisfy the compact section requirement, but are fully effective (i.e., $w/t < (w/t)_{lim}$ according to Eq. 1.3), the effects of small initial deflections may possibly create a slightly non-uniform field of bending moments combined with axial stresses. In this case yielding may start locally in extreme fibers, which would provide the conditions for the second mode of plastic deformations (plastic flow).
3) In tests with coldformed box sections,[25] the presence of high residual stresses due to the forming process was noticed. The effect of high residual

stresses would be that yielding spreads gradually, contained by elastic portions of material.

The author has concluded that the theory of plastic deformations used for interpreting inelastic buckling of hot-rolled sections for plastic design, was not applicable to the coldformed stiffened sections tested within the present program. Therefore, to adapt the classical bifurcation-stability theory to the problem of plastic critical strains by using material constants from the elastic and strainhardening range of the stress-strain curve did not seem to be justified.

1.5 Summary

In the first part of this chapter, as a general background, the failure modes of coldformed, stiffened compression flanges were discussed on the basis of previous experimental and analytical research and established theories. The discussion was then directed at the reserves of inelastic resistance of coldformed stiffened sections, which are obtained from inelastic stress-redistribution across the depth of the beam section, i.e., from web plastification. In this context, the problem that deserves most attention is the capacity of the compression flange to sustain plastic strains, which, in certain cases (symmetric sections and eccentric sections with neutral axis closer to the compression flange) will determine whether there can be any inelastic reserve capacity at all.

The discussion of the compression flange failure modes indicated that significant plastic strains in the compression

flange corners prior to failure can only be obtained for compression flanges that are practically fully effective at incipient yielding. This brings up the problem of plastic compression flange buckling at the essentially constant stress level σ_y, at various points of the yield plateau of the compression flange stress strain curve.

In this context, the literature on inelastic flange buckling of hotrolled sections for plastic design is of some interest, since it applies to the same type of structural steel with extended yield plateau and subsequent strainhardening. The theory which is found in this field, ignores in its analytical approach the yield plateau, and applies classical bifurcation-stability theory to the strainhardening range. Physically, this has been justified by a special theory of plastic deformations of steel, according to which a "dynamic jump" takes place in the slip planes from incipient yielding to incipient strainhardening. The theory therefore contends, that strains in the range of the yield plateau exist only as an average between strains at incipient yielding and strainhardening.

This theory was not considered applicable in the present context of coldformed sections above the limiting w/t-ratio for plastic design. The plastic behavior within the present experimental investigation was found to be better represented by the assumptions of continuous and homogeneous plastic deformations of the theory of plastic flow, which has found much

experimental support in the past in connection with elastically contained plastic zones and non-uniform stress fields. In the present case the elastic containment is provided by the relatively thick webs.

Analytical aspects will not be pursued beyond these general observations. Information of practical importance will be obtained on the basis of the experimental program, which will be presented in the following chapter.

CHAPTER 2

EXPERIMENTAL INVESTIGATION OF STIFFENED SECTIONS

2.1 Experimental Program

2.1.1 Material

Beam sections were formed from commercial grade structural steel sheets of 10, 12, 16 and 20 gage thickness. The 10, 12 and 16 gage sheets were hotrolled, the 20 gage sheets coldreduced. The sheets were selected on the basis of preliminary tension coupon tests to ensure that the stress-strain curves had the desired properties of a well-defined sharp yield point, yield plateau and subsequent strainhardening. Detailed properties obtained from standard tension coupon tests are listed in Table 2.1. Yield points of the 10, 12 and 20 gage sheets are in the vicinity of 36 ksi, of the 16 gage sheets around 40 ksi. The extension of the yield plateau was found satisfactory. Properties both parallel and transverse to the rolling direction were compared. Since the differences were small, only the properties parallel to the rolling direction, i.e., parallel to beam axes, are listed.

2.1.2 Beam Sections and Fabrication

Section geometries are shown schematically in Fig. 2.1. Dimensions, taken from direct measurements of the test specimens, are listed in detail in Table 2.2. The values for web

depth B and tension flange width C are average values of the dimensions at each side of the section, since perfect symmetry is usually not achieved in the actual fabrication of the cold-formed section. But deviations from symmetry did not exceed ± 2/100 in. The thickness t did not differ perceptibly within the same cross-section. It did vary slightly over the beam length, as did all other dimensions. All measurements in Table 2.2 are taken at midsection of the beams, representing good average values over the central portion of the beam length, which, as will be seen, is the critical portion of the test specimens.

All test specimens are open or closed hat-sections, i.e., stiffened sections, with a compression flange supported by a web at either side. Classification of the specimens is based on (1) the w/t-ratio of the compression flange, (2) general differences in shape, as explained below.

The w/t-ratios in Table 2.2 are computed according to the definition of the AISI design provisions,[10] with

$$w = A - 2t - 2R \tag{2.1}$$

The ratios cover a range $32 < w/t < 120$, with special emphasis on the range of moderate ratios between $w/t = 33$ and $w/t = 42$, to test the capacity of compression flanges to sustain significant plastic strains. A total of ten specimens in this range has been evaluated. The test program was not designed to investigate the advanced postcritical behavior of stiffened

compression flanges per se, since it is well established. However, specimens with ratios of 73.5 and 120.2 were tested for direct information about the circumstances of failure in the advanced postcritical range after substantial yielding of the tension flanges.

The following general distinctions can be made between the section geometries of the test specimens, although the basic form in each case is the hat-section. (1) Five open sections were designed with considerable eccentricity of the centroidal axis to obtain initial yielding and web plastification in tension prior to initial yielding in compression. These are initialed HA. (2) Two sections, initialed HB, were designed with opposite eccentricity to obtain initial yielding in compression. This was achieved by spot-welding a plate to the lips of the tension flange which was taken from the same material as the hat. (3) Five open sections, HL, were designed to obtain approximately balanced conditions.

The beam specimens were formed on a press brake with the axis of the beam parallel to the rolling direction of the sheet. Corner radii, desired to conform with industrial sections, were obtained by padding the passive die with strips of sheet steel. The radii are of the order of magnitude of the sheet thickness (see Table 2.2). In the design of the sections it was deliberately attempted to keep corner workhardening effects mild through the relative proportioning of corner and flat areas. For all compression flanges, the proportions

of flats to corners are, at least, 20:1. For tension flanges, type HA, at least 10:1, type HB 20:1 and type HL 5:1. The web depth of the specimens was restricted by the forming process, but a satisfactory compromise between beam depth and length was obtained.

The length of the specimens is L = 72". Width and depth of all sections are of the same order of magnitude. Large differences in compression flange w/t-ratios were mainly obtained by using steel sheets of different thickness.

2.1.3 Set-up, Loading Procedure and Measurements

The schematic test set-up is shown in Fig. 2.2. Symmetric loads are applied at the third points, creating a range of constant moment over a length about 5 to 6 times the compression flange width, which, in the postcritical range, accommodates about 3 full wave lengths. Web stiffeners in the form of diaphragms are fitted into the section and tack-welded to the webs at load points and supports, to prevent premature failure by web crushing, and to maintain the original section geometry throughout loading.

The specimens were loaded by a hydraulic testing machine. A loading program in the elastic range was planned according to prior computations. Intervals of measurement in the inelastic range were determined by increments of compression flange strain in fractions of yield strain. These fractions were kept small enough to be always reasonably close to the failure value, if failure was to occur unexpectedly. Failure

was defined as the attainment of maximum load and the onset of load shedding, but measurements were continued into a limited range after initial load shedding. Even though the load was applied at a slow rate, a certain relaxation was always observed in the advanced inelastic range, manifesting itself by a slight dropping of the load after the testing machine was stopped. During the relaxation period, the deflection measurements did not change at all, and the strain measurements were only affected to a negligible degree. As the loading proceeded, the drop of load was immediately recovered, at a rate which was apparently similar to the initial elastic behavior of the section.

Fig. 2.2 shows a typical instrumentation of a test specimen. As indicated, deflections were measured at the load points and at midspan by dial gages with a sensitivity of 1/1000 in. All strain measurements were obtained from resistance wire strain gages SR-4, type A12, 1 in long. A complete set of strain measurements was always taken at midsection. According to the numbering of the strain gages in Fig. 2.2, this includes gages 3 and 4 on the tension flanges, gages 9 and 10 on both edges of the compression flange, and gages 11 and 12 on the upper and lower surface at the centerline of the compression flange. The gages at midsection were applied symmetrically on both halves of the cross-section to check symmetry of behavior and to obtain average strain values. Gages 3 and 4 on the tension flanges were always used at the

beginning of the testing procedure to correct transversal eccentricity of the load, if necessary. Gages (3,9) and (4,10), taken as pairs, established the local beam curvature at midsection. Gages (11,12) and (13,14) were applied to determine both the local average axial strain at the center-line of the compression flange and the local curvature in the flange. Hence, these gages indicated deviations from uniform strain distribution across the flange, as well as out-of-plane distortions. The pair (13,14) was used in addition to the pair (11,12) to increase the probability that at least one pair of gages was near to a point of maximum amplitude of potential out-of-plane distortions. Gages 1 and 2 on the tension flange near the load points were used to center the load in the longitudinal direction, if necessary. Compression flange strains near the load points were measured by gages 5 and 6. These gages were useful in determining the onset of local failure if it occurred near one of the load points. The gage pairs (1,5) and (2,6) established values of the beam curvature near the loadpoints, gages 7 and 8 in addition to gage 9 provided important information about the uniformity of the yield process in longitudinal direction over a central 6 inch interval of the compression flange.

The beam curvature was not only measured locally by the strain gage pairs (1,5), (3,9), (4,10), and (2,6), but also as an average value over the whole interior portion of the beam, by the slope measurements of the two inclinometers indicated

in Fig. 2.2. These inclinometers were a combination of a small level and a micrometer.

The absolute values of out-of-plane compression flange distortions were directly measured by a moveable dial gage of high sensitivity (1/10000 in), which was mounted on a bridge of adjustable width, spanning the distance between the edges of the compression flange. The data obtained from this instrument will be reported as far as necessary for a general judgment on the visual appearance of out-of-plane compression flange distortions. However, insights in the inelastic performance of the compression flanges are gained mainly from the changes in out-of-plane deflections with increasing load. The changes, however, are more accurately represented by the curvature data obtained from the strain gage pairs (11,12) and (13,14). Therefore, except for visual appearance, the discussion of the compression flange behavior will be based on the strain gage data.

2.2 Background for Evaluation of Experimental Data

Before going into the details of the test data, the general approach taken in the data evaluation will be outlined. The evaluation will essentially center around (1) the failure criterion, (2) the moment curvature relationships.

The significance of the behavior of the compression flanges, both with respect to failure criterion and moment-curvature relationship was discussed in Chapter 1. The principal classification of the test specimens will therefore be

determined by the classification of the compression flanges according to their main parameter, the w/t-ratio. The important reference value of the w/t-ratios in the context of inelastic behavior is the limiting ratio for fully effective width, $(w/t)_{lim}$, as computed from Eq. 1.3. This value divides the specimens theoretically in two categories, those that are fully effective at initial yielding of the compression flange, and those with reduced effective width. The following terms will be used in the classification of the specimens.
(1) Ratios in the range $w/t < (w/t)_{lim}$ will be considered low ratios, (2) ratios $w/t > (w/t)_{lim}$, but in the close vicinity of $(w/t)_{lim}$, will be called moderate ratios, (3) ratios $w/t >> (w/t)_{lim}$ will be considered high ratios. Accordingly it is seen from Table 2.3, which will be discussed in detail later, that 4 specimens of low ratios and 6 specimens of moderate ratios were tested. For the ten specimens of Table 2.3, the yield points are around $\sigma_y = 36$ ksi, for which, from Eq. 1.3

$$(w/t)_{lim} = \frac{221}{\sqrt{\sigma_y}} = 37$$

For the two test specimens with high w/t-ratios, the values of w/t and $(w/t)_{lim}$ are listed in Table 2.6.

Evaluation of the Experimental Moment-Curvature Relationships with Respect to a General Analysis

It is the intent of this investigation to translate the results from the test data into rules for a general analysis

which is independent of individual geometric configurations and dimensions. The word "general" is, of course, applied within the limits of coldformed, stiffened sections. The approach which offers itself naturally to obtain information of a general nature, is a comparison with the conventional and somewhat idealized theory of beam behavior which is reviewed in Appendix 2.1. The equations of conventional beam theory are given by Eqs. A2.1-1 to A2.1-5 for an elastic-perfectly plastic stress-strain law, which is assumed to apply uniformly over the cross-section. This set of equations will establish the theoretical moment-curvature relationships in the elastic and inelastic ranges, for prescribed and constant section geometry. This type of theoretical relationship will be used for comparison with the experimental moment-curvature relationships of specimens with low and moderate ratios. The comparison in the range of low ratios shall be discussed first.

In the case of low ratios, good agreement between theoretical and experimental moment-curvature relationships must be expected in the elastic range up to and including the yield moment, if care is taken in the measurements, and in the determination of the material yield point of each specimen. Discrepancies in this respect were, in fact, negligible within the present experimental program for low ratios. Good agreement with respect to the stiffness (EI) and the yield moment is important for a valid comparison in the range of inelastic behavior.

With respect to differences between theoretical and experimental moment-curvature curves in the inelastic range it must certainly be taken into account, that imponderabilities in the execution of the experiments and imperfections of the real specimens as compared to the theoretical model may be of greater significance in the inelastic range than in the elastic range. Differences of this type would be of statistical nature. However, if similar differences between the theoretical and experimental moment-curvature relationships in the inelastic range occur consistently, it may be assumed that there must be a rational explanation. These differences may result from as many causes as there are idealizations in Eq. A2.1-1 to A2.1-5, including the assumption of fully effective geometry. However, inferences on specific causes will be possible on the basis of previous research, and experimental measurements beyond those that lead directly to the experimental moment-curvature relationship. Thus, it will be necessary to take into consideration the effects of corner-strainhardening produced by the coldforming process. This characteristic of coldformed shapes was extensively investigated at Cornell University.[24] Further, the effectiveness of the compression flanges in the range of plastic deformations may be approached with some apprehension. Clues on this aspect were sought by measurements of the compression flange curvature. From a practical point of view, however, there will be a tendency to complicate as little as possible the simplified set of equa-

tions of beam theory, unless they are unsafe by more than a negligible degree, or unless complications of analysis are justified by substantial gains in economy. Both theoretical and experimental moment-curvature relationships will be exhibited graphically for all specimens.

For high ratios ($w/t >> (w/t)_{lim}$) the effective compression flange width will no longer be constant throughout the elastic range. Therefore, beam analysis prior to initial yielding is based not only on the set of equations A2.1-1 to A2.1-5, but in addition, according to the AISI Specifications,[10] on the effective width equation given in general form by Eq. 1.2. In its final form, this equation is written as follows

$$\frac{b_{eff}}{t} = \frac{326}{\sqrt{\sigma}}\left[1 - \frac{71.3}{(w/t)\sqrt{\sigma}}\right] \qquad \text{for } \sigma > \sigma_{lim} \qquad (2.2)$$

$$b_{eff} = w \qquad \text{for } \sigma \leq \sigma_{lim} \qquad (2.3)$$

b is the effective width of the compression flange. σ is given in k/in^2. The stress σ_{lim} is not mentioned in the AISI design provisions. Instead, the two ranges are determined in terms of

$$(w/t)_{lim} = \frac{221}{\sqrt{\sigma}} \qquad (2.4)$$

However, to avoid confusion, $(w/t)_{lim}$ will be used in the present discussion only in connection with initial yielding of the compression flange, where $\sigma = \sigma_y$ in Eq. 2.4. σ_{lim} is

obtained by solving Eq. 2.2 for σ and setting $b = 2$, or by solving Eq. 2.4 for σ, using the actual w/t.

The compression flange width is now not treated as a constant in the beam equations, but as a variable according to a specified additional equation. Eq. 2.2, however, is only intended to apply up to initial yielding in the compression flange. Theoretical moment-curvature relationships based on the effective width equation will therefore not be established beyond this point. But, there is no theoretical obstacle to continue moment-curvature relationships based on Eq. A2.1-1 to A2.1-5 and Eq. 2.2 beyond the yield moment, as long as only the tension flange is yielding. This has not been done yet, since the AISI Specifications consider incipient yielding as the strength criterion, regardless of whether it occurs in the tension or compression flange. Therefore, for specimens with $w/t > (w/t)_{lim}$, and initial yielding at the tension flange, a comparison in the inelastic range between the theoretical moment-curvature-relationships derived from Eq. 2.2, and the experimental moment-curvature relationships will be of interest.

Details about the computation of the theoretical moment-curvature relationships are given in Appendix 2.1. The curvature ϕ was always used as the independent variable to be prescribed. Usually, values of ϕ were chosen to be identical with those measured at successive load steps in the experiments.

Remarks on the Elastic Stiffness of the Test Specimens

For specimens with low w/t-ratios, theoretical and experimental curves should show good agreement with respect to the elastic stiffness EI. For all specimens with low and moderate w/t-ratios, this agreement was obtained within a margin of at most ±2.0%. Similarly for high ratios, there should be good agreement of the elastic stiffness in the initial elastic range, i.e., for $\sigma < \sigma_{lim}$. In general it was observed, for sections with comparable widths and depths, that discrepancies may be the higher the smaller the sheet thickness. Differences are possible since stiffnesses for theoretical and experimental moment-curvature relationships were obtained from completely different sets of measurements. Stiffness values for theoretical curves were based on the measured dimensions of the cross-section, whereas the experimental stiffness values were obtained from measured values of load and curvature. For example, for specimen HA5-20 (see Table 2.2) with w/t = 120.2 and 20 gage sheet, the stiffness values of theoretical and experimental curves showed a difference of 6% in the low, linear elastic range which was not found to be due to any definite error in measurement. It seemed desirable to eliminate this discrepancy to obtain comparable conditions in the more advanced range of non-linear elastic behavior and inelastic behavior. This has been done by distributing the error of 6% in stiffness to the individual dimension measurements, giving each linear dimension equal weight. Since the

moment of inertia has the dimension (L^4), this method implies that each linear dimension be corrected by a factor

$$e = \sqrt[4]{1.06} = 1.015 \qquad (2.5)$$

Similar corrections seem to be important when determining the effective width directly from the moment-curvature behavior of the test specimen, i.e., if an effective width equation is to be verified (for example for unstiffened sections).

The elastic modulus E = 29,500 ksi was always used when working with the equations of beam theory. This value was not considered a possible source of error, due to the good agreement of computed and experimental stiffness values for low and moderate w/t-ratios.

Computational Evaluation with Respect to Failure Criterion

Since the purpose of this investigation is to study the inelastic strength of coldformed sections, the pertinent failure criterion is directly connected with local failure of the compression flange at or after initial yielding. There is no valid theory to deal with the problem of compression flange failure of coldformed sections in the inelastic range. A failure criterion will therefore be established empirically from experimental data for the compression flanges of varying w/t-ratios. Once a compression flange failure criterion is specified, it will be used in design applications to determine ultimate moment and ultimate curvature. For this purpose the

just discussed set of equations for the moment-curvature relationships in the inelastic range will be used subsequently.

2.3 Behavior of Specimens in the Range of Low and Moderate w/t-Ratios

2.3.1 Experimental Observations on Failure Mode; Definition of Failure

Since the beam specimens were tested in a hydraulic testing machine, readings were taken at an essentially constant state of deflection. This allows load-deflection measurements beyond the maximum load into the load shedding range. In particular, it allows detailed observations on the circumstances of failure. Flange distortions were not visible upon inspection prior to maximum load. At the point of maximum load, however, clearly visible out-of-plane deflections in the form of incipient local buckles were initiating. As further deflections were imposed on the beam, the amplitude of this local buckling half-wave would increase with decreasing load in a continuous fashion and at a visible rate. At this stage, additional deformations were confined to the weakened region where local failure had occurred. Simultaneously, strains outside the zone of local failure showed some unloading. Eventually, the pattern of the buckle would change from the smoothly waved into a grossly distorted, kinked shape, accompanied by a rapid drop of load. There was some gradation within this general type of behavior, over the range of w/t-ratios, according to the following observations.

The specimens of low ratios ($w/t < (w/t)_{lim}$) were in a

state of advanced section plastification, with significant plastic strains in the compression flange, as buckling distortions were initiating. At this point, the maximum load could still be kept at almost its maximum level over a certain range of additional deflections before load shedding became pronounced. After failure initiation, the amplitude of the local buckle increased very gradually with increasing deflections.

At the upper end of the spectrum of ratios, in the beams with $w/t \approx 42$, the compression flanges failed upon or shortly after reaching the yield stress. Flange distortions again were not visible prior to maximum load. However at the point of maximum load the compression flanges began to bulge locally at a fast rate into a half-wave pattern, which continued even as the testing machine was stopped, until the amplitude had reached approximately five times the flange thickness. The half-wave then assumed a kinked shape after some additional beam deflections. The drop of load was pronounced as soon as the point of maximum load was passed. The failure region of these beams was usually located in the central portion of the beam, around midsection, in contrast to beams of lower ratios where local failure always occurred near one of the load points. From strain gages in the close vicinity of local failure it could be determined that, as the buckle developed, it was initially accompanied by considerable local section plastification, both from the tension and compression side, although the load was decreasing.

Definition of Failure

The failure point in the behavior of the beams shall be defined as the point of maximum load just prior to load shedding. For specimens with low w/t-ratios this point can sometimes only be clearly defined by incipient visible buckling distortions, since the drop of load may initially be very slow. From here on, the maximum load will be called either failure load or ultimate load, P_u, and correspondingly, the failure load will determine ultimate moment M_u, ultimate curvature ϕ_u, and ultimate compressive strain $\varepsilon_{c,u}$. The word failure will be used as an attribute synonymously with "ultimate." Since local failure is obviously determined by the loss of stability of the compression flange in the plastic range, the ultimate compressive strain will also be called the critical compressive strain in the plastic range.

2.3.2 Plastic Behavior of Compression Flanges

Uniformity of Yielding in Longitudinal Direction

The critical compression flange strains will be established in the following from strain gage measurements. However, since the strain gages measure local strain values in a region of constant moment, it is necessary to ensure that the measurements selected are really representative of the flange just prior to the plastic stability limit.

Elastic and plastic strain distributions along the webs within the constant moment zone are plotted in Figs. 2.3 and 2.4 for two typical specimens. Fig. 2.3 shows the strain

distribution for specimen HL1-10 (w/t = 32.3) as measured by three gages (7, 8, and 9 in Fig. 2.2) over a six inch interval at midspan. Fig. 2.4 shows the strain distribution for HL3-10 (w/t = 38.3) as measured by four gages (5, 6, 7, and 9 in Fig. 2.2) over the major part of the constant moment region. Certain irregularities are always present. For HL1-10 they occur in the initial plastic range, indicated by reading 8, but it is seen that at the last reading, R11, at incipient load shedding, the distribution is surprisingly uniform. Hence, although failure did not occur within the interval of measurements, but close to the load point, it was considered justified to select the indicated value at midsection as a representative critical compression strain. Specimen HL3-10 at first yields in a uniform manner. At a later stage the strains near the load points increase faster than the strains at midsection, which can be explained as the effect of local disturbances near load application on a flange whose ratio is slightly above $(w/t)_{lim}$. The straight lines between points of measurement in Fig. 2.4 may be somewhat misleading, since the outer measurements may have local significance only. But it may be concluded that flanges around the limit ratio and above are more sensitive to disturbances in the process of yielding, than lower ratios. The value selected as the critical strain in this case is the average ultimate strain near midsection, to ensure that effects of local disturbances are excluded. Failure, in fact, occurred subsequently at the left load point

in Fig. 2.4, as might be expected from the strain measurements.

In general, particularly for ratios w/t < 37, the yield process was uniform in the longitudinal direction and continuous with increasing load. This can be expected as long as web plastification is not complete, that is, as long as there is any appreciable elastic resistance left in the webs.

Symmetry across the flange was checked by gages 9 and 10 (Fig. 2.2). Differences between these two gages were negligibly small for all specimens, and are therefore not further discussed.

Out-of-Plane Flange Distortions

Figs. 2.5 and 2.6 deal with the strain distribution across the flange and out-of-plane flange distortions for specimen HL1-10 (w/t = 32.3). The behavior is typical for all flanges that reach into the range of plastic strains (compare Figs. 2.7 and 2.8 for HA3-12, w/t = 41.2). In Fig. 2.5, the strains measured on the inner and outer surface at the centerline of the compression flange are plotted vs. the edge strain, both individually and as an average. If the axial strains (average over the flange thickness) were uniform across the flange, the dashed line in Fig. 2.5 would have to be obtained for both gages (11 and 12) and their average. Throughout the elastic range the strain distribution was uniform. Small differences result from a plate curvature corresponding to the beam curvature. A drastic change in behavior

is observed at initial yielding of the flange. At this point the measurements register a sudden deviation between the inner and outer surface strains at center, indicating that plate distortions have taken place. Thereafter the axial compressive strain at center (average between gages 11 and 12) increases continuously, although at a smaller rate than the edge strain (gages 9, 10).

In Fig. 2.6, the flange curvature at center is plotted vs. the edge strain for the same specimen. The elastic curvature is followed by an abrupt increase at initial yielding and then a steady, very slow increase over a long range of plastic edge strains. The curve ends just after failure initiation.

The curvature beyond incipient yielding in Fig. 2.6 (i.e., beyond yield strain level as marked) results from out-of-plane deflections in the form of a somewhat irregular wave pattern over the region of constant moment. Although the deflections were measureable they were not visible, since they did not exceed $\delta_{max} = 1.5/100$ in prior to failure. The flange curvature is approximately proportional to out-of-plane deflections. The scale in terms of δ_{max} (maximum amplitude) is also indicated in Fig. 2.6.

Conclusions from Figs. 2.5 and 2.6

The compression flange is plane in the elastic range, except of course, that it has a curvature in the longitudinal direction, identical with the beam curvature. With incipient yielding the plane configuration is no longer stable and the

flange deflects, over a very short load interval, into a slightly deflected shape which again constitutes apparently a stable equilibrium configuration. The deflected shape is measurable, but invisible to the naked eye. In this state, large increments of plastic strain at the edges of the flange produce only small increments in flange deflections, up to a point where the deflected shape is no longer stable. At reading R10 in Figs. 2.5 and 2.6, the final limit of stability is reached. Following R10, deflections δ_{max} begin to increase visibly under small increments of additional edge strain, accompanied by a drop of load, which constitutes failure. The edge strain recorded at R10 has therefore been defined as the critical compressive strain of specimen HL1-10, or the ultimate compressive strain $\varepsilon_{c,u}$. The strains between R10 and R11 in Figs. 2.5 and 2.6 do not represent the behavior at or near the location of local buckling (which was close to a load point).

A possible loss of strength of the compression flange in the plastic range prior to failure can, if at all, only be observed in the moment-curvature relationships, which will be discussed subsequently. It cannot be measured directly.

The ten specimens of low and moderate w/t-ratios span a range from $w/t = .88\ (w/t)_{lim}$ to $w/t = 1.14\ (w/t)_{lim}$ (see Table 2.6). Figs. 2.5 and 2.6 are representative for the compression flange behavior in the low range of w/t-ratios ($w/t < (w/t)_{lim}$). An example for the compression flange behavior at

the upper end of this range is given in Figs. 2.7 and 2.8 for HA3-12, with $w/t = 41.2 = 1.12\ (w/t)_{lim}$. In this case, an abrupt increase of flange curvature occurs at edge strains somewhat below the yield strain ε_y. Apparently, in the neighborhood of this w/t-ratio, the effects of initial deflections create a non-uniform stress field where incipient yielding in extreme fibers occurs at corner strains appreciably below ε_y. However, the plots show that this flange, after an initial change in its deflected shape, remains stable, and sustains axial strains (average over thickness) into the plastic range, even at its centerline (gages 11, 12). The flange deflections between R7 and R11 remain invisible to the eye. The resistance of the compression flange does not seem to be significantly impaired in this range, as compared to the fully effective section, according to the moment curvature relationship of the specimen which will be presented later. Following R11, the flange becomes unstable with rapidly increasing plastic buckling distortions and a simultaneous loss of resistance of the section at a fast rate. R11 therefore determines $\varepsilon_{c,u}$ for HA3-12.

Sections with w/t-ratios similar to HA3-12 did not produce consistent values of ultimate compressive strain. E.g., HA4-12 failed just after reaching a corner strain ε_y. It may be concluded that, as the corner strains reach ε_y, the state of equilibrium of the compression flanges in this range of w/t-ratios is very sensitive with respect to imperfections.

The ultimate compressive strains $\varepsilon_{c,u}$ for all ten specimens are given in Fig. 2.9 and Table 2.3 to be presented next.

Critical Compression Flange Strains in the Plastic Range

In Fig. 2.9 the plastic critical strains of all beams, evaluated as discussed, are plotted vs. the w/t-ratios. It is noted that the yield points for all test specimens are within the range $36 < \sigma_y < 37.7$ ksi, that is, the results are comparable with respect to the yield stress.

There is a considerable scatter of test results for ratios $w/t > (w/t)_{lim} \simeq 37$, with the smallest failure strains falling just above the yield strain. In contrast, the critical strains for $w/t < 34$ show good consistency and exceed three times the yield strain. Although only three values are available in this range, they comprise the three different types of hat sections, balanced conditions (HL1-10), first yielding at the tension flange (HA1-10) and first yielding at the compression flange (HB1-10), the last two with considerable eccentricity of the neutral axis. Critical or ultimate strains $\varepsilon_{c,u} = 3\varepsilon_y$, as indicated in Fig. 2.9 are therefore considered reliable in this range.

Numerical values of the experimental ultimate compressive strains are listed in Table 2.3 for increasing w/t-ratios. In the same table they are put in context with the overall deformational behavior of the sections, represented by the ultimate tensile strains and curvatures, all listed as ratios with respect to their values at initial yielding. Although the

ultimate compressive strains for the first three sections in Table 2.3 are nearly the same, the corresponding curvatures show a large difference which is due to the different type of section geometry.

It is proposed to use the straight line shown in Fig. 2.9 as a reasonable and safe approximation for determining critical edge strains initiating flange failure. These flange failure strains will be used in the design approach discussed later.

2.3.3 Moment-Curvature Relationships

Experimental moment-curvature relationships for the specimens with low and moderate w/t-ratios are plotted in Figs. 2.10 to 2.19. The curvatures are obtained from strain gage readings, usually taken at midsection (average of gages (3,9) and (4,10)). The evaluation of the compressive strains in the plastic range, to exclude local effects, was described previously. The average curvatures over the constant moment region, obtained from inclinometer readings, are in good agreement, but tend to be slightly larger in the inelastic range. This can be attributed to local effects at the load points, included in the inclinometer measurements.

The experimental moment-curvature relationships are compared to theoretical moment-curvature relationships obtained on the basis of beam theory as described in Section 2.2. All curves are normalized with respect to initial yielding of the fully effective section. The computed bounds to the inelastic

range, moment at initial yield and full plastic moment, are indicated in the graphs. The plastic moment is a computed theoretical value. Postultimate behavior has been omitted, since load shedding is of no particular interest beyond the general description given earlier. It is seen that measured and calculated curves agree very satisfactorily.

Ultimate Moments and Ultimate Curvatures

Numerical data on ultimate moments and curvatures are collected in Tables 2.4 and 2.5. Table 2.4 presents the results in the form of ratios from two points of view:

1) Ratios with reference to initial yielding in Cols. 6 and 7

These ratios indicate available reserves of inelastic resistance and inelastic curvature, respectively. The initial yield values M_y are computed values, but, for all practical purposes, are identical with the experimentally measured values. The first three rows refer to sections of type HA with pronounced eccentricity and initial yielding in tension. In this case the reserves of inelastic resistance prior to initial yielding of the compression flange is indicated in Col. 4. It is seen to be a major fraction of the maximum possible reserve, i.e., that corresponding to the computed full plastic moments, listed for all sections in Col. 5. Plastic moment ratios are naturally much higher for the eccentric sections (first five rows) than for the balanced sections (last five rows). The geometric eccentricity of the sections

can roughly be compared on the basis of the values y_t/d in Col. 3. y_t is the distance between neutral axis and tension flange. Col. 6 shows that the experimental reserves of inelastic resistance are in general significant. The ultimate curvature ratios given in Col. 7 reflect to some degree the variations of the critical compressive strains.

2) Ratios between experimental and computed ultimate values in Cols. 8 and 9

The computed values were obtained from the conventional beam equations, Eqs. A2.1-1 to A2.1-5, given in Appendix 2.1, applied to the fully effective section. For calculating $M_{u,ctd}$ and $\phi_{u,ctd}$, the actual experimental critical compressive strains were used, as given in Fig. 2.9. Using the strains corresponding to the proposed straight lines on Fig. 2.9 would have given slightly more conservative results, with one exception.

The results of this evaluation with respect to strength are either quite accurate or else slightly conservative. A larger variation is obtained for the curvatures. The deviations from 1.0 can primarily be explained by the effects of corner strainhardening above the yield strain. Since the sections are not symmetric, corner strainhardening effects will make different contributions on tension and compression flange, and thus shift the neutral axis from its ideal position. This effect can decrease the curvature and increase the strength, or vice versa, if compared to the idealized section.

Still, the effect seems to be relatively mild. More details will be given in discussing the moment-curvature graphs.

Graphical Comparison of Experimental and Theoretical Moment-Curvature Relationships

The moment-curvature graphs are given in Fig. 2.10 to 2.19 in ascending order of w/t. The graphs show very good agreement in the elastic range, and predicted yield moments seem to be as accurate as practically possible. It seems that mainly two causes are responsible for some discrepancies between experimental and computed curves in the inelastic range: (1) Some loss in compression flange effectiveness. (2) Corner workhardening effects, although they have deliberately been kept mild through the relative proportioning of the corner and flat areas.

Beginning in the late elastic range or with initial yielding of the compression flanges near the corners, it can generally be observed that the experimental moments are slightly smaller than the computed moments, indicating that possibly small losses in compression flange effectiveness may have occurred. This effect is relatively more pronounced for sections HL2-10 and HL3-10 in Figs. 2.13 and 2.14, respectively. The loss of effectiveness does, however, not seem to continue at an appreciable rate into the state of plastic deformations of the compression flange. Hence, as long as plastic deformations can be sustained, corner workhardening effects, although mild, soon seem to compensate for the initial loss in

effectiveness and, as failure occurs, the experimental values have usually reached or slightly exceeded the computed values which account neither for loss in effectiveness nor for corner workhardening. More specific observations shall be reported separately for the ranges of low and moderate ratios.

1) Low Ratios ($w/t < (w/t)_{lim} = 37$), Figs. 2.10 to 2.13

Figs. 2.10, 2.11 and 2.13 represent sections of the type HB and HL with initial yielding in compression or balanced conditions, respectively. The diagrams indicate that the compression flanges might have a small loss in effectiveness approximately at the point of their initial yielding, coinciding with the sudden increase in out-of-plane deflections as indicated in Figs. 2.5 to 2.8. This loss does not seem to increase in the plastic range. Instead, the experimental moments follow the computed moments closely, and, in all cases, reach slightly higher values at failure. Fig. 2.11 shows the moment-curvature curves for specimen HA1-10, with initial yielding in tension, where much of the inelastic reserve of resistance is obtained before the compression flange yields. Within this portion of the inelastic range, the diagram does not show any appreciable discrepancy between experimental and theoretical curve. In the advanced inelastic range, the experimental moments are slightly higher than computed, probably due to mild corner workhardening effects. In general, for the four specimens of low ratios, the experimental and theoretical moment-curvature relationships are in good

agreement, and the experimental failure values reach or exceed slightly the corresponding computed values.

2) Moderate Ratios ($37 < w/t < 42$), Figs. 2.14 to 2.19

In the moderate range, the experimental w/t-ratios cluster around the two values $w/t \approx 38.5$ and $w/t \approx 41.5$, which are above $(w/t)_{lim} = 37$. The yield moment and yield curvature, marked in the graphs, are those computed for the fully effective section. Some of the graphs show small deviations from the computed curves prior to M_y, but the differences between M_y for the fully effective section and the actual experimental yield moment are less than 3% in all cases.

However, the compression flanges are capable of sustaining various amounts of plastic deformations, and do apparently not undergo any appreciable loss of compression flange effectiveness after initial yielding at the corners and before local failure. At failure, the experimental moments exceed the moments computed for the fully effective sections, but usually by insignificant amounts. This again may be ascribed to mild corner workhardening effects. The inconsistency of the amounts of ultimate curvature among the different specimens corresponds of course to the scatter of the critical compressive strains in Fig. 2.9. The agreement between experimental and computed curves in Figs. 2.14 to 2.19 is very good in some cases and is in general very satisfactory.

2.3.4 Conclusions and Failure Criterion for Inelastic Design

General

In the usual case of gravity load, attainment of maximum load and incipient load shedding of a beam is defined as failure. In the tests, load shedding was always caused by the loss of stability of the compression flange in the range of plastic deformations. This loss of stability was evident as the compression flange in the state of plastic strains began to bulge visibly from an apparently plane configuration into a local buckling wave, which grew steadily into an excessively distorted and finally kinked shape. The point where the plastic limit of stability is reached is well defined in a careful testing procedure, and can be measured in terms of plastic strains in the corners of the compression flange. These were called the critical strains in the plastic range.

Inelastic Behavior of the Compression Flanges Prior to Failure

In view of the theory of selective yielding in connection with plastic design, discussed in Chapter 1, Sec. 1.4, the yield process in the compression flanges was examined with respect to its uniformity over the region of constant moment. With the exception of minor irregularities in the range of moderate w/t-ratios, mainly due to disturbances at the load points, it can be stated that the yield process was generally uniform over the constant moment region and continuous with increasing load.

For all specimens of low and moderate w/t-ratios, out-of-plane compression flange distortions were not visible to the naked eye prior to failure, i.e., prior to the plastic stability limit of the flange. Measurements, however, indicate that a marked change in the geometric configuration of the flange takes place around incipient yielding at the corners, when the flange suddenly adjusts to a new, deflected geometric configuration. From there on the deflections increase approximately proportional to the plastic strains (Fig. 2.6), until the critical strain is reached. But the rate at which the deflections increase is so slow, that just prior to failure the maximum out-of-plane deflections, measured for any specimen, were $\delta_{max} < 2/100$ in $\approx$ b/200.

Experimental Critical Strains and Design Failure Criterion

The results for the critical compressive strains are plotted vs. the w/t-ratios in Fig. 2.9, for a yield strength $\sigma_y \approx 36$ ksi. The individual experimental results are identified by the names of the specimens. The group names HA, HB and HL denote sections with initial yielding in tension, compression, or balanced conditions, respectively. No obvious differences are discernible in the test results in Fig. 2.9, that could be attributed to the distinction between the section geometries. One is therefore left with the parameter w/t as the principal geometric parameter.

The objective is now to deduce a failure criterion in terms of critical compressive strains, for the design with w/t-ratios in the low and moderate range. The values of critical compressive strains obtained for w/t < 34 are apparently consistent, at a plastic strain level of somewhat larger than $\varepsilon_{c,u}/\varepsilon_y = 3$. In contrast, the critical compressive strains for ratios 38 < w/t < 42 show a considerable scatter, which may be caused by a high imperfection sensitivity in this range. A general failure criterion in this range may be chosen as a reasonable lower bound to the scatter. On this basis, a design failure criterion in terms of critical compressive strains is proposed as given by the straight lines in Fig. 2.9. Accordingly, in analytical terms, the following critical compressive strains can be used in the inelastic design of stiffened coldformed sections as the failure criterion. It shall first be expressed for $\sigma_y = 36$ ksi, i.e.,

$$\left.\begin{aligned} \varepsilon_{c,u}/\varepsilon_y &= 1 && \text{for} \quad \frac{w}{t} > 40 \\ \varepsilon_{c,u}/\varepsilon_y &= \frac{1}{3}(41 - \frac{w}{t}) + \frac{2}{3} && \text{for } 34 < \frac{w}{t} < 40 \\ \varepsilon_{c,u}/\varepsilon_y &= 3 && \text{for} \quad \frac{w}{t} < 34 \end{aligned}\right\} \sigma_y = 36 \text{ ksi} \qquad (2.6)$$

Introducing $(w/t)_{lim}$ as a general parameter, Eqs. 2.6 can be written as follows

$$\begin{aligned} \varepsilon_{c,u}/\varepsilon_y &= 1 && \text{for } w/t > 1.08(w/t)_{lim} \\ \varepsilon_{c,u}/\varepsilon_y &= 14.5 - 12.5 \times \frac{w/t}{(w/t)_{lim}}, && \text{for } .92(\frac{w}{t})_{lim} < \frac{w}{t} < 1.08(\frac{w}{t})_{lim} \\ \varepsilon_{c,u}/\varepsilon_y &= 3 && \text{for } w/t < .92(w/t)_{lim} \end{aligned} \qquad (2.7)$$

The failure criterion above was derived from test results where the yield stress was close to σ_y = 36 ksi. It may be reasonably assumed that the bounds of the failure criterion depend on σ_y in a form similar to that in which $(w/t)_{lim}$ depends on σ_y. For stiffened flanges, this form is given by Eq. 1.3, i.e., $(w/t)_{lim} = 221/\sqrt{\sigma_y}$. It is of interest in this context, that the w/t-ratios for hotrolled sections that qualify for plastic design are defined in a similar form, e.g., $w/t = 190/\sqrt{\sigma_y}$ for box sections.[11] A lower value $150/\sqrt{\sigma_y}$ has recently been proposed and documented.[25]

If the assumption introduced in the last paragraph is justified, it is possible to use Eqs. 2.7 for variable values of $(w/t)_{lim}$, where $(w/t)_{lim}$ depends on σ_y, as defined by Eq. 1.3. However, the range in which the yield stress may vary should be limited with some caution, unless additional tests are made for yield stresses significantly different from $\sigma_y \approx 36$ ksi. It is therefore recommended, that Eqs. 2.7 should only be used if $\sigma_y \leq 45$ ksi.

Ultimate Moment and Ultimate Curvature

It is proposed that the compressive strain failure criterion given above be used in design to determine ultimate moment and ultimate curvature of the beam section. This requires a set of equations representative of the inelastic moment-curvature behavior of the actual beam. In the calculations for Tables 2.4 and 2.5, and Figs. 2.10 to 2.19, computations have been carried out with the conventional equations of

beam theory for the fully effective section, which are given in Appendix 2.1, Eqs. A2.1-1 to A2.1-5. This approach was not only used to compare the experimental and computed moment-curvature relationships in full (Figs. 2.10 to 2.19), but was also applied in particular to compare experimental and computed values of ultimate moment and ultimate curvature (Table 2.4, Cols. 8 and 9). The computed values were established for the actual measured critical compressive strains (Table 2.3 and Fig. 2.9). It was found that the accuracy of the computed values for ultimate moment and curvature can hardly be improved. Similarly, there is a general good agreement between experiment and computation at all stages of the moment-curvature relationships. The equations of beam theory, as given by Eqs. A2.1-1 to A2.1-5, in combination with the fully effective section, can therefore be considered a valid basis for inelastic analysis throughout the range $w/t \leq 42$ for $\sigma_y = 36$ ksi of the present investigation, or, in general, for $w/t \leq 1.15\ (w/t)_{lim}$.

Finally, Table 2.6 compares the experimental ultimate moments with the design ultimate moments computed with the beam equations for fully effective section, and the design failure criterion of ultimate compressive strain (Eq. 2.7; straight line fit of Fig. 2.9). The design approach predicts safe and conservative ultimate moment values for nine out of ten specimens. One design value overestimates the experimental result, which was expected on the basis of Fig. 2.9, and

seemed to be acceptable within the context of generally conservative results. This establishes the design approach for partial section plastification in the range of w/t-ratios below or in the neighborhood of $(w/t)_{lim}$.

2.4 Ultimate Strength of Specimens in the Range of High w/t-Ratios and Failure Criterion for Inelastic Design

Two specimens were tested with high ratios, i.e., $w/t >> (w/t)_{lim}$, so that their flanges could reach an advanced postcritical state prior to initial yielding of the compression flanges. They were designed with significant initial eccentricity to undergo web plastification from the tension side. The compression flange ratios were w/t = 73.5 for HA4-16 and w/t = 120.2 for HA5-20.

Observations on Failure Modes

The compression flanges of both specimens showed a well-defined wave pattern of postcritical out-of-plane deflections prior to failure.

Numerical results are summarized in Tables 2.7 and 2.8. Table 2.7, in the last 4 columns, lists experimental failure strains and their ratios with respect to the yield strain. As expected according to the discussion in Chapter 1, local failure is obtained with incipient yielding of the compression flanges at the corners. Col. 10 indicates that yielding in tension is substantial for HA4-16, less so for HA5-20. In the latter section the initial eccentricity of the neutral axis is substantially reduced at high loads by postcritical loss of

compression flange effectiveness. This shift of the neutral axis may be expressed in terms of the ratio y_t/d. Thus, for HA5-20, the position of the neutral axis dropped from y_t/d = .62 to y_t/d = .53, between the beginning of loading and failure, respectively. The corresponding drop for HA4-16 was only from y_t/d = .62 to y_t/d = .57. Accordingly, in column 3 the inelastic reserve strength is considerably larger for HA4-16 than for HA5-20.

The ratios in columns 3 to 8 relate experimental results to values computed from the effective width approach. The ratios of reserves of inelastic resistance in Cols. 3 and 4 are meaningful only if the experimental values at initial yielding compare well with the computed values at initial yielding. This comparison has been made in Cols. 5 and 6. The validity of the reduced effective width approach to determine ultimate loads is checked in Cols. 7 and 8.

There is practically no difference in calculated vs. observed initial yield moments for HA4-16. For HA5-20 the experimental initial yield load is 5% low as compared to the analytical value. Ultimate experimental loads check within 2% with the analytical values for both specimens. Curvatures at ultimate load show the same good agreement.

A judgment can also be made from the graphs in Figs. 2.20 and 2.21. Considering some experimental imponderabilities, effective particularly in the inelastic range, there is reasonable agreement between experimental and analytical

results, indicating that the actual beam behavior is well represented by the effective width approach in combination with an elastic-plastic stress distribution on the tension side.

Failure Criterion for Design

For sections with large w/t-ratios it may be concluded, that a reliable ultimate strength design can be applied in the postcritical range, based on (1) a compression flange failure criterion $\varepsilon_{c,u}/\varepsilon_y = 1$; (2) the conventional beam equations, as given in Appendix 2.1; and (3) the Winter effective width equation, given by Eq. 2.2. This will not affect the conventional allowable stress design of sections with initial yielding at the compression flange, since in this case the yield moment is identical with the ultimate strength of the section (i.e., $\varepsilon_c = \varepsilon_y = \varepsilon_{c,u}$). However, for sections with initial yielding at the tension flange, it allows us to take advantage of inelastic reserves of resistance gained from web plastification on the tension side.

The computation of the ultimate moment for a section with reduced effective width is no more complicated than for a fully effective section, and the design approaches with respect to the ultimate moment, that will be developed in Chapter 3, will be equally applicable to both cases. This is due to the fact that, with a failure criterion $\varepsilon_{c,u}/\varepsilon_y = 1$, the effective width of the compression flange can be determined *a priori* from the Winter effective width equation (Eq. 2.2).

However, the amount of plastification from the tension side at failure will depend on the position of the neutral axis at failure. For certain sections with high w/t-ratios, the compression flange effective width can be reduced by so much, that the initial eccentricity of the neutral axis will be substantially reduced or even reversed.

CHAPTER 3

ANALYSIS OF THE STATICALLY DETERMINATE BEAM FOR PARTIAL SECTION PLASTIFICATION

The preceding chapter has determined that the design of coldformed steel beams for ultimate load carrying capacity has to be based on a compressive strain failure criterion. A strain failure criterion has not yet been used in steel design, and will therefore require that design methods be demonstrated that are efficient, and suitable for practical needs. Inelastic design methods for coldformed beams must, in the regular case, be applicable to asymmetric sections. An attempt will be made in Chapters 3 to 5, to establish practical design methods in a systematic manner.

The analysis will be derived from beam theory, assuming that the section remains plane in the deformed state, not only in the elastic range, but also in the inelastic range, and that the uniaxial stress-strain law is valid between longitudinal stresses and deformations. It was shown in the preceding chapter by comparison of experiment and beam theory that these assumptions are justified for all practical purposes.

The compressive strain failure criterion as a function of the width to thickness ratio and the yield strength of the

material has been discussed in detail in the previous chapter. The inelastic capacity of coldformed steel beams will be evaluated in particular with respect to the maximum and minimum value of the established failure strain criterion, i.e., according to Eq. 2.7, $\varepsilon_{c,u}/\varepsilon_y = 3$ for $w/t \geq .92\ (w/t)_{lim}$, and $\varepsilon_{c,u}/\varepsilon_y = 1$ for $w/t \geq 1.08\ (w/t)_{lim}$, respectively. This will establish the general approach, according to which intermediate failure strains can later be evaluated. The demonstration for the limiting values of the strain criterion will in addition serve for a general assessment of the results of inelastic design of coldformed beams. The following introductory remarks shall be made with respect to the selected compressive strain values.

(1) $\varepsilon_{c,u} = 3\varepsilon_y$. Under this condition the stress distribution across the flange will be considered uniform over the actual flange width, at a stress level of σ_y. This was shown by experiment to be a valid assumption.

(2) $\varepsilon_{c,u} = \varepsilon_y$. In this case, inelastic structural reserves can only be expected from web plastification on the tension side. The compression flange will be in the postcritical state, or at the transition to the postcritical state, at failure, and will therefore be treated according to the effective width design provisions of the present AISI Specifications. For sections that belong to this category, the limiting condition of elastic, allowable stress design is defined as initial yielding of the tension flange, which

requires an iteration procedure to determine effective compression flange width and allowable moment. In contrast, if the compressive strain failure criterion of inelastic design is applied, the effective width of this category of sections can be determined at the outset, since for $\varepsilon_{c,u} = \varepsilon_y$ the effective width is obtained from the postcritical effective width formula with $\sigma_{max} = \sigma_y$. There is then only one category of sections left, for which the allowable stress design coincides for all practical purposes with the design for ultimate strength. These are the sections in the postcritical range with initial yielding at the compression flange.

For unstiffened flanges, plastic failure strains are not yet established experimentally; they may depend not only on w/t-ratio and yield strength, but also on the distance of lateral beam bracing. Once these critical compressive strains have been established, it will be possible to apply the design method, developed in the present chapter, to both stiffened and unstiffened sections.

The inelastic load carrying capacity of an indeterminate system will be determined by two components. (1) The increased resistance of the beam section due to partial section plastification. (2) An additional resistance of the system due to partial moment redistribution. The first component is determined by the section parameters and the compressive failure strain. The second component results from the inelastic rotation of partially developed hinges, which depends in

addition on system and loading parameters. The second component, of course, does not apply to the statically determinate system, which will be the subject of investigation of the present chapter.

The treatment of the inelastic behavior of coldformed, statically determinate beams will be organized as follows. In Sec. 3.1, the moment-curvature relationship in the elastic and inelastic range will be discussed in principle, in terms of the parameters involved. In Sec. 3.2, a design approach will be developed for the ultimate resistance of a coldformed, eccentric section with a failure criterion of ultimate compressive strain.

3.1 General Considerations of Similarity in the Flexural Behavior of Monosymmetric Coldformed Sections

A methodical approach requires that all aspects of similarity be taken advantage of, i.e., that the number of independent parameters be reduced to a minimum. For example, the moment-curvature-relationship of a doubly symmetric flanged section can be described by a function of 7 independent variables

$$M = M(\phi, \sigma_y, E, b, d, t_w, t_{fl}) \qquad (3.1)$$

Notations are illustrated in Fig. 3.1. Hence, to obtain the general behavior with respect to the moment-curvature relationship, families of curves of the two variables M and ϕ could be constructed with respect to 6 independent parameters.

Since there are two primary dimensional units, force and length, the number of parameters could immediately be reduced to 4, in the form of a non-dimensional equation. But the actual equations of equilibrium of the section can easily be established. They will show that the number of parameters can be reduced even further, so that the problem can finally be expressed by a one-parameter family of curves, where the remaining arguments take the form

$$\frac{M}{\sigma_y t_w d^2} = f\left(\frac{\phi d}{\varepsilon_y} , \bar{\beta}_1\right) \tag{3.2}$$

with the geometric parameter

$$\bar{\beta}_1 = \frac{A_{fl}}{A_w} = \frac{bt_{fl}}{dt_w} \tag{3.3}$$

The remaining parameters in Eq. 3.2 are the normalized variables of moment and curvature, which, in the following, will be represented by the notation

$$m = \frac{M}{\sigma_y t_w d^2} , \quad \kappa = \phi d \tag{3.4}$$

The moment-curvature behavior is now expressed by a family of curves created by a single geometric parameter β_1. The analysis will, however, be based on a somewhat more general type of section, the monosymmetric section, which is not symmetric about the axis of bending. This loss of symme-

try introduces two new independent geometric dimensions, i.e., we must now distinguish between the different widths and thicknesses of the tension and compression flange, b_t, b_c and t_t, t_c, respectively. In the non-dimensional form of the moment-curvature relationship, corresponding to Eq. 3.2, however, there will be only one additional parameter and it will now look as follows,

$$m = f(\frac{\kappa}{\varepsilon_y} , \bar{\bar{\beta}}_1, \bar{\bar{\beta}}_2) \tag{3.5}$$

with the two geometric parameters

$$\bar{\bar{\beta}}_1 = \frac{A_t}{A_w} = \frac{b_t t_t}{dt_w} , \quad \bar{\bar{\beta}}_2 = \frac{A_c}{A_w} = \frac{b_c t_c}{dt_w} \tag{3.6}$$

At this point we will reduce the problem specifically to the coldformed monosymmetric section. A section prototype is shown in Fig. 3.1. Being formed from steel sheets, the thickness of all flat elements composing the section, will be the same. For sections symmetric with respect to the vertical axis, the coldforming technique will, however, often imply that there are two webs. These can either result from a single forming process in the case of hat and tubular sections, or, in the case of I-sections, by connecting two channels back to back. The geometric parameters for flexural behavior about one principal axis, as given above, do not distinguish between these types of sections and, therefore, cover all of them. Considering that

$$t_{fl} = t = \frac{1}{2} \sum t_w \tag{3.7}$$

we obtain the following simplifications for the $\bar{\bar{\beta}}$-parameters

$$\bar{\bar{\beta}}_1 = \frac{b_t}{2d} , \quad \bar{\bar{\beta}}_2 = \frac{b_c}{2d} \tag{3.8}$$

This form is not yet quite satisfactory. To assess trends in structural reserves it seems to be more suggestive to express the degree of eccentricity of a monosymmetric section in one single parameter. This can be done by the trivial transformation,

$$\beta_1 = \frac{\bar{\bar{\beta}}_1 + \bar{\bar{\beta}}_2}{2} = \frac{b_t + b_c}{4d} , \quad \beta_2 = \frac{\bar{\bar{\beta}}_1 - \bar{\bar{\beta}}_2}{2} = \frac{b_t - b_c}{4d} \tag{3.9}$$

It is now seen that β_2 vanishes in the symmetric case and must therefore be a measure for the degree of eccentricity of the neutral axis. For $\beta_2 > 0$, initial yielding occurs at the compression flange, for $\beta_2 < 0$ at the tension flange. β_1 may be considered a parameter that represents the relative distribution of material between flanges and webs, the flange areas taken as an average. The degenerate case $\beta_1 = 0$ stands for the solid rectangular section, which has the highest shape factor of all symmetric sections. For large β_1, the web area will be small relative to the flange area. Hence, web plastification will produce smaller reserves of inelastic resistance.

So far, the failure condition has not yet been introduced in the moment-curvature relationship. It is expressed by the failure strain of the compression flange $\varepsilon_{c,u}$. First, the

following auxiliary equation relates the curvature to the maximum compressive strain $\varepsilon_{c,max}$,

$$\phi = \frac{\varepsilon_{c,max}}{y_c} \tag{3.10}$$

where y_c defines the distance between the compression flange and the neutral axis. In normalized terms, Eq. 3.10 takes the form

$$\frac{\kappa}{\varepsilon_y} = \frac{\varepsilon_{c,max}}{\varepsilon_y} \frac{d}{y_c} \tag{3.11}$$

y_c/d depends on β_1, β_2 and, possibly, in the inelastic range, on the curvature, as determined by the equilibrium condition of the section $\int_A \sigma dA = 0$. Hence, Eq. 3.11 simply represents a transformation from compression strain into curvature, i.e.,

$$\frac{\kappa}{\varepsilon_y} = f(\frac{\varepsilon_{c,max}}{\varepsilon_y}, \beta_1, \beta_2) \tag{3.12}$$

Substituting Eq. 3.12 into Eq. 3.5, and considering the transformation of the geometric parameters according to Eq. 3.9, we can write the moment-curvature relationship in terms of the following arguments,

$$m = f(\frac{\varepsilon_{c,max}}{\varepsilon_y}, \beta_1, \beta_2) \tag{3.13}$$

We may now introduce the failure condition $\varepsilon_{c,max} = \varepsilon_{c,u}$, and obtain

$$m_u = f(\frac{\varepsilon_{c,u}}{\varepsilon_y} , \beta_1, \beta_2) \qquad (3.14)$$

In the graphical representation of Eq. 3.14, any of the three arguments on the right-hand side can be chosen as the independent variable, with the two others being used as parameters, the choice of the variable depending on the object of interpretation. Each point of the curves will always represent a failure condition.

The detailed equations for the moment-curvature relationships in normalized terms are given in Appendix 3.1 for the elastic and inelastic range. This Appendix will be discussed within the next section.

Further Remarks

(1) Although the analysis has been limited to coldformed, monosymmetric sections, a generalization with respect to independent thicknesses of all flat elements is trivial and does not require additional geometric parameters. It only requires that the β-parameters be generalized as follows

$$\beta_1 = \frac{A_t + A_c}{2 \sum A_w} , \quad \beta_2 = \frac{A_t - A_c}{2 \sum A_w} \qquad (3.15)$$

It can be verified that this form reduces to the form of Eq. 3.9, if applied to coldformed sections. Therefore, whatever solutions will be derived for monosymmetric, coldformed sections can also be applied to hotrolled sections, if this should be desirable, or to coldformed sections of the channel

and Z-type, if for some reason they are considered restricted to the case of simple bending parallel to the plane of the web.

(2) The stress state in the flanges is idealized by considering only the average stress in the middle plane of the flanges. The resulting error will be negligible for the thin-walled coldformed sections this analysis is mainly concerned with, but would not always be negligible for thick hotrolled flanges. As an additional simplification, corner rounds are not considered in rigorous fashion.

(3) Stiffening lips of flanges are not included in the present analysis. Every additional geometric element, not included in the prototype considered above, like stiffening lips on flanges, with a dimension independent of the other geometric dimensions, will introduce an additional geometric parameter in the normalized moment-curvature relationship. Each additional parameter, however, would multiply the number of diagrams in a general graphical solution. But it seems, that practical needs are well served if only the following types of coldformed shapes are covered. (i) The hat section without stiffening lips, but possibly closed by a connected plate. The plate dimension can always be included into the flange dimension. This type of section may be used for individual floor and roof joists, but is usually obtained as the individual geometric unit of floor decks. This case would be covered by the parameters β_1 and β_2 as chosen above.

(ii) Symmetric floor joists of the I-type, with stiffening lips of equal depth on both top and bottom flanges. In this case the inelastic problem can again be solved with two geometric parameters. The eccentricity parameter will be eliminated, but one parameter for the lip depth will be introduced instead. This will, of course, be a set of parameters different from case (i), and therefore require a separate derivation of solutions. The following analysis will only apply to case (i), and to symmetric and eccentric I-shapes without stiffening lips.

3.2 Ultimate Resistance in Bending

Long-hand sample computations of the ultimate resistance of monosymmetric, coldformed sections without stiffening lips, with a compressive strain failure criterion $\varepsilon_{c,u} = 3\varepsilon_y$, are demonstrated in Appendix 3.2 for prescribed section geometry. The first sample computation is carried out for a section with initial yielding in tension. In this case, obviously, both flanges will have yielded at failure. In a second example, a section is chosen with initial yielding at the compression flange. In this case it is not certain at the outset whether the tension flange has yielded at failure. This requires an initial guess with respect to the elastic-plastic stress distribution across the section at failure, which must be checked as the first solution is obtained.

This approach to the individual problem, although straightforward, is not very efficient. It solves the problem

of determining the ultimate load carrying capacity of a beam with given section dimensions, but requires a trial and error procedure for the more usual problem of finding an adequate section for prescribed ultimate load.

The drawback of trial and error procedure and repeated analysis can be eliminated by the analysis with normalized arguments, as outlined in the preceding section. Furthermore, the examination of the normalized moment-curvature relationship shows the following. Since by definition

$m_u = \frac{M_u}{\sigma_y t d^2}$ and $m_y = \frac{M_y}{\sigma_y t d^2}$, we have $\frac{M_u}{M_y} = \frac{m_u}{m_y}$. With

$m = m(\frac{\varepsilon_{c,max}}{\varepsilon_y}, \beta_1, \beta_2)$, i.e., $m_u = m(\frac{\varepsilon_{c,u}}{\varepsilon_y}, \beta_1, \beta_2)$,

$m_y = m(1, \beta_1, \beta_2)$, it becomes obvious, that the ratio between the dimensional values of the ultimate moment and the yield moment, M_u/M_y, also, depends only on the three parameters $\frac{\varepsilon_{c,u}}{\varepsilon_y}, \beta_1, \beta_2$. With the number of parameters limited to three, it becomes possible and practical to present the ratios M_u/M_y graphically for all coldformed sections that can be described by β_1 and β_2. The ratio M_u/M_y is obviously of great practical interest, since it establishes the gains of ultimate strength design over the traditional design for initial yielding. The normalized approach does not only render a graphical presentation possible, but also allows determination of the ratios M_u/M_y without the need to specify the beam cross-

section in all its geometric dimensions. The parameters β_1 and β_2 will only require that the shape be determined within geometric similarity, not including the thickness t. The yield strength has, of course, no effect on the ratio, unless it changes the failure criterion $\varepsilon_{c,u}/\varepsilon_y$. Thus, we will now consider numerical solutions for M_u/M_y, and their graphical representation.

The normalized equations of the moment-curvature relationship are elementary and therefore transferred into Appendix 3.1. The three types of elastic and inelastic stress-distributions that must be considered are shown in Appendix 3.1, Fig. A3.1-1. The stress-distribution will be in state I if it is purely elastic, in state II if one flange is yielded whereas the other flange is still elastic, and in state III if both flanges are yielded. If there were lips, there would be additional types of stress distributions, as previously shown in Appendix 2.1. The transition from one state to the other will mark a discontinuity in the second derivative of the moment-curvature relationship. The moment-curvature relationship must therefore be derived separately for each state from the equilibrium and compatibility conditions of the section. Appendix 3.1 then gives the equations for the position of the neutral axis and the moment-curvature relationship in terms of normalized arguments, and defines the transition points on the moment-curvature relationship from one state to the other. The moment-curvature equations have simple algebraic forms in

state I and state III, due to the fact that in these states the position of the neutral axis is fixed. In state II however, where the position of the neutral axis is shifting, the moment-curvature equation is a much more complicated algebraic function. Appendix 3.1 finally introduces the compressive strain failure criterion, and the transformation from ultimate compressive strain into ultimate curvature.

The analysis in Appendix 3.1 was programmed and solved for the ultimate resistance of beam sections with a reasonable range of geometric parameters β_1 and β_2, and the failure criterions $\varepsilon_{c,u} = 3\varepsilon_y$ and $\varepsilon_{c,u} = \varepsilon_y$. The analysis has also been solved, for reasons of comparison, for $\varepsilon_{c,u} = \infty$, which represents $\phi,\kappa = \infty$ and full section plastification. The results can be presented in two ways.

1) $$m_u = f\left(\frac{\varepsilon_{c,u}}{\varepsilon_y}, \beta_1, \beta_2\right)$$

where $$m_u = \frac{M_u}{\sigma_y t d^2}$$

2) $$\frac{m_u}{m_y} = \frac{M_u}{M_y} = \bar{f}\left(\frac{\varepsilon_{c,u}}{\varepsilon_y}, \beta_1, \beta_2\right) \qquad (3.16)$$

The first alternative would be somewhat more convenient for design purposes, as will be seen. However, the second alternative is more meaningful with respect to evaluating inelastic reserve capacity.

Numerical results are presented in Figs. 3.2 to 3.5. In

Figs. 3.2 and 3.3, the results are plotted for the failure condition $\varepsilon_{c,u} = 3\varepsilon_y$. Both figures represent the same results, but in different representations. In Fig. 3.2, the eccentricity parameter β_2 is chosen as the variable along the horizontal axis. Values on the vertical axis represent symmetric sections. β_1 is used as a parameter for individual curves. Hence, this representation singles out the effect of eccentricity on the ratio M_u/M_y. As can be expected, the gains in economy as compared to the design for initial yielding become more pronounced with increasing eccentricity. It has been mentioned before that the design for initial yielding is the less economical, the larger the difference between the stress extremes of the elastic stress distribution. Hence, for the large differences in the extreme stresses produced by sections with significant eccentricity, the economic gains of plastic stress redistribution are most pronounced. These gains are, of course, relative to initial yielding and do not imply that eccentric sections are more economical than symmetric sections. The curves in Fig. 3.2 are somewhat unsymmetric with respect to the axis $\beta_2 = 0$, since for $\beta_2 < 0$ the section yields first in tension, for $\beta_2 > 0$ first in compression, whereas the failure criterion in both cases refers to the compression flange. For large positive values β_2, the failure condition can be reached before the tension flange reaches initial yielding. The points where this transition occurs are marked in Fig. 3.2. Eccentricities of this size

will, however, not often be found in the usual range of section geometries.

In Fig. 3.3, β_1 is used as the variable along the horizontal axis and β_2 is constant for individual curves. β_1 relates the average area of the flanges to the area of the webs. With decreasing values of β_1, the web areas become larger relative to the flange areas, and the gains due to web plastification become more pronounced. Thus, the curves are declining with increasing β_1. The rate of decline is particularly strong in the range $.2 < \beta_2 < .6$, but levels off beyond that range. The curves are cut off at $\beta_1 = .2$, since flanged sections with lower β_1-parameters are unusual.

The dashed lines in Figs. 3.2 and 3.3 give the results for $\varepsilon_c = \infty$, i.e., full section plastification. These results show by comparison that, with a failure criterion $\varepsilon_{c,u} = 3\varepsilon_y$, the ultimate moments are already very close to the full plastic moments. In Fig. 3.2, the dashed lines are, of course, symmetric to the vertical axis, since for $\varepsilon_c = \infty$ it does not matter any more which flange has yielded first.

Figs. 3.4 and 3.5 show the results for the failure condition $\varepsilon_{c,u} = \varepsilon_y$, in a representation corresponding to Figs. 3.2 and 3.3, respectively. Inelastic reserves of strength can only be obtained for eccentric sections with initial yielding in tension, i.e., $\beta_2 < 0$. For example, for $\beta_2 = -.10$, which can be considered a moderate eccentricity, strength reserves between 10% and 20% can usually be obtained. Hence, this case is worth while considering in practical applications.

Design Applications

Figs. 3.2 to 3.5 can directly be used in the design of coldformed, statically determinate beams for ultimate strength, governed by a compressive strain failure criterion. Similar diagrams can be established for intermediate strain values. They can be applied as discussed below.

Problem 1

Given: Span Length, Yield Strength σ_y and Section Geometry

Required: Ultimate Load Carrying Capacity

General Solution: With given section geometry, the parameters β_1 and β_2 (defined by Eq. 3.9 for the coldformed section with double webs, and by Eq. 3.15 for the general case) and the w/t-ratio can be computed. The w/t-ratio and yield strength will determine the compressive failure strain. In addition, the dimensional yield moment can be computed. The compressive failure strain will determine the diagram from which to select the ratio M_u/M_y according to parameters β_1 and β_2. For example, for $w/t \leq .92\ (w/t)_{lim}$ and $\sigma_y = 36$ ksi, we obtain from Eq. 2.7, $\varepsilon_{c,u}/\varepsilon_y = 3$, hence use Fig. 3.2. The ultimate load carrying capacity can now be determined as easily as the yield load. A numerical example is given in Appendix 3.3, Example 1.

Problem 2

Given: Span Length, Yield Strength σ_y and Ultimate Load w_u

Required: Adequate Section Dimensions

General Solution: Select a coldformed shape for the design

problem within general geometric proportions. No consideration has yet to be given to the thickness t. With this initial choice, the parameters β_1 and β_2 (Eqs. 3.9 or 3.15) are defined. An additional choice is required for the w/t-ratio, to define the compressive failure strain. E.g., we may select $w/t \leq .92\ (w/t)_{lim}$, i.e., from Eq. 2.7, $\varepsilon_{c,u}/\varepsilon_y = 3$, and use Fig. 3.2 to determine the ratio M_u/M_y. We will use the notation p_S for the ratio M_u/M_y. We can now compute the yield load w_y, since the inelastic load factor is

$$p_u = \frac{w_u}{w_y} = p_S = \frac{M_u}{M_y} = \frac{m_u}{m_y} \ . \tag{3.17}$$

I.e., $w_y = w_u/p_S$, and the design can be carried out for initial yielding.

However, the two parameters β_1 and β_2 are not sufficient to determine the dimensional yield moment M_y, but they will determine the normalized yield moment m_y. m_y can be computed from Eqs. A3.1-8, A3.1-4 and A3.1-1. The computation is no more involved than the computation of the dimensional M_y. It only requires that the equilibrium conditions of the section be arranged in dimensionless form, as done in Appendix 3.1. m_y can also be given in a simple graph as a function of β_1 and β_2, as done in Fig. 3.6. Then, by definition

$$m_y = \frac{M_y}{\sigma_y t d^2} \ , \quad \text{i.e.,} \quad td^2 = \frac{M_y}{\sigma_y m_y}$$

With $M_y = w_y L^2/8$,

$$td^2 = \frac{w_y L^2}{8\sigma_y m_y} \tag{3.18}$$

The right-hand side of the above equation is now a known numerical value. If values for t and d are chosen to satisfy Eq. 3.18, the beam will have an ultimate load carrying capacity equal to the required load carrying capacity.

The design procedure above requires a final check of the w/t-ratio to verify the initial failure strain criterion. The values of t and d can always be adjusted to obtain the initially selected w/t, but the resulting dimensions will not always be reasonable and might require a second computation with modified w/t.

A numerical example is given in Appendix 3.3, Example 2. If, after the first choice of dimensions t and d, Eq. 3.18 is not exactly satisfied, and if the resulting w/t-ratio does not exactly match the initially selected w/t-ratio, the chosen dimensions will be safe, if

1) the resulting w/t-ratio is smaller than the initially selected w/t-ratio

2) $td^2 > \frac{w_u L^2}{8\sigma_y m_u}$.

The choice of dimensions t and d will not affect the normalized ultimate moment m_u or the ratio M_u/M_y as long as the β-parameters are not changed.

Limitations to the Inelastic Reserve of Resistance from Structural Considerations

Fig. 3.2 indicates that inelastic reserves of resistance can reach more than 60% of the yield moment, in the case of eccentric sections. Structural design should however be guided by the principle that local yielding should not occur under service load conditions. This principle should be ensured with a certain reserve margin. Thus, it may be decided that initial yielding should not occur until a load of 1.20 × service load is reached. In this case we require $w_y \geq 1.20\, w_{S.L.}$, where $w_{S.L.}$ is the service load. With a safety factor of 1.66 we obtain the ultimate load as $w_u = 1.66\, w_{S.L.}$. I.e.,

$$\frac{w_u}{w_y} \leq \frac{1.66}{1.20} = 1.40 \tag{3.19}$$

Hence, if Condition 3.19 were accepted, the ratios $p_S = M_u/M_y$ $(= w_u/w_y)$ may not exceed the value 1.40, and the diagrams in Figs. 3.2 to 3.5 must be used accordingly.

CHAPTER 4

PLASTIC ROTATIONS OF PARTIALLY PLASTIC HINGES

The analysis of plastic rotations of partial hinges will serve two purposes which are, (i) deflection computations of coldformed beams at ultimate load, (ii) the analysis of the ultimate load carrying capacity of indeterminate coldformed beams, if plastic design, based on full moment redistribution, cannot be applied. Deflection computations for ultimate load are of minor importance in structural design, since deflection criteria are applied to service load conditions for which the structure should behave elastically. The following analysis will therefore mainly be carried out with respect to ultimate strength computations of indeterminate coldformed beams.

The rotation capacities of coldformed asymmetric shapes will in the following be strictly derived from the idealized mechanical principles of beam theory, in connection with the compressive strain failure criterion of Eq. 2.7 (which excludes the strainhardening range of the stress-strain curve). A knife-edge support will be assumed for partial hinges at interior supports.

4.1 Analysis of the Partial Hinge

In developing the analysis it is helpful to look at the case of unloading from the elastic-plastic state, i.e., from a load state $P = P^* > P_y$. Unloading will occur in a purely

elastic manner. After unloading bending moments will have disappeared, but a state of residual deflections will be left in the beam, originating from a residual hinge rotation θ_p, which is due to prior plastic deformations over the hinge length, and, therefore, will be called the plastic rotation component of the partial hinge.

If the beam is reloaded until the previous load value P* is obtained, its behavior will be completely elastic. Hence, the total rotation over the hinge length of the partial hinge is obtained as

$$\theta = \theta_{el} + \theta_p \tag{4.1}$$

where θ is the total rotation of the partial hinge, θ_{el} the linear and recoverable rotation component, corresponding to the load P*, and θ_p the non-linear, residual or plastic rotation component. A solution is desired for the plastic component which is responsible for moment redistribution, i.e.,

$$\theta_p = \theta - \theta_{el} \tag{4.2}$$

Rotation components are obtained by integration of corresponding curvature components over the length of the partial hinge. The curvature components are illustrated by a sketch in Fig. 4.1. ϕ_{el} is the curvature for an imagined elastic behavior of the section in the region of the partial hinge, i.e., $\phi_{el} = M/EI$, for $M > M_y$. With a total curvature ϕ at a point within the partial hinge, we define

$$\phi_p = \phi - \phi_{el} \tag{4.3}$$

The rotation θ_p then is the area defined by the ordinates ϕ_p, i.e., in general terms

$$\theta_p = \int_H (\phi(x) - \phi_{el}(x))dx \tag{4.4}$$

where H is the total hinge length.

To solve the integral, the moment-curvature relationships must be solved for ϕ. At a point x inside a partial hinge, the curvature $\phi(x)$ then will be a function of the corresponding moment ordinate M(x), the section geometry, the yield stress and the elastic modulus, i.e.,

$$\phi(x) = F(M(x), \text{Geometry}, \sigma_y, E) \tag{4.5}$$

Hence, the integral will depend on the moment distribution M(x) over the hinge length. The usual problems of structural design will involve only a very limited number of functions M(x). For single concentrated loads, M(x) will be linear. It can be expected that a linearized M(x) can be used over the short length of partial hinges at interior supports. For partial hinges in spans under uniform load, M(x) will be parabolic with the origin of the parabola in the center of the hinge. In view of the final results, the detailed analysis will be limited to linear moment distribution M(x).

As shown in Chapter 3, in a normalized analysis the number of section parameters can be reduced significantly. If the normalized moment-curvature relationships, given in

Appendix 3.1, are solved for the normalized curvature $\kappa = \phi d$, Eq. 4.5 takes the following form

$$\kappa(x) = \varepsilon_y F(m(x), \beta_1, \beta_2) \tag{4.6}$$

where $m(x) = M(x)/\sigma_y t d^2$, and the geometric parameters are defined by Eq. 3.9. This form is valid both for elastic behavior (state I) and for inelastic behavior (states II and III). Substituting $\phi(x) = \kappa(x)/d$ in Eq. 4.4 we obtain

$$\theta_p = \frac{\varepsilon_y}{d} \int_H \left(\frac{\kappa(x)}{\varepsilon_y} - \frac{\kappa_{el}(x)}{\varepsilon_y} \right) dx \tag{4.7}$$

With Eq. 4.6

$$\theta_p = \frac{\varepsilon_y}{d} \int_H (F - F_{el}) dx \tag{4.8}$$

Solution for Linear Moment Distribution

A typical partial hinge of an asymmetric coldformed section at an interior support is shown in Fig. 4.2, with the notations that will be used in the following analysis. With the discontinuities of the moment-curvature relationship at the transition from state II to state III, the integrals of Eqs. 4.7 or 4.8 become the sum of two integrals on each side of the support, i.e., an integral over state II and an integral over state III. For state III, the moment-curvature relationship, given by Eq. A3.1-12, can be solved for κ in closed form, and integration in closed form becomes possible. In state II, as indicated in Appendix 3.1, closed form

solution of the moment-curvature relationship for κ is not possible. Therefore, state II was solved by programmed computation, with a Newton iteration procedure to solve the moment-curvature relationship for κ and integration according to Simpson's rule. The closed form integration shall be outlined below. For symmetric sections state III will apply to the total partial hinge.

Closed Form Integration over State III

Without loss in generality, the demonstration can be restricted to the portion of the partial hinge on the left side of the support. The linear moment distribution M(x), with origin of x at the center of the partial hinge, is given by

$$M(x) = M_{max} - V_{\ell} x \tag{4.9}$$

With $V_{\ell} = \frac{1}{h_{\ell}} (M_{max} - M_{III,min})$, we obtain

$$M(x) = M_{max} - (M_{max} - M_{III,min}) \frac{x}{h_{\ell}} \tag{4.10}$$

This equation can directly be written in normalized form, i.e.

$$m(x) = m_{max} - (m_{max} - m_{III,min}) \frac{x}{h_{\ell}} \tag{4.11}$$

At failure $m_{max} = m_u$, and

$$m(x) = m_u - (m_u - m_{III,min}) \frac{x}{h_{\ell}} \tag{4.12}$$

Eq. A3.1-14 gives the moment-curvature relationship of state III. Solving this equation for κ/ε_y, and substituting Eq. 4.12, we obtain

$$\frac{\kappa(x)}{\varepsilon_y} = \frac{1}{\sqrt{3/2\ (m_p - m(x))}} = \frac{1}{\sqrt{3/2\ (m_p - m_u + (m_u - m_{III,min})\ x/h_\ell)}} \tag{4.13}$$

The elastic curvature component is obtained from Eq. A3.1-5 as

$$\frac{\kappa_{el}(x)}{\varepsilon_y} = \frac{m(x)}{i} = \frac{1}{i}\ (m_u - (m_u - m_{III,min})\ \frac{x}{h_\ell}) \tag{4.14}$$

Substituting the last two expressions in Eq. 4.7, and integrating, the following result is obtained.

$$(\theta_p)_{III,\ell} = \frac{\varepsilon_y}{d}\ h_\ell \left[2\ \frac{\sqrt{3/2(m_p - m_{III,min})} - \sqrt{3/2(m_p - m_u)}}{3/2(m_p - m_{III,min})} - \frac{1}{2i}\ (m_u + m_{III,min}) \right] \tag{4.15}$$

According to Eqs. A3.1-14 and A3.1-16

$$m_u = m_p - \frac{2}{3}\left(\frac{\varepsilon_y}{\kappa_u}\right)^2 , \quad m_{III,min} = m_p - \frac{2}{3}\left(\frac{1}{2} - |\beta_2|\right)^2$$

respectively, and according to Eq. A3.1-13

$$m_p = 2(\beta_1 - \beta_2{}^2 + \frac{1}{4})$$

i is a normalized moment of inertia (= I/td^3) which is given by Eqs. A3.1-4 and A3.1-1 in terms of β_1 and β_2. Obviously, the expression in brackets in Eq. 4.15 depends only on the two geometric section parameters β_1 and β_2 and on the failure value κ_u/ε_y. κ_u/ε_y can be obtained from the failure criterion in terms of $\varepsilon_{c,u}/\varepsilon_y$, given by Eq. 2.7, by transformation

according to Eq. A3.1-20.

If the notation ζ_{lin} is introduced for the expression in brackets, we obtain

$$(\theta_p)_{III,\ell} = \frac{\varepsilon_y}{d} h_\ell \zeta_{lin,III} \tag{4.16}$$

where

$$\zeta_{lin,III} = \bar{f}(\kappa_u/\varepsilon_y, \beta_1, \beta_2) = f(\varepsilon_{c,u}/\varepsilon_y, \beta_1, \beta_2)$$

The subscript of ζ refers to linear moment distribution.

The rotation θ_p in this case was shown to be linear in the hinge length h_ℓ. This result can be derived without solving the integration. It is observed that in Eq. 4.12 for $m(x)$ the variable of integration and the hinge length h_ℓ form a dimensionless ratio, and that h_ℓ occurs only in connection with this ratio. This means that x and h_ℓ occur only as a ratio in the integrand of Eq. 4.7. Thus, a substitution of the variable of integration can be carried out, with $\xi = \frac{x}{h_\ell}$, $dx = h_1 d\xi$. Eq. 4.7 can now be written in the form

$$(\theta_p)_{III,\ell} = \frac{\varepsilon_y}{d} h_\ell \underbrace{\int_{\xi=0}^{1} \left(\frac{\kappa(\xi)}{\varepsilon_y} - \frac{\kappa_u(\xi)}{\varepsilon_y}\right) d\xi}_{\zeta_{lin,III}} \tag{4.17}$$

The same equation is obtained over the length h_r on the right hand side of the support. The sum of the two integrals will be

$$(\theta_p)_{III} = \frac{\varepsilon_y}{d} h \zeta_{lin,III} \tag{4.18}$$

A similar procedure has been applied to the portions of the partial hinge in state II, with a total hinge length (H-h). Again the rotation is linear in the corresponding hinge length, since this characteristic depends only on the equation for the moment distribution m(x). In general form the rotation over state II is

$$(\theta_p)_{II} = \frac{\varepsilon_y}{d} (H-h)\zeta_{lin,II} \tag{4.19}$$

where $\zeta_{lin,II} = g(\varepsilon_{c,u}/\varepsilon_y, \beta_1, \beta_2)$ has been solved by numerical procedure.

With $\theta_p = (\theta_p)_{II} + (\theta_p)_{III}$

$$\theta_p = \frac{\varepsilon_y}{d} H\underbrace{[(1-\frac{h}{H})\zeta_{lin,II} + \frac{h}{H}\zeta_{lin,III}]}_{\zeta_{lin}} \tag{4.20}$$

Since

$$\frac{h}{H} = \frac{m_u - m_{III,min}}{m_u - m_y} = f(\varepsilon_{c,u}/\varepsilon_y, \beta_1, \beta_2)$$

the expression in brackets in Eq. 4.20 will still only be a function of $\varepsilon_{c,u}/\varepsilon_y$, β_1, β_2.

Thus, the general form of the plastic rotation over the total length of the partial hinge under linear moment distribution can be given as

$$\theta_p = \frac{\varepsilon_y}{d} H\, \zeta_{lin} \tag{4.21}$$

where $\zeta_{lin} = (1-\frac{h}{H})\zeta_{lin,II} + \frac{h}{H}\zeta_{lin,III} = f(\varepsilon_{c,u}/\varepsilon_y, \beta_1, \beta_2)$.

The function ζ_{lin} has been solved for a reasonable range of section parameters β_1 and β_2 and for the two failure conditions $\varepsilon_{c,u}/\varepsilon_y = 3$ ($w/t \leq .92(w/t)_{lim}$, from Eq. 2.7), and $\varepsilon_{c,u}/\varepsilon_y = 1$ ($w/t \geq 1.08(w/t)_{lim}$). The results are presented as two families of curves in Fig. 4.3. With these graphs the explicit integration of the plastic rotation components is eliminated for all symmetric and asymmetric sections of the corresponding range of parameters, and as long as the moment distribution over the hinge length is linear or can be linearized. An evaluation of the ζ-function with respect to symmetric cross-sections will be given next.

4.2 Discussion of ζ-Functions for Symmetric Sections

Curvature and compressive strain are related by the equation $\phi = \varepsilon_c/y_c$, where y_c is the distance between neutral axis and compression flange. For symmetric sections $y_c = d/2$, and therefore $\phi = 2\varepsilon_c/d$.

At incipient yielding of the symmetric section $\phi_y = 2\varepsilon_y/d$, at failure $\phi_u = 2\varepsilon_{c,u}/d$. Also, $\phi_u/\phi_y = \varepsilon_{c,u}/\varepsilon_y$ (therefore, for symmetric sections, the failure criterion of Eq. 2.7 can be given in terms of curvature).

In connection with symmetric sections, the ζ-functions find a simple physical interpretation. From Eq. 4.21 (but dropping the subscript)

$$\zeta = \frac{\theta_p d}{H\varepsilon_y} \tag{4.22}$$

With an average plastic curvature component, defined by $\phi_{p,av} = \theta_p/H$, and with $\phi_y = 2\varepsilon_y/d$, we obtain

$$\zeta = 2 \frac{\phi_{p,av}}{\phi_y} \tag{4.23}$$

We can define a reference rotation $\theta_y = \phi_y H$ $(= M_y H/EI)$ and obtain

$$\frac{\theta_p}{\theta_y} = \frac{1}{2} \zeta \tag{4.24}$$

According to Fig. 4.3, for $\varepsilon_{c,u}/\varepsilon_y = 3$, and for symmetric sections ($\beta_2 = 0$), $.4 < \theta_p/\theta_y < .5$. Since θ_p is the plastic rotation component of a partial hinge at failure, Eq. 4.24 expresses the rotation capacity of the partial hinge.

4.3 Comparison of Rotation Capacity with Rotation Requirements of Plastic Design

The ultimate load carrying capacity of a structure reaches an upper limit with the attainment of a collapse mechanism, created by a sufficient number of plastic hinges. This upper limit can be established by the analytical principles of the plastic design method, which is especially simple in its application to redundant beams.

Research with respect to the ultimate strength of redundant steel beams and frames was therefore mainly directed at defining compression flange w/t-ratios that allow enough hinge rotation to qualify a steel section for plastic design. One approach to establish a criterion for sections for plastic

design is to compare experimentally obtained rotation capacities against computed rotation requirements. The computation of rotation requirements shall therefore be outlined.

A convenient analytical approach to follow the load-deflection (or load-hinge rotation) behavior of a structure until the collapse mechanism is reached, is derived from an idealized elastic-perfectly plastic moment-curvature relationship. Accordingly, a section is assumed to behave elastic until the plastic moment M_p is reached. Under further loading the point where M_p has been reached will act as a hinge, where rotations can take place under the constant resistance M_p. This idealization eliminates the partially plastic hinge and does not take into account the actual finite hinge length. Load-deflection curves based on this method are straight line approximations that form an upper bound to the experimental smooth load deflection curves. In particular, this method assigns to each plastic hinge a distinct hinge rotation value at the attainment of the collapse mechanism, which, for beams, can be computed quite easily. The maximum hinge angle in the structure, thus computed, can be used as a rotation requirement for plastic design (θ_c).

Maximum hinge angles have been computed on this basis for different types of structures.[13] They are usually normalized with respect to a rotation θ_{rL}, defined as $\theta_{rL} = \phi_r L$, where $\phi_r = M_p/EI$ and L is a reference span length. With these definitions a rotation requirement for plastic design can be

expressed in the general form (the notation for rotation requirement shall be RR, for rotation capacity RC)

$$RR = \frac{\theta_c}{\theta_{rL}} = \frac{\theta_c}{\phi_r L} = \frac{\theta_c EI}{M_p L} \tag{4.25}$$

In the actual smooth load deflection curve the attainment of a collapse mechanism cannot be associated with a distinct point in the load-deflection curve. Rather, this curve will approach the limiting load carrying capacity of the mechanism asymptotically as long as local failure does not occur. A rotation requirement should principally only guarantee that the actual load carrying capacity comes sufficiently close to the limiting load carrying capacity of the mechanism. With respect to this principle, the computed values $\theta_c/\phi_r L$ seem to be artificial in certain cases. E.g., for highly indeterminate structures, where a mechanism requires a large number of hinges, the load carrying capacity of the mechanism can practically be reached before the last hinge forms. Examples have been presented for gable frames, where 98% of the load carrying capacity of the mechanism is already reached at maximum hinge rotations of 1/3 or 1/2 the computed value $\theta_c/\phi_r L$.[13] However, for beams, which require at most three hinges for a mechanism, $\theta_c/\phi_r L$ may be considered a valid rotation requirement.

On this background, the plastic rotation capacity derived from the failure criterion of Eq. 2.7 shall be evaluated for the example of a beam over two equal spans with uniformly

distributed load over both spans, with a cross-section as defined by the parameters $\beta_1 = .6$, $\beta_2 = -.2$, $w/t \leq .92(w/t)_{lim}$ (i.e., from Eq. 2.7, $\varepsilon_{c,u}/\varepsilon_y = 3$). More information for the example is not needed to compare rotation capacity with rotation requirement. The beam system represents a regular design problem, and the section parameters are well within the practical range. The result will therefore serve for a good assessment of the moment redistribution capacity, to be expected within the present approach, as compared to full moment redistribution defined by the collapse mechanism.

Rotation Requirement

For this particular example, the computed hinge rotation at the interior support, as the mechanism is obtained, is

$$\frac{\theta_c}{\theta_{rL}} = \frac{\theta_c}{\phi_r L} = .308 \tag{4.26}$$

This value is obtained from the analysis of a collapse mechanism in the endspan. For comparison with the rotation capacity it shall be modified as follows (introducing $\theta_{rH} = \phi_r H = M_p H/EI$).

$$RR = \frac{\theta_c}{\theta_y} = \frac{\theta_c}{\theta_{rL}} \left(\frac{\theta_{rL}}{\theta_{rH}}\right) \left(\frac{\theta_{rH}}{\theta_y}\right) \tag{4.27}$$

With $\theta_{rL} = \phi_r L = M_p L/EI$ and $\theta_{rH} = \phi_r H \rightarrow \theta_{rL}/\theta_{rH} = L/H$. With $\theta_y = \phi_y H = M_y H/EI$ and $M_p \simeq M_u \rightarrow \theta_{rH}/\theta_y \simeq M_u/M_y$. Therefore, Eq. 4.27 can be written as

$$RR = \frac{\theta_c}{\theta_y} = .308 \frac{L}{H} \frac{M_u}{M_y} \tag{4.28}$$

The hinge length in the case of a statically determinate beam with concentrated load at midspan is given, as can easily be verified, by

$$\frac{H}{L} = 1 - \frac{M_y}{M_u} \tag{4.29}$$

A rough approximation for the hinge length at the interior support can be obtained by linearizing the moment distribution between the inflection points ($x \simeq .25L$ on each side of the support), and by applying Eq. 4.29 to the beam portion between the inflection points, i.e., to the length $L' \simeq .5L$. Hence, $H/L \simeq .5\ H/L'$. Fig. 3.2, with $\beta_1 = .6$, $\beta_2 = -.2$, gives $M_u/M_y = 1.30$. I.e., we obtain from Eq. 4.29 $H/L' = 1 - 1/1.30 = .23$, and $H/L = .5 \times .23 = .115$. Hence, from Eq. 4.28

$$RR = \frac{\theta_c}{\theta_y} = .308 \times \frac{1}{.115} \times 1.30 = 3.5$$

Rotation Capacity

According to Eq. 4.21, $\theta_p = \frac{H}{d} \varepsilon_y \zeta_{lin}$. With $\theta_y = \phi_y H = M_y H/EI$, we obtain

$$RC = \frac{\theta_p}{\theta_y} = \frac{\varepsilon_y \zeta}{\phi_y d} = \frac{\varepsilon_y \zeta}{\kappa_y}$$

From Fig. 4.3 with $\beta_1 = .6$, $\beta_2 = -.2 \rightarrow \zeta_{lin} = .78$. From Eq. A3.1-7

$$\frac{\kappa_y}{\varepsilon_y} = \frac{2\beta_1 + 1}{\beta_1 + |\beta_2| + \frac{1}{2}} = 1.7$$

I.e.,

$$RC = \frac{\theta_p}{\theta_y} = \frac{.78}{1.7} = .46$$

Comparison

Rotation requirement and rotation capacity now are in comparable form, i.e.,

$$RR = \frac{\theta_c}{\theta_y} = 3.5 \qquad RC = \frac{\theta_p}{\theta_y} = .46$$

and

$$\frac{RC}{RR} = \frac{.46}{3.5} = \frac{1}{7.8}$$

Conclusion

The plastic rotations allowed by the failure criterion of Eq. 2.7 are relatively small fractions of the required hinge rotation for full moment redistribution. For the above example, the inelastic load factor for full moment redistribution is

$$\frac{w_u}{w_y} = \frac{M_p}{M_y} + .46\,\frac{M_p}{M_y} = 1.30 + .60 = 1.90$$

where the second component is due to full moment redistribution. With the given rotation capacity we can expect roughly ($M_u \simeq M_p$),

$$\frac{w_u}{w_y} = 1.30 + .065 = 1.365$$

I.e., partial moment redistribution in this case increases the load carrying capacity by approximately 6%, which is a relatively small increase as compared to full moment redistribution, but may be worthwhile considering.

However, the following qualifying aspects with respect to the present approach to plastic rotations of partial hinges should be considered. The failure criterion of ultimate compressive strain was derived from experimental measurements in a constant moment region. The results may be conservative in the case of steep moment gradients at interior supports. More importantly, the previous analysis for plastic rotations of partial hinges may be unrealistic, though conservative, with respect to the mathematical assumption of a knife edge support. In the actual case the peak curvature may be spread over a finite length by the width of a bearing plate. This could conceivably have a drastic effect on the plastic rotations that can be obtained from a partial hinge. A similar effect is obtained, e.g., if compressive strains can be sustained beyond the yield plateau into the strainhardening range, or if a material is gradually strainhardening. However, the present analysis suggests that, on the other hand, the assumption of constant distribution of maximum curvature over the total hinge length would produce distorted, and highly unconservative results for the hinge rotation capacity under moment gradient.

Therefore, definite conclusions on plastic rotation of partial hinges and partial moment redistribution will need additional research on continuous beams. The present investigation will give conservative applicable results, but is also intended as a framework for further investigation.

When plastic design, i.e., full moment redistribution cannot be applied, the ultimate load carrying capacity must be determined by inelastic analysis for partial moment redistribution with a compressive strain failure criterion. This problem was investigated with regard to a practical design approach. The result will be presented in the following chapter.

It was mentioned above that in plastic design for full moment redistribution plastic zones over a finite hinge length and partial hinges are eliminated from the analysis by the simplifying assumptions of bilinear moment curvature relationship and point hinge. These simplifications will obviously not be applicable with a failure criterion that applies to the maximum compressive strain at the center of a partial hinge. In this case, the partial hinge must be represented correctly in the analysis to establish the relationship between failure criterion and hinge rotation. The ζ-functions will be an important part of such an analysis for partial moment redistribution.

CHAPTER 5

INELASTIC ANALYSIS OF REDUNDANT BEAMS

5.1 General Approach to Partial Moment Redistribution Analysis

The point of the redundant system, where the yield moment M_y will be reached first, can be determined by elastic analysis. Incipient yielding at this point will establish the yield load P_y. Under continued loading, the first partial hinge will form, followed at a higher load level by a second partial hinge, etc. Depending on the design parameters and the failure criterion in terms of ultimate compressive strain, failure may occur anywhere in the range between incipient yielding of the system and final unrestraint plastic flow as the collapse mechanism is approached. In between these two bounds, a unique solution of elastic-plastic analysis can only be obtained by following the load history.

In a genuine computer design method, e.g., the finite element method, this would be reflected by an incremental procedure, where the response of the system would be computed for a sequence of small load or deformation increments, followed at each step by a modification of the stiffness properties according to the progression of plasticity, and by a check with respect to the failure condition.

The present investigation does not aim at a computer application of this type. It seemed to be more useful as an

introductory contribution, to use a conventional analytical approach to partial moment redistribution, but with special consideration of practical applications. The computer will only be used in an auxiliary function. Within this approach, the load history must be followed in steps from initial yielding at one point of the system to initial yielding at the next point. Whenever initial yielding occurs at a new point of the system, it will mark a discontinuity in behavior. It will therefore be necessary to distinguish between load intervals according to the number of existing partial hinges, and to define the inelastic behavior in each load interval by a different set of equations. The load interval where only one partial hinge exists will be called the one-hinge load interval. If failure occurs in this load range, it will be a one-hinge failure mode, etc. The equations in each load interval from which the ultimate load carrying capacity can be computed in connection with the failure criterion will be called design equations.

In a rigorous long-hand analysis of an individual system we must start by establishing and solving the design equations for the one-hinge failure mode. The solution will give the true ultimate load carrying capacity only, if the yield moment has not been exceeded at any other point of the system. Otherwise, the analysis must be continued by solving the one-hinge load interval for its limiting condition, incipient yielding at the location of the second partial hinge. This

limiting state will be the initial condition for the two-hinge load interval. The equations for the two-hinge interval must now be established and solved, etc. It can be anticipated that the solution of a particular design problem by long-hand analysis can become very involved. In addition, although the mechanical principles and the analytical procedure can be formulated in general terms, explicit equations can only be established for the particular case. The mathematical development of partial moment redistribution in the present chapter will therefore only be presented to the extent justified by the final outcome.

It will be shown that, for the compressive strain failure criterion given by Eq. 2.7, the plastic rotation of a partial hinge is relatively small. Moment redistribution will therefore be so limited that the one-hinge failure mode is obtained for most practical design problems. Thus, the mathematical development will only be given in detail for the one-hinge failure mode, where the design equations can still be formulated in fairly general terms. A safe approximation for failure outside the one-hinge failure mode will however be possible.

Even the one-hinge failure failure mode can be solved in a practical way only due to a significant simplification in the treatment of the rotation integrals, introduced in Chapter 4, Sec. 4.1. The integration of the plastic rotation of a partial hinge is the numerically most involved and error-prone

part of the design equations. However, as shown in Chapter 4, Sec. 4.1, a graphical representation of the rotation integrals becomes possible for the two important cases of linear and parabolic moment distribution, since in these cases the integrals depend only on the ratio between ultimate compressive strain and yield strain, and on a small number of geometric section parameters. Hence, it will be possible to remove the integration from the solution of the design equations for the one-hinge failure mode.

But, even if the mathematical problem is reduced to the one-hinge failure mode, and with the auxiliary graphs for the rotation integrals, the longhand analysis cannot yet be considered simple enough for frequent applications in structural design. A complete design solution for frequently occurring types of systems is therefore envisioned on the basis of design diagrams along the following lines.

There are essentially two groups of parameters, (1) the parameters of the section in which we will include the geometric parameters, the materials properties (E, σ_y) and the ultimate compressive strain, (2) the parameters of the beam system, in which we will include the ratios between the span lengths, the load case and the boundary conditions. The section geometry shall be constant throughout the beam. As mentioned before, the total inelastic reserve of resistance is made up (1) by the inelastic strength reserves of the section, and (2) by the reserves due to partial moment redistribution.

The first component, which depends only on the section parameters, was the subject of Chapter 3, Sec. 3.1 and 3.2, in connection with the statically determinate beam. Design diagrams were presented in Figs. 3.2 to 3.5 for the ratio between ultimate moment and yield moment, M_u/M_y, in terms of only three parameters, i.e., two geometric parameters β_1 and β_2 (Eqs. 3.9) and the ratio between ultimate compressive strain and yield strain $\varepsilon_{c,u}/\varepsilon_y$. These parameters suffice to determine M_u/M_y correctly for the coldformed monosymmetric sections defined in Chapter 3. The present chapter will deal exclusively with the second component, i.e., the inelastic reserves of the redundant beam due to moment redistribution. This component will not only depend on the section parameters (in the form of β_1, β_2 and $\varepsilon_{c,u}/\varepsilon_y$), but also on the system parameters. System parameters, however, can only be dealt with efficiently in design diagrams, if systems that are comparable with respect to load case and span length ratios are represented by a common bound to their inelastic reserves from moment redistribution.

With this solution for the redistribution component, both components of the total inelastic reserve of resistance will be given by graphs in terms of section parameters β_1, β_2, $\varepsilon_{c,u}/\varepsilon_y$, but with the understanding that the moment redistribution component is a safe and good approximation only for a certain domain of system parameters. Thus, a small number of

design graphs will apply to the whole practical range of section parameters and to the most frequently used systems.

Formulation of Design Problem

The derivation of partial moment redistribution analysis is straightforward in principle if a solution for the ultimate load carrying capacity is desired. In this case, the ultimate load carrying capacity is treated as the unknown of the problem, whereas the parameters of the section and structural system are considered as the independent variables to be specified. In the usual design problem, however, the inverse problem has to be solved. The ultimate load will be specified, whereas adequate section dimensions are looked for. The design approach on the basis of design diagrams, as outlined above, in connection with non-dimensional analysis, will allow a simple direct solution to the inverted problem, which will be given later in this chapter. In the following analytical derivations, however, the ultimate load carrying capacity will, for simplicity, be treated as the unknown.

Basic Analytical Principles

We assume that the system is initially stress-free and consider a one-parameter load case, with a load value exceeding the yield load, i.e., $P = P^* > P_y$. Plastic deformations will have occurred around at least one critical section. Unloading will take place in a purely elastic manner, and will leave the beam with a residual moment distribution. Renewed

loading up to P* would therefore also be purely elastic. Hence, the moment distribution can be split into the following components.

$$M(x) = M_{el}(x) + M_{res}(x) \tag{5.1}$$

$M_{el}(x)$ represents the elastic moment distribution corresponding to the actual inelastic load value P*. It is therefore obtained by elastic analysis for the load value P* and does not require further elaboration. The residual moment distribution $M_{res}(x)$ is due to the plastic deformations that are taking place as $P > P_y$. This component will be treated in detail in Sec. 5.2.

The components of Eq. 5.1 are shown graphically in Fig. 5.3, for a beam with two equal spans under uniform load, as shown in Fig. 5.1. The first partial hinge, which will always be identified by subscript 1, will form in the example at the interior support. It can be visualized that plastic rotations at the interior support will produce a residual moment component at the interior support, opposite to the elastic moment. Therefore, if Eq. 5.1 is applied to the interior support, we can write more explicitly

$$|M_1| = |M_{1,el}| - |M_{1,res}| \tag{5.2}$$

The second partial hinge, whose location will be identified by the subscript 2, will form in the spans, as indicated in Fig. 5.3. The total moment at point 2, according to Fig. 5.3,

will be

$$|M_2| = |M_{2,el}| + |M_{2,res}| \tag{5.3}$$

If failure occurs at the first partial hinge, M_1 will have reached the magnitude of the ultimate resistance of the section at point 1, $M_{u,1}$. $M_{u,1}$ shall always be taken as an absolute value. Hence, with Eq. 5.2, failure of the system is expressed by the equation

$$M_{u,1} = |M^f_{1,el}| - |M^f_{1,res}| \tag{5.4}$$

Superscript f identifies the moment components as failure values.

Failure will not always occur at the first partial hinge. In all cases, however, we must make an initial assumption on the "critical" section where failure will occur, before we can solve the analysis for the ultimate load carrying capacity. This assumption can be verified once a solution is obtained, and will possibly have to be corrected, which would require a new analysis.

5.2 The Residual Moment Component

5.2.1 Residual Moment Distribution and Plastic Rotation of the Partial Hinge

In the preceding chapter, the hinge angle has been split into an elastic and a plastic component. The plastic component θ_p has been identified with the residual rotation, producing a state of residual displacements in the statically

determinate system after unloading. In the redundant system, these residual displacements are restrained by the support conditions, and will produce a state of residual moments.

The residual moment distribution, thus produced, must be in equilibrium with the support reactions alone, since no external load is present after unloading. Hence, this moment distribution is that of a statically determinate system on which the support reactions act like external loads. Therefore, the residual moment distribution must be linear, and will represent a state of self-equilibrium of the system. For the example in Fig. 5.1, the residual moment distribution can easily be visualized according to these rules. It is given by the linear equation,

$$M_{res}(x) = M_{1,res} \frac{L-|x|}{L} , \quad x \gtrless 0 \qquad (5.5)$$

if the origin of x is taken at the interior support. The relationship between the plastic hinge angles and the parameter $M_{1,res}$ of the residual moment distribution for the example in Fig. 5.1 can be computed as follows.

The first partial hinge will form at the interior support. After a certain plastic rotation at point 1, additional partial hinges will form in the spans at points 2 and 2'. We consider the statically determinate case after unloading from this state. Fig. 5.2 shows the residual deformational pattern. The residual deflection of the statically determinate case at point 1, $\delta_{p,1}$, can be computed from the plastic hinge

rotation components by elementary computation. With a sign convention as shown in Fig. 5.2 we obtain

$$\delta_{p,1} = -\frac{1}{2} L(\theta_{p,1} - 2\frac{L-a_2}{L}\theta_{p,2}) \tag{5.6}$$

The computation of $\delta_{p,1}$ according to Eq. 5.6 implies a slight idealization, since the plastic rotations of the partial hinges have been lumped into a point at each hinge.

$\delta_{p,1}$ is now treated like an initial deflection and compatibility with the support restraint at point 1 is imposed. The result of this analysis will be,

$$M_{1,res} = \frac{3}{2}\frac{EI}{L}(\theta_{p,1} - 2\theta_{p,2}\frac{L-a_2}{L}) \tag{5.7}$$

Within the one-hinge load interval we can set $\theta_{p,2} = 0$. In this case Eq. 5.7 reduces to

$$M_{1,res} = \frac{3}{2}\frac{EI}{L}\theta_{p,1} \tag{5.8}$$

Eq. 5.7 can be expressed in general form for the two-hinge load interval and the general system as follows,

$$M_{1,res} = \frac{EI}{L_{max}}(C_1\theta_{p,1} - C_2\theta_{p,2}) \tag{5.9}$$

The coefficients C_1 and C_2 are derived from elastic analysis, as demonstrated above, and L_{max} will be the reference span length. The rotation components enter the equation successively with increasing load.

5.2.2 Analysis of the Residual Moment at Failure

The analysis of the residual moment component at failure will lead to the solution of the design problem of ultimate load carrying capacity of the redundant beam. As mentioned in Sec. 5.1, the mathematical derivations for this analysis will be given in the following only for the one-hinge failure mode. This limitation is justified by the results obtained for the more regular types of systems, which constitute a large majority of all design problems. The design equations for the one-hinge failure mode can be formulated in a general way, valid for all systems, with one exception: Systems under uniform load, with initial yielding in the span require certain modifications. If failure occurs within the one-hinge failure mode, local failure will occur at the first partial hinge. The critical section for which the design equations must be solved, is therefore the section where initial yielding of the system occurs, which is determined by elastic analysis. The validity of the one-hinge failure mode must, of course, be checked, once the solution is obtained. The latter problem will be treated in Sec. 5.4.

One-hinge Failure Mode with Hinge at Interior Support

In Chapter 4, the plastic rotation of a partial hinge has been connected to the maximum compressive strain at hinge center by means of the ζ-functions, in the form (compare Eq. 4.21)

$$\theta_p = \varepsilon_y \frac{H}{d} \zeta$$

H is the length of the partial hinge and ζ depends only on the parameters (β_1, β_2, $\varepsilon_{c,u}/\varepsilon_y$) and on the moment distribution function M(x). Numerical results have been derived for linear moment distribution and are given in Fig. 4.3, for ζ_{lin}, for the two compressive strain failure conditions $\varepsilon_{c,u}/\varepsilon_y = 3$ and $\varepsilon_{c,u}/\varepsilon_y = 1$. Plastic rotations obtained from the latter critical compressive strain, however, are too small to be worth while considering. Only the failure criterion $\varepsilon_{c/u}/\varepsilon_y = 3$ will be considered in the remainder of this chapter. The functions ζ_{lin} will be correct only for systems under single loads, but they can also be used with very good accuracy for partial hinges at interior supports, if the system is under uniform load. This amounts to a linearization of the moment distribution at the interior support over the hinge length, which can be justified as follows.

The moment distribution, as derived from the free-body-diagram with the origin of x at the interior support, is given by the equation

$$M(x) = M_1 + x(V_{1,\ell} - \frac{wx}{2}) \tag{5.10}$$

Linearization implies that the term $\frac{wx}{2}$ is neglected in the above equation over the hinge length, i.e., within the range $x \leq H_{1,\ell}$. Hence, for $x \leq H_{1,\ell}$, we require that $\frac{wx}{2} << V_{1,\ell}$. But $V_{1,\ell}$ is of the order of magnitude $\frac{wL}{2}$. The above inequality is therefore satisfied, if $\frac{wH_{1,\ell}}{2} << \frac{wL}{2}$, i.e., if $H_{1,\ell} << L$. It has been shown that the hinge length is usually a very

small portion of the span length, and thus the error introduced by neglecting the term $\frac{wx}{2}$ over the hinge length is, in fact, negligible.

The plastic rotation of the partial hinge at an interior support can now be written in general as

$$\theta_{p,1} = \varepsilon_y \frac{H_1}{d} \zeta_{1in} \tag{5.11}$$

If Eq. 5.9 is adapted to the one-hinge failure mode (i.e., $C_2 = 0$), and Eq. 5.11 is substituted for $\theta_{p,1}$, we obtain

$$M_{1,res} = C_1 \frac{\sigma_y I}{L} \frac{H_1}{d} \zeta_{1in} \tag{5.12}$$

We can now choose the rotation integrals ζ_{1in} for the ultimate compressive strain, and will obtain, with Eq. 5.12, the residual moment at failure,

$$M^f_{1,res} = C_1 \frac{\sigma_y I}{L} \frac{H^f_1}{d} \zeta_{1in} \tag{5.13}$$

The superscript f denotes that the variables in the equation refer to the state of failure of the system.

The hinge length H^f_1 depends on the actual moment distribution at failure. For linear or linearized moment distribution over the hinge length, the hinge length on either side of the interior support is expressed by the equations

$$H^f_{1,\ell} = \frac{M_{u,1} - M_y}{|V^f_{1,\ell}|}, \quad H^f_{1,r} = \frac{M_{u,1} - M_y}{|V^f_{1,r}|} \tag{5.14}$$

where $V^f_{1,\ell}$ and $V^f_{1,r}$ are the shear forces on either side of the interior support (at the state of failure). The total hinge length is given by

$$H^f_1 = H^f_{1,\ell} + H^f_{1,r} = (M_{u,1} - M_y)\left(\frac{1}{|V^f_{1,\ell}|} + \frac{1}{|V^f_{1,r}|}\right) \qquad (5.15)$$

Summarizing the preceding analysis, the design equations for the one-hinge failure mode with partial hinge at an interior support, have the following general form.

$$M_{u,1} = |M^f_{1,el}| - |M^f_{1,res}| \qquad (5.16a)$$

$$|M^f_{1,res}| = C_1 \frac{\sigma_y I}{L} \frac{H^f_1}{d} \zeta_{lin} \qquad (5.16b)$$

$$H^f_1 = (M_{u,1} - M_y)\left(\frac{1}{|V^f_{1,\ell}|} + \frac{1}{|V^f_{1,r}|}\right) \qquad (5.16c)$$

If this set of equations is solved for $M^f_{1,el}$, the ultimate load carrying capacity is simply obtained from the elastic relationship between ultimate load and $M^f_{1,el}$, i.e., from

$$|M^f_{1,el}| = \alpha_1 P_u L \ , \quad \text{or} \quad |M^f_{1,el}| = \alpha^*_1 w_u L^2 \qquad (5.16d)$$

in the case of single loads or uniformly distributed loads, respectively. α and α^* are the coefficients of elastic analysis.

The solution in closed form of this set of equations shall now be demonstrated for the sample system of Fig. 5.1, where the first partial hinge will be located at the interior

support, and therefore, within the one-hinge failure mode, local failure will occur at the interior support.

For this system, the shear force $V^f_{1,\ell}$ can be expressed by the components of the actual moment distribution as follows.

With $|V^f_{1,\ell}| = \frac{w_u L}{2} + \frac{M_{u,1}}{L}$, and $w_u = \frac{8|M^f_{1,el}|}{L^2}$, we obtain

$$|V^f_{1,\ell}| = \frac{1}{L}\,(4|M^f_{1,el}| + M_{u,1}) \tag{5.17}$$

With symmetry of the system, $V^f_{1,\ell} = V^f_{1,r}$. Eq. 5.16c can now be written in the form

$$H^f_1 = 2L\,\frac{(M_{u,1} - M_y)}{4|M^f_{1,el}| + M_{u,1}} \tag{5.18}$$

If the last expression is substituted for H^f_1 in Eq. 5.16b, and Eq. 5.16b is substituted for $M^f_{1,res}$ into Eq. 5.16a, we obtain, with $C_1 = 3/2$

$$M_{u,1} = |M^f_{el,1}| - 3\,\frac{\sigma_y I}{d}\,\frac{M_{u,1} - M_y}{4|M^f_{1,el}| + M_{u,1}}\,\zeta_{lin} \tag{5.19}$$

where the only unknown is $M^f_{1,el}$. Some rearrangement of this equation finally leads to the quadratic in $M^f_{1,el}$

$$|M^f_{1,el}|^2 - \frac{3}{4}\,M_{u,1}|M^f_{1,el}| - \frac{1}{4}(M^2_{u,1} + (M_{u,1} - M_y)\,3\,\frac{\sigma_y I}{d}\,\zeta_{lin}) = 0 \tag{5.20}$$

With the solution for $M^f_{1,el}$, the load carrying capacity can be determined from the elastic relationship

$$w_u = \frac{8|M^f_{1,el}|}{L^2} \tag{5.21}$$

For less regular systems, the closed form solution can become considerably more involved. In this case, an iterative solution will be more convenient, where the shear forces $V^f_{1,\ell}$ and $V^f_{1,r}$ are initially determined from the elastic moment distribution for limiting moment $M_{u,1}$. Eqs. 5.16 can now be solved approximately. In a second iterative cycle, the shear forces will be determined for the improved moment distribution, etc. Particularly if the residual moment component is small, the first solution in the iterative analysis will be very close to the exact solution.

The solution of the inelastic design problem for partial moment redistribution requires the elastic analysis of the system with respect to, (1) the actual load case and system, (2) the relationship between the residual moment at the critical section and the plastic rotation of the partial hinge. The elastic computations have to be carried out in terms of parameters not yet numerically known, and will produce the elastic coefficients required in the design equations (Eqs. 5.16). Both the elastic moment distribution for the given load case, and the residual moment distribution, and therefore any combination of the two components will satisfy the equilibrium conditions. The compatibility conditions are satisfied everywhere as soon as a partial hinge with plastic rotation θ_p is fit into the system at the critical section. For

this purpose there is one free variable left, the hinge length H. The design equations can now be interpreted as the condition under which the boundary conditions at the end points of the hinge are satisfied, i.e., continuity of slope and moment, where the moment at the end points on both sides must be equal to the yield moment. These conditions have been implicitly satisfied in the derivation of the design equations.

5.3 The Process of Inelastic Moment Redistribution Through Inelastic Load History

The process of inelastic moment redistribution, from initial yielding at load P_y to the final failure mechanism at load P_p (P is here considered a load parameter which can represent any type of load), is illustrated for an example in the diagram of Fig. 5.4. In this diagram, the absolute values of the two peak moments in the endspan of the shown beam are plotted vs. the load, for a load range $0 < P < P_p$. All variables are normalized with respect to initial yielding of the structure. The left endspan will be the critical span in the given case, developing the first failure mechanism of the structure, if no other restrictions are imposed. The first partial hinge will develop at the interior support ("1"), which has the maximum absolute moment of the elastic moment distribution. The second partial hinge will develop in the endspan at point "2." No other partial hinge will form in the structure before the failure mechanism is obtained. The smooth curves in the inelastic range represent the actual

behavior for gradual plastification of the section and gradual hinge development, on which the preceding analysis is based. These curves are only drawn schematically. But, it may be assumed that the actual, smooth behavior is well represented, since the curves are drawn to fit an envelope, provided by a stepwise analysis according to the plastic hinge method (discussed in Chapter 4, Sec. 4.3). In particular, the plastic hinge method will establish tangents at initial yielding of the beam, and as the failure mechanism is obtained. As the failure mechanism is obtained under load P_p, the two peak moments in the endspan will be equal, both having reached the full plastic moment M_p.

On this background, we will now impose a strain failure criterion that produces an ultimate moment M_u at 1 ($M_{u,1}$). $M_{u,1}$ establishes the failure point F in Fig. 5.4, on the curve for M_1. A line parallel to the moment axis through point F intersects the line of linear behavior associated with M_1 at $M^f_{1,el}$. The difference between $M^f_{1,el}$ and $M_{u,1}$ has been identified as the residual moment component $M^f_{1,res}$, according to Eq. 5.4, where

$$M_{u,1} = |M^f_{1,el}| - |M^f_{1,res}|$$

Similarly, the line through F will determine the components of the moment M_2, according to the equation (compare Eq. 5.3)

$$|M^f_2| = |M^f_{2,el}| + |M^f_{2,res}|$$

Thus, the shaded areas in the diagram indicate the residual moment components throughout the possible inelastic load history. But the deviation from linear behavior of the moments at the moment peaks is also exactly what is meant by inelastic moment redistribution. Hence, there is a direct parallel between inelastic moment redistribution and the residual moment components. The diagram furnishes exact values of the residual moment components for the final failure mechanism.

The failure point F also establishes the ultimate load P_u. Similarly to the treatment of the moments, a horizontal line through F will now determine a load component for linear behavior, P_S, and a second component for the deviation from linear behavior, P_R, satisfying the relationship

$$P_u = P_S + P_R \tag{5.24}$$

If the moments are taken as ratios with respect to the yield moment M_y, and the load values as ratios with respect to the yield load P_y (as done in Fig. 5.4), the following relationships can be established from Fig. 5.4

$$\frac{P_u}{P_y} = \frac{|M^f_{1,el}|}{M_y}\,, \quad \frac{P_S}{P_y} = \frac{M_{u,1}}{M_y} \quad \text{and} \quad \frac{P_R}{P_y} = \frac{|M^f_{1,res}|}{M_y} \tag{5.25}$$

These relationships are only true with respect to the moments at the first partial hinge. They could have been established by mere theoretical reasoning. The load ratios will be

important in the later design approach and shall therefore be given the special notation, $p_u = P_u/P_y$, $p_S = P_S/P_y$ and $p_R = P_R/P_y$. Hence,

$$p_u = p_S + p_R \tag{5.26}$$

The meaning of the load factor components becomes evident from Eq. 5.25. p_S would be obtained for linear elastic analysis with limiting moment M_u instead of M_y. Hence, it depends solely on the geometric section parameters β_1 and β_2, and on the compressive strain failure condition $\varepsilon_{c,u}/\varepsilon_y$, and represents the inelastic reserves of load carrying capacity due to section plastification. The component p_R reflects the deviation from linear, elastic behavior and is therefore the contribution of inelastic moment redistribution. The load factors will directly indicate the economical savings in inelastic design.

5.4 Design Approach for Partial Moment Redistribution

The remainder of this chapter will deal with the problem to reduce moment redistribution analysis into a systematic and practical design approach, which will ultimately consist in the use of diagrams for the inelastic load factors. For this purpose, Sec. 5.4.1 will deal with the problem of the section parameters. In Sec. 5.4.2, results of partial moment redistribution will be presented for a prescribed sample system, but for the whole practical domain of geometric section

parameters. An evaluation with respect to system parameters will follow in Sec. 5.4.3.

5.4.1 The Section Parameters

The coldformed simply eccentric section was discussed in detail in Chapter 3, for the primary purpose of reducing the section parameters to the smallest possible number necessary for a correct description of inelastic section performance. Moreover, the parameters were selected in a special form, to allow a direct evaluation of the effects of section eccentricity. As a result, two non-dimensional geometric parameters β_1 and β_2 were obtained, which are defined by Eqs. 3.9. Geometrically similar sections will always have identical values for β_1 and β_2, but the similarity need not include the thickness t, which does not occur in β_1 and β_2. Elastic modulus, yield stress and ultimate compressive strain can be combined in the one parameter $\varepsilon_{c,u}/\varepsilon_y$, which represents the failure criterion of the coldformed section. Hence, it has been shown, that the inelastic behavior of the section, in particular the ratios between ultimate moment and yield moment M_u/M_y, are defined by the three non-dimensional parameters β_1, β_2 and $\varepsilon_{c,u}/\varepsilon_y$.

The use of this set of non-dimensional parameters to represent the section and the failure criterion implies that all equations of the analysis be transformed into a normalized form, compatible with the non-dimensional section parameters.

It has been shown in Chapter 3, that with respect to moment and curvature the following normalization must be applied,

$$m = \frac{M}{\sigma_y t d^2} , \quad \kappa = \phi d$$

where m and κ are called the normalized moment and curvature, respectively. This normalization of moment and curvature will determine the normalized form of all the other variables in the analysis. In this respect, it is not necessary to transform equations individually into normalized form. It will suffice to determine the normalized form of the remaining variables from any of the basic equations of the analysis. As an example, the normalized forms of the uniform load w and the span length L shall be derived from the equation between uniform load and maximum moment of the statically determinate beam,

$$M = \frac{wL^2}{8}$$

If M is normalized as shown above, we obtain

$$m = \frac{M}{\sigma_y t d^2} = \frac{wL^2}{8\sigma_y t d^2} = \frac{1}{8} \frac{w}{\sigma_y t} \left(\frac{L}{d}\right)^2$$

We set $\bar{w} = \frac{w}{\sigma_y t}$ and $\ell = \frac{L}{d}$ and can write $m = \frac{\bar{w}\ell^2}{8}$. $\bar{w}$ and ℓ are by definition the normalized uniform load and beam length. Similarly, all remaining variables can be normalized. A list of the variables of the analysis and their corresponding

normalized forms is given in Table 5.1. The notation of the normalized variables has been distinguished from the dimensional variables either by switching from capital to small letters, or by using a bar. All equations of the analysis can now be normalized by simply replacing the dimensional variables by their normalized counterparts. It is seen from the list in Table 5.1 that every dimensional variable could have been normalized by forming the dimensionless product between the variable and the quantities $(\sigma_y t)$ and d.

Once this transformation into dimensionless products is established, dimensional and non-dimensional analysis will be completely identical. Thus, the design equations of the one-hinge failure mode with first partial hinge at the support (Eqs. 5.16) can directly be written in normalized form as follows

$$m_{u,1} = |m^f_{1,el}| - |m^f_{1,res}| \tag{5.27a}$$

$$m^f_{1,res} = C_1 i \frac{\bar{H}^f_1}{\ell} \zeta_{1in} \tag{5.27b}$$

$$\bar{H}^f_1 = (m_{u,1} - m_y) \frac{1}{|v^f_{1,\ell}|} + \frac{1}{|v^f_{1,r}|} \tag{5.27c}$$

$$|m^f_{1,el}| = \alpha_1 \bar{w}_u \ell^2 \tag{5.27d}$$

The solution of this set of equations for the example system of Fig. 5.1 was given in dimensional form by Eqs. 5.20 and 5.21. Again, these equations can directly be transformed as follows

$$(m^f_{1,el})^2 - \frac{3}{4} m_{u,1} |m^f_{1,el}| - \frac{1}{4}(m^2_{u,1} + (m_{u,1}-m_y)3i\zeta_{lin}) = 0 \quad (5.28)$$

$$\bar{w}_u = \frac{8|m^f_{1,el}|}{\ell^2} \quad (5.29)$$

With the background of Chapter 3, it is now obvious that the main objective of normalized analysis has been achieved. The quantities $m_{u,1}$, m_y, i, and ζ_{lin} are functions of the section parameters β_1, β_2, $\varepsilon_{c,u}/\varepsilon_y$. Hence, the section is now represented by the smallest possible number of parameters in the desired form. Explicit equations are given in Appendix 3.1 for $m_{u,1}$, m_y and i. The functions $m_u/m_y = m_{u,1}/m_y$ and m_y have been plotted in Figs. 3.2 to 3.5 and Fig. 3.6, respectively. i is obtained from Eq. A3.1-8 as follows

$$i = m_y \frac{\beta_1 + |\beta_2| + \frac{1}{2}}{2\beta_1 + 1} \quad (5.30)$$

ζ_{lin} is plotted in Fig. 4.3. Thus, if the section parameters are prescribed, the values of $m_{u,1}$, m_y, i and ζ_{lin} will be defined. If Eq. 5.28 is solved for $m_{1,el}$, Eq. 5.29 can be solved for $\bar{w}_u$. The dimensional ultimate load can be computed from

$$w_u = \bar{w}_u \sigma_y t \quad (5.31)$$

Inversion of the Design Problem

The use of normalized analysis provides an additional significant advantage: It allows a direct and efficient solution for the inverted design problem, where the ultimate load

is specified, whereas the section dimensions are the unknowns. Of course, the section must be defined prior to the analysis to the extent that values for β_1, β_2 and $\varepsilon_{c,u}/\varepsilon_y$ must be selected ($\varepsilon_{c,u}/\varepsilon_y$ will depend on w/t according to Eq. 2.7). But these values will not define the section dimensions completely. β_1 and β_2 will only determine the proportions of the section geometry, not including the thickness t. E.g., we obtain from Eqs. 5.29 and 5.31,

$$w_u = \frac{8|m^f_{1,el}|\sigma_y t}{(L/d)^2}$$

This equation can be rearranged in the form

$$td^2 = \frac{w_u L}{8|m^f_{1,el}|\sigma_y} \tag{5.32}$$

If w_u is specified in the design problem, the right-hand side of Eq. 5.32 will be a known value. We are now free to choose t and d in any combination that satisfies Eq. 5.32 and which is consistent with the failure condition $\varepsilon_{c,u}/\varepsilon_y$. These aspects of non-dimensional analysis have been discussed more extensively in connection with the statically determinate beam in Chapter 3, Sec. 3.2, and are demonstrated by design examples in Appendix 3.3.

Inelastic Load Factors

Inelastic load factors have been defined in Sec. 5.3 by Eqs. 5.25 and 5.26 in terms of dimensional moment ratios.

Since $\frac{m}{m_y} = \frac{M}{M_y}$, the inelastic load factors are also directly obtained as the ratios of the non-dimensional moments, i.e.,

$$p_u = \frac{|m^f_{1,el}|}{m_y} , \quad p_S = \frac{m_{u,1}}{m_y} , \quad p_R = \frac{|m^f_{1,res}|}{m_y} \qquad (5.33)$$

5.4.2 Results for the Sample System of Fig. 5.1

Eqs. 5.28 and 5.29, which represent the solution of partial moment redistribution analysis for the system given in Fig. 5.1 (two-span beam under uniform load), have been solved for the practical domain of parameters β_1 and β_2, and for $\varepsilon_{c,u}/\varepsilon_y = 3$. The results are plotted in Figs. 5.5 to 5.7 in terms of inelastic load factors. These graphs will allow a general assessment of the contribution of inelastic moment-redistribution to the total inelastic reserve of the cold-formed redundant beam system. In addition, they will show the range of validity of the one-hinge failure mode.

The eccentricity parameter β_2 is chosen as the variable on the horizontal axis, whereas β_1 is used as a constant parameter for each curve. In this representation, the values for symmetric sections lie along the vertical axis. To the left of the vertical axis are the sections that yield initially in tension, to the right are the sections that yield initially in compression. The curves cannot be symmetric, since the strain failure criterion always refers to the compression flange.

The results for the total inelastic load factor p_u are plotted in Fig. 5.5(a) in solid lines. The dashed lines indicate the load factors p_S. The difference between p_u and p_S is due to inelastic moment redistribution, representing the component p_R. The results for the component p_R will be discussed in more detail below.

In Fig. 5.5(b), the moment ratios in the span, corresponding to the load factors p_u in Fig. 5.5(a), are plotted as a check for initial yielding in the span, particularly, since the analysis was carried out for the one-hinge failure mode. It is seen that a second partial hinge does not form in the span prior to failure, with the exception of extreme section geometries with initial yielding in tension. The boundary where this transition to the two-hinge failure mode occurs, i.e., $M_2/M_y = 1$, is shown in the graph. For the majority of practical sections, the peak moment M_2 in the span remains considerably below the yield moment as failure occurs.

The component p_S does not depend on system and load case, but is identical with the moment ratios M_u/M_y which were evaluated in Chapter 3 and plotted in Fig. 3.2. The principal result of the inelastic analysis of redundant beams is the contribution of inelastic moment redistribution to the ultimate load carrying capacity, represented by the load factor component p_R, which is plotted for the example in separate graphs, in Figs. 5.6 and 5.7. Whereas in Fig. 5.6 the gains of inelastic moment redistribution are related to the yield

load, in Fig. 5.7 they are related to the total inelastic reserve in load carrying capacity, p_u-1. It is seen from the latter graph that, in general, the contribution of moment redistribution to the total inelastic reserve will vary between 10% and 20%. This means that the major inelastic reserve is provided by the inelastic strength reserve of the cross-section, rather than by moment redistribution.

The relatively small contribution of moment redistribution is due to the generally small plastic rotations of partial hinges at an interior support under idealized assumptions (e.g., knife edge support, perfectly plastic material). This could be anticipated, since, inspecting Eq. 4.15, it is seen that the integral over the plastic curvature component at an interior support, i.e., the plastic rotation of the partial hinge, is mathematically finite for $\varepsilon_{c,max} = \infty$ or $\phi_{max} = \infty$. Fig. 5.9 shows the bound of the redistribution load factors for $\varepsilon_{c,max} = \infty$. The curves are now symmetric, but the redistribution load factors are still very moderate. They will, for the majority of section geometries, not even allow a second partial hinge in the span to form. Accordingly, a full plastic hinge, as used in plastic design, can never be obtained mathematically if strainhardening of the material is not considered. This proves that the strainhardening property of structural steel is essential to obtain a collapse mechanism. But, since the strain failure criterion $\varepsilon_{c,u}/\varepsilon_y = 3$ for coldformed sections does not reach into the strainhardening

The results for the total inelastic load factor p_u are plotted in Fig. 5.5(a) in solid lines. The dashed lines indicate the load factors p_S. The difference between p_u and p_S is due to inelastic moment redistribution, representing the component p_R. The results for the component p_R will be discussed in more detail below.

In Fig. 5.5(b), the moment ratios in the span, corresponding to the load factors p_u in Fig. 5.5(a), are plotted as a check for initial yielding in the span, particularly, since the analysis was carried out for the one-hinge failure mode. It is seen that a second partial hinge does not form in the span prior to failure, with the exception of extreme section geometries with initial yielding in tension. The boundary where this transition to the two-hinge failure mode occurs, i.e., $M_2/M_y = 1$, is shown in the graph. For the majority of practical sections, the peak moment M_2 in the span remains considerably below the yield moment as failure occurs.

The component p_S does not depend on system and load case, but is identical with the moment ratios M_u/M_y which were evaluated in Chapter 3 and plotted in Fig. 3.2. The principal result of the inelastic analysis of redundant beams is the contribution of inelastic moment redistribution to the ultimate load carrying capacity, represented by the load factor component p_R, which is plotted for the example in separate graphs, in Figs. 5.6 and 5.7. Whereas in Fig. 5.6 the gains of inelastic moment redistribution are related to the yield

load, in Fig. 5.7 they are related to the total inelastic reserve in load carrying capacity, p_u-1. It is seen from the latter graph that, in general, the contribution of moment redistribution to the total inelastic reserve will vary between 10% and 20%. This means that the major inelastic reserve is provided by the inelastic strength reserve of the cross-section, rather than by moment redistribution.

The relatively small contribution of moment redistribution is due to the generally small plastic rotations of partial hinges at an interior support under idealized assumptions (e.g., knife edge support, perfectly plastic material). This could be anticipated, since, inspecting Eq. 4.15, it is seen that the integral over the plastic curvature component at an interior support, i.e., the plastic rotation of the partial hinge, is mathematically finite for $\varepsilon_{c,max} = \infty$ or $\phi_{max} = \infty$. Fig. 5.9 shows the bound of the redistribution load factors for $\varepsilon_{c,max} = \infty$. The curves are now symmetric, but the redistribution load factors are still very moderate. They will, for the majority of section geometries, not even allow a second partial hinge in the span to form. Accordingly, a full plastic hinge, as used in plastic design, can never be obtained mathematically if strainhardening of the material is not considered. This proves that the strainhardening property of structural steel is essential to obtain a collapse mechanism. But, since the strain failure criterion $\varepsilon_{c,u}/\varepsilon_y = 3$ for coldformed sections does not reach into the strainhardening

range of mild structural steel, the plastic rotations are very limited. The analytical assumption of a knife edge support was discussed in Chapter 4, Sec. 4.3.

Fig. 5.8 shows the redistribution component p_R for a compressive strain failure criterion $\varepsilon_{c,u}/\varepsilon_y = 1$. Plastic rotations in this case can be obtained for initial yielding in tension, but are so limited for sections with moderate eccentricities that moment redistribution may as well be neglected. This would still allow us to design with a load factor p_S, considering only the increased resistance of the section due to partial section plastification.

5.4.3 The System Parameters (Approximate Approach)

Once the inelastic load factor p_u has been determined for a given system and load case, the final solution of the design problem becomes simple. The inelastic load factor as defined by Eq. 5.26 is $p_u = P_u/P_y = p_S + p_R$, where the notation P indicates the general parameter of a one-parameter load case, p_S is the component of the ultimate strength of the section, and p_R is the moment redistribution component. Assuming that the load P_u is specified in the design problem (design load × safety factor), the yield load P_y can be computed from $P_y = P_u/p_u$. The dimensions of the section can now be determined from elastic design for the yield load. The difficulties of the analysis arise of course in the computation of p_u.

According to the treatment of the section parameters in Sec. 5.4.1, the section will be represented by two geometric

parameters β_1 and β_2, and the compressive strain failure criterion $\varepsilon_{c,u}/\varepsilon_y$.

On this background it is desired to derive graphs for the inelastic load factors p_u that are either valid for general system parameters or, at least, for a frequently occurring limited domain of system parameters, to avoid an explicit analysis of moment redistribution in the individual design problem. Since the component p_S is determined by the ratio M_u/M_y, it depends on section parameters only. However, section and system parameters must be considered in connection with the moment redistribution component p_R. A treatment with respect to system parameters will now only concern the component p_R. Principally, two approximate approaches can be considered.

1) Moment redistribution analysis is not carried out at all. In this case we consider an elastic analysis of the redundant system with limiting moment M_u instead of M_y as a substitute for the rigorous analysis with moment redistribution. Since $p_R = 0$ certainly is a lower bound to the redistribution ratios of all systems, this approach is valid for all system parameters. The analysis will, of course, be simplified considerably if moment redistribution analysis does not have to be carried out. But the approach must, in general, be judged by the loss in economical advantage, since the reserves of the system due to moment redistribution are neglected. A good judgment of the economical significance of components p_S and

p_R can be made from the results for the two-span beam under uniform load, which were presented in Sec. 5.4.2 for the whole domain of practical section parameters, and for the largest ultimate compressive strain allowed by the failure criterion of Eq. 2.7. The results show that the component p_R is rather insignificant in the example, amounting only to less than 20% of the total inelastic reserves. This approach will therefore be of practical importance.

2) Even though the component p_R may be small, an alternative will be offered to the approach outlined above where moment redistribution is included in the design, although for a strictly limited domain of system parameters. The solution that will be given is illustrated by the diagram of Fig. 5.6, where p_R is plotted for the whole domain of section parameters, and for ultimate compressive strain $\varepsilon_{c,u}/\varepsilon_y = 3$, but only for one particular example system. However, it will be possible to combine comparable systems into one diagram of this type, where the redistribution ratio p_R is a lower bound to the group of comparable systems. For example, the beam over two equal spans under uniform load can be considered a special case of all systems over an arbitrary number of equal spans under uniform load. Moreover, the restriction to equal span lengths can be liberalized. Hence, this approach shall be demonstrated for systems under uniform load with an arbitrary number of spans whose lengths do not differ by more than 20%.

The two methods will be outlined in the following in more detail, beginning with the more general approach (1).

5.4.3.1 Elastic Design of Redundant Beams for Limiting Moment M_u

If moment redistribution analysis is not carried out, elastic analysis of the redundant beam for limiting moment M_u instead of M_y can be examined as a substitute for the rigorous analysis with moment redistribution. In particular, it must be examined if the governing load case and the critical section (where the limiting condition of the design is reached first) are the same as in elastic design for initial yielding. For, the ultimate resistance of an eccentric section is usually different for positive and negative moment, i.e., at the support and in the span. For this reason, the ultimate resistance at the first partial hinge has been identified as $M_{u,1}$, at the second partial hinge as $M_{u,2}$. In addition, the actual moment distribution at the ultimate load computed from the simplified inelastic analysis will not be correctly represented by the elastic moment distribution, but will still have an elastic and a residual moment component.

The governing load case of elastic design (producing the maximum moment of the elastic moment envelope) will be called the primary load case. If the primary load case produces the maximum moment of the elastic moment envelope at a support, the corresponding secondary load case shall by definition produce the maximum span-moment of the elastic moment envelope.

In this case, the primary load case will produce the first partial hinge at a support, the secondary load case in a span. Vice versa, if the primary load case produces the first partial hinge in a span, the secondary load case will by definition produce the first partial hinge at a support.

Due to the effects of the residual moment component and of different ultimate moments at the support and in the span, governing load case and critical section of inelastic analysis need not be the same as in elastic analysis. For the primary load case, the failure condition may first be reached at the first partial hinge (same critical section as in elastic design) for $M_{u,1}$, or at the second partial hinge for $M_{u,2}$. Or the secondary load case may govern the design (with possibilities of failure at first and second partial hinge). Hence, four values for the ultimate load carrying capacity can be computed for four different alternatives of failure. The lowest of these four values will govern the design.

For the limited rotation capacities of the partial hinges in the present context, two of these four alternatives can be eliminated by inspection. For example, we assume the maximum moment of the elastic moment envelope at the support. The primary load case will then create the most unfavorable condition for all support moments, whereas the secondary load case will create the most unfavorable condition for all span moments. Failure at the support will now be considered only in connection with the primary load case, failure in the span

only in connection with the secondary load case. I.e., we have to examine only two alternatives of failure: (1) primary load case with failure at its first partial hinge, (2) secondary load case with failure at its first partial hinge. These failure conditions shall now be expressed analytically.

The notation used until now (M_1 = moment at first partial hinge, M_2 = moment at second partial hinge) is not convenient in the comparison of different load cases, since subscripts 1 and 2 do not refer to identical points of the system for different load cases. We shall therefore define two fixed points a and b of the system, where a is determined by the first partial hinge of the primary load case, b by the first partial hinge of the secondary load case. Instead of a general load parameter P we shall use the notation w for uniformly distributed load. The coefficients α are those occurring in the elastic relationships $M = \alpha w L^2_{max}$. Subscripts will be used for α, which define the point of the system and the load case. The α-coefficients are illustrated by sketches for a special example in Table 5.1.

The governing yield load w_y of elastic design for M_y is determined by the primary load case. Hence,

$$w_y = \frac{M_y}{\alpha_{a,1} L^2} \tag{5.34}$$

1) Ultimate Load Carrying Capacity of the Primary Load Case with Local Failure at First Partial Hinge ($M_{u,a}$)

Adapting Eq. 5.4

$$M_{u,a} = |M^f_{a,el}| - |M^f_{a,res}|$$

Ultimate load carrying capacity according to Eq. 5.16d

$$w_{u,1} = \frac{|M^f_{a,el}|}{\alpha_{a,1} L^2} = \frac{1}{\alpha_{a,1} L^2} (M_{u,a} + |M^f_{a,res}|) \qquad (5.35)$$

It is seen from Eq. 5.35 that the residual moment component can safely be dropped. In this case,

$$w_{u,1} \simeq \frac{M_{u,a}}{\alpha_{a,1} L^2} \qquad (5.36)$$

The ultimate load carrying capacity $w_{u,1}$ is now obtained approximately, but safely, from the elastic analysis of the primary load case with limiting condition $M_{u,a}$. The inelastic load factor according to Eq. 5.35 is obtained by dividing both sides of Eq. 5.35 by w_y and using Eq. 5.34, i.e.,

$$p_{u,1} = \frac{w_{u,1}}{w_y} = \underbrace{\frac{M_{u,a}}{M_y}}_{p_{S,1}} + \underbrace{\frac{|M^f_{a,res}|}{M_y}}_{p_{R,1}} \qquad (5.37)$$

The last equation defines the inelastic load factor and its components for the primary load case.

2) Ultimate Load Carrying Capacity of the Secondary Load Case with Local Failure at First Partial Hinge ($M_{u,b}$)

Adapting Eq. 5.4

$$M_{u,b} = |M^f_{b,el}| - |M^f_{b,res}|$$

Ultimate load carrying capacity according to Eq. 5.16d

$$w_{u,2} = \frac{|M^f_{b,el}|}{\alpha_{b,2} L^2} = \frac{1}{\alpha_{b,2} L^2} (M_{u,b} + |M^f_{b,res}|) \qquad (5.38)$$

Again, we can safely drop the residual moment component. In this case

$$w_{u,2} \simeq \frac{M_{u,b}}{\alpha_{b,2} L^2} \qquad (5.39)$$

Hence, a safe approximate ultimate load carrying capacity is obtained from elastic analysis with limiting condition $M_{u,b}$. Dividing both sides of Eq. 5.38 by w_y and using Eq. 5.34

$$p_{u,2} = \frac{w_{u,2}}{w_y} = \underbrace{\frac{\alpha_{a,1}}{\alpha_{b,2}} \frac{M_{u,b}}{M_y}}_{p_{S,2}} + \underbrace{\frac{\alpha_{a,1}}{\alpha_{b,2}} \frac{|M^f_{b,res}|}{M_y}}_{p_{R,2}} \qquad (5.40)$$

If the redistribution components $p_{R,1}$ and $p_{R,2}$ are dropped in Eqs. 5.37 and 5.40, the following approximate, but safe, inelastic load factors are obtained for the primary and secondary load case,

$$p_{u,1} = \frac{M_{u,a}}{M_y} \tag{5.41}$$

$$p_{u,2} = \frac{\alpha_{a,1}}{\alpha_{b;2}} \frac{M_{u,b}}{M_y} \tag{5.42}$$

respectively. The smaller value of the two load factors will govern the design.

The ratios $M_{u,a}/M_y$ and $M_{u,b}/M_y$ are given by Figs. 3.2 to 3.5 for the whole domain of section parameters β_1 and β_2, and for $\varepsilon_{c,u}/\varepsilon_y = 1$ ($w/t \geq 1.08(w/t)_{lim}$) and $\varepsilon_{c,u}/\varepsilon_y = 3$ ($w/t \leq .92(w/t)_{lim}$).

Since $M_{u,a}$ and $M_{u,b}$ denote the ultimate resistance of a section for positive and negative moment, the same flange will in one case be a tension flange, in the other case a compression flange. This means, according to Eq. 3.9, that the parameter β_2 changes its sign. However, the failure criterion $\varepsilon_{c,u}/\varepsilon_y$ may also be different at the two points a and b, which would require the use of different graphs to determine $M_{u,a}/M_y$ and $M_{u,b}/M_y$.

It may be desirable to furnish additional graphs, besides those given in Figs. 3.2 to 3.5, for intermediate ultimate compressive strains, e.g., $\varepsilon_{c,u}/\varepsilon_y = 2$. If a graph for the exact ultimate compressive strain according to Eq. 2.7 (in the range $.92(w/t)_{lim} < w/t < 1.08(w/t)_{lim}$) does not exist, it will always be safe to use a graph based on a lower ultimate compressive strain.

Summarizing, elastic analysis with limiting conditions $M_{u,a}$ and $M_{u,b}$ can be used safely in connection with the failure criterion of Eq. 2.7. In this case solely the inelastic reserves of strength of a section are taken advantage of. However, two different inelastic load factors must be determined for two load cases, one of which produces the maximum support moment of the elastic moment envelope, the other the maximum span moment. The smaller load factor governs the design. If the governing load factor has been established from Eqs. 5.41 and 5.42, it can be applied in the subsequent design procedure to determine the yield load of the system. The section can then be dimensioned for the yield load.

5.4.3.2 Alternative Approach with Lower Bound Moment Redistribution Component for Restricted Domain of Section Parameters and System Parameters

An alternative approach shall now be discussed, which will take into account the moment redistribution component p_R of the inelastic load factor, but only for a limited domain of system parameters which is thought to occur frequently in practical design. In this approach the redistribution component will be plotted, as a lower bound to a group of comparable systems, in the form of Fig. 5.6, i.e., for the whole practical range of section parameters β_1 and β_2, and for the failure criterion $\varepsilon_{c,u}/\varepsilon_y = 3$ (valid in the range $w/t \leq .92(w/t)_{lim}$, according to Eq. 2.7).

The lower bound ratios will be established on the basis of the following restrictions.

1) $L_{min} \geq .8L_{max}$, but the number of spans is arbitrary.
2) Live load and dead load are uniformly distributed loads.
3) The governing load case is identical with the governing load case of elastic design for M_y (primary load case).
4) Failure occurs in the one-hinge load interval.

Systems that satisfy restrictions (1) and (2) will usually not satisfy restrictions (3) and (4) in the whole range of section parameters. But the ratios p_R, derived on the basis of all four restrictions, will be safe only in those cases where all restrictions are satisfied. This requires special safeguards with respect to restrictions (3) and (4). In the following, the lower bound curves of p_R shall be established. Subsequently, safeguards with respect to restrictions (3) and (4) shall be derived.

Lower Bound of Moment Redistribution Components p_R

Two and three span systems will be evaluated as prototypes with the assumption that the results can be extended to an arbitrary number of spans without further verification. All combinations of two and three span systems with $L_{max} = 1$ and $L_{min} = .8$ are shown in sketches in Table 5.1, Col. 2, together with their primary load cases. Seven different combinations are possible. In all cases the primary load case will produce the first partial hinge at the first interior support, indicated as point a. The location of the maximum

span moment of the primary load case is indicated as point b (which coincides in all cases with the location of the maximum span moment of the secondary load case).

The numerical evaluation is based on a dead load to live load ratio $w_D/w_L = 1:4$.

According to restriction (4), only the one-hinge failure mode will be considered. General design equations for moment redistribution, valid for the one-hinge failure mode with first partial hinge at support, are given by Eqs. 5.27a-d in normalized form. These equations have been solved for $|m^f_{1,el}|$ (Eq. 5.28) for a particular case. Similarly they can be solved for the component $|m^f_{1,res}|$. To do this, the shear forces, in an approximation, shall be computed for the elastic moment distribution with limiting moment $M_{u,a}$, rather than for the actual inelastic moment distribution. The error is small, and certainly has no effect within the present purpose of deriving a lower bound for p_R. Hence, we use

$$v_{a,\ell} = \gamma_{a,\ell}\bar{w}_u\ell \qquad \text{and} \qquad v_{a,r} = \gamma_{a,r}\bar{w}_u\ell$$

where the coefficients γ are elastic coefficients of the shear distribution. We will also use the elastic coefficients α of the moment distribution, e.g.,

$$|m^f_{a,el}| = \alpha_{a,1}\bar{w}_u\ell^2$$

Subscript a refers to point a of the systems. Only α is generally written with a second subscript indicating the load case.

Including the above definitions in the set of equations given by Eqs. 5.27a-d, and considering the present modification of the subscripts (a instead of 1), the equations can be solved in the form of the following quadratic,

$$(m^f_{a,res})^2 + |m^f_{a,res}|m_{u,a} - i(m_{u,a} - m_y)C_a\alpha_{a,1}(\frac{1}{\gamma_{a,}} + \frac{1}{\gamma_{a,r}})\zeta_{lin} = 0 \tag{5.43}$$

It is seen that system parameters (C_a, $\alpha_{a,1}$, $\gamma_{a,\ell}$, $\gamma_{a,r}$) can be combined by the following notation

$$S = C_a\alpha_{a,1}(\frac{1}{\gamma_{a,\ell}} + \frac{1}{\gamma_{a,r}}) \tag{5.44}$$

If Eq. 5.43 is divided by m_y^2, and with $p_R = |m^f_{a,res}|/m_y$, and Eq. 5.44, we obtain

$$p_R^2 + p_R\frac{m_{u,a}}{m_y} - \frac{i}{m_y}(\frac{m_u}{m_y} - 1)\zeta_{lin}S = 0 \tag{5.45}$$

which has the solution

$$p_R = \frac{1}{2}\left[-\frac{m_u}{m_y} \oplus \sqrt{(\frac{m_u}{m_y})^2 + 4\frac{i}{m_y}(\frac{m_u}{m_y} - 1)\zeta_{lin}S}\right] \tag{5.46}$$

The encircled positive sign is valid since $p_R > 1$. System parameters occur only and exclusively in the quantity S. As can easily be verified, the lower bound of p_R to all system parameters is obtained for the minimum value of S for all system parameters. S has therefore been evaluated for the seven systems of Table 5.1, which represent the whole group of

systems defined by restriction (1). $\alpha_{a,1}$, $\gamma_{a,\ell}$, $\gamma_{a,r}$ (primary load case) and C_a are listed in Cols. 3 to 6 in Table 5.1. The values of S are given in Col. 7. Comparing the results in Col. 7, we find that S_{min} pertains to system (1), the same system that has been evaluated as an example for moment redistribution analysis in Sec. 5.4.2. Therefore, it can be concluded that the graphs of Fig. 5.6, established for system (1), represent a safe lower bound to the redistribution component p_R for the whole group of systems, as long as restrictions (3) and (4) are satisfied. Fig. 5.6 can now be considered the design diagram for p_R for these systems.

To test the deviation between the exact values of p_R and the lower bound, particular lower bound values of p_R ($p_{R,LB}$) for $S_{min} = .6000$ (system (1)) and upper bound values ($p_{R,UB}$) for $S_{max} = .6575$ (system (6)) were computed from Eq. 5.46, for two points with representative section parameters. The result was

i) For $\beta_1 = 1.2$, $\beta_2 = 0$, $(M_u/M_y = 1.06) \rightarrow p_{R,UB}/p_{R,LB} = 1.088$

ii) For $\beta_1 = .6$, $\beta_2 = -.3$, $(M_u/M_y = 1.40) \rightarrow p_{R,UB}/p_{R,LB} = 1.083$

It can be concluded that, for $M_u/M_y \leq 1.40$, and for all systems

$$p_{R,UB}/p_{R,LB} < 1.09 \qquad (5.47)$$

It is seen that the lower bound is a good approximation to the actual values of p_R within this group of systems.

Safeguard to Ensure Failure by One-Hinge Failure Mode

According to restriction (4), the values of p_R in Fig. 5.6 are valid only, if failure occurs within the one-hinge load interval, i.e., before a second partial hinge can form in the structure. This condition is in general not satisfied in the whole domain of section parameters of Fig. 5.6. A safeguard must therefore be derived.

If the moment at b (maximum span moment) just reaches the yield moment as failure occurs at the first partial hinge at a, we obtain from Eq. 5.3

$$|M_b| = M_y = |M^f_{b,el}| + |M^f_{b,res}|$$

The load carrying capacity for this special case is given as follows

$$w_u = \frac{|M^f_{b,el}|}{\alpha_{b,1} L^2_{max}} = \frac{1}{\alpha_{b,1} L^2_{max}} (M_y - |M^f_{b,res}|) \qquad (5.48)$$

The load factor is, with Eq. 5.34 ($\alpha_{a,1} = \alpha_a$),

$$p_u = \frac{w_u}{w_y} = \frac{\alpha_{a,1}}{\alpha_{b,1}} \left(1 - \frac{|M^f_{b,res}|}{M_y}\right) \qquad (5.49)$$

Yielding at b is excluded, if

$$p_u < \frac{\alpha_{a,1}}{\alpha_{b,1}} \left(1 - \frac{M^f_{b,res}}{M_y}\right) \qquad (5.50)$$

The residual moment distribution is linear. If points a and b belong to the endspan, the residual moment distribution is

given by Eq. 5.5. This applies to all systems in Table 5.2, except system (5), where b is in the interior span. With Eq. 5.5, setting x = .6L,

$$\frac{|M^f_{b,res}|}{M_y} = .4\,\frac{|M^f_{a,res}|}{M_y} = .4p_R \tag{5.51}$$

This condition is conservative for system (5) and can therefore be used for all systems. Condition 5.50 is conservative if p_R is an upper bound to the exact values of p_R. This upper bound is given by Eq. 5.47. Hence,

$$\frac{|M^f_{b,res}|}{M_y} < .4 \times 1.09 p_{R,LB} = .44 p_{R,LB} \tag{5.52}$$

Since $p_{R,LB}$ stands for the redistribution ratios of the design diagram in Fig. 5.6, we drop the second subscript. Substituting Eq. 5.52 in Eq. 5.50, we obtain

$$p_u < \frac{\alpha_{a,1}}{\alpha_{b,1}} (1 - .44p_R) \tag{5.53}$$

where p_R must be taken from Fig. 5.6. This condition must be satisfied to ensure restriction (4).

Safeguard with Respect to Failure in Second Load Case

According to restriction (3), the values p_R of the design diagram in Fig. 5.6 are valid only, if the primary load case governs the design. This restriction is certainly satisfied if the design load factor p_u is smaller than the inelastic load factor $p_{u,2}$ of Eq. 5.42 for the secondary load case

without moment redistribution. Hence, with Eq. 5.42 we obtain the desired safeguard as follows

$$p_u < \frac{\alpha_{a,1}}{\alpha_{b,2}} \frac{M_{u,b}}{M_y} \tag{5.54}$$

The coefficients $\alpha_{a,1}$ are listed in Table 5.2, Col. 3. The load configuration of the secondary load case is indicated in Table 5.3. The span moments at b are the maximum moments in this load case, and the maximum span moments of all possible load cases. Coefficients $\alpha_{b,2}$ are given in Table 5.3, Col. 3, ratios $\alpha_{a,1}/\alpha_{b,2}$ in Col. 4.

Final Remarks

The design for the systems defined by restrictions (1) and (2) can now be based on an inelastic load factor p_u which includes the moment redistribution component by a safe, but good approximation. p_u can be determined by two design diagrams, Fig. 3.2 for the component p_S, and Fig. 5.6 for the component p_R. However, the approach is only valid in the domain of section parameters where the two additional restrictions (3) and (4) are satisfied. This requires that two simple safeguards be checked, given by Eqs. 5.53 and 5.54. If any of the restrictions (1) to (4) is not satisfied, recourse must be taken to the simplified design approach of Sec. 5.4.3.1, where moment redistribution analysis is not carried out.

A design example is given in Appendix 5.1.

5.5 Proposed Modification of Hinge Rotation Analysis Pending Additional Tests with Continuous Systems

The partial moment redistribution analysis of the present chapter is based on a rational analysis of hinge rotation capacities as developed in Chapter 4. However, it seems that the hinge rotation capacities are overly conservative due to the assumption of a knife edge support. This assumption is so restrictive that it is not possible, on this basis, to establish a connection between computed hinge rotation capacities and the actual rotation requirements for full moment redistribution. This is true even for w/t-ratios below 30 (σ_y = 36 ksi) where ultimate compressive strains higher than $\varepsilon_{c,u}/\varepsilon_y$ = 3.0 may be obtained. However, test results reported in Ref. 25 indicate that the width of bearing plates may significantly affect the hinge rotation capacity. An extension of the analysis of Chapter 4, taking into account the width of bearing plates, shall therefore be outlined as a suggestion for further experimental investigation. This analytical outline shall be demonstrated for the example of Chapter 4, Sec. 4.3.

Fig. 5.10 is a modification of Fig. 4.1, illustrating a proposed analytical simplification of the support pressure over a bearing plate width by means of two single forces at distance s. The resulting inelastic curvature distribution is also indicated. For this curvature distribution Eq. 4.21 can be modified as follows,

$$\theta_p = \frac{H-s}{d}\,\varepsilon_y \zeta_{lin} + \phi_{p,u}\, s$$

With $$\phi_{p,u} = \frac{\varepsilon_{c,u}}{y_c}$$

$$\theta_p = \frac{H}{d}\,\varepsilon_y \left[\left(1 - \frac{s}{H}\right)\zeta_{lin} + \frac{s}{H}\underbrace{\left(\frac{\varepsilon_{c,u}}{\varepsilon_y}\,\frac{d}{y_c}\right)}_{\zeta_{vec}}\right]$$

With $\beta_2 = -0.2$ (negative sign indicating initial yielding in tension) and $\varepsilon_{c,u}/\varepsilon_y = 3.0$, we obtain from Eq. A3.1-20

$$\frac{\varepsilon_{c,u}}{\varepsilon_y}\,\frac{d}{y_c} = \zeta_{vec} = \frac{\kappa_u}{\varepsilon_y} = \frac{\varepsilon_{c,u}}{\varepsilon_y}\,\frac{1}{\frac{1}{2} - |\beta_2|} = 10$$

For the sake of a dimensional illustration we assume L = 72 in, d = 4.0 in (L/d = 18) and s = 3 in. With H/L = .115, H = .115 × 72 = 8.3 in, and s/H = 3/8.3 = .363. Hence,

$$\theta_p = \frac{H}{d}\,\varepsilon_y[4.125]$$

Also, $$RC = \frac{\theta_p}{\theta_y} = 4.125\,\frac{\varepsilon_y}{\phi_y d} = 4.125\,\frac{\varepsilon_y}{\kappa_y}$$

With $$\frac{\kappa_y}{\varepsilon_y} = 1.7,$$

$$RC = 4.125/1.7 = 2.4$$

The rotation requirement for the example of Sec. 4.3 is RR = 3.5. Hence,

$$RC/RR = 2.4/3.5 = 1/1.46$$

and $$w_u/w_y = 1.30 + .60/1.46 = 1.30 + .41 = 1.71$$

The component (.41) is due to partial moment redistribution. It is approximately five times the value obtained with the assumption of a knife edge support in Sec. 4.3, and 69% of the value for full moment redistribution. This shows that hinge rotations are very sensitive with respect to the parameter s/H (for comparable systems, H/d is approximately constant, therefore s/H can equivalently be expressed by s/d), and it seems worthwhile to investigate this parameter by tests on continuous beams. Obviously, the results in Chapter 5 for s/H = 0 are conservative, since a knife edge support does in reality not occur.

CHAPTER 6

DESIGN APPLICATION AND OUTLOOK ON FUTURE RESEARCH

The present investigation has been primarily concerned with (1) a compressive strain failure criterion for coldformed stiffened sections, and (2) analytical techniques to deal with partial section plastification and partial moment redistribution in practical design (elastic-plastic analysis), with particular consideration of sections with eccentricity of the neutral axis in the load direction. The design applications of the present investigation shall now be reviewed separately for determinate and indeterminate beams.

6.1 Design Applications for Determinate Beams

The results of this investigation are considered directly applicable to strength design of determinate coldformed beams with stiffened cross-sections and material yield strengths in the neighborhood of $\sigma_y \simeq 36$ ksi (say, $\sigma_y < 45$ ksi). This means, the results are applicable to beams that are comparable to the test specimens of the present investigation. Certain questions that will arise in the design of such beams shall be discussed in the following.

6.1.1 Stiffening Plates at Partial Hinges at Concentrated Loads

The cross-section should be stiffened at points of concentrated loads, where a partial hinge will develop, by a

stiffening plate which connects to both webs. This stiffening plate must be designed to fulfill three different functions:

(i) In case of concentrated loads, it must stiffen the webs to prevent web crippling prior to flexural failure.

(ii) Also in case of concentrated loads, it has to support the compression flange, and transmit the vertical concentrated load directly into the web, to prevent concentrated loads from acting on an unsupported compression flange in the sensitive region of the partial hinge, thus affecting the ultimate compressive strain.

(iii) It has to preserve the original geometry of the cross-section until flexural failure occurs. This requirement concerns mainly open hat-sections, where the eccentric arrangement of the tension flanges with respect to the midplane of the webs will create a tendency of the tension flanges for lateral displacements.

Such stiffening plates were used in the present beam tests at the load points, whereas no additional stiffeners were used throughout the region of constant maximum moment in the mid-third of the beam specimens. Under these conditions pure flexural failure was obtained with very good agreement between experimental and computed ultimate values of moment and

curvature, where the computed values were obtained from beam theory for pure bending.

6.1.2 Imperfections at Load Points in Spite of the Presence of Stiffening Plates

Local failure occurred near the load points in most cases, but in some cases well within the constant moment region. The fact that local failure did not necessarily occur at load points indicates that effects of imperfections at load points, if the cross-section is properly stiffened, are of a similar order of magnitude as the effects of imperfections throughout the beam. In all cases, the compressive strain failure criterion was established from measurements that were taken at points removed from the vicinity of local plastic buckling, and therefore were not affected by localized phenomena in connection with failure. Thus, the measured ultimate compressive strains can be considered safe with respect to the effects of local disturbances in the beam tests. No special precautions were taken in the beam tests to reduce imperfections and to model ideal behavior.

6.1.3 Shear Forces

With respect to the presence of shear in a partial hinge it seems justified to adopt the established guidelines of plastic design (see Ref. 13, Chapter 6), since shear forces will have no appreciable influence on ultimate compressive strains, and will certainly become more critical the more web plastification has progressed. With regard to the first

argument, shear forces will not require special consideration in connection with a compressive strain failure criterion (which is replaced in plastic design); with regard to the second argument the guidelines of plastic design (full web plastification) will be conservative.

It has been shown in Ref. 13 that the plastic analysis of combined shear and bending moment can lead to a reduced plastic moment resistance M_{ps} (as compared to the full plastic moment M_p) in the case of low ratios between shear span "a" and beam depth d (the shear span in the case of concentrated loads is given by the ratio M_{max}/V). It is shown in Ref. 13 that the analysis furnishes significantly reduced plastic moments M_{ps} for ratios $a/d < 4.0$ (in the present beam tests $a = L/3$, $L/d \approx 18$, hence $a/d \approx 6$). However, the experimental correlation in Ref. 13 shows that reductions of the full plastic moment M_p are usually not yet observed for values a/d as low as $a/d = 2.0$, and become significant only for $a/d \approx 1.0$. The final design recommendation in Ref. 13 is given by the rule that the plastic moment need not be modified unless $V > \frac{\sigma_y}{\sqrt{3}} t_w d$. This formula can be used as a conservative rule with respect to the ultimate moment M_u in the case of partial web plastification.

The present beam tests did not indicate unfavorable effects of the shear forces at the load points on the ultimate values of moment and curvature.

6.1.4 Uniform Moment and Moment Gradient

The ultimate compressive strain failure criterion of Eq. 2.7 was obtained from experimental measurements in a region of uniform moment. It must be expected that critical compressive strains are altered to some degree by moment gradients. Again, the research for plastic design can supply valuable information. This research shows that maximum compressive strains under moment gradient reach higher values than under uniform moment. It is reported in Ref. 13, for compact sections, that local buckling in a uniform moment region usually occurs when strain hardening commences, whereas under moment gradient maximum compressive strains reach into the strain hardening range. Thus it can be extrapolated that the failure criterion of Eq. 2.7, established from measurements for uniform moment, is conservative in the case of moment gradient.

6.1.5 Material Yield Strength and Stress-Strain Relationship

The compressive strain failure criterion of Eq. 2.7 should not be applied in connection with material yield strengths $\sigma_y > 45$ ksi. It is not possible to draw rational conclusions from the present investigation for $\sigma_y \approx 36$ ksi for significantly different ranges of material yield strength, say $\sigma_y = 60$ ksi, since as of now no analytical relationship is known between the lengths of the compression flange yield plateaus and the material yield strength. This would require at the present state of knowledge a complete additional test

program to establish compressive strain failure criterions for, say, a material yield of 60 to 65 ksi. If this were done, other values could probably be interpolated. It must also be noted especially that the failure criterion of Eq. 2.7 applies only to steel of $\sigma_y < 45$ ksi with a yield plateau.

6.2 Design Applications to Continuous Beams

The compressive strain failure criterion of Eq. 2.7 is a local failure criterion which depends essentially on the compression flange w/t-ratio and the yield strength, not on particular aspects of the beam system. It will be applicable to continuous beams under the same conditions of section geometry (stiffened compression flanges) and yield strength ($\sigma_y < 45$ ksi) for which this failure criterion was derived from statically determinate beam specimens. The only generalization concerning this failure criterion, which is made without explicit experimental investigation, is its application to cases of varying moment gradients. In this cases the failure criterion is conservative (see Sec. 6.1.4).

To obtain the optimal strength and rotation capacity of a partial hinge, it is necessary to ensure that pure flexural failure governs the design. This requires that the cross-section at a partial hinge under concentrated load or support reaction be properly stiffened by a stiffening plate which is connected to both webs while giving support to the compression flange, and that the effect of shear force on the ultimate values of moment and curvature be negligible. These two

aspects are discussed in Secs. 6.1.1 to 6.1.3. With this background, the compressive strain failure criterion together with inelastic analysis for pure bending will be applicable to design problems.

Inelastic analysis of continuous beams at present is severely restricted by the lack of a compressive strain failure criterion for unstiffened flanges. In the case of continuous beams it must be considered that the top flange is in compression in the spans, the bottom flange at the supports. For upright, open hat sections the bottom flanges are unstiffened flanges for which a compressive strain failure criterion does not yet exist. Hence, in such cases, inelastic design cannot yet be applied for the usual continuous systems where incipient yielding occurs at the supports. However, particularly in the case of cellular floor decks, hat sections are often closed by plates, or are used upside down. Then, the compression flanges at interior supports are stiffened, and inelastic design can be applied.

6.3 Subjects for Further Investigation

On the basis of the previous discussion the following subjects for future investigation are suggested:

Experimental

(1) Modification of compressive strain failure criterion of Eq. 2.7 for steels with yield strength $\sigma_y > 45$ ksi.

(2) Compressive strain failure criterion for unstiffened flanges.

(3) The influence of bearing plate widths on the plastic rotation capacity of partial hinges. Note: Preferably this would include testing of continuous beams. Rotation capacities should not only be established by direct measurements in the zone of partial hinges, but also by comparing the experimental load carrying capacity with the computed limiting load carrying capacity associated with the failure mechanism.

(4) Determination of limit w/t-ratios for plastic design of coldformed sections.

Analytical

(1) Establishment of design graphs for partial moment redistribution analysis (compare Fig. 5.6) which include the parameter s/d as discussed previously (see Sec. 5.5).

(2) Extension of design approach to symmetric I-sections with stiffening lips.

SUMMARY

Inelastic design of coldformed stiffened beams with failure in the elastic-plastic domain has been the subject of this investigation. This means design for partial section plastification and, for continuous beams, for partial moment redistribution on the basis of an ultimate compressive strain failure criterion. It closes the gap between plastic design, where the local failure criterion of the section is replaced by the criterion of unconstraint plastic flow of the system (collapse mechanism), and linear allowable stress design. It is of special importance for coldformed sections which do not usually qualify for plastic design.

Optimal performance of a beam section and system is obtained if the design is governed by pure flexural failure, since the primary inelastic reserves originate from section plastification in bending (including plastic rotations due to such section plastification). The principal endeavor in Chapters 1 to 5 has therefore been the investigation of inelastic reserves in pure bending. Chapter 6 points out that shear forces reduce the inelastic reserves obtained in pure bending only in unusual cases (a conclusion derived from the research in connection with plastic design), and that it is possible to eliminate unfavorable local effects at points

where concentrated loads or reactions are transmitted into the beam, by proper detailing of these points. Thus, for usual design problems the analysis can be carried out for bending only with a failure criterion of ultimate compressive strain (as an inelastic stability criterion of the compression flange).

The two central subjects in the preceding chapters are therefore the experimental investigation of a compressive strain failure criterion and its application for design purposes to coldformed beams in pure bending. These two subjects shall now be summarized.

Compressive Strain Failure Criterion (Experimental Part)

Chapter 1 gives an evaluation of failure modes of compression flanges on the background of previous research. This review describes the domain of compression flange w/t-ratios for which experimental data are needed. In this domain compression flange stress-strain curves have a yield plateau of varying length, depending essentially on w/t-ratio and yield strength. Chapter 1 also examines modes of plastic deformations of mild steel, and determines that presently no analytical solution for the length of yield plateaus of the compression flange stress-strain curves is possible.

Chapter 2 reports the present experimental program, and gives an evaluation of the test results with respect to ultimate compressive strains and moment-curvature relationships. The ultimate compressive strains are determined as the limit

of inelastic stability of equilibrium of the compression flange, which coincides with incipient load shedding, i.e., failure of the statically determinate test specimens. Experimental results for ultimate compressive strains are shown, together with a proposed failure criterion, in Fig. 2.9. The analytical formulation of the failure criterion is given by Eq. 2.7. It is further shown that the inelastic analysis for pure bending with the conventional beam equations produces moment-curvature relationships that are in good agreement with the experimentally measured moment-curvature curves.

The experimental failure criterion has presently only been established for coldformed stiffened compression flanges with a material yield strength $\sigma_y < 45$ ksi. Failure criterions for unstiffened flanges and for different ranges of material yield strengths require additional experimental investigations.

Elastic-Plastic Strength Analysis

The section prototype of the present analysis is symmetric about the plane of loading, but may have an arbitrary eccentricity of the neutral axis in the plane of loading. This generality is important in applications to coldformed sections which are not usually doubly symmetric. The section prototype does not distinguish between stiffened and unstiffened flanges, a distinction which only concerns the failure criterion.

A systematic approach to determining the strength of a section under partial section plastification with the limiting condition of a compressive strain failure criterion is given in Chapter 3. The moment-curvature relationships are normalized to reduce the analysis to the smallest possible number of parameters. As a result, design graphs for the ratios between ultimate moment and yield moment can be established in terms of only two geometric parameters, with the ratio between ultimate compressive strain and yield strain ($\varepsilon_{c,u}/\varepsilon_y$) as the only additional parameter. The geometric parameters are chosen in such a form, that one parameter (β_2) vanishes in the case of symmetry about an axis normal to the load plane; thus β_2 is a measure of the eccentricity of the centroidal axis. The second geometric parameter (β_1) is the ratio between flange and web areas (see Eqs. 3.9 and 3.15). Stiffening lips have presently not been included.

Chapter 4 establishes the rigorous analysis of the plastic rotation of partial hinges. The rotations of partial hinges in normalized form (rotation capacity) depend on section parameters β_1, β_2, $\varepsilon_{c,u}/\varepsilon_y$, and on the moment distribution function. Of particular importance, and therefore evaluated, is the linear moment distribution which is used to determine the rotation capacity of partial hinges at interior supports. The rotation capacities can thus be plotted independently of system parameters (see Fig. 4.3).

Chapter 5 establishes practical methods for strength design of continuous beams based on a strain failure criterion. It is shown that an approximate design can always be used, based on elastic analysis of the system and the limiting condition M_u (ultimate moment). This takes advantage only of the inelastic reserves of the cross-section. But beyond the inelastic reserves of the section, continuous beams have an additional reserve of load carrying capacity due to partial moment redistribution. The redistribution component depends on the rotation capacity of the partial hinge and on system and load case. Partial moment redistribution analysis is outlined in its general approach in Chapter 5. It is greatly simplified by auxiliary graphs for the plastic rotation capacity of partial hinges (Fig. 4.3). However, since the analysis is still somewhat involved for design purposes, it is proposed that explicit moment redistribution analysis is eliminated from design applications by direct design graphs for the redistribution component with an approximate treatment of system parameters. This is done by selecting a group of comparable systems, determining the system with the lowest redistribution component among all systems of the group, and thus defining the lower bound redistribution component. The design graphs then depend only on the parameters β_1, β_2, $\varepsilon_{c,u}/\varepsilon_y$, and apply to a restricted domain of system parameters (see Fig. 5.6).

The design approach of Chapters 3 to 5 allows the direct proportioning of the section for partial section plastification and partial moment redistribution if the load is specified, eliminating trial and error procedures.

The analysis in Chapters 4 and 5 (rotation capacity and moment redistribution) is a rigorous application of beam theory, conservatively assuming a knife edge support which produces a sharp peak in the inelastic curvature distribution over the partial hinge. However, rotation capacities are considerably larger for the more realistic support condition of finite bearing widths, since it must then be assumed that the curvature peak is spread over a finite length and rounded. This effect will deserve more attention in experiment and analysis. A possible approach to further investigation is indicated at the end of Chapter 5.

BIBLIOGRAPHY

I. General References

1. Winter, G., "Commentary on the 1968 Edition of the Specification for the Design of Coldformed Steel Structural Members," American Iron and Steel Institute, N.Y., 1970.

2. Freudenthal, A. M., "The Inelastic Behavior of Engineering Materials and Structures," John Wiley & Sons, N.Y., Chapman & Hall, Ltd., London, 1950.

3. Hoff, N. J., "The Analysis of Structures," John Wiley & Sons, 1966.

4. Gerard, G., "Introduction to Structural Stability Theory," McGraw-Hill, 1962.

5. Timoshenko, S. and Gere, J. M., "Theory of Elastic Stability," McGraw-Hill, 2nd Edition, 1961.

6. Prager, W., "An Introduction to Plasticity," Addison-Wesley, 1959.

7. Prager, W., and Hodge, P. G., "Theory of Perfectly Plastic Solids," Dover, 1951.

8. Bridgman, P. W., "Dimensional Analysis," Yale University Press, New Haven, 1943.

9. Langhaar, H. L., "Dimensional Analysis and Theory of Models," John Wiley & Sons, 1951.

II. Specifications and Commentaries to Specifications

10. Specifications for the Design of Coldformed Steel Structural Members, 1968 Edition, American Iron and Steel Institute, N.Y., 1970. (Commentary see Ref. 1.)

11. Specifications for the Design, Fabrication and Erection of Structural Steel for Buildings, AISC, N.Y., 1969.

12. Commentary on the AISC Specification, AISC, N.Y., 1969.

13. Plastic Design in Steel, a Guide and Commentary, AISC, N.Y., 1971.

III. Special References

14. Von Kármán, T., Sechler, E. E., and Donnell, L. H., "The Strength of Thin Plates in Compression," Trans. ASME, Vol. 54, p. 53, 1932.

15. Winter, G., "Strength of Thin Steel Compression Flanges," Trans. ASCE, Vol. 112, 1947.

16. Winter, G., "Performance of Thin Steel Compression Flanges," IABSE, Third Congress, Liège, Preliminary Publication, p. 317, 1948.

17. Gerard, G., "Handbook of Structural Stability; Part IV - Failure of Plates and Composite Elements," Technical Note 3784, NACA, Washington, D.C., 1957.

18. Graves-Smith, T. R., "The Ultimate Strength of Locally Buckled Columns of Arbitrary Length," Ph.D. Thesis, Cambridge University, 1966.

19. Johnson, A. L., "The Structural Performance of Austenitic Stainless Steel Members," Ph.D. Thesis, Cornell University, 1967.

20. Von Kármán, T., "Untersuchungen über Knickfestigkeit," Forschungsarbeiten, No. 81, Berlin, 1910.

21. Von Kármán, T., with Dunn, L. G., and Tsien, H. S., "The Influence of Curvature on the Buckling Characteristics of Structures," Journ. Aero. Sci., Vol. 7, p. 276, 1940.

22. Drucker, D. C., and Onat, E. T., "On the Concept of Stability of Inelastic Systems," Journ. Aero. Sci., Vol. 21, p. 543, 1954.

23. Lay, M. G., "Flange Local Buckling in Wide Flange Shapes," Journal of the Structural Division, ASCE, Vol. 91, ST6 (4554), 1965.

24. Britvec, S. J., Chajes, A., Karren, K. W., Uribe, J., and Winter, G., "Effects of Cold Work in Coldformed Steel Structural Members," Cornell Engineering Research Bulletin, No. 70-1, 1970.

25. Korol, R. M., and Hudoba, J., "Plastic Behavior of Hollow Structural Sections," Journal of the Structural Division, ASCE, Vol. 98, ST5 (8872), 1972.

APPENDIX 2.1

ANALYTICAL BASIS FOR M-ϕ RELATIONSHIP

ACCORDING TO BEAM THEORY

The behavior of a beam section under pure bending about one principal axis can be described by the following set of equations

$$\sigma^* = E\varepsilon^* \qquad \text{for } \varepsilon^* < \varepsilon_y$$
$$\sigma^* = \sigma_y \qquad \text{for } \varepsilon^* \geq \varepsilon_y \qquad \text{(A2.1-1)}$$

$$\phi = \frac{\varepsilon^*}{\bar{y}^* - \bar{y}_o} \qquad \text{(A2.1-2)}$$

$$y_p = \frac{\varepsilon_y}{\phi} = \frac{\varepsilon_y}{\varepsilon^*}\,(\bar{y}^* - \bar{y}_o) \qquad \text{(A2.1-3)}$$

for $\varepsilon^* < \varepsilon_y$:

$$\sum H = 0 = \int_A \sigma dA = \sigma^* \int_{A_{el}} \frac{\bar{y} - \bar{y}_o}{\bar{y}^* - \bar{y}_o}\, dA + \sigma_y \int_{A_{pl}} dA \qquad \text{(A2.1-4a)}$$

$$\sum M_i = M = \int_A \sigma y dA = \sigma^* \int_{A_{el}} \frac{(\bar{y} - \bar{y}_o)^2}{\bar{y}^* - \bar{y}_o}\, dA + \sigma_y \int_{A_{pl}} (\bar{y} - \bar{y}_o) dA \qquad \text{(A2.1-5a)}$$

for $\varepsilon^* \geq \varepsilon_y$

$$\sum H = 0 = \sigma_y \int_{A_{el}} \frac{\bar{y} - \bar{y}_o}{y_p}\, dA + \sigma_y \int_{A_{pl}} dA \qquad \text{(A2.1-4b)}$$

$$\sum M_i = M = \sigma_y \int_{A_{el}} \frac{(\bar{y} - \bar{y}_o)^2}{y_p}\, dA + \sigma_y \int_{A_{pl}} (\bar{y} - \bar{y}_o) dA \qquad \text{(A2.1-5b)}$$

Eq. A2.1-1 is the elastic-plastic stress-strain law. Eq. A2.1-2 reflects the principle that the section remains plane in bending. ε^* is a parameter of the linear strain-distribution at the point defined by $\bar{y}^*$. $\bar{y}^*$ is not a variable of the beam equations. It may, e.g., define the position of a strain gage by which the strain ε^* is measured. $\bar{y}_o$ determines the position of the neutral axis. Fig. A2.1-1 illustrates the coordinate systems. Eq. A2.1-3 establishes the boundary between elastic and plastic zones of the section, where y_p is the distance from the neutral axis to this boundary. A2.1-4a and A2.1-5a are the equilibrium conditions of the section for the elastic-perfectly plastic stress-strain law, if $\bar{y}^*$ denotes a point within the elastic zone ($\varepsilon^* < \varepsilon_y$). A_{el} indicates integration over the elastic portion of the section, A_{pl} integration over the plastic portion. These portions are defined by y_p. If $\bar{y}^*$ denotes a point in the plastic zone ($\varepsilon^* > \varepsilon_y$), the equilibrium conditions are given by Eqs. A2.1-4b and A2.1-5b. The variables of the section in bending throughout the loading history are

$$\varepsilon^*,\ \sigma^*,\ \bar{y}_o,\ y_p,\ \phi \text{ and } M \qquad \text{(A2.1-6)}$$

There are five independent equations and six variables. Choosing one independent variable, any of the remaining variables can be expressed as a function of the independent variable.

In Chapter 2, an ultimate compressive strain failure

criterion is established for coldformed stiffened beams (see Eq. 2.7). In this case $\varepsilon^* = \varepsilon_{c,u}$ is specified, and any of the remaining variables can be computed from Eqs. A2.1-1 to A2.1-5.

In Tables 2.4 and 2.5 values M_{ctd} and ϕ_{ctd} were computed from ultimate compressive strains. In this case, $\varepsilon_{c,u}$ was not determined by Eq. 2.7, but, directly measured values $\varepsilon_{c,u}$ from the individual experiments where used in the computation. It was intended to check the validity of the idealized beam equations (A2.1-1 to A2.1-5) in predicting realistic experimental values M_u and ϕ_u, if the computation is based on ultimate compressive strains.

If M-ϕ relationships, based on the effective width formula, Eq. 2.2, are computed, there will be as many additional equations as there are additional unknowns. Again, with one independent variable specified, all other variables can be computed.

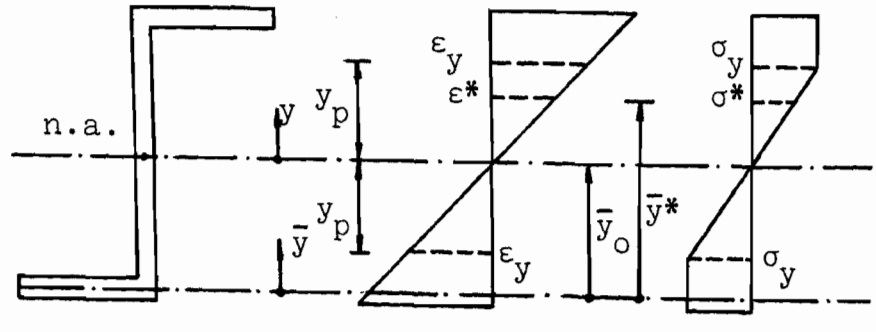

Fig. A2.1-1

NOTATIONS FOR THE EQUATIONS OF BEAM THEORY

APPENDIX 3.1

MOMENT-CURVATURE RELATIONSHIP OF MONOSYMMETRIC SECTION IN NON-DIMENSIONAL FORM

It is convenient to define the geometric variables initially with reference to the flange where initial yielding occurs. Index "1" and "2" shall refer to the flange that yields first and second, respectively. The β-parameters with respect to this definition shall be distinguished with a *-superscript and given as follows

$$\beta_1^* = \frac{b_1 + b_2}{4d} \quad , \quad \beta_2^* = \frac{b_2 - b_1}{4d}$$

β_2^* in this form is always positive, since $b_2 > b_1$. We will first introduce the possible stress distributions across the section, throughout the elastic and inelastic moment-curvature relationship. Consistent with Chapter 3, stiffening lips will not be taken into account.

1) Stress-Distribution between Discontinuities

The section prototype and the three possible stress-distributions across the section in the elastic and inelastic range are shown in Fig. A3.1-1, together with the notations used in the following equations. The stress-distributions shall be identified as State I in the elastic range, State II as long as only one flange is yielding and State III if both flanges are yielding.

2) Non-Dimensional Moment-Curvature Relationships

The non-dimensional equations will be fully derived for the elastic state to demonstrate the procedure. For the following states, the equations will be given without the elementary derivations.

State I

The equilibrium condition for the horizontal stresses is $\int_A \sigma dA = 0$, where A denotes integration over the area of the cross-section. With $\sigma = E\phi y$, the condition can be simplified as follows

$$E\phi \int_A y dA = 0$$

or

$$\int_A y dA = 0$$

For the section prototype of Fig. A3.1-1 this produces the following equation

$$(b_1 y_1 - b_2 y_2 + 2 \times \frac{1}{2} y_1^2 - 2 \times \frac{1}{2} y_2^2) = 0$$

With $y_2 = d - y_1$

$$y_1(b_1 + b_2 + 2d) - d^2 - b_2 d = 0$$

$$\frac{y_1}{d} = \frac{1 + \frac{b_2}{d}}{\frac{b_1 + b_2}{d} + 2}$$

With $\frac{b_2}{d} = 2(\beta_1^* + \beta_2^*)$ and $\frac{b_1 + b_2}{d} = 4\beta_1^*$ we obtain

$$\frac{y_1}{d} = \frac{\beta_1^* + \beta_2^* + \frac{1}{2}}{2\beta_1^* + 1} = \frac{1}{2} + \frac{\beta_2^*}{2\beta_1^* + 1} \qquad \text{(A3.1-1)}$$

The equilibrium condition between internal and external moment is expressed by

$$\int_A \sigma y dA = E\phi \int_A y^2 dA = M$$

For the section prototype of Fig. A3.1-1, this produces the following equation

$$M = E\phi t(b_1 y_1^2 + b_2 y_2^2 + 2 \times \frac{1}{3} y_1^3 + 2 \times \frac{1}{3} y_2^3)$$

With $y_2 = d - y_1$

$$M = E\phi t\left(b_1 y^2 + b_2 (d-y_2)^2 + \frac{2}{3} y_1^3 + \frac{2}{3}(d-y_1)^3\right)$$

With $\frac{b_1}{d} = 2(\beta_1^* - \beta_2^*)$, $\frac{b_2}{d} = 2(\beta_1^* + \beta_2^*)$ and, taking d^3 out of the parentheses, we obtain

$$M = E\phi t d^3 2[(\beta_1^* - \beta_2^*)(\frac{y_1}{d})^2 + (\beta_1^* + \beta_2^*)(1 - \frac{y_1}{d})^2 + \frac{1}{3}(\frac{y_1}{d})^3 + \frac{1}{3}(1 - \frac{y_1}{d})^3]$$

We can now divide both sides by σ_y to write the equation in the following form

$$\frac{M}{\sigma_y t d^2} = \frac{\phi d}{\varepsilon_y} 2[(\beta_1^* - \beta_2^*)(\frac{y_1}{d})^2 + (\beta_1^* + \beta_2^*)(1 - \frac{y_1}{d})^2 + \frac{1}{3}(\frac{y_1}{d})^3 + \frac{1}{3}(1 - \frac{y_1}{d})^3] \qquad \text{(A3.1-2)}$$

where $\frac{y_1}{d}$ is defined by Eq. A3.1-1. All arguments in the above equation are dimensionless. With notations

$$m = \frac{M}{\sigma_y t d^2}, \quad \kappa = \phi d \tag{A3.1-3}$$

and

$$i = 2[(\beta_1^* - \beta_2^*)(\frac{y_1}{d})^2 + (\beta_1^* + \beta_2^*)(1 - \frac{y_1}{d})^2 + \frac{1}{3}(\frac{y_1}{d})^3 + \frac{1}{3}(1 - \frac{y_1}{d})^3] \tag{A3.1-4}$$

we obtain

$$m = i \frac{\kappa}{\varepsilon_y} \tag{A3.1-5}$$

The normalized curvature κ depends on the strains in the flanges in the following way

$$\frac{\kappa}{\varepsilon_y} = \frac{\varepsilon_1}{\varepsilon_y} \frac{d}{y_1} = \frac{\varepsilon_2}{\varepsilon_y} \frac{d}{y_2} \tag{A3.1-6}$$

This transformation is true throughout the elastic and inelastic moment-curvature relationship.

State I terminates with initial yielding at flange 1, as $\varepsilon_1 = \varepsilon_y$. From Eq. A3.1-6

$$\frac{\kappa_y}{\varepsilon_y} = \frac{d}{y_1} = \frac{2\beta_1^* + 1}{\beta_1^* + \beta_2^* + \frac{1}{2}} \tag{A3.1-7}$$

and

$$m_y = i \frac{\kappa_y}{\varepsilon_y} = i \frac{2\beta_1^* + 1}{\beta_1^* + \beta_2^* + \frac{1}{2}} \tag{A3.1-8}$$

State II

After initial yielding at flange 1, but before initial yielding at flange 2

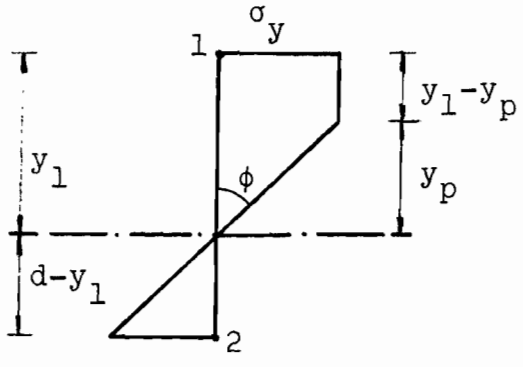

$$\phi = \frac{\varepsilon}{y}$$

Elastic: $\sigma = E\phi y$

Plastic: $\sigma = \sigma_y$

$$\sum H = 0 = \int_A \sigma dA = E\phi \int_{A_{el}} y dA + \sigma_y \int_{A_{pl}} dA$$

$$\longrightarrow \quad E\phi t[-2\times\tfrac{1}{2}y_p^{\,2} + 2\times\tfrac{1}{2}(d-y_1)^2 + b_2(d-y_1)]$$

$$- \sigma_y t[2(y_1-y_p) + b_1] = 0$$

With $y_p = \frac{\varepsilon_y}{\phi}$, dividing the equation by $E\phi t$ and d^2

$$-(\frac{\varepsilon_y}{\phi d})^2 + (1 - \frac{y_1}{d})^2 + \frac{b_2}{d}(1 - \frac{y_1}{d}) - 2\,\frac{\varepsilon_y}{\phi d}\,\frac{y_1}{d} + 2(\frac{\varepsilon_y}{\phi d})^2 - \frac{b_1}{d}\,\frac{\varepsilon_y}{\phi d} = 0$$

With $\phi d = \kappa$, after some rearrangement, we obtain

$$(\frac{y_1}{d})^2 - 2\,\frac{y_1}{d}(1 + \frac{\varepsilon_y}{\kappa} - \frac{1}{2}\,\frac{b_2}{d}) - \frac{b_1}{d}\,\frac{\varepsilon_y}{\kappa} + \frac{b_2}{d} + 2(\frac{\varepsilon_y}{\kappa})^2 = 0$$

With $\frac{b_1}{d} = 2(\beta_1^* - \beta_2^*)$ and $\frac{b_2}{d} = 2(\beta_1^* + \beta_2^*)$

$$\left(\frac{y_1}{d}\right)^2 - 2\,\frac{y_1}{d}\left[1 + \frac{\varepsilon_y}{\kappa} - (\beta_1^* + \beta_2^*)\right] - 2\,\frac{\varepsilon_y}{\kappa}(\beta_1^* - \beta_2^*)$$

$$+ 2(\beta_1^* + \beta_2^*) + 2\left(\frac{\varepsilon_y}{\kappa}\right)^2 = 0 \qquad \text{(A3.1-9)}$$

$$\sum M_i = M = \int_A \sigma y dA = E\phi \int_{A_{el}} y^2 dA + \sigma_y \int_{A_{pl}} y dA$$

i.e.,

$$M = E\phi t\left[b_2(d-y_1)^2 + 2\times\frac{1}{3}(d-y_1)^3 + 2\times\frac{1}{3}y_p^3\right]$$

$$+ \sigma_y t\left[b_1 y_1 + 2\,(y_1 - y_p)\,\frac{1}{2}(y_1 + y_p)\right]$$

With $m = \dfrac{M}{\sigma_y t d^2}$ and $\dfrac{\kappa}{\varepsilon_y} = \dfrac{\phi d}{\varepsilon_y}$, and making the geometric variables dimensionless, this equation can be rearranged as follows

$$m = 2\left\{\frac{\kappa}{\varepsilon_y}\left[(\beta_1^* + \beta_2^*)\left(1 - \frac{y_1}{d}\right)^2 + \frac{1}{3}\left(1 - \frac{y_1}{d}\right)^3\right]\right.$$

$$\left. + \frac{y_1}{d}(\beta_1^* - \beta_2^*) + \frac{1}{2}\left(\frac{y_1}{d}\right)^2 - \frac{1}{6}\left(\frac{\varepsilon_y}{\kappa}\right)^2\right\} \qquad \text{(A3.1-10)}$$

Eq. A3.1-9 shows that the position of the neutral axis is a function of $\frac{\kappa}{\varepsilon_y}$ (i.e., the curvature), and therefore is not constant. Eq. A3.1-9 is a quadratic equation in y_1/d. If the solution is substituted in Eq. A3.1-10, we obtain the normalized moment-curvature relationship, without any additional unknown. However, the result is a rather complicated algebraic function which cannot be solved in closed form for κ. As long as we are merely interested in the moment-curvature relationship, κ can be treated as the independent variable,

and a solution for κ is not required. However, in determining the plastic rotation of a partial hinge, integration over the curvature must be carried out, which requires an explicit solution of the moment-curvature relationship for κ. In this case a numerical procedure will have to be employed to obtain solutions for specified numerical values.

The bounds of state II are derived from the neighboring states I and III.

State III

Both flanges are yielding

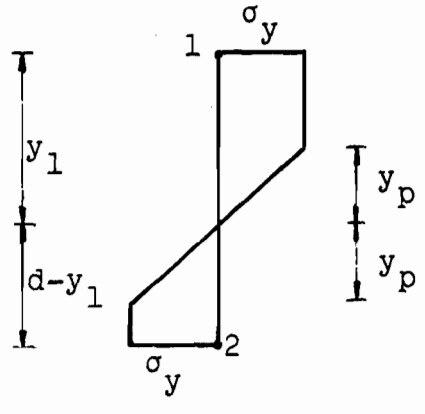

$$\sum H = 0 = E\phi \int_{A_{el}} y\,dA + \sigma_y \int_{A_{pl}} dA$$

$$\sum M_i = M = E\phi \int_{A_{el}} y^2\,dA + \sigma_y \int_{A_{pl}} y\,dA$$

$\sum H = 0$ (the elastic areas cancel each other out)

$$b_1 - b_2 + 2(y_1 - y_p) - 2(d - y_1 - y_p) = 0$$

$$4\,\frac{y_1}{d} - 2 - 4\beta_2^* = 0$$

$$\frac{y_1}{d} = \frac{1}{2} + \beta_2^* \qquad \text{(A3.1-11)}$$

From $\sum M_i = M$

$$m = 2[\beta_1^* - (\beta_2^*)^2 + \frac{1}{4} - \frac{1}{3}(\frac{\varepsilon_y}{\kappa})^2] \qquad \text{(A3.1-12)}$$

The full plastic moment is obtained as $\kappa \to \infty$. Eq. A3.1-12 then reduces to

$$m_p = 2[\beta_1^* - (\beta_2^*)^2 + \frac{1}{4}] \qquad \text{(A3.1-13)}$$

and Eq. A3.1-12 can be written in the form

$$m = m_p - \frac{2}{3}(\frac{\varepsilon_y}{\kappa})^2 \qquad \text{(A3.1-14)}$$

Transition from state II to state III occurs as $\varepsilon_2 = \varepsilon_y$. From

$$\frac{\kappa}{\varepsilon_y} = \frac{\varepsilon_2}{\varepsilon_y}\frac{d}{y_2} = \frac{\varepsilon_2}{\varepsilon_y}\frac{1}{1 - y_1/d}$$

we obtain

$$\frac{\kappa_{II,max}}{\varepsilon_y} = \frac{\kappa_{III,min}}{\varepsilon_y} = \frac{1}{\frac{1}{2} - \beta_2^*} \qquad \text{(A3.1-15)}$$

and

$$m_{II,max} = m_{III,min} = m_p - \frac{2}{3}(\frac{1}{2} - \beta_2^*)^2 \qquad \text{(A3.1-16)}$$

We can now also bound the range of state II. From Eq. A3.1-7 and Eq. A3.1-15, the range of state II is defined by

$$\frac{2\beta_1^* + 1}{\beta_1^* + \beta_2^* + \frac{1}{2}} \leq \frac{\kappa_{II}}{\varepsilon_y} \leq \frac{1}{\frac{1}{2} - \beta_2^*} \qquad \text{(A3.1-17)}$$

3) Failure Condition

The failure condition is given in terms of a compression strain failure condition. Since the variables above do not distinguish between tension and compression flange, but between first and second yielding, we must now correlate the two reference systems. The compressive failure strain shall be identified by the notation $\varepsilon_{c,u}$. The geometric parameters with respect to tension and compression flange are

$$\beta_1 = \frac{b_t + b_c}{4d}, \quad \beta_2 = \frac{b_t - b_c}{4d} \qquad \text{(A3.1-18)}$$

The transformation from compressive failure strain into curvature is given by the equation

$$\frac{\kappa_u}{\varepsilon_y} = \frac{\varepsilon_{c,u}}{\varepsilon_y} \frac{d}{y_c} \qquad \text{(A3.1-19)}$$

Case 1

The tension flange yields first, therefore $b_1 = b_t$, $\varepsilon_1 = \varepsilon_t$, $y_1 = y_t$ and $b_2 = b_c$, $\varepsilon_2 = \varepsilon_c$, $y_2 = y_c$. Further

$$\beta_1^* = \frac{b_t + b_c}{4d} = \beta_1$$

and

$$\beta_2^* = -\frac{b_t - b_c}{4d} = -\beta_2$$

However, for case 1, $b_c > b_t$ and therefore

$$\beta_2^* = |\beta_2|$$

Therefore, Eq. A3.1-1 to A3.1-17 will all be valid in the

given form for parameters β_1 and β_2, if β_1^* is replaced by β_1, and β_2^* is replaced by $|\beta_2|$.

Failure can only occur within state III or at the transition to state III. With $y_c = y_2$ we obtain from Eq. A3.1-19 and Eq. A3.1-11

$$\frac{\kappa_u}{\varepsilon_y} = \frac{\varepsilon_{c,u}}{\varepsilon_y}\,\frac{d}{y_2} = \frac{\varepsilon_{c,u}}{\varepsilon_y}\,\frac{1}{(1 - y_1/d)} = \frac{\varepsilon_{c,u}}{\varepsilon_y}\,\frac{1}{\frac{1}{2} - |\beta_2|} \qquad \text{(A3.1-20)}$$

and from Eq. A3.2-13

$$m_u = m_p - \frac{2}{3}\left(\frac{\varepsilon_y}{\kappa_u}\right)^2$$

Case 2

The compression flange yields first, therefore $b_1 = b_c$, $\varepsilon_1 = \varepsilon_c$, $y_1 = y_c$ and $b_2 = b_t$, $\varepsilon_2 = \varepsilon_t$, $y_2 = y_t$. Further

$$\beta_1^* = \beta_1 \quad \text{and} \quad \beta_2^* = \frac{b_t - b_c}{4d} = \beta_2$$

Since $b_t > b_c$, β_2 will always be positive. Hence, if desired, we can again write $\beta_2^* = |\beta_2|$. Thus we see that Eq. A3.1-1 to Eq. A3.1-17 are true in the given form with respect to the β-parameters both for case 1 and case 2, if β_1^* is replaced by β_1 and β_2^* is replaced by $|\beta_2|$. The moment-curvature relationships do therefore not depend on the sign of the β_2-parameter in any case. This will be different for the failure condition. Failure in case 2 can occur in state II or state III. If failure occurs in state III we have

$$\frac{\kappa_u}{\varepsilon_y} = \frac{\varepsilon_{c,u}}{\varepsilon_y}\,\frac{d}{y_1} = \frac{\varepsilon_{c,u}}{\varepsilon_y}\,\frac{1}{\frac{1}{2}+|\beta_2|}$$

and (A3.1-21)

$$m_u = m_p - \frac{2}{3}\left(\frac{\varepsilon_y}{\kappa_u}\right)^2$$

By comparison of Eq. A3.1-20 and A3.1-21 it is seen that the failure values of the two cases in state III are different. Failure will occur in state III, only if

$$\frac{\kappa_u}{\varepsilon_y} = \frac{\varepsilon_{c,u}}{\varepsilon_y}\,\frac{1}{\frac{1}{2}+|\beta_2|} > \frac{1}{\frac{1}{2}-|\beta_2|} \qquad \text{(A3.1-22)}$$

If condition A3.1-22 is not satisfied, failure will occur in state II. The ultimate normalized curvature is obtained as follows. From Eq. A3.1-19,

$$\frac{y_c}{d} = \frac{\varepsilon_{c,u}}{\varepsilon_y}\left(\frac{\varepsilon_y}{\kappa_u}\right) \qquad \text{(A3.1-23)}$$

Substituting this equation into Eq. A3.1-9, we obtain

$$\left(\frac{\varepsilon_{c,u}}{\varepsilon_y}\,\frac{\varepsilon_y}{\kappa_u}\right)^2 - 2\,\frac{\varepsilon_{c,u}}{\varepsilon_y}\,\frac{\varepsilon_y}{\kappa_u}\left(1+\frac{\varepsilon_y}{\kappa_u}+\beta_1+|\beta_2|\right)$$

$$-\frac{2\varepsilon_y}{\kappa_u}\left(\beta_1-|\beta_2|\right)+2(\beta_1+|\beta_2|)+\left(\frac{\varepsilon_y}{\kappa_u}\right)^2 = 0$$

This is a quadratic equation in κ_u as follows

$$2\left(\frac{\kappa_u}{\varepsilon_y}\right)^2(\beta_1 + |\beta_2|) - \frac{\kappa_u}{\varepsilon_y}\left[2\,\frac{\varepsilon_{c,u}}{y}\,(1 + \beta_1 + |\beta_2|) + 2(\beta_1 - |\beta_2|)\right]$$

$$- \left(\frac{\varepsilon_{c,u}}{\varepsilon_y} - 1\right) = 0 \qquad \text{(A3.1-24)}$$

This equation must be solved for κ_u. With κ_u known, we also know y_c/d from Eq. A3.1-23. We can now substitute the values of κ_u and y_c/d into Eq. A3.1-10, for κ and y_1/d, respectively, to obtain the normalized ultimate moment m_u.

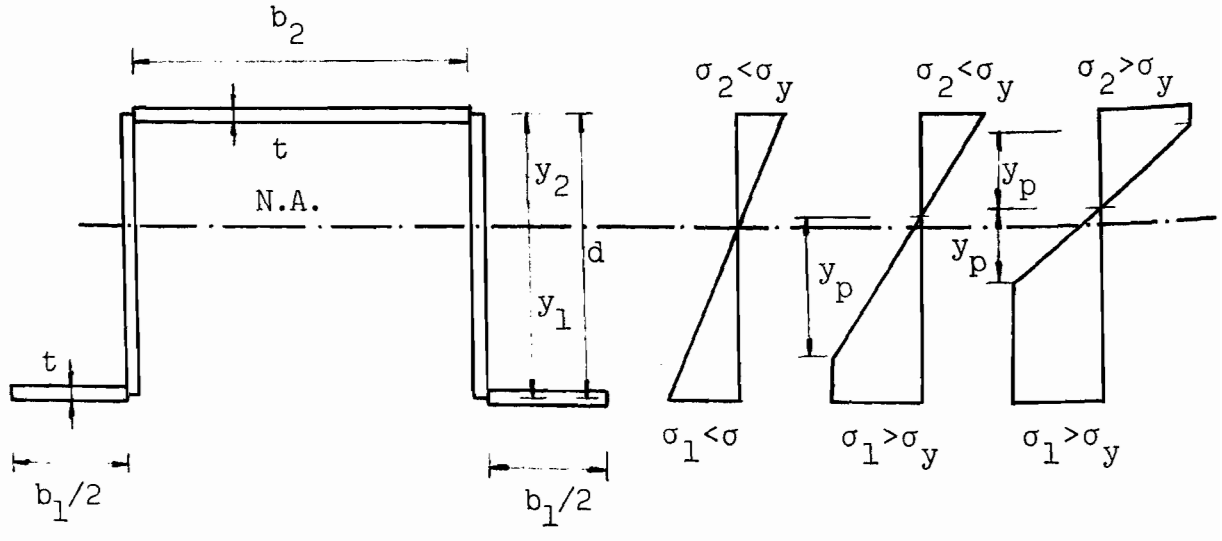

Fig. A3.1-1

ELASTIC AND INELASTIC STRESS DISTRIBUTIONS
FOR THE PROTOTYPE SECTION

APPENDIX 3.2

DIMENSIONAL COMPUTATION OF ULTIMATE MOMENT FOR ECCENTRIC COLDFORMED SHAPES WITH COMPRESSIVE STRAIN FAILURE CRITERION

Example 1: Initial Yielding in Tension

(A graphical solution for this example will be given in Appendix 3.3, Example 1.)

Given: (a) Specified minimum yield point σ_y = 36 ksi

(b) Dimensions of cross-section as follows

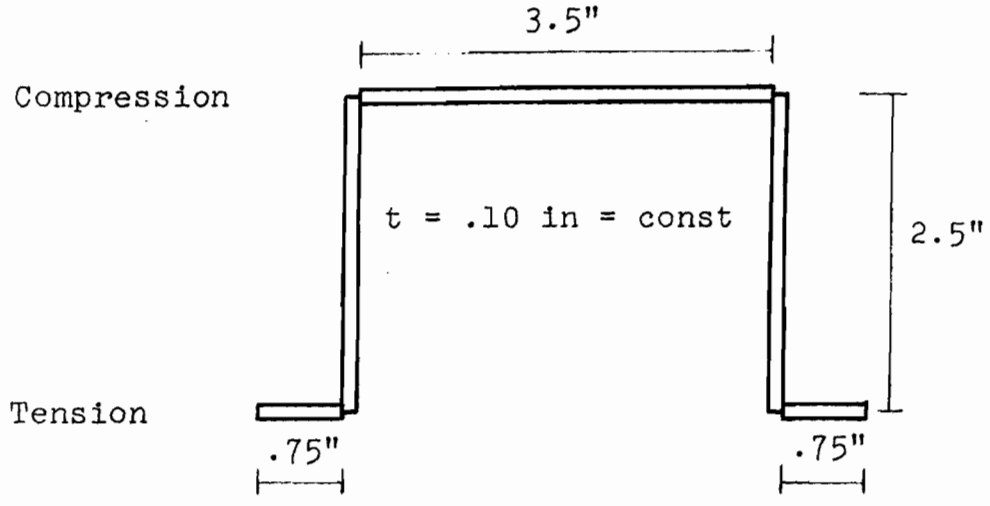

Required: Ultimate moment M_y and inelastic reserve strength in terms of M_u/M_y

Solution:

a) Failure Criterion:

With corner radius R ≈ .10 in → $w/t = \frac{3.5 - .2}{.10} = 33.$

According to failure criterion of Eq. 2.7, with $(w/t)_{lim}$ = 37 → $w/t < .92(w/t)_{lim} = 34$, i.e., $\varepsilon_{c,u}/\varepsilon_y = 3$.

b) Yield Moment

	Area, in^2	$\bar{y}$, in	$A\bar{y}$, in^2	y, in	Ay^2, in^4	I_o, in^4
Compression Flange	.10×3.5 = .35	0	0	1.00	.3500	∿0
Webs	2×.10×2.5 = .50	1.25	.625	-.25	.0312	$2\times\frac{d^3t}{12}$ = .2604
Tension Flange	.10×1.5 = .15	2.50	.375	-1.50	.3375	∿0
	$\sum A = 1.00$		$\sum A\bar{y} = 1.000$		$\sum Ay^2 = 0.7187$	
					$I_o = .2604$	
					$I = .9791\ in^4$	

$$y_c = \frac{1.00}{1.00} = 1.00 \text{ in}, \quad y_t = 1.50 \text{ in}$$

$$M_y = \frac{\sigma_y I}{y_t} = \frac{36 \times .9791}{1.50} = 23.498 \text{ k-in} = 1.958 \text{ k-ft}$$

c) Ultimate Moment

By inspection, both flanges will have yielded prior to failure. Hence, the shape of the stress-distribution across the section at failure is known, i.e.

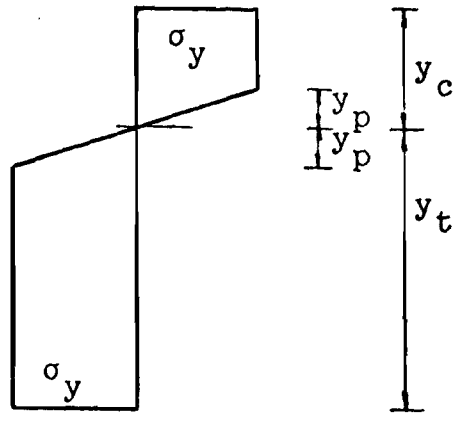

Equilibrium condition $\sum H = 0$

$$\sigma_y t[b_c + 2\times(y_c - y_p) + 2\times\tfrac{1}{2} y_p - 2\times\tfrac{1}{2} y_p - 2\times(y_t - y_p) - b_t] = 0$$

$$b_c + 2y_c - 2y_t - b_t = 0$$

With $y_t = d - y_c$

$$b_c + 4y_c - 2d - b_t = 0$$

$$y_c = \tfrac{1}{4}(b_t - b_c + 2d) = \tfrac{1}{4}(1.50 - 3.50 + 5.0) = .75 \text{ in.}$$

$$\underline{y_t} = 2.50 - .75 = \underline{1.75 \text{ in.}}$$

Compatibility condition (linear strain distribution)

$$\frac{\varepsilon_{c,u}}{\varepsilon_y} = \frac{y_c}{y_p} \rightarrow y_p = y_c \frac{\varepsilon_y}{\varepsilon_{c,u}} = \frac{.75}{3} = .25 \text{ in}$$

$$y_c - y_p = .75 - .25 = .50 \text{ in}$$

$$y_t - y_p = 1.75 - .25 = 1.50 \text{ in}$$

Equilibrium condition $\sum M_i = M_u$

$$M_u = \sigma_y t[b_c y_c + 2\times(y_c - y_p)(y_p + \tfrac{1}{2}(y_c - y_p)) + 2\times\tfrac{2}{3} y_p^2$$

$$+ 2\times(y_t - y_p)(y_p + \tfrac{1}{2}(y_t - y_p)) + b_t y_t)]$$

$$= 36\times.10[3.5\times.75 + 2\times.25\ (.25 + \tfrac{1}{2}\times.50) + 2\times\tfrac{2}{3}\times.25^2$$

$$+ 2\times1.50\times(.25\times(.25 + \tfrac{1}{2}\times1.50) + 1.50\times1.75]$$

$$\underline{M_u} = 36 \times .10 \times 8.833 = 31.80 \text{ k-in} = \underline{2.65 \text{ k-ft}}$$

Finally

$$\frac{M_u}{M_y} = \frac{2.65}{1.958} = 1.353$$

and the problem is solved.

Example 2: Initial Yielding in Compression

The problem is the same as in Example 1, but a different section is used with initial yielding in compression. In this case, for high eccentricity of the neutral axis, the tension flange may not have yielded at failure. The computation of the ultimate moment, if the tension flange has not yielded, shall be demonstrated in the following.

Cross-section and dimensions:

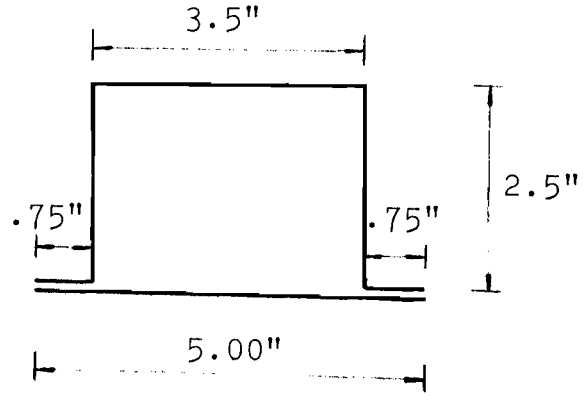

a) Failure Criterion same as before, $\varepsilon_{c,u}/\varepsilon_y = 3.$

b) Yield Moment

	Area, in^2	$\bar{y}$, in	$A\bar{y}$, in^3	y, in	Ay^2, in^4	I_o, in^4
Compression Flange	.10×3.5 = .35	0	0	1.50	.7875	∿0
Webs	2×.10×2.5 = .50	1.25	.625	.25	.0312	.2604
Tension Flange	.10×1.50 .10×5.00 = .65	2.50	1.625	-1.00	.6500	∿0
	$\sum A = 1.50$	$\sum A\bar{y} = 2.250$		$\sum Ay^2 = 1.4687$		
				$I_o = .2604$		
				$I = 1.7291\ in^4$		

$$y_c = \frac{2.25}{1.50} = 1.50 \text{ in.}$$

$$M_y = \frac{36 \times 1.7291}{1.50} = 41.4984 \text{ k-in} = 3.4582 \text{ k-ft}$$

c) Ultimate Moment

By inspection it cannot be said with certainty whether the tension flange has yielded at failure.

First, assume the tension flange has yielded (same stress diagram as in Example 1). The formula for the position of the neutral axis can be taken from Example 1, i.e.,

$$y_c = \frac{1}{4}(b_t - b_c + 2d) = \frac{1}{4}(6.5 - 3.5 + 5.0) = 2.00 \text{ in}$$

$$y_t = d - y_c = .50 \text{ in}$$

$$y_p = \frac{2.00}{3} = .666 \text{ in}$$

Since $y_p > y_t$, the tension flange has not yielded at failure! Therefore, stress-diagram at failure

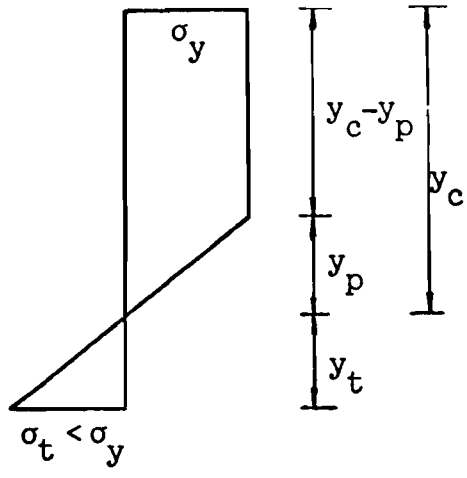

$$\sum H = 0$$

$$\sigma_y t[b_c + 2(y_c - y_p) + 2\times\frac{1}{2}y_p - 2\times\frac{1}{2}y_t\,\frac{\sigma_t}{\sigma_y} - b_t\,\frac{\sigma_t}{\sigma_y}] = 0$$

As before, $y_p = \frac{1}{3}\,y_c$, $y_t = d - y_c$. Also

$$\frac{\varepsilon_t}{\varepsilon_c} = \frac{y_t}{y_c} \rightarrow \varepsilon_t = \varepsilon_c\,\frac{y_t}{y_c} = \varepsilon_c\,\frac{d - y_c}{y_c}$$

$$\frac{\sigma_t}{\sigma_y} = \frac{\varepsilon_t}{\varepsilon_y} = \frac{\varepsilon_c}{\varepsilon_y}\,\frac{d - y_c}{y_c} = 3\,\frac{d - y_c}{y_c} = 3$$

Hence,

$$b_c + \frac{4}{3}\,y_c + \frac{1}{3}\,y_c - 3\,\frac{(d-y_c)^2}{y_c} - 3b_t\,\frac{d-y_c}{y_c} = 0$$

$$y_c^2 - \frac{3}{4}\,y_c(b_c + 6d + 3b_t) + \frac{9}{4}\,(d^2 + b_t d) = 0$$

$$y_c^2 - 28.500\,y_c + 50.625 = 0$$

$$\underline{y_c} = \frac{28.500 \ominus \sqrt{812.25 - 202.50}}{2} = \underline{1.9035\ \text{in}}$$

$$y_t = 2.5000 - 1.9035 = .5965 \text{ in}$$

$$y_p = \frac{1.9035}{3} = .6345 > y_t \rightarrow \text{ok.}$$

$$y_c - y_p = 1.2690 \text{ , } \quad \frac{\sigma_t}{\sigma_y} = 3\,\frac{y_t}{y_c} = 3 \times \frac{.5965}{.6345} = .9401$$

$$\sum M = M_u$$

$$M_u = \sigma_y t[b_c y_c + 2(y_c - y_p)(y_p + \tfrac{1}{2}(y_c - y_p)) + 2\times \tfrac{1}{3} y_p^2 + 2\times \tfrac{1}{3} y_t^3 \frac{\sigma_t}{\sigma_y}$$

$$b_t y_t \frac{\sigma_t}{\sigma_y}]$$

$$= 36\times.10[3.5\times1.9035 + 2\times1.2690\times(.6345 + \tfrac{1}{2}\times1.2690)$$

$$+ \tfrac{2}{3}\times.6345^2 + \tfrac{2}{3}\times.5965^2\times.9401 + 6.5\times.5965\times.9401]$$

$$= 36\times.10\times14.0194 = 50.4698 \text{ k-in} = 4.2058 \text{ k-ft}$$

$$\underline{M_u} = \underline{4.2058 \text{ k-ft}}$$

With $M_y = 3.4582$ k-ft

$$\underline{\frac{M_u}{M_y}} = \frac{4.2058}{3.4582} = \underline{1.216}$$

The problem is solved.

APPENDIX 3.3

EXAMPLES FOR GRAPHICAL ULTIMATE STRENGTH DESIGN APPROACH FOR STATICALLY DETERMINATE BEAMS WITH ECCENTRIC SECTIONS

Example 1: Computation of Ultimate Load Carrying Capacity for Specified Section Dimensions

Given: (a) $\sigma_y = 3$ ksi

(b) Section geometry and dimensions, see Appendix 3.2, Example 1

(c) Beam under uniform load, Safety Factor = 1.66

(d) Span length L = 9 ft.

Required: Service load w_{SL} from ultimate strength design

Solution:

For the section in Appendix 3.2, Example 1, the following β-parameters are computed, according to Eq. 3.9. With $b_c = 3.5$, $b_t = 1.5$, $d = 2.5$

$$\beta_1 = \frac{b_t + b_c}{4d} = \frac{1.5 + 3.5}{10} = .5; \quad \beta_2 = \frac{b_t - b_c}{4d} = \frac{1.50 - 3.5}{10} = -.2$$

Dimensional yield moment, from Appendix 3.2, Example 1,

$$M_y = 1.958 \text{ k-ft}$$

Failure criterion from Eq. 2.7, as before,

$$\varepsilon_{c,u}/\varepsilon_y = 3$$

Hence, for graphical solution use design graphs of Fig. 3.2 or Fig. 3.3. From the graphs, with $\beta_1 = .5$, $\beta_2 = -.2$

$$\frac{M_u}{M_y} = p_S = 1.353$$

By definition $M_u = p_S M_y = 1.353 \times 1.958 = 2.649$ k-ft

$$w_u = \frac{8M_u}{L^2} = \frac{8 \times 2.649}{9^2} \times 1000 = 261 \text{ \#/ft}$$

Since $w_u = w_{S.L.} \times S.F.$, $w_{S.L.} = \frac{261}{1.66} = 157$ #/ft

and the problem is solved.

Example 2: Design of a Section for Specified Ultimate Load by Normalized Design Approach

Given: (a) $\sigma_y = 36$ ksi.

(b) Uniformly distributed load; Safety Factor = 1.66. Service load (live load + dead load), $w_{S.L.}$ = 120 #/ft.

(c) Span length L = 12 ft.

Required: Adequate section dimensions

Solution:

In dimensional design this problem would require a trial and error procedure. In an approach with normalized variables, a direct solution is possible by the following procedure.

(a) Select relative geometric proportions of the cross-section, not considering the sheet thickness t.

E.g.,

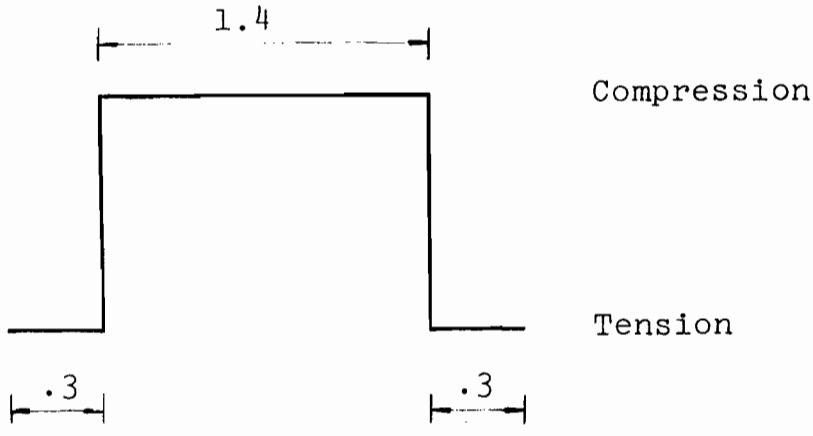

By inspection, initial yielding will occur at the tension flange. The geometric parameters, as defined by Eq. 3.9, of the normalized analysis, are

$$\beta_1 = \frac{b_t + b_c}{4d} = \frac{.06 + 1.4}{4} = .5$$

$$\beta_2 = \frac{b_t - b_c}{4d} = \frac{.6 - 1.4}{4} = -.2$$

(b) According to the failure criterion of Eq. 2.7,

$$\varepsilon_{c,u}/\varepsilon_y = 3 \text{ for } w/t \leq .92(w/t)_{lim}$$

For $\sigma_y = 36$ ksi, from the AISI design provisions, Ref. 10,

$$(w/t)_{lim} = \frac{221}{\sqrt{\sigma_y}} = \frac{221}{\sqrt{36}} = 37$$

Use $w/t \leq .92(w/t)_{lim} = 34$, i.e., $\varepsilon_{c,u}/\varepsilon_y = 3$.

(c) Ultimate load

$$w_u = w_{S.L.} \times \text{S.F.} = 120 \times 1.66 = 199 \text{ \#/ft}$$

Required ultimate moment

$$M_u = \frac{w_u L^2}{8} = \frac{199 \times 12^2}{8} = 3.582 \text{ k-ft}$$

(d) Inelastic load factor and yield load

$$p_u = \frac{w_u}{w_y} = p_S = \frac{M_u}{M_y} = \frac{m_u}{m_y} = 1.353$$

Hence,

$$w_y = \frac{w_u}{p_S} = \frac{199}{1.353} = 147 \text{ \#/ft}$$

We can now design for initial yielding, i.e., for M_y. However, since the section geometry is already determined to some degree, this has to be done by an analysis with normalized variables.

(e) Dimensioning of section. The normalized analysis of the moment-curvature relationship is given in Appendix 3.1. The normalized moment is $m = \frac{M}{\sigma_y t d^2}$. I.e., $m_y = \frac{M_y}{\sigma_y t d^2}$.

With $M_y = \frac{M_u}{p_S}$, we obtain $m_y = \frac{M_u}{p_S \sigma_y t d^2}$, from which

$td^2 = \frac{M_u}{m_y p_S \sigma_y}$. Hence, we have to determine the normalized yield moment m_y. m_y is given in graphical form in Fig. 3.6, as a function of β_1 and β_2. With $\beta_1 = .5$, $\beta_2 = -.2 \rightarrow$ $m_y = 1.04$. Hence,

$$td^2 = \frac{M_u}{m_y p_S \sigma_y} = \frac{3.582}{1.04 \times 1.353 \times 36} \times 12 = .845$$

Use $t = .10$ in ($\sim 12^{ga}$ sheet)

$\rightarrow d = \sqrt{8.449} = 2.907$ in

From the initial sketch of the geometric proportions of the section, $b_c = 1.4 \times d = 4.07$ in.

Check w/t-ratio with respect to initial assumption.

With corner radius $R \simeq .10$ in

$$w/t = \frac{4.07 - .2}{.10} = 38.7 > 34 \rightarrow \text{no good!}$$

Use $t = .11$ in $\rightarrow d = \sqrt{7.681} = 2.77$ in

$$b_c = 1.4 \times 2.77 = 3.88 \text{ in}$$

$$w/t = \frac{3.88 - .2}{.11} = 33.45 < 34 \rightarrow \text{ok!}$$

Final Dimensions

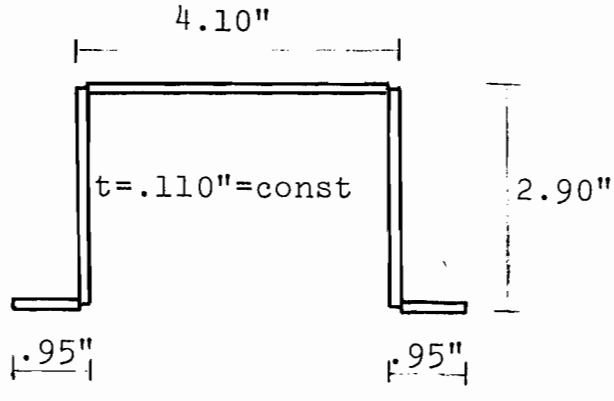

The problem is solved.

APPENDIX 5.1

DESIGN EXAMPLE FOR INELASTIC DESIGN OF REDUNDANT BEAM

Given: Steel with specified minimum yield point σ_y = 36 ksi.
Beam system and critical load case of elastic design (primary load case)

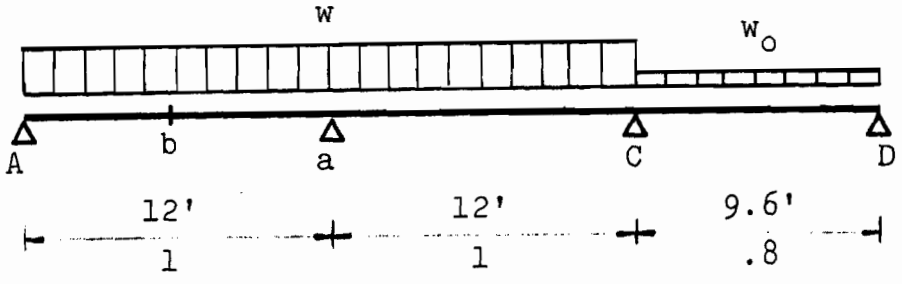

w_D = 30 #/ft, w_L = 120 #/ft

$w = w_D + w_L$ = 150 #/ft

Coefficients of elastic design

Primary load case (as indicated above)

from Handbook (Anger), also see Tables 5.1 and 5.2

$$M_a = \alpha_{a,1} wL^2_{max} = .1138\ wL^2_{max}$$

$$M_b = \alpha_{b,1} wL^2_{max} = .0746\ wL^2_{max}$$

Secondary load case

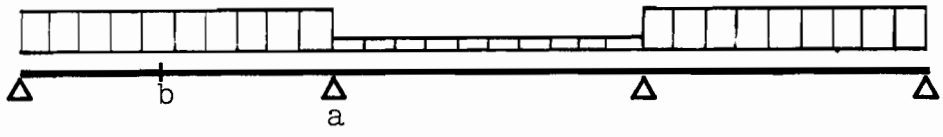

$$M_b = \alpha_{b,2} wL^2_{max} = .0938\ wL^2_{max}$$

Select type of cross-section

Only the relative dimensions of the section are needed (the thickness t does not have to be considered at all).

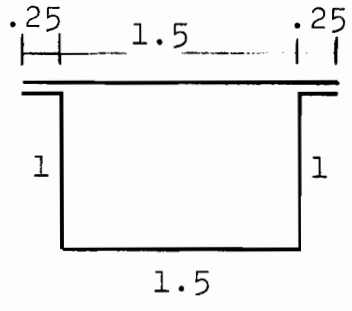

t = const

The geometric parameters needed for the graphical solution are β_1 and β_2 as defined by Eq. 3.9. For the selected proportions, (1) at interior support

$$\beta_1 = \frac{b_t + b_c}{4d} = \frac{2.5 + 1.5}{4} = 1.0$$

$$\beta_2 = \frac{b_t - b_c}{4d} = \frac{2.5 - 1.5}{4} = +.25 \quad (b_t \text{ refers to top flange})$$

(2) in span (b_t refers to bottom flange) $\beta_1 = 1.0$, $\beta_2 = -.25$

a) Design without moment redistribution

(Only the inelastic strength reserves of the section are considered.)

According to the failure criterion of Eq. 2.7 for $w/t < .92(w/t)_{lim} \rightarrow \varepsilon_{c,u}/\varepsilon_y = 3$. Use $w/t < .92(w/t)_{lim}$, i.e., for $\sigma_y = 36$ ksi, $w/t < 34$. The ratios $p_S = M_u/M_y$ can now be found from Fig. 3.2 (or Fig. 3.3)

At support, with $\beta_1 = 1.0$, $\beta_2 = .25 \rightarrow \frac{M_{u,a}}{M_y} = 1.20$

In span, with $\beta_1 = 1.0$, $\beta_2 = -.25 \rightarrow \frac{M_{u,b}}{M_y} = 1.23$

Inelastic load factor, assuming failure in primary load case, from Eq. 5.41

$$p_{u,1} = \frac{M_{u,a}}{M_y} = 1.20$$

assuming failure in secondary load case, from Eq. 5.42

$$p_{u,2} = \frac{\alpha_{a,1}}{\alpha_{b,2}} \frac{M_{u,b}}{M_y} = \frac{.1138}{.0938} \times 1.23 = 1.49$$

$p_{u,1}$ governs, i.e.,

$$p_{u,1} = p_u = \frac{w_u}{w_y} = 1.20$$

Design of Section (safety factor = 1.66)

$$w_u = 1.66 \times 150 = 250 \text{ \#/ft}$$

$$w_y = \frac{w_u}{p_u} = \frac{250}{1.20} = 207 \text{ \#/ft}$$

Design section with proportions given above by elastic design for initial yielding, i.e., for w_y. The dimensionless moment m_y can be computed from Appendix 3.1, Eqs. A3.1-1, A3.1-4, A3.1-8 for given values β_1, β_2. For simplicity use graphs Fig. 3.6, from which the following value is found

$$m_y = .963$$

By definition (Eq. 3.4)

$$m = \frac{M}{\sigma_y t d^2}, \text{ i.e., } td^2 = \frac{M_y}{\sigma_y m_y}$$

With $M_y = .1138\ w_y L_{max}^2$,

$$td^2 = \frac{.1138 \times .207 \times 12^2}{36 \times .963} \times 12 = 1.175 \text{ in}^3$$

Use t = .130 in ($\sim$ 10 gage)

$$d = \sqrt{\frac{1.175}{.130}} = 3.0 \text{ in}$$

From initial sketch of cross-section

$$b_{bottom} = 3.0 \times 1.5 = 4.5 \text{ in (= compression flange)}$$

Check w/t-ratio

$$w = b_c - 2t = 4.50 - .26 = 4.24 \text{ in}$$

$$w/t = \frac{4.24}{.130} = 32.5 < 34$$

Final dimensions

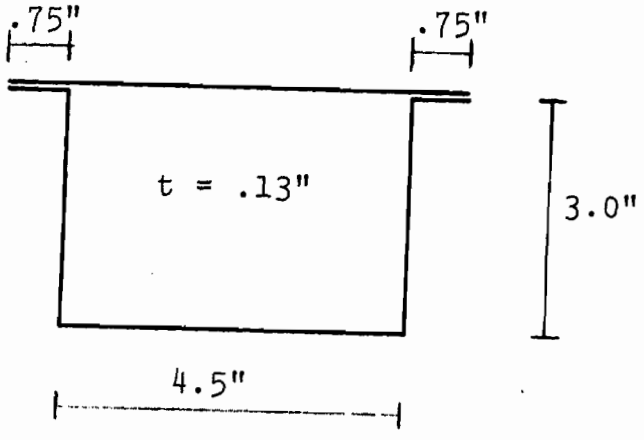

b) Design with moment redistribution

The design with moment redistribution has four restrictions:

(1) $L_{min}/L_{max} \geq .8$. In the given case $L_{min}/L_{max} = .8$, i.e., this condition is satisfied.

(2) It is only valid for uniform load w, which is also satisfied.

(3) and (4) Governing load case identical with governing load case of elastic design and failure within one-hinge failure mode (only one partial hinge at failure).

The last two restrictions must be checked by the formulas given in Eq. 5.54 and 5.53, respectively. According to Eq. 5.26, the inelastic load factor is $p_u = p_S + p_R$. If restrictions (3) and (4) apply,

$$p_S = \frac{M_{u,a}}{M_y}$$

i.e., $p_u = 1.20$ (from above);

p_R, the redistribution component, can be determined from the graphs of Fig. 5.6. With $\beta_1 = 1.0$ and $\beta_2 = +.25$

$$p_R = .029 \simeq .03$$

I.e., $p_u = 1.20 + .03 = 1.23$

Check condition 5.54:

$$p_u < \frac{\alpha_{a,1}}{\alpha_{b,2}} \frac{M_{u,b}}{M_y} = 1.49$$

(as above), satisfied since $p_u = 1.23 < 1.49$.

Check condition 5.53:

$$p_u < \frac{\alpha_{a,1}}{\alpha_{b,1}} (1 - .44\ p_R) = \frac{.1138}{.0746} (1 - .44 \times .03)$$

$$= 1.51, \text{ satisfied.}$$

Hence, the inelastic load factor $p_u = 1.23$ is valid for the given problem. The design can now continue in the same manner as above (design without moment redistribution) but with a slightly increased inelastic load factor.

Table 2.1. Material Properties

Sheet	Yield Stress (ksi)	Ultimate Tensile Strength (ksi)	Yield Strain* (E = 29,500 ksi)	Strain at Beginning Strainhardening
10-1	36.0		.00122	.00960
10-9	36.0	49 (Avg.)	.00122	.01600
10-10	37.4		.00127	.01800
12-1	37.0		.00125	.02000
12-2	36.0	48 (Avg.)	.00122	.01840
12-6	36.4		.00124	.02360
12-8	37.4		.00127	.02520
16-2	40.4	53	.00137	.02700
20-4	34.5	48	.00117	.02400

*Computed yield strains with E = 29,500 ksi.

Table 2.2. Geometry of Stiffened Sections

Specimen	Sheet	A (in)	B	C	D	E	t	R	w/t
HA1-10	10-1	5.075	3.235	1.540	-	-	.138	.125	33.0
HA2-12	12-1	4.725	3.245	1.510	-	-	.105		41.2
HA3-12	12-2	4.700	3.249	1.493	-	-	.103	.100	41.2
HA4-16	16-2	4.730	3.250	.750	-	-	.061	.062	73.5
HA5-20	20-4	4.755	3.255	.745	-	-	.038	.062	120.2
HB1-10	10-1	5.151	3.162	1.550	7.620	-	.138	.125	33.5
HB2-12	12-2	4.725	3.344	1.498	7.285	-	.103	.100	41.9
HL1-10	10-10	4.780	3.285	2.245	-	.532	.132	.125	32.3
HL2-10	10-10	5.340	3.620	2.220	-	.747	.131	.125	36.8
HL3-10	10-9	5.725	3.980	2.265	-	.989	.136	.125	38.3
HL4-12	12-6	4.437	3.008	1.995	-	.508	.103	.100	38.6
HL5-12	12-8	4.375	3.270	2.022	-	.778	.102	.100	38.4

Table 2.3. Experimental Strain Measurements at Failure
Critical Compressive Strains $(w/t)_{lim} \approx 37$

Specimen	w/t	ε_y (10^{-6} $\frac{in}{in}$)	Tension Strains		Critical Compressive Strains		$\frac{\phi_{ult}}{\phi_y}$
			$\varepsilon_{t,ult}$ (10^{-6} $\frac{in}{in}$)	$\frac{\varepsilon_{t,ult}}{\varepsilon_y}$	$\varepsilon_{c,ult}$ (10^{-6} $\frac{in}{in}$)	$\frac{\varepsilon_{c,ult}}{\varepsilon_y}$	
HL1-10	32.3	1270	2835	2.25	4119	3.25	2.92
HA1-10	33.0	1220	5790	4.75	3995	3.28	4.78
HB1-10	33.5	1220	1190	.98	4146	3.40	2.74
HL2-10	36.8	1270	2252	1.78	2987	2.35	2.15
HL3-10	38.3	1220	2433	2.00	2610	2.34	2.11
HL5-12	38.4	1270	1247	.99	1450	1.14	1.13
HL4-12	38.6	1240	1882	1.54	1821	1.47	1.55
HA2-12	41.2	1260	2069	1.64	1260	1.00	1.61
HA3-12	41.2	1220	3880	3.18	2180	1.80	2.89
HB2-12	41.9	1220	978	.80	1507	1.24	1.34

Table 2.4. Moment and Curvature Ratios

Specimen	w/t	$\frac{y_t}{d}$	$\frac{M_{yc}}{M_y}$	$\frac{M_p}{M_y}$	$\frac{M_{u,exp}}{M_y}$	$\frac{\phi_{u,exp}}{\phi_y}$	$\frac{M_{u,exp}}{M_{u,ctd}}$	$\frac{\phi_{u,exp}}{\phi_{u,ctd}}$
1	2	3	4	5	6	7	8	9
HA1-10	33.0	.573	1.21	1.31	1.36	4.78	1.05	.90
HA2-12	41.2	.568	1.19	1.29	1.23	1.61	1.04	1.00
HA3-12	41.2	.566	1.22	1.29	1.31	2.89	1.03	1.05
HB1-10	33.5	.354	-	1.30	1.26	2.74	1.02	.99
HB2-12	41.9	.358	-	1.31	1.12	1.34	1.03	1.01
HL1-10	32.3	.490	-	1.17	1.16	2.92	1.00	.97
HL2-10	36.8	.508	-	1.16	1.13	2.15	1.00	.93
HL3-10	38.3	.501	-	1.16	1.16	2.11	1.02	1.04
HL4-12	38.6	.492	-	1.16	1.16	1.55	1.06	1.06
HL5-12	38.4	.490	-	1.20	1.06	1.13	.99	1.04

Table 2.5. Dimensional Moment and Curvature Values

Specimen	I (in^4)	M_y (k-ft)	ϕ_y (10^{-6} $\frac{1}{in}$)	M_{yc} (k-ft)	M_p (k-ft)	$M_{u,exp}$ (k-ft)	$\phi_{u,exp}$ (10^{-6} $\frac{1}{in}$)	$M_{u,ctd}$ (k-ft)	$\phi_{u,ctd}$ (10^{-6} $\frac{1}{in}$)
1	2	3	4	5	6	7	8	9	10
HA1-10	3.137	5.12	663	6.20	6.71	6.98	3159	6.68	3550
HA2-12	2.355	4.06	690	4.76	5.16	4.98	1110	4.76	1100
HA3-12	2.360	3.88	668	4.71	4.99	5.08	1924	4.90	1700
HB1-10	5.378	7.98	604	-	10.37	10.10	1653	9.96	1660
HB2-12	4.349	6.12	572	-	8.01	6.89	766	6.62	695
HL1-10	3.746	6.98	759	-	8.20	8.10	2211	8.07	2280
HL2-10	4.931	8.48	699	-	9.83	9.55	1501	9.59	1620
HL3-10	6.663	10.10	612	-	11.70	11.72	1297	11.40	1250
HL4-12	2.286	4.56	812	-	5.29	5.24	1275	4.99	1195
HL5-12	2.790	5.16	753	-	6.19	5.48	852	5.52	822

Table 2.6. Comparison between Experimental and Design Ultimate Moments

Specimen	$\frac{w/t}{(w/t)_{lim}}$ *	$\left(\frac{\varepsilon_{c,u}}{\varepsilon_y}\right)_{design}$ **	$\varepsilon_{c,u}$	$M_{u,des}$ (k-ft)	$M_{u,exp}$ (k-ft)	$\frac{M_{u,exp}}{M_{u,des}}$
1	2	3	4	5	6	7
HA1-10	.90	3.0	3660	6.68	6.98	1.05
HA2-12	1.14	1.0	1250	4.76	4.98	1.04
HA3-12	1.12	1.0	1220	4.71	5.08	1.07
HB1-10	.91	3.0	3660	9.81	10.10	1.03
HB2-12	1.14	1.0	1220	6.12	6.89	1.12
HL1-10	.89	3.0	3810	8.05	8.10	1.00
HL2-10	1.02	1.7	2150	9.40	9.55	1.02
HL3-10	1.04	1.5	1820	10.10	11.72	1.16
HL4-12	1.05	1.4	1740	4.99	5.24	1.06
HL5-12	1.06	1.3	1650	6.05	5.48	0.91

*$(w/t)_{lim}$ based on actual yield strength.

**From Eq. 2.7.

Table 2.7. Experimental Results for Stiffened Sections in the Postcritical Range ($(w/t)_{lim}$ for HA4-16 = 34.8, for HA5-20 = 37.6)

Specimen	w/t	Inelastic Reserves		Comparison of Experiment and Computation				Ultimate Strains			
		$\frac{M_{u,exp}}{M_{y,W}}$	$\frac{\phi_{u,exp}}{\phi_{y,W}}$	$\frac{M_{y,exp}}{M_{y,W}}$	$\frac{\phi_{y,exp}}{\phi_{y,W}}$	$\frac{M_{u,exp}}{M_{u,W}}$	$\frac{\phi_{u,exp}}{\phi_{u,W}}$	$\varepsilon_{t,u}$	$\frac{\varepsilon_{t,u}}{\varepsilon_y}$	$\varepsilon_{c,u}$	$\frac{\varepsilon_{c,u}}{\varepsilon_y}$
1	2	3	4	5	6	7	8	9	10	11	12
HA4-16	73.5	1.20	1.55	1.00	.95	1.015	1.095	2280	1.63	1397	1.00
HA5-20	120.2	1.06	1.17	.95	.98	.98	.98	1389	1.18	1150	.98

Index "W" - computed on the basis of the Winter effective width equation.

Table 2.8. Dimensional Values of Moment-Curvature Relationship

Specimen	w/t	σ_y	Fully Effective		Reduced Effective Width				Experiment			
			$M_{y,f}$	$\phi_{y,f}$	$M_{y,W}$	$\phi_{y,W}$	$M_{u,W}$	$\phi_{u,W}$	$M_{y,exp}$	$\phi_{y,exp}$	$M_{u,exp}$	$\phi_{u,exp}$
1	2	3	4	5	6	7	8	9	10	11	12	13
HA4-16	73.5	41.1	1.905	683	1.809	740	2.150	1050	1.815	700	2.18	1150
HA5-20	120.2	34.5	1.035	572	.927	672	1.006	806	.880	660	.985	789

Table 5.1. System of Dimensionless Variables for Normalized Analysis

All variables are normalized with respect to units $\sigma_y t$ and d.

Definition	Dimensional Term	Non-Dimensional Term
Moment	M	$\frac{M}{\sigma_y t d^2} = m$
Curvature	ϕ	$\phi d = \kappa$
Elastic Stiffness	EI	$\frac{EI}{\sigma_y t d^3} = \frac{i}{\varepsilon_y}$
	$\sigma_y I$	$\frac{\sigma_y I}{\sigma_y t d^3} = i$
Coordinate of Section	y	$y/d = \eta$
Beam Coordinate	x	$x/d = \xi$
Distributed Load	w	$\frac{w}{\sigma_y t} = \bar{w}$
Concentrated Load	P	$\frac{P}{\sigma_y t d} = \bar{P}$
Shear Force	V	$\frac{V}{\sigma_y t d} = v$
Span Length	L	$L/d = \ell$
Hinge Length	H	$H/d = \bar{H}$
Sample Equations	$M = EI\,\phi$	$m = \frac{i}{\varepsilon_y}\kappa$
	$M(x) = Vx - \frac{wx^2}{2}$	$m(\xi) = v\xi - \frac{\bar{w}\xi^2}{2}$
	$M_{res} = C\,\frac{\sigma_y I}{L}\,\frac{H}{d}\,\zeta$	$m_{res} = C\,i\,\bar{H}\,\frac{1}{\ell}\,\zeta$

Table 5.2. Evaluation of Systems for Partial Moment Redistribution (Primary Load Case; w_D/w_L = 1:4)

Sketch Illustrating Elastic Coefficients of System (3)

Primary Load Case

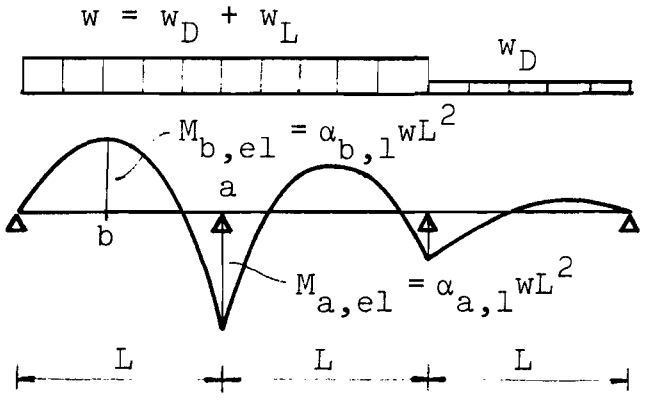

Secondary Load Case

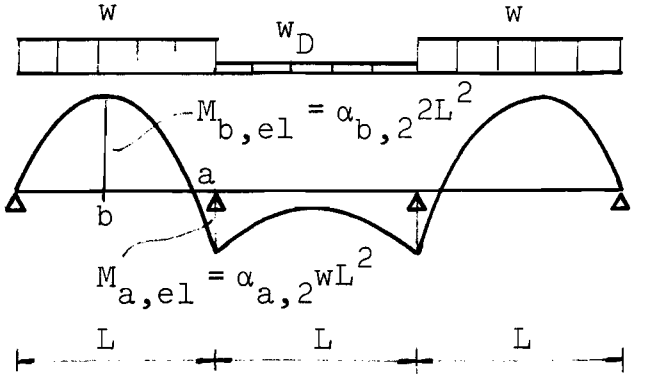

#	System, Primary L.C.	$\alpha_{a,1}$	$\gamma_{a,\ell}$	$\gamma_{a,r}$	C_a	S	$\alpha_{b,1}$	$\frac{\alpha_{a,1}}{\alpha_{b,1}}$
1	2	3	4	5	6	7	8	9
(1)	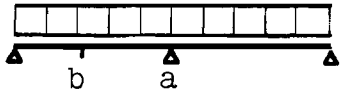 b a 1 : 1	.1250	.6250	.6250	1.5000	.6000 = min	.0703	1.778
(2)	 b a 1 : .8	.1050	.5313	.6050	1.6666	.6186	.0780	1.346

Table 5.2 (continued)

#	System, Primary L.C.	$\alpha_{a,1}$	$\gamma_{a,\ell}$	$\gamma_{a,r}$	C_a	S	$\alpha_{b,1}$	$\frac{\alpha_{a,1}}{\alpha_{b,1}}$
1	2	3	4	5	6	7	8	9
(3)	$w = w_D + w_L$ w_D  b a 1 : 1 : 1	.1133	.6134	.5667	1.6000	.6154	.0747	1.517
(4)	 b a 1 : 1 : .8	.1138	.6138	.5688	1.6119	.6213	.0746	1.525
(5)	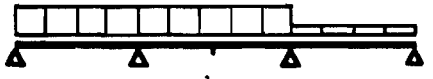 a b .8 : 1 : .8	.0918	.5152	.5320	1.8060	.6334	.0406	1.772
(6)	 b a 1 : .8 : 1	.1010	.5990	.4893	1.7532	max .6575	.0806	1.253
(7)	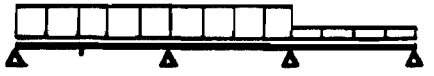 b a 1 : .8 : .8	.0999	.5999	.4887	1.7647	.6546	.0800	1.249

Table 5.3. Evaluation of Systems for Partial Moment Redistribution (Secondary Load Case; w_D/w_L = 1:4)

#	Sketch for Secondary L.C.	$\alpha_{b,2}$	$\frac{\alpha_{a,1}}{\alpha_{b,2}}$
(1)	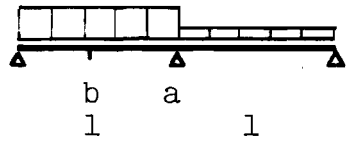	.0907	1.378
(2)	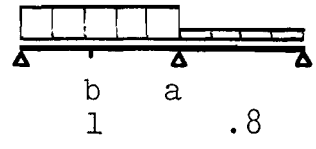	.0897	1.170
(3)	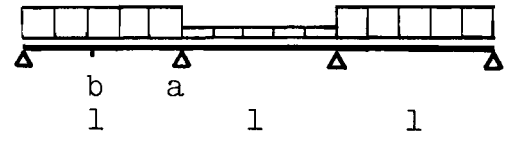	.0970	1.168
(4)	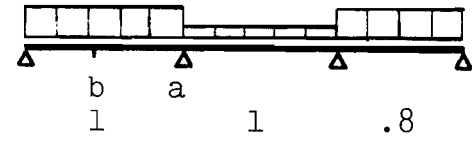	.0938	1.213
(5)	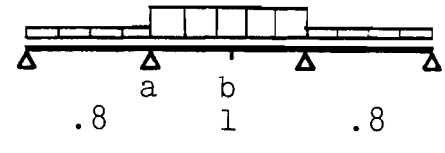	.0937	1.417
(6)	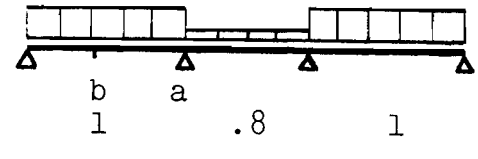	.0960	1.052
(7)	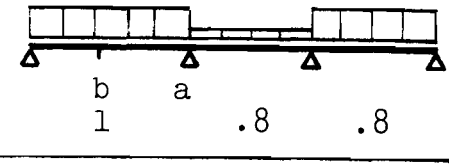	.0926	1.078

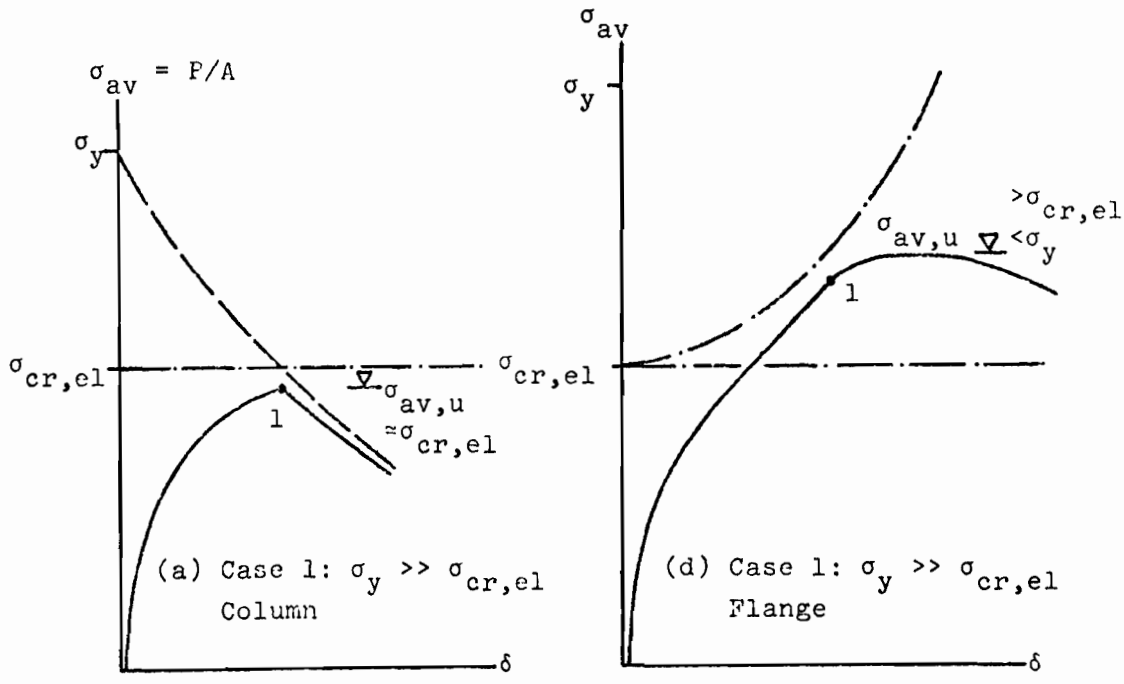

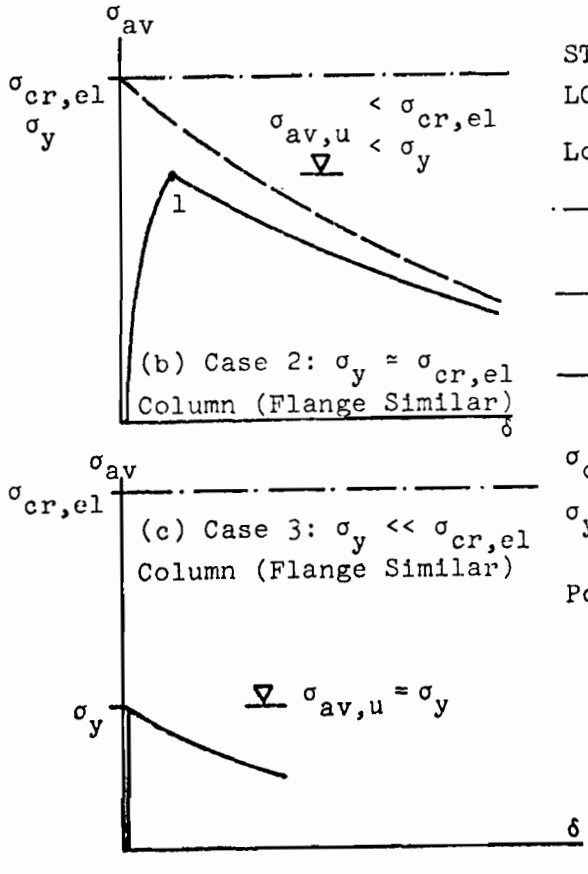

Fig. 1.1

STRUCTURAL BEHAVIOR UNDER AXIAL LOAD WITH INITIAL IMPERFECTIONS

Load-deflection behavior

·——·—— after bifurcation at $\sigma_{cr,el}$

———— after bifurcation at σ_y

——— based on small initial deflections

$\sigma_{cr,el}$... elastic critical load

σ_y..... yield load in undeflected state

Point 1.. initial yielding in deflected state

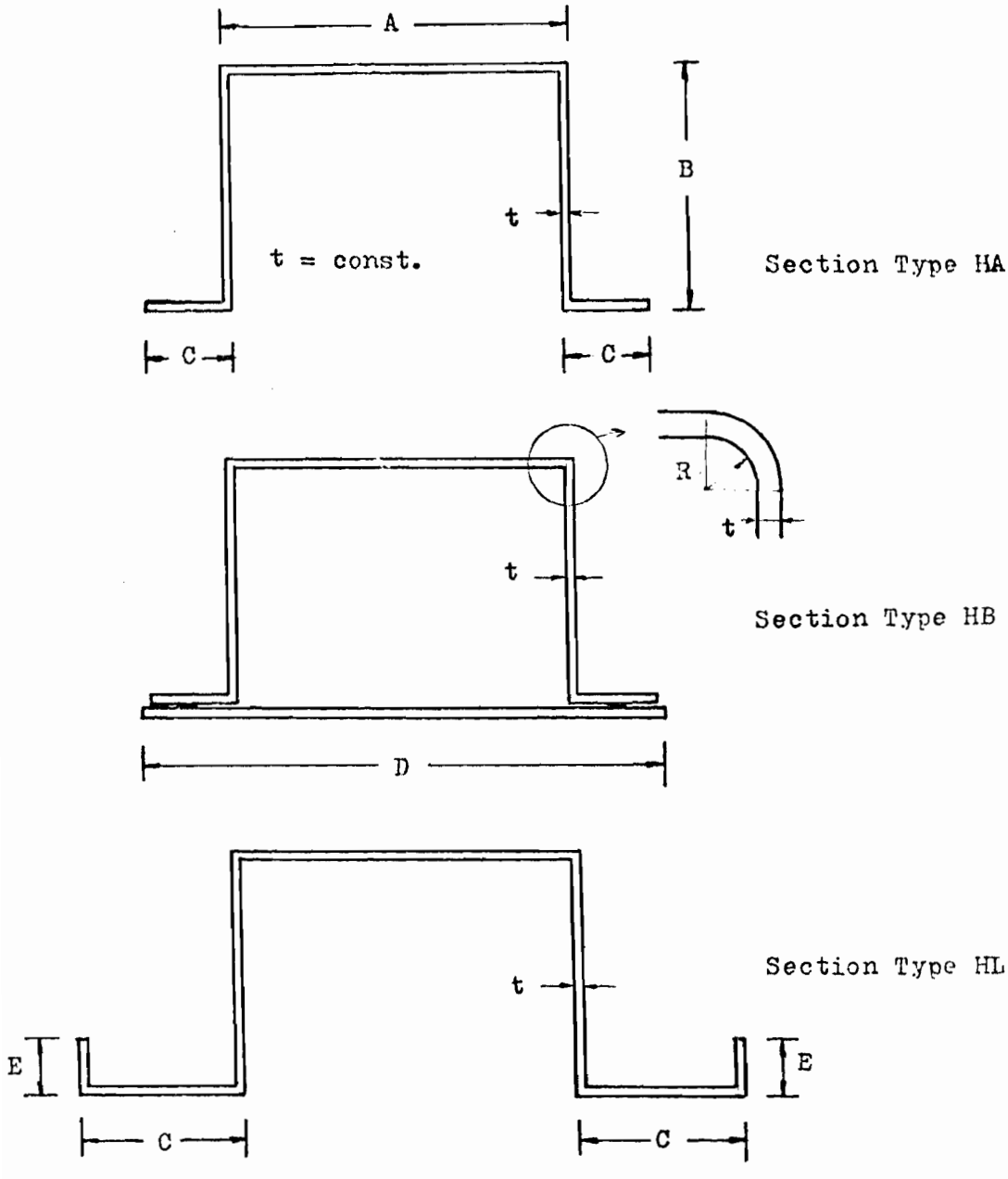

Fig. 2-1 SECTION GEOMETRIES

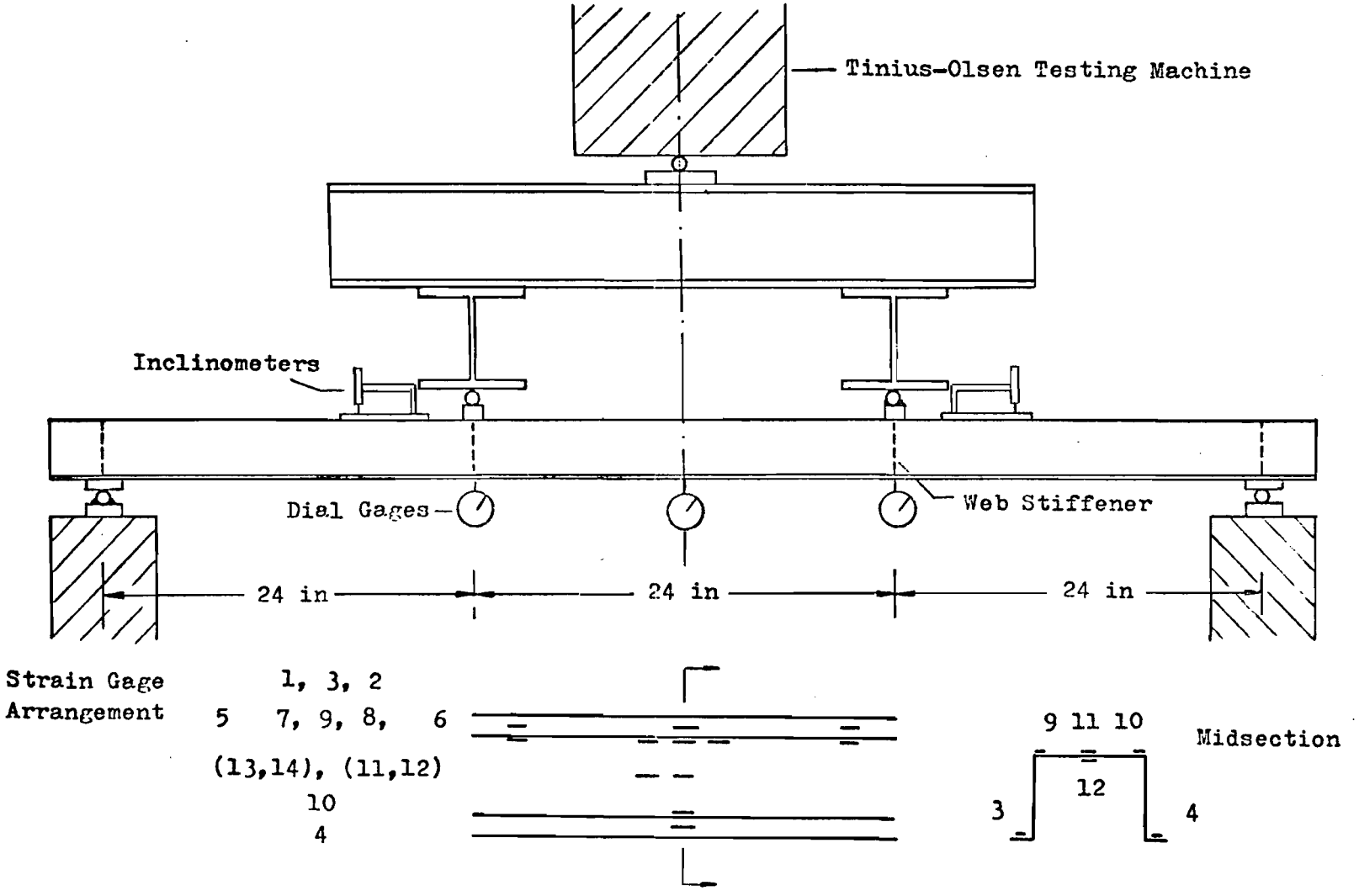

Fig. 2.2 : TEST SET-UP AND INSTRUMENTATION

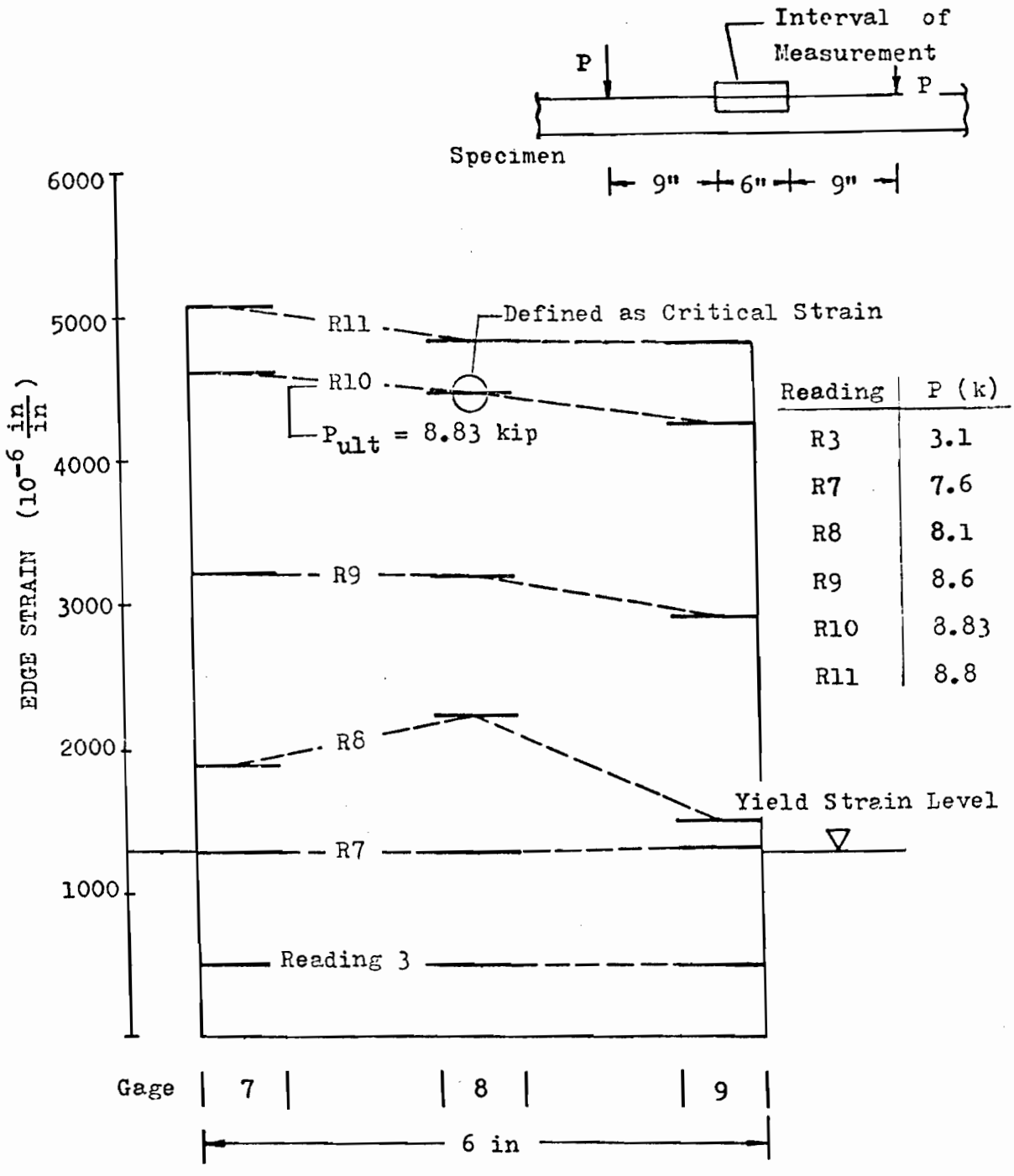

Fig. 2-3 LONGITUDINAL STRAIN DISTRIBUTION IN COMPRESSION FLANGE
SPECIMEN HL1-10 w/t = 32.3

Reading	P (k)
R4	8.1
R6	10.6
R7	11.1
R8	11.68
R9	11.72

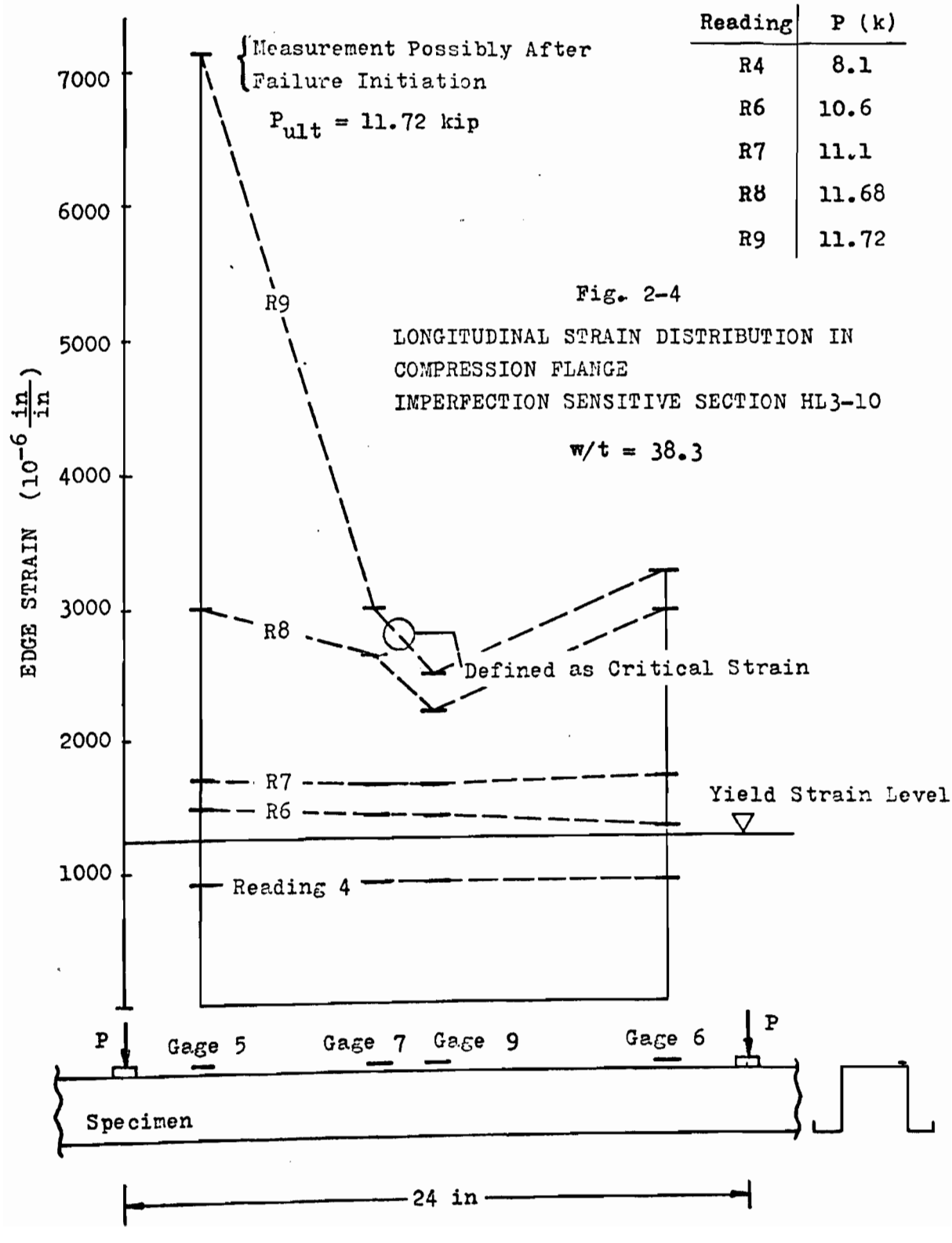

Fig. 2-4

LONGITUDINAL STRAIN DISTRIBUTION IN COMPRESSION FLANGE
IMPERFECTION SENSITIVE SECTION HL3-10

w/t = 38.3

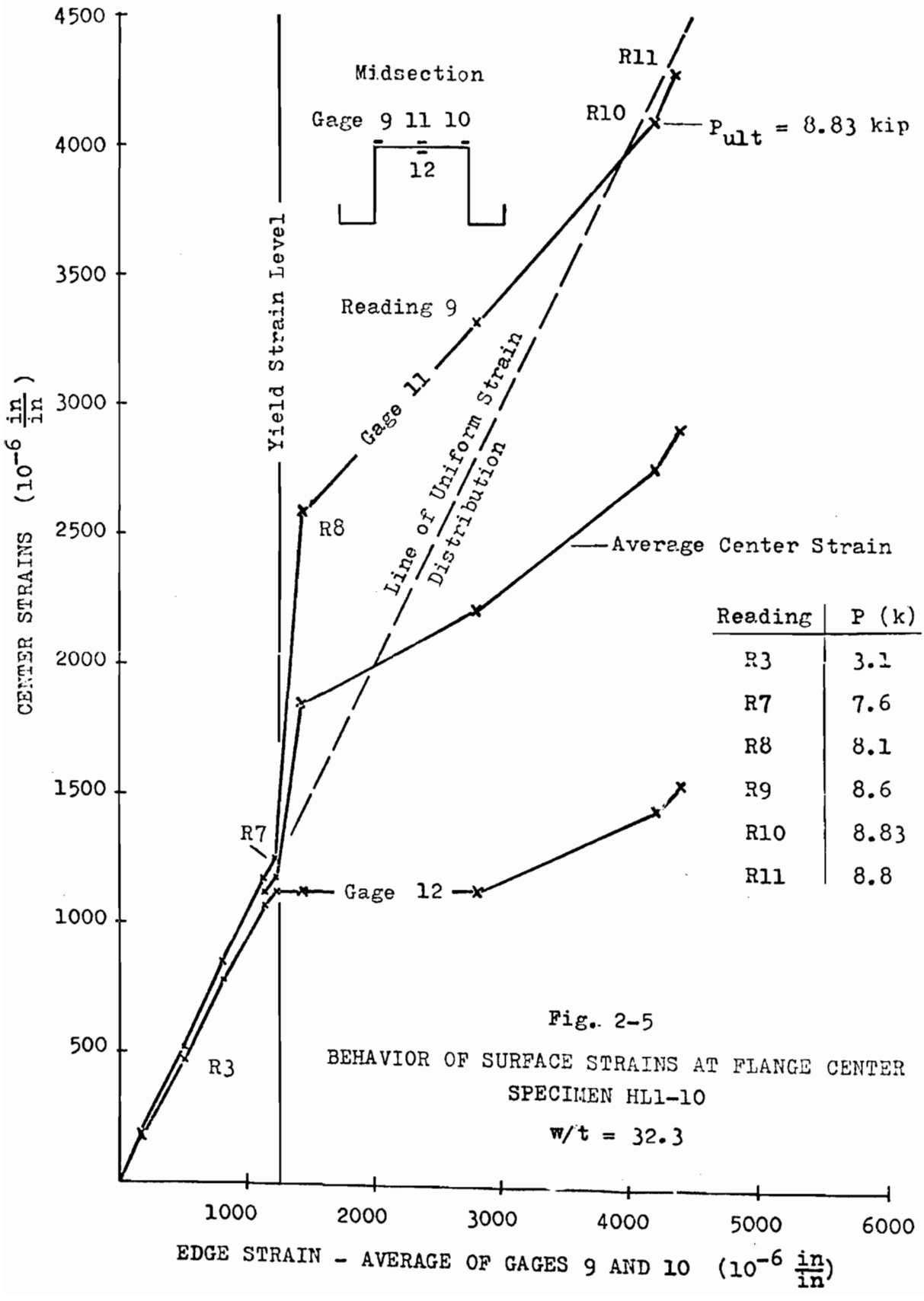

Reading	P (k)
R3	3.1
R7	7.6
R8	8.1
R9	8.6
R10	8.83
R11	8.8

Fig. 2-5

BEHAVIOR OF SURFACE STRAINS AT FLANGE CENTER

SPECIMEN HL1-10

w/t = 32.3

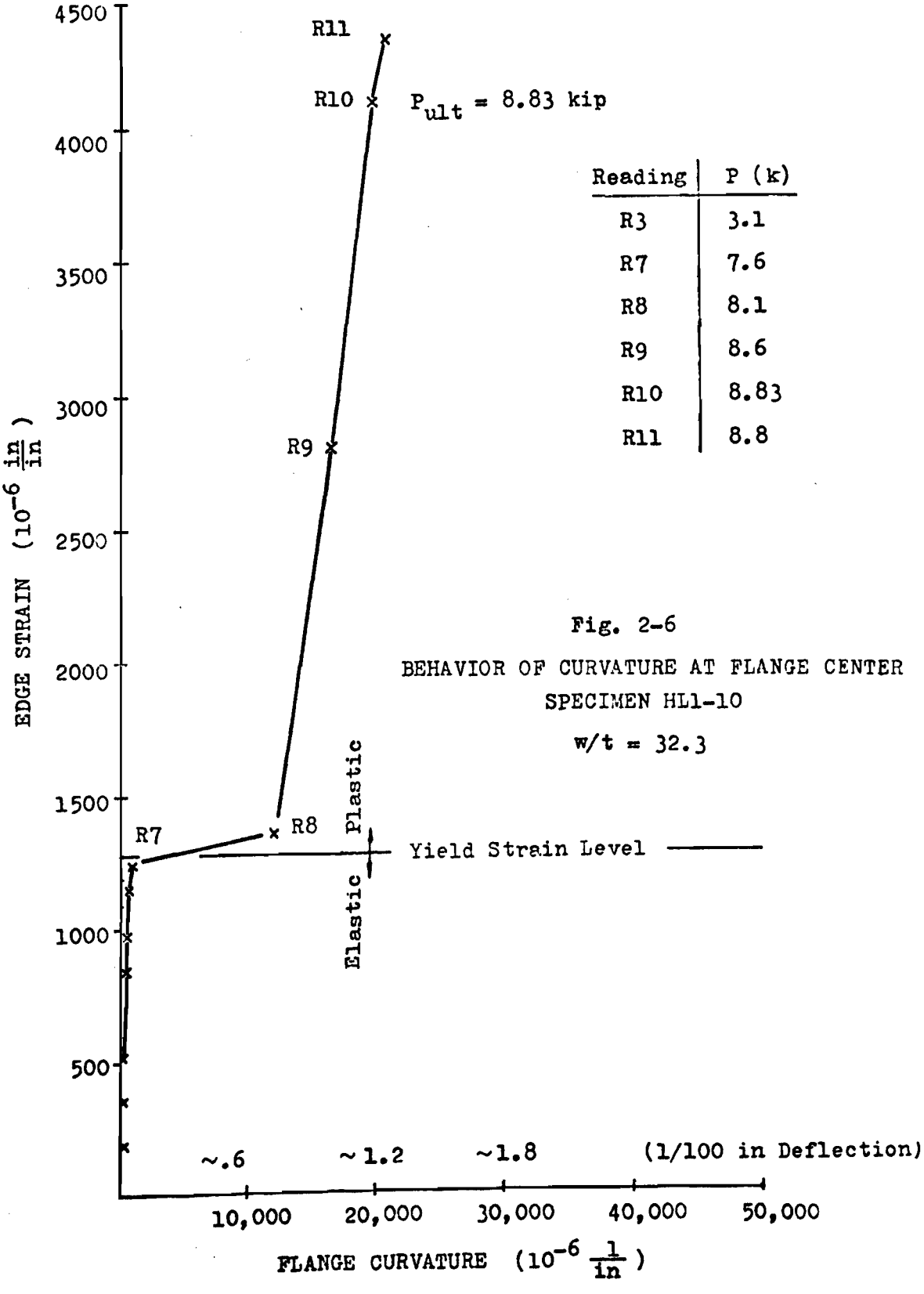

Reading	P (k)
R3	3.1
R7	7.6
R8	8.1
R9	8.6
R10	8.83
R11	8.8

Fig. 2-6

BEHAVIOR OF CURVATURE AT FLANGE CENTER
SPECIMEN HL1-10
w/t = 32.3

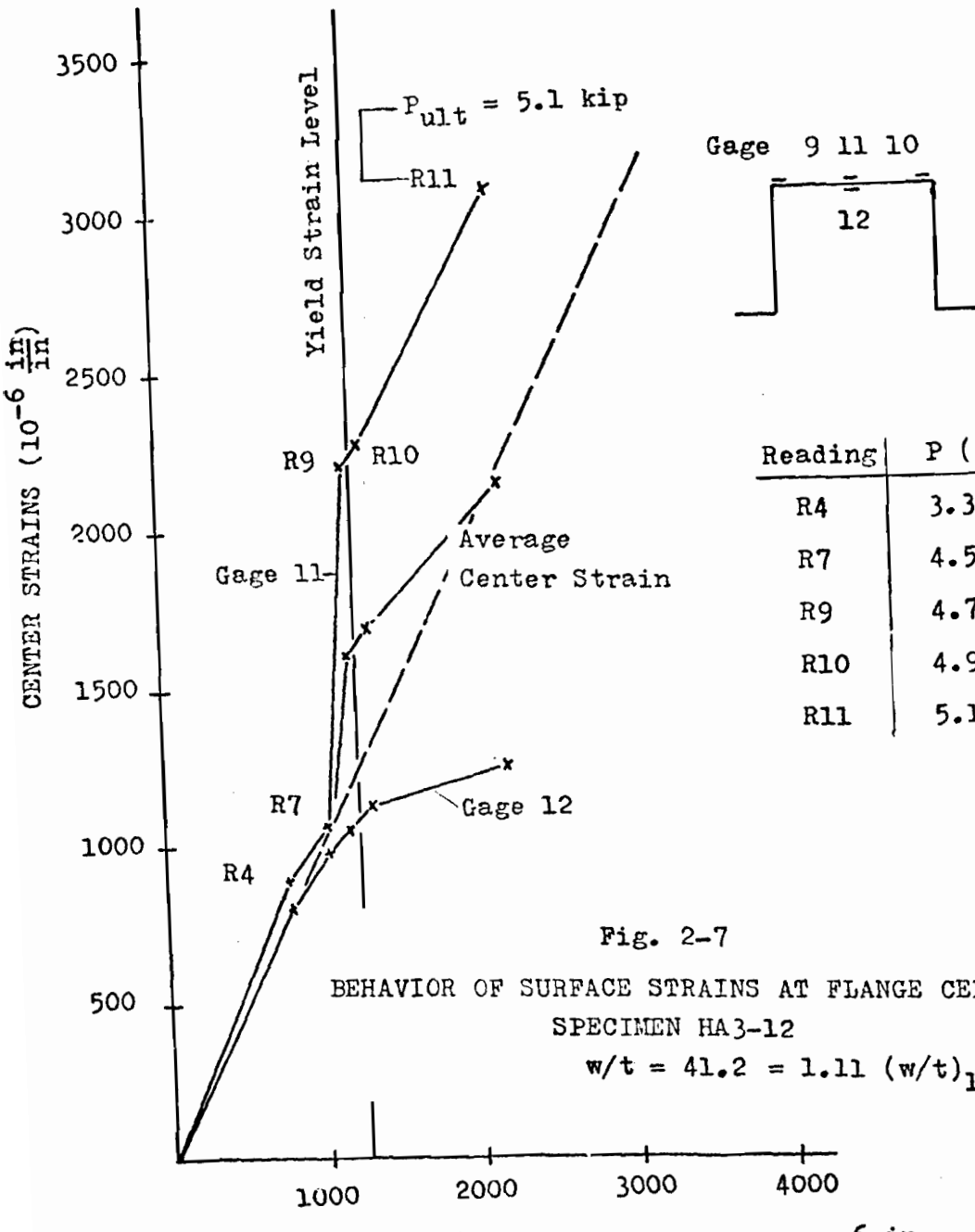

Reading	P (k)
R4	3.3
R7	4.5
R9	4.7
R10	4.9
R11	5.1

Fig. 2-7

BEHAVIOR OF SURFACE STRAINS AT FLANGE CENTER
SPECIMEN HA3-12
$w/t = 41.2 = 1.11\ (w/t)_{lim}$

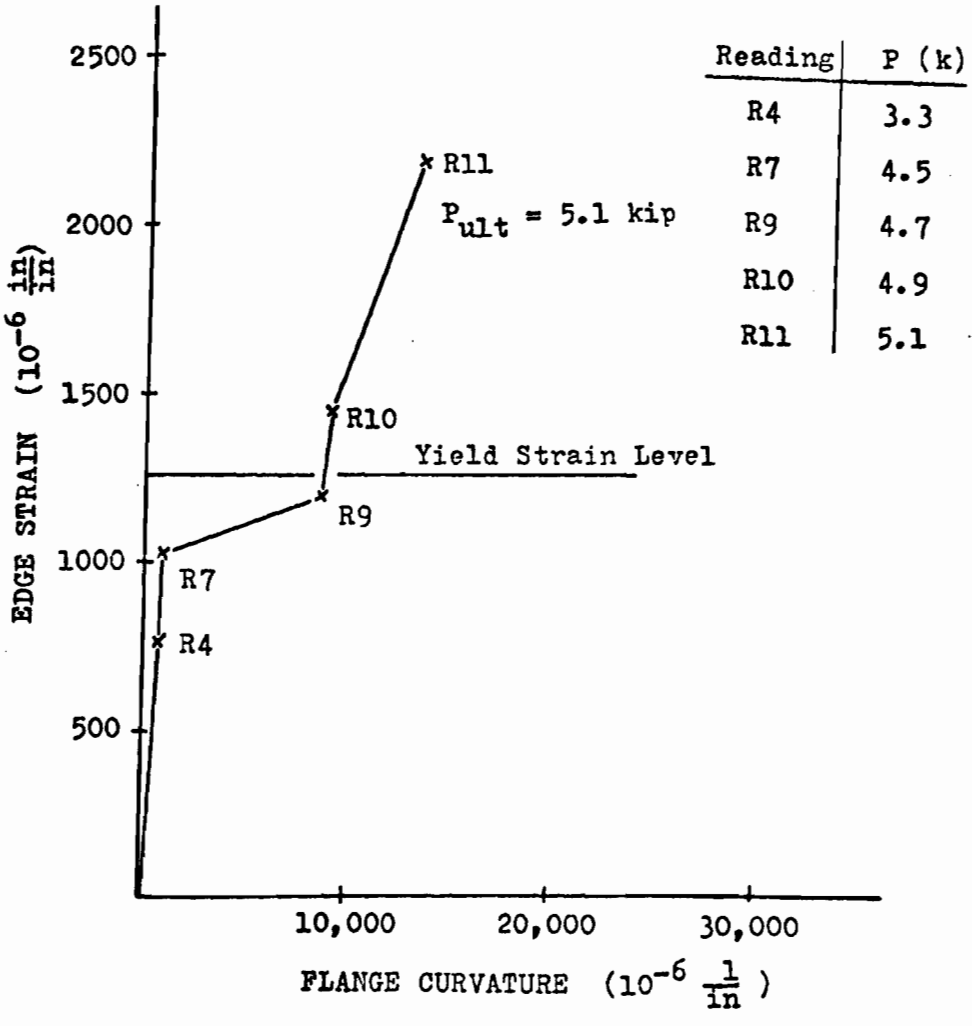

Fig. 2-8

BEHAVIOR OF CURVATURE AT FLANGE CENTER
SPECIMEN HA3-12

$w/t = 41.2 = 1.11\ (w/t)_{lim}$

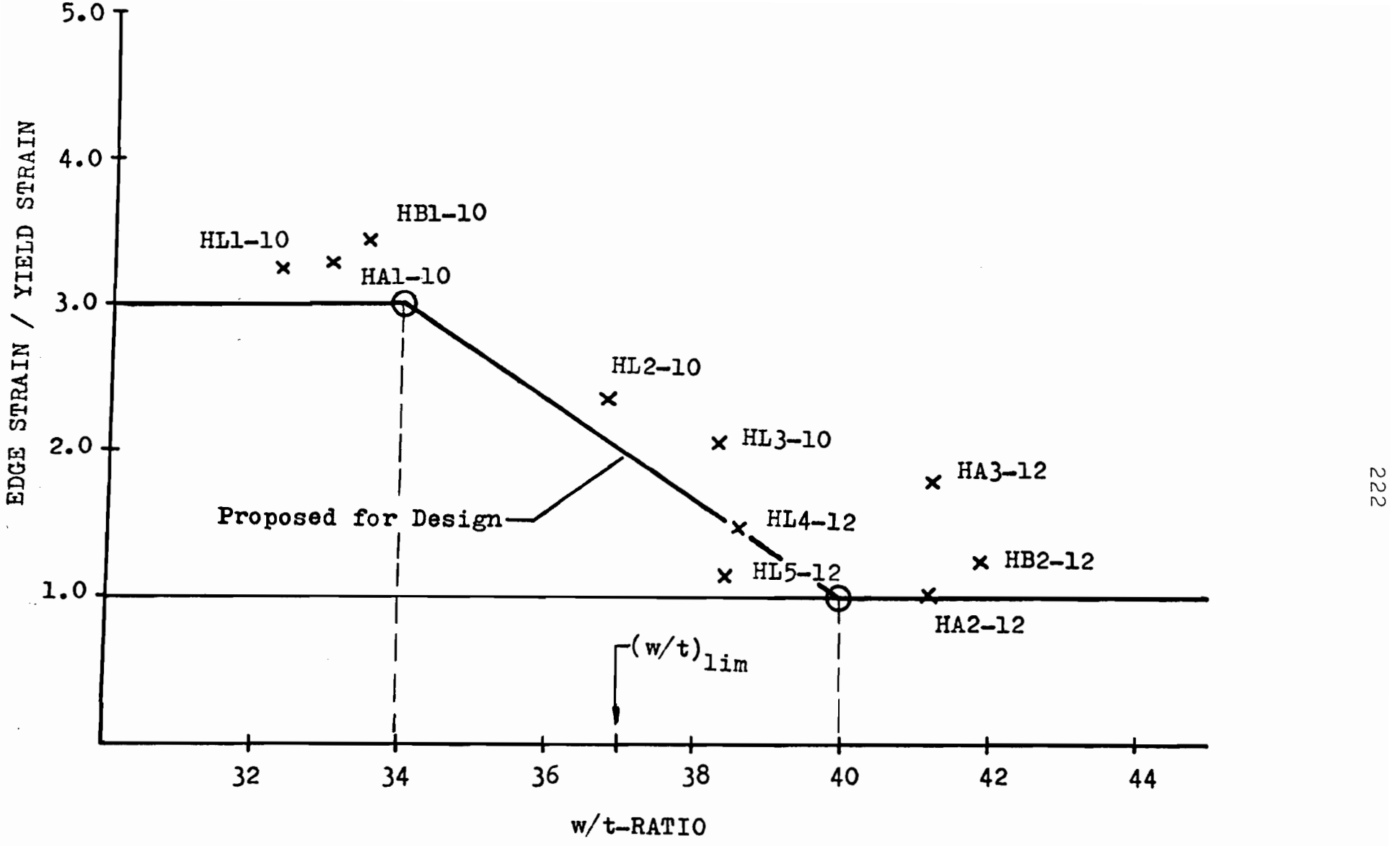

Fig. 2-9 CRITICAL COMPRESSION FLANGE STRAINS $(\varepsilon_{c,u}/\varepsilon_y)$

$36^{ksi} < 6 \leq 37.4^{ksi}$

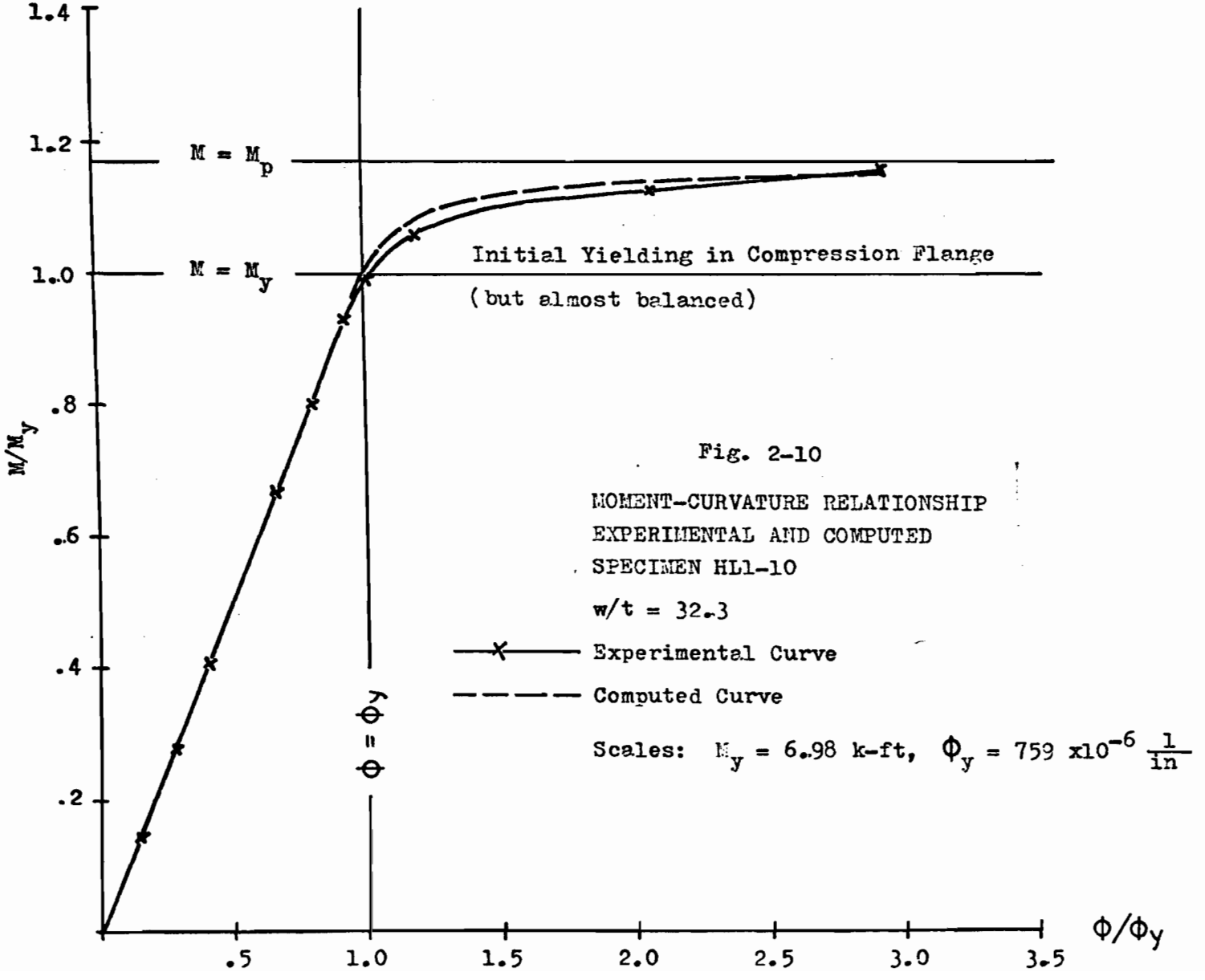

Fig. 2-10

MOMENT-CURVATURE RELATIONSHIP
EXPERIMENTAL AND COMPUTED
SPECIMEN HL1-10

w/t = 32.3

Experimental Curve

Computed Curve

Scales: M_y = 6.98 k-ft, $\Phi_y = 759 \times 10^{-6} \frac{1}{in}$

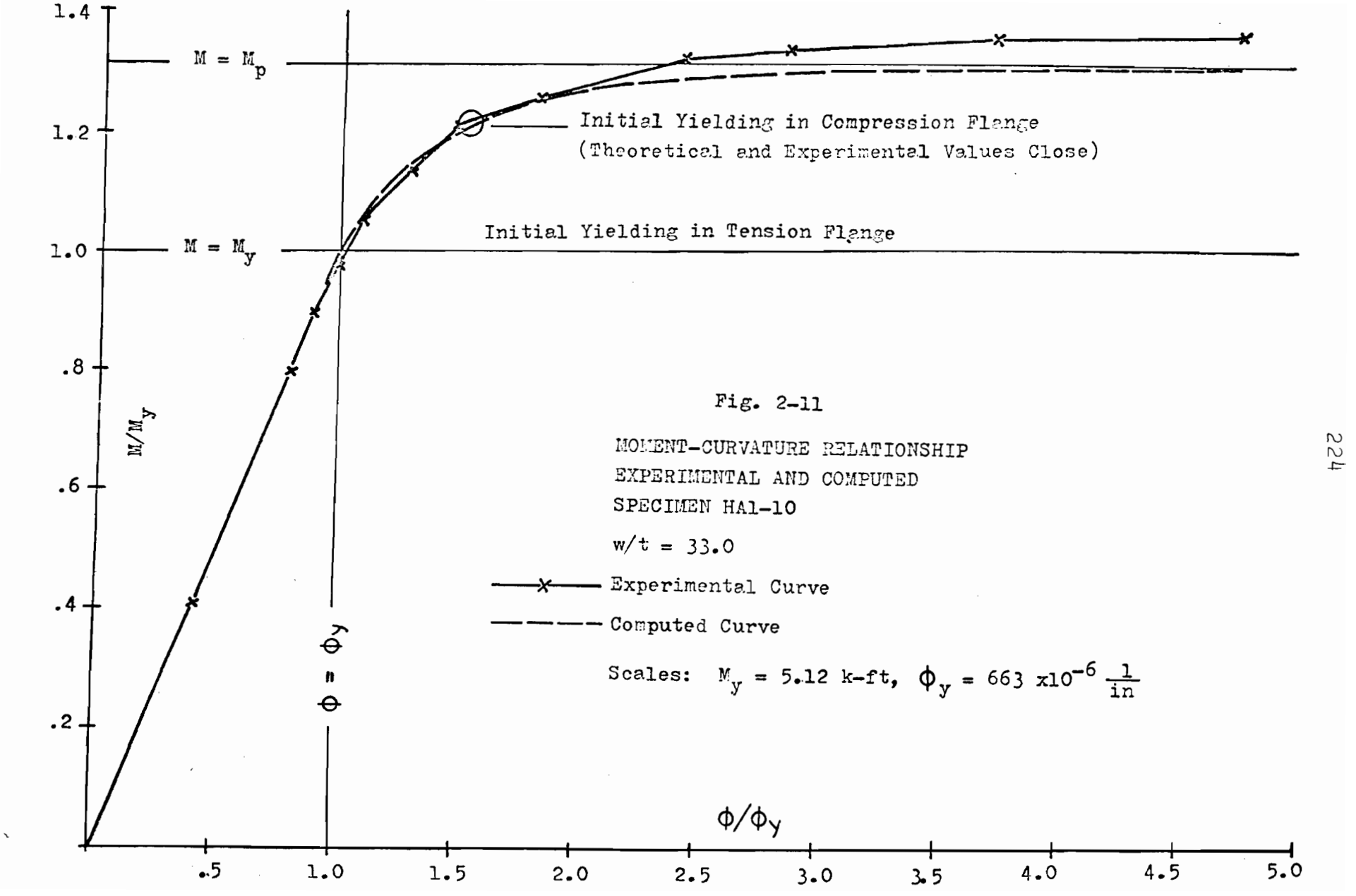

Fig. 2-11

MOMENT-CURVATURE RELATIONSHIP
EXPERIMENTAL AND COMPUTED
SPECIMEN HA1-10

w/t = 33.0

—×— Experimental Curve

— — — Computed Curve

Scales: M_y = 5.12 k-ft, $\phi_y = 663 \times 10^{-6} \frac{1}{in}$

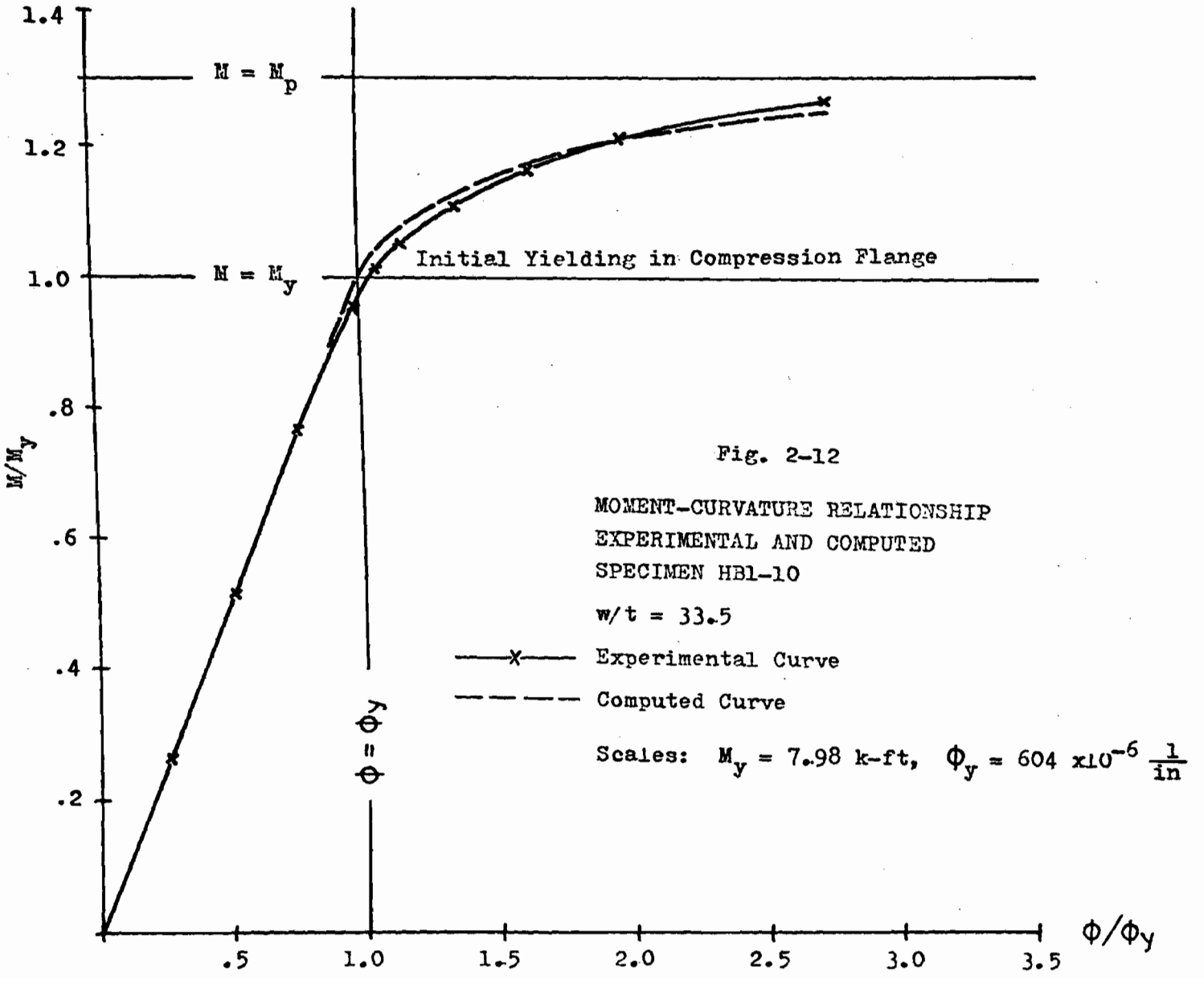

Fig. 2-12

MOMENT-CURVATURE RELATIONSHIP
EXPERIMENTAL AND COMPUTED
SPECIMEN HB1-10

w/t = 33.5

—×— Experimental Curve

— — — Computed Curve

Scales: M_y = 7.98 k-ft, $\phi_y = 604 \times 10^{-6} \frac{1}{in}$

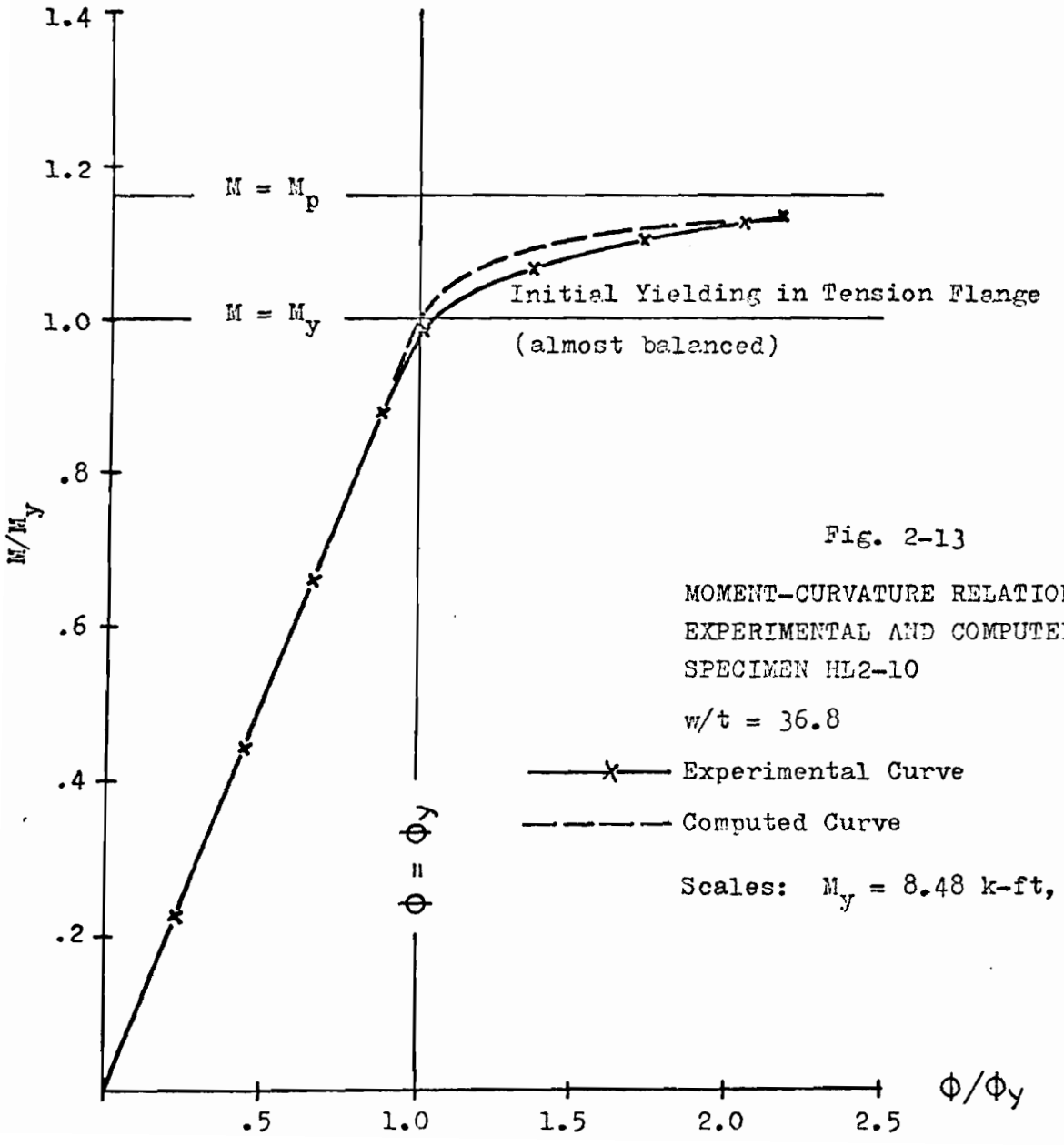

Fig. 2-13

MOMENT-CURVATURE RELATIONSHIP
EXPERIMENTAL AND COMPUTED
SPECIMEN HL2-10

w/t = 36.8

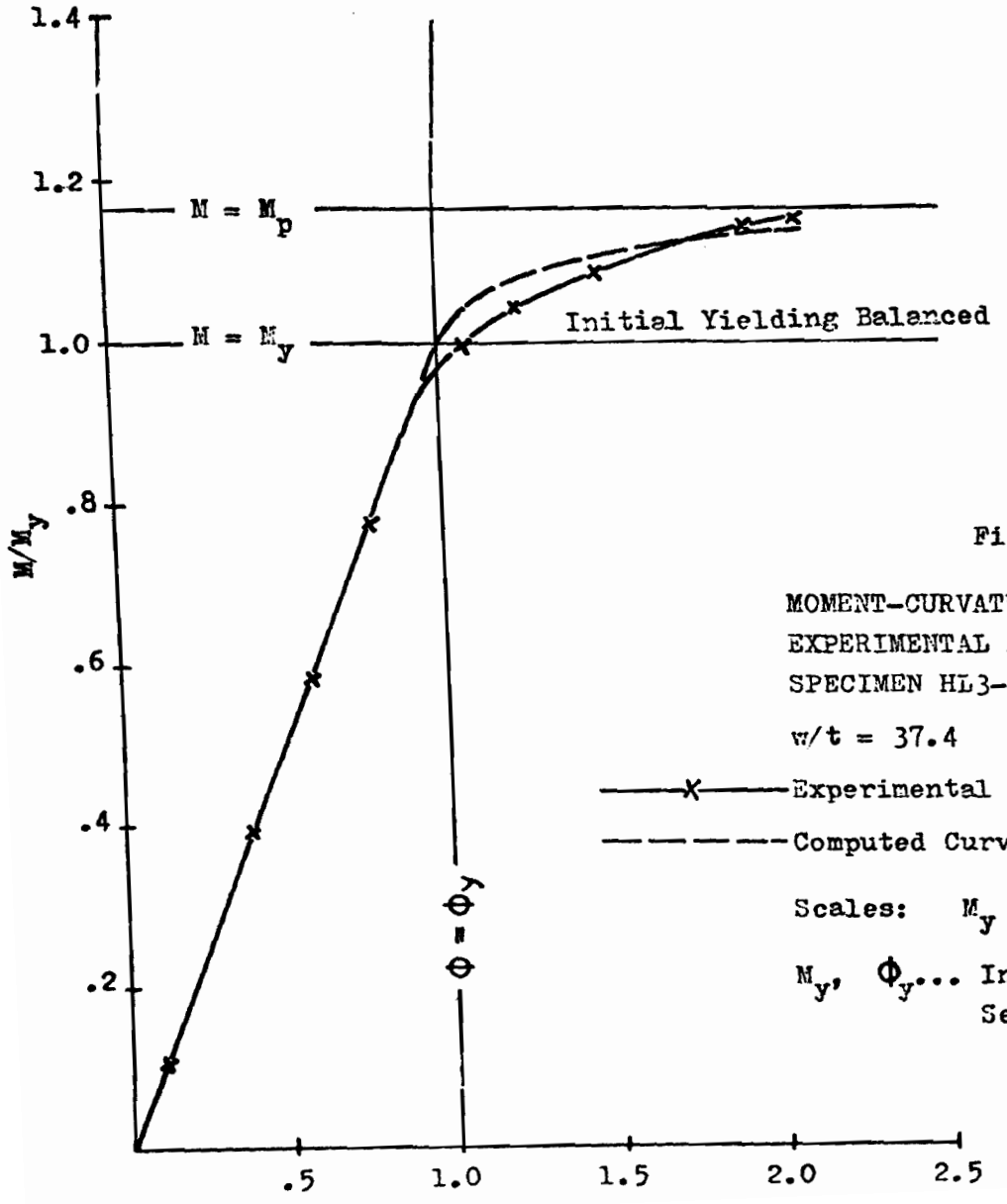

Fig. 2-14

MOMENT-CURVATURE RELATIONSHIP
EXPERIMENTAL AND COMPUTED
SPECIMEN HL3-10

w/t = 37.4

——×——Experimental Curve

— — — —Computed Curve for Fully Effective Section

Scales: M_y = 10.10 k-ft, $\Phi_y = 612 \times 10^{-6} \frac{1}{in}$

M_y, Φ_y... Initial Yielding of Fully Effective Section

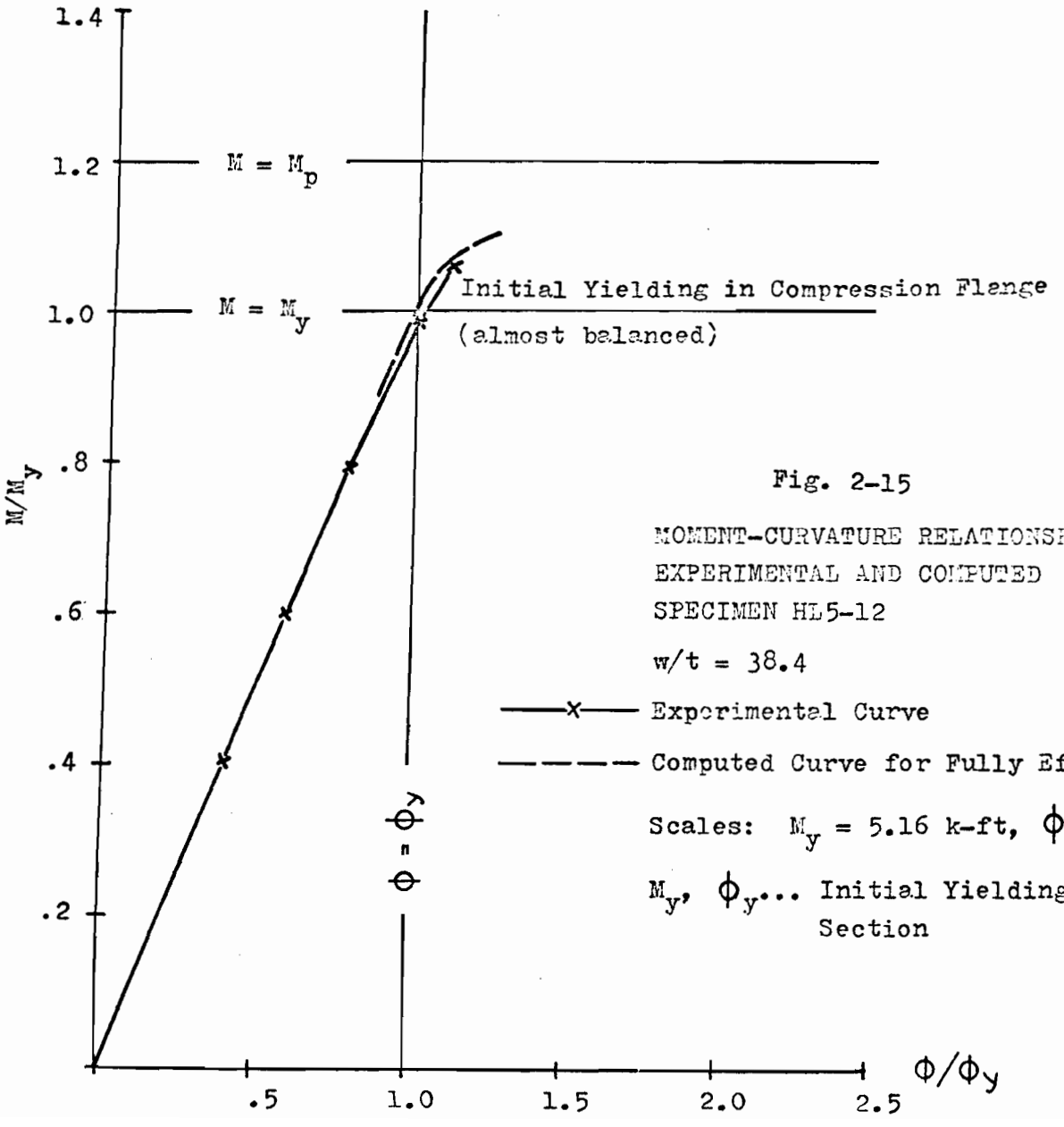

Fig. 2-15

MOMENT-CURVATURE RELATIONSHIP
EXPERIMENTAL AND COMPUTED
SPECIMEN HL5-12

w/t = 38.4

——×—— Experimental Curve

— — — — Computed Curve for Fully Effective Section

Scales: M_y = 5.16 k-ft, $\phi_y = 753 \times 10^{-6} \frac{1}{in}$

M_y, ϕ_y... Initial Yielding of Fully Effective Section

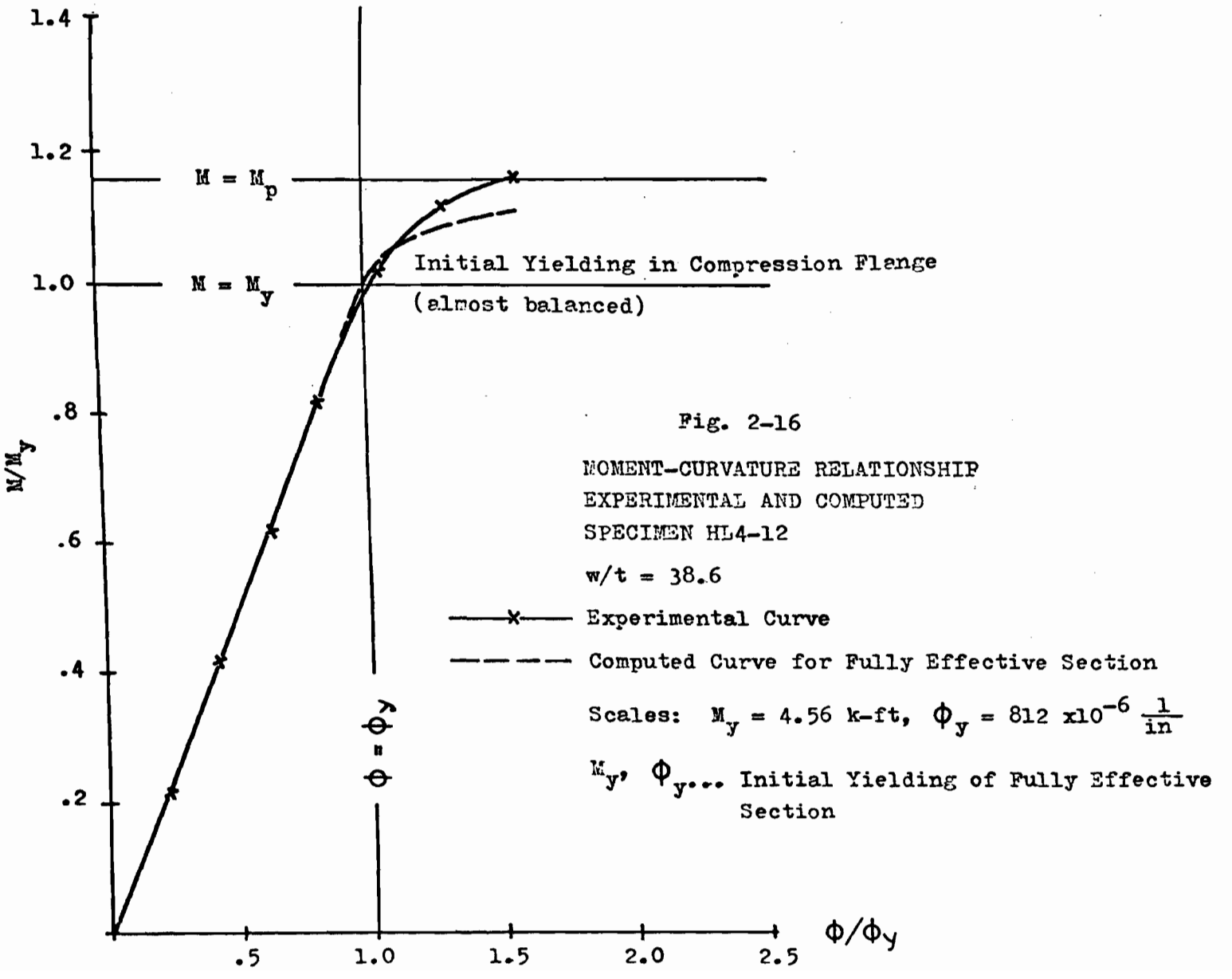

Fig. 2-16

MOMENT-CURVATURE RELATIONSHIP
EXPERIMENTAL AND COMPUTED
SPECIMEN HL4-12

w/t = 38.6

——×—— Experimental Curve

– – – – Computed Curve for Fully Effective Section

Scales: M_y = 4.56 k-ft, $\Phi_y = 812 \times 10^{-6} \frac{1}{in}$

M_y, Φ_y... Initial Yielding of Fully Effective Section

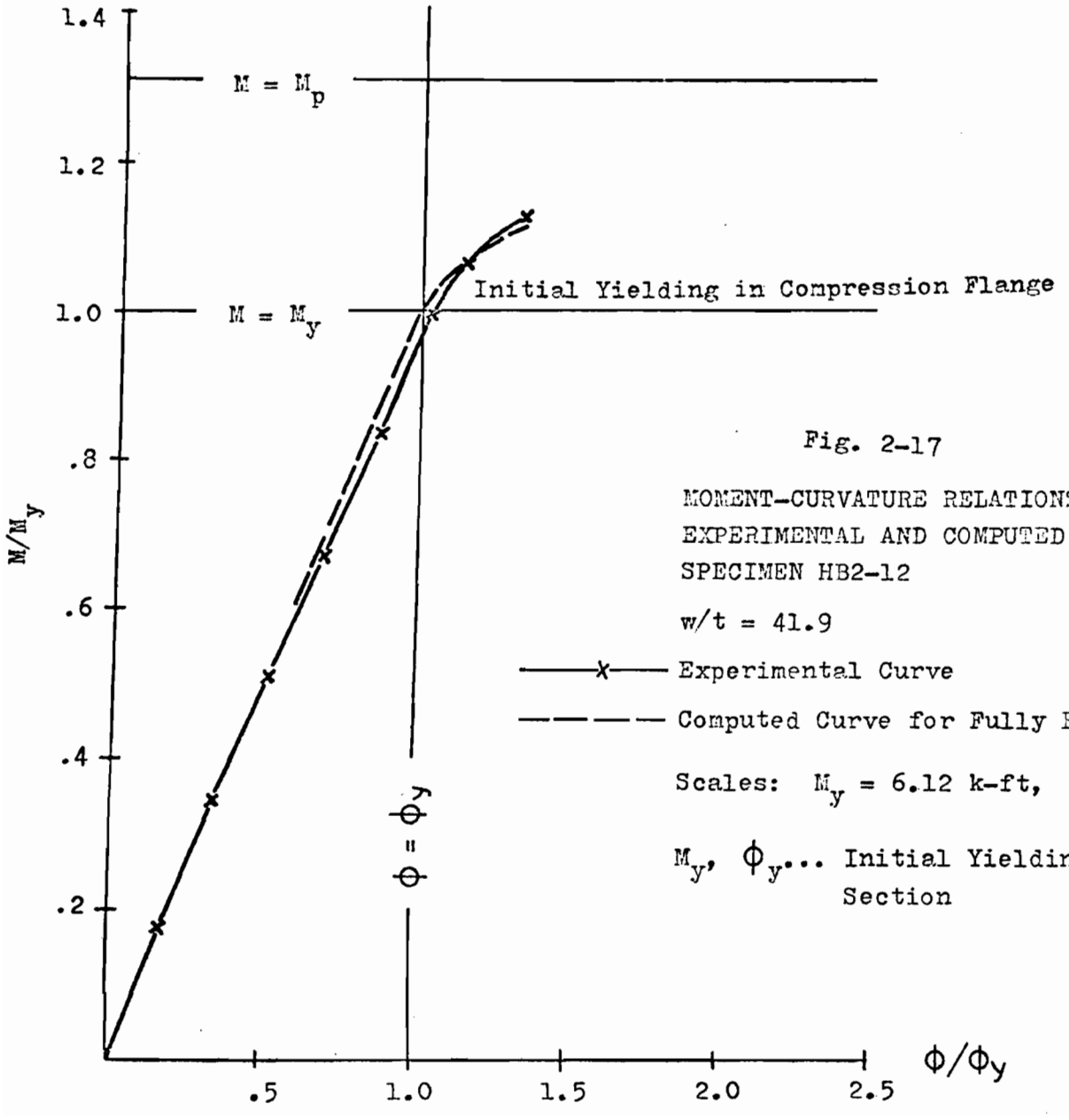

Fig. 2-17

MOMENT-CURVATURE RELATIONSHIP
EXPERIMENTAL AND COMPUTED
SPECIMEN HB2-12

w/t = 41.9

——x—— Experimental Curve

— — — — Computed Curve for Fully Effective Section

Scales: M_y = 6.12 k-ft, $\Phi_y = 572 \times 10^{-6} \frac{1}{in}$

M_y, Φ_y... Initial Yielding of Fully Effective Section

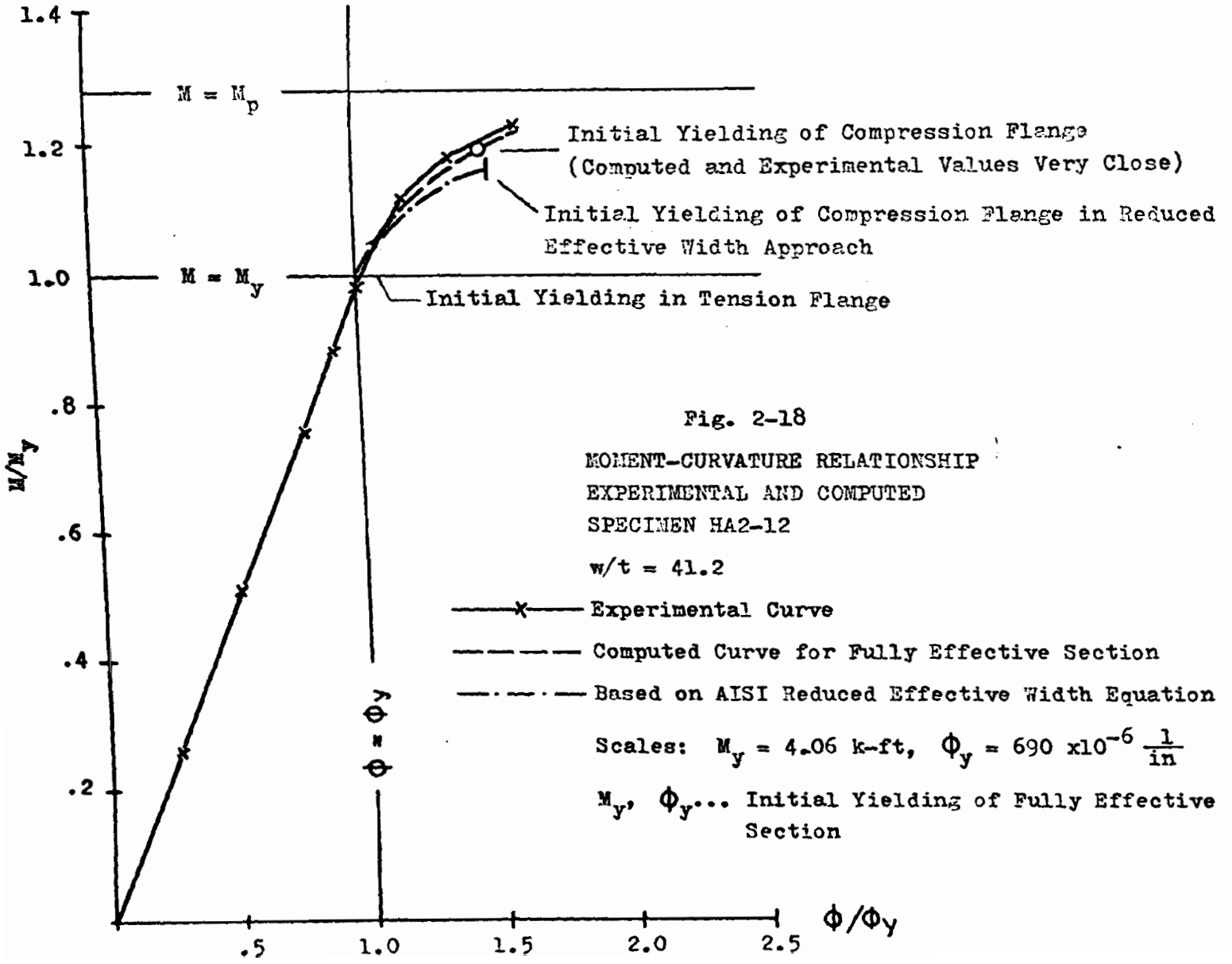
1.4
1.2
1.0
.8
.6
.4
.2
M/My
M = Mp
M = My
Initial Yielding of Compression Flange
(Computed and Experimental Values Very Close)
Initial Yielding of Compression Flange in Reduced
Effective Width Approach
Initial Yielding in Tension Flange
.5
1.0
1.5
2.0
2.5
Φ/Φy
Fig. 2-18
MOMENT-CURVATURE RELATIONSHIP
EXPERIMENTAL AND COMPUTED
SPECIMEN HA2-12
w/t = 41.2
Experimental Curve
Computed Curve for Fully Effective Section
Based on AISI Reduced Effective Width Equation
Scales: My = 4.06 k-ft, Φy = 690 x10^-6 1/in
My, Φy... Initial Yielding of Fully Effective
Section

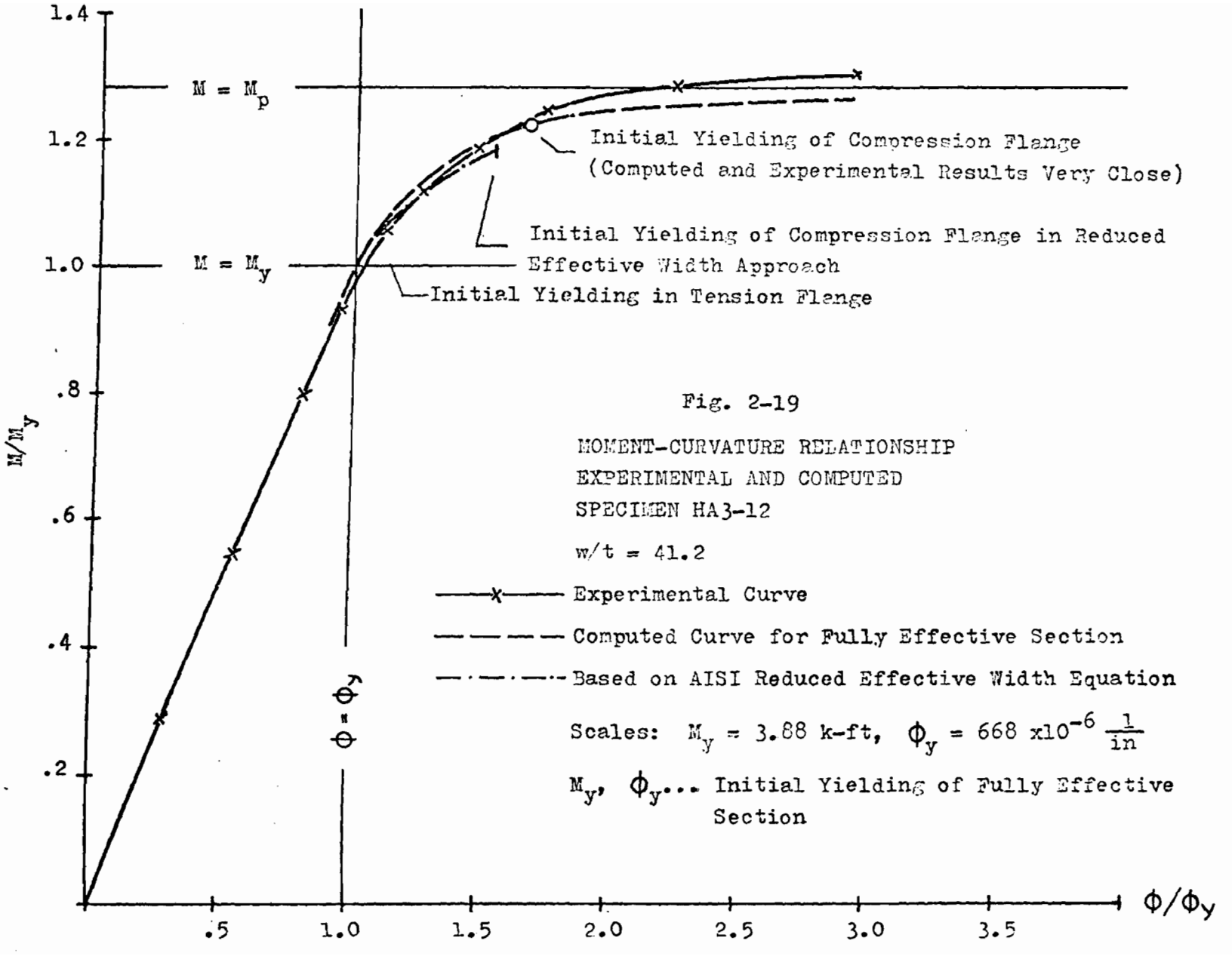

Fig. 2-19

MOMENT-CURVATURE RELATIONSHIP
EXPERIMENTAL AND COMPUTED
SPECIMEN HA3-12

w/t = 41.2

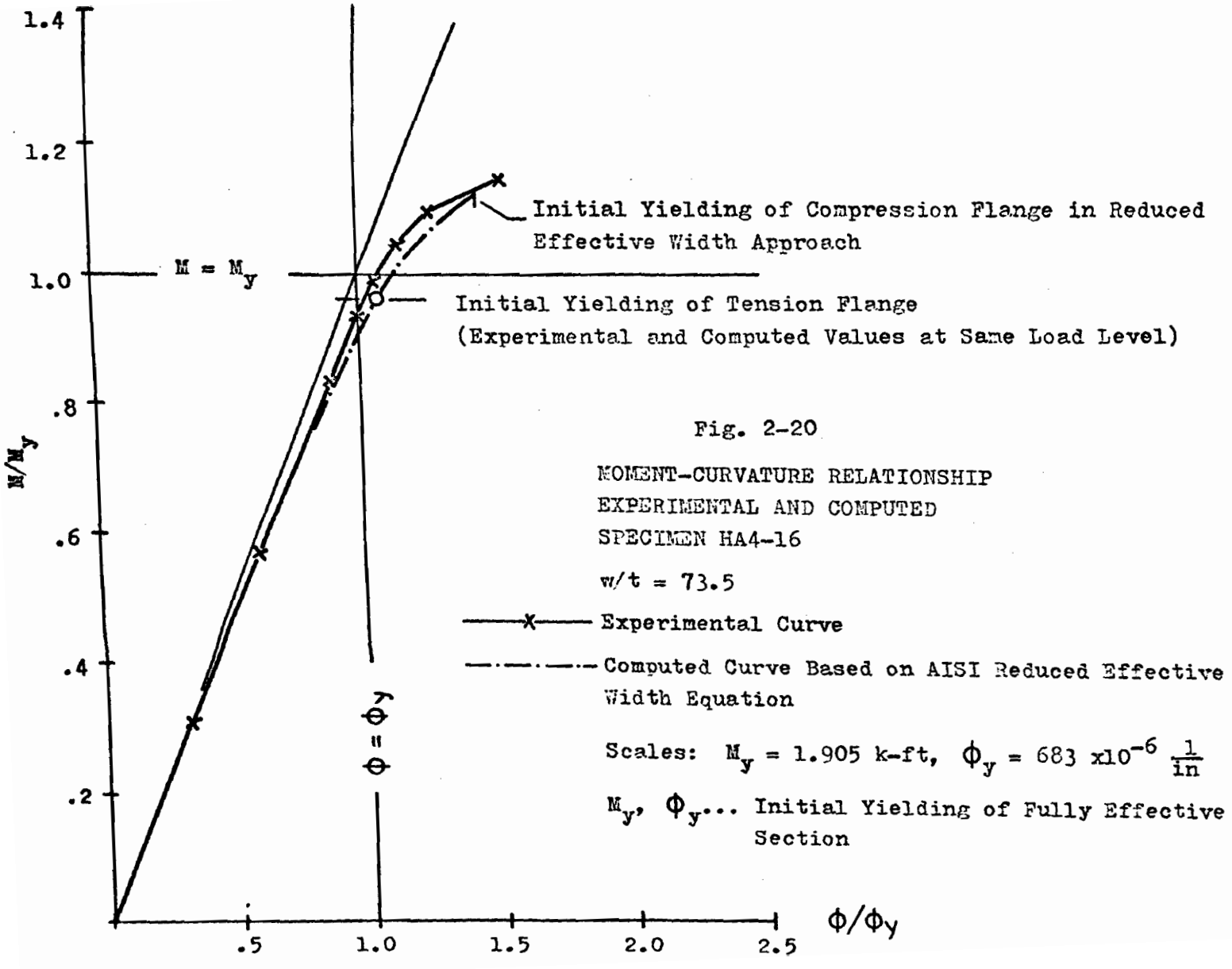

Fig. 2-20

MOMENT-CURVATURE RELATIONSHIP
EXPERIMENTAL AND COMPUTED
SPECIMEN HA4-16

w/t = 73.5

——x—— Experimental Curve

—·—·—·— Computed Curve Based on AISI Reduced Effective Width Equation

Scales: M_y = 1.905 k-ft, $\phi_y = 683 \times 10^{-6} \frac{1}{in}$

M_y, ϕ_y... Initial Yielding of Fully Effective Section

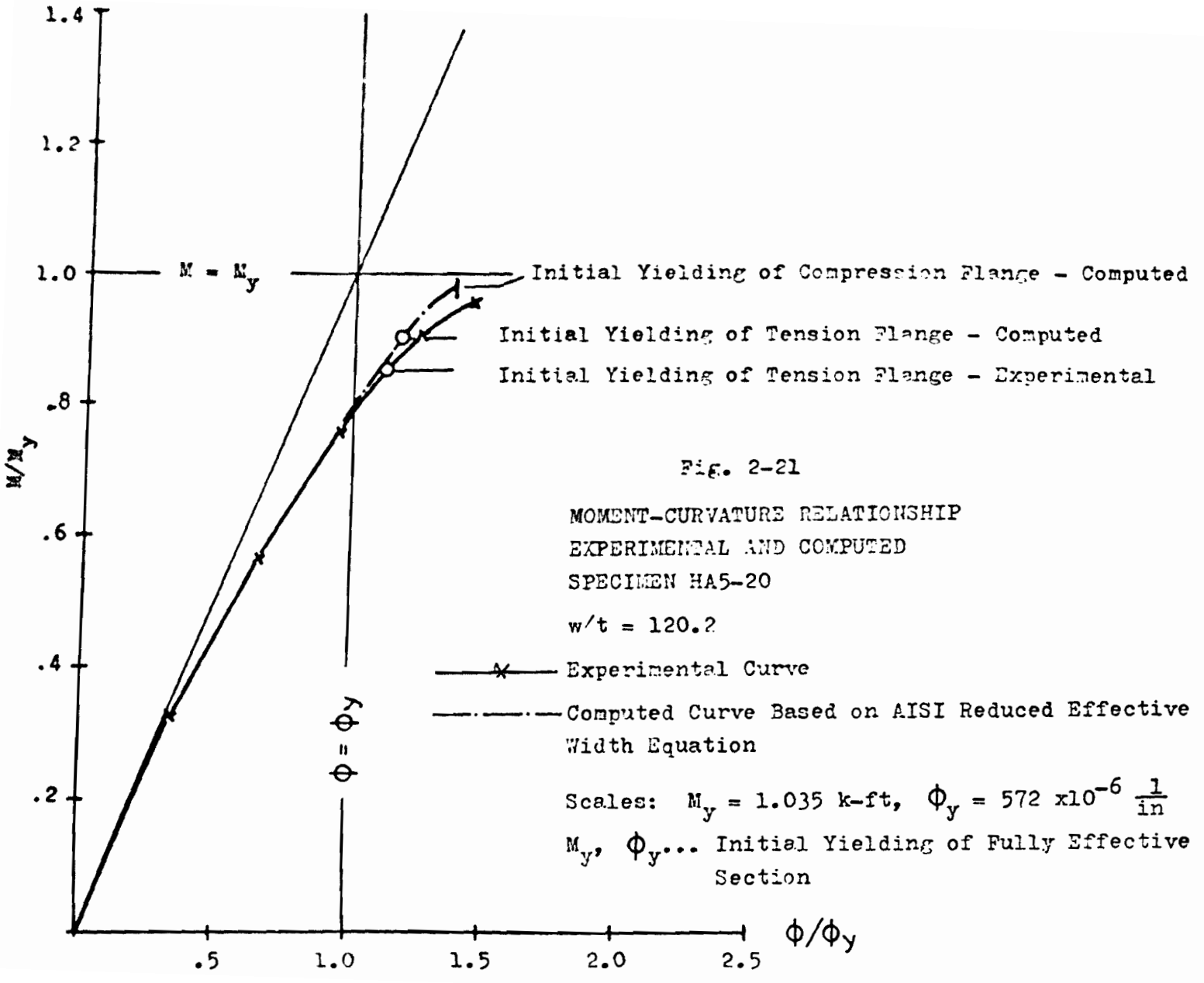

Fig. 2-21

MOMENT-CURVATURE RELATIONSHIP
EXPERIMENTAL AND COMPUTED
SPECIMEN HA5-20

w/t = 120.2

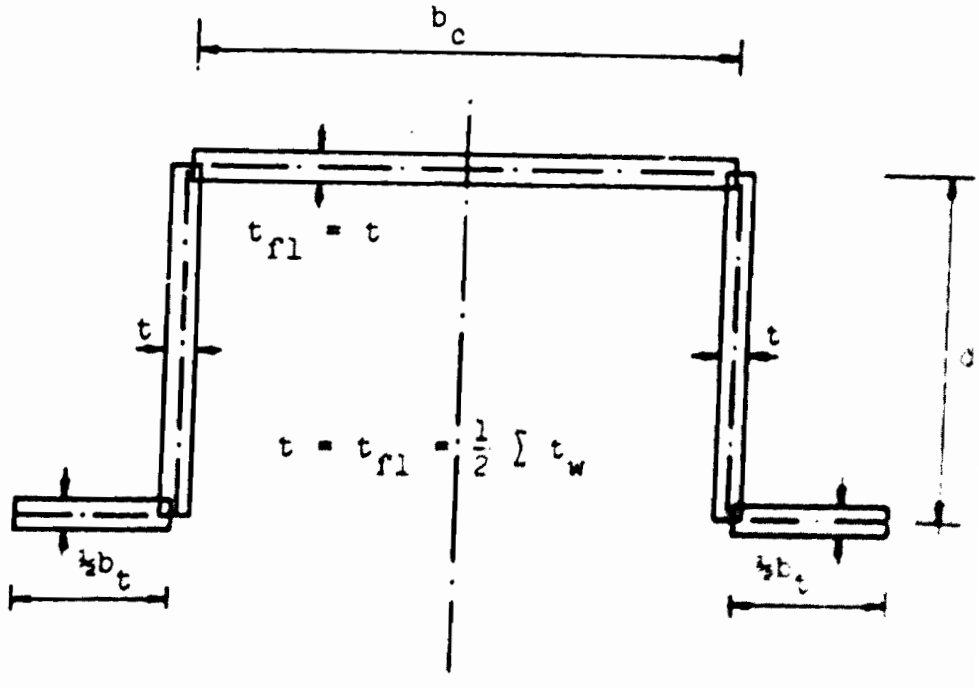

Fig. 3.1

MONOSYMMETRIC, COLDFORMED SECTION AS USED IN ANALYSIS

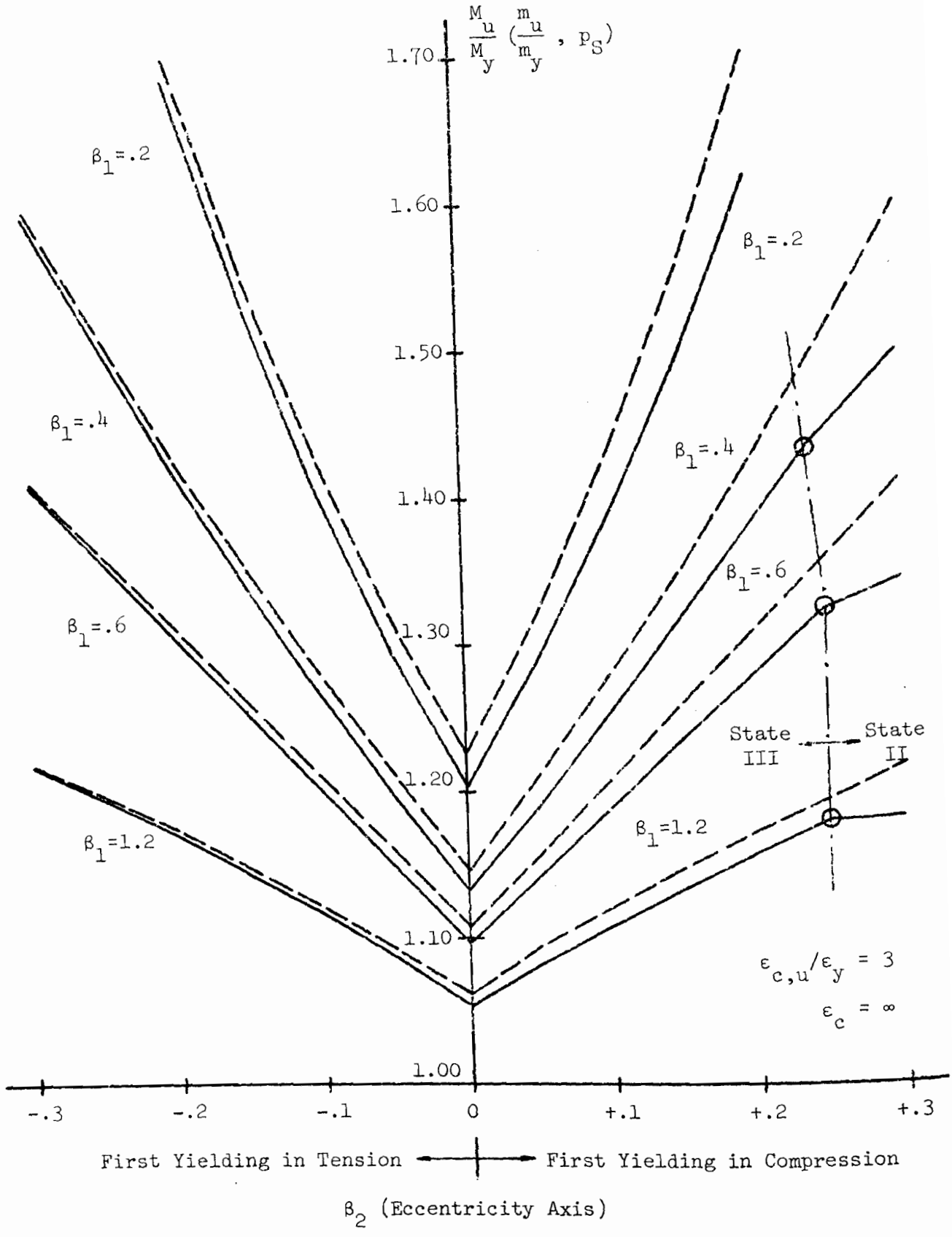

Fig. 3.2 INELASTIC RESERVES OF RESISTANCE OF THE MONOSYMMETRIC COLDFORMED SECTION [FAILURE CRITERION $\varepsilon_{c,u}/\varepsilon_y = 3$]

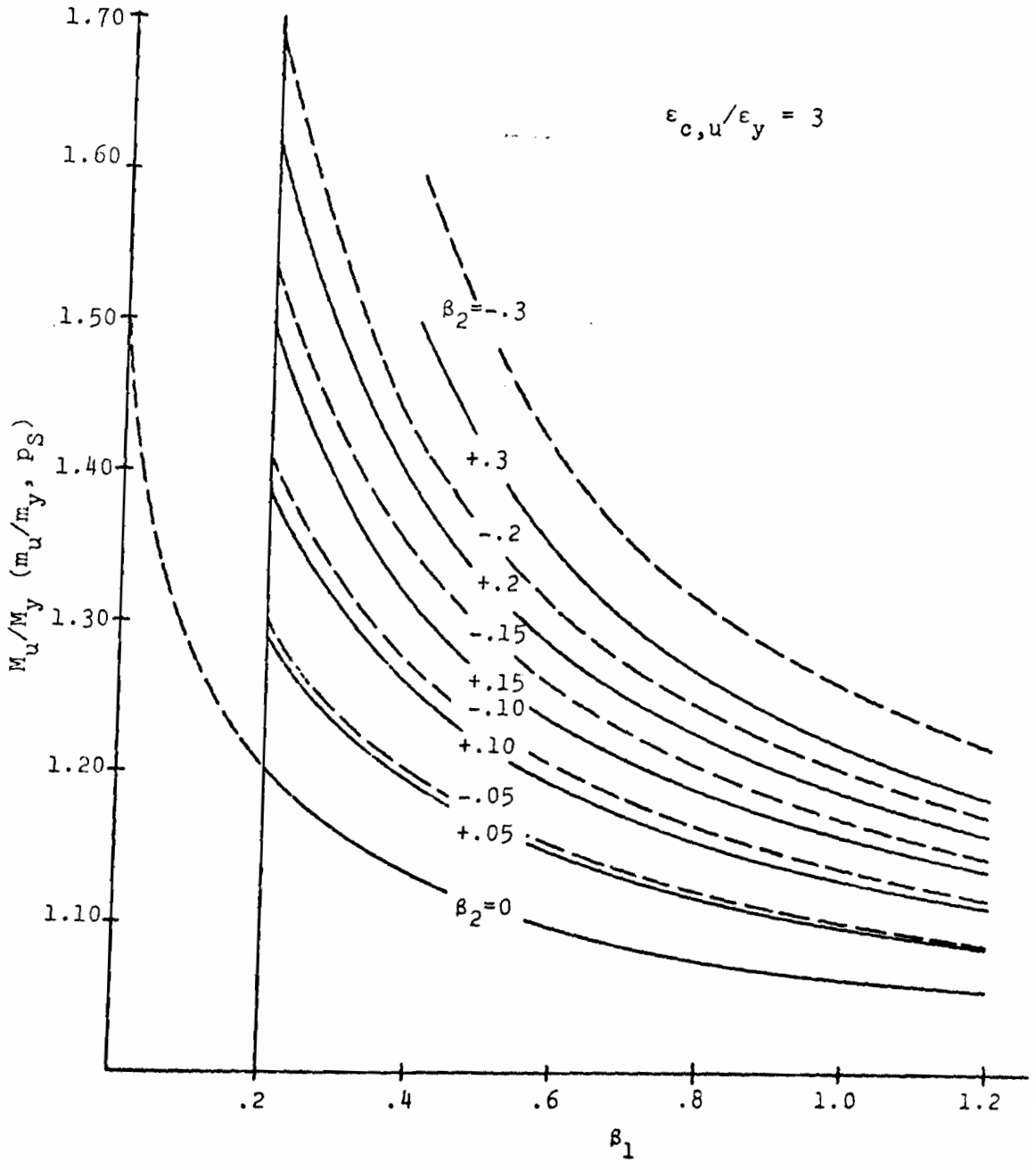

Fig. 3.3 INELASTIC RESERVES OF RESISTANCE OF THE MONOSYMMETRIC COLDFORMED SECTION FAILURE CRITERION $\varepsilon_{c,u}/\varepsilon_y$ = 3

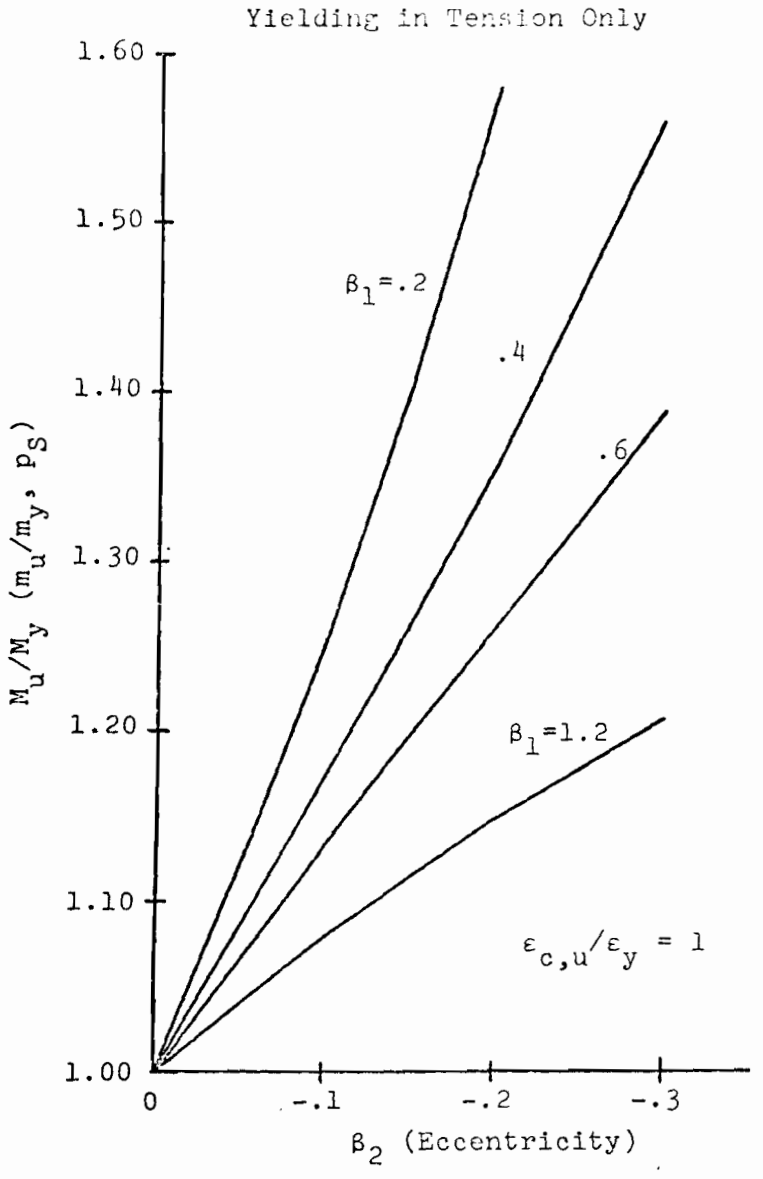

ig. 3.4 INELASTIC RESERVES OF RESISTANCE FOR MONOSYMMETRIC COLDFORMED SECTION FAILURE CRITERION $\varepsilon_{c,u}/\varepsilon_y$ = 1

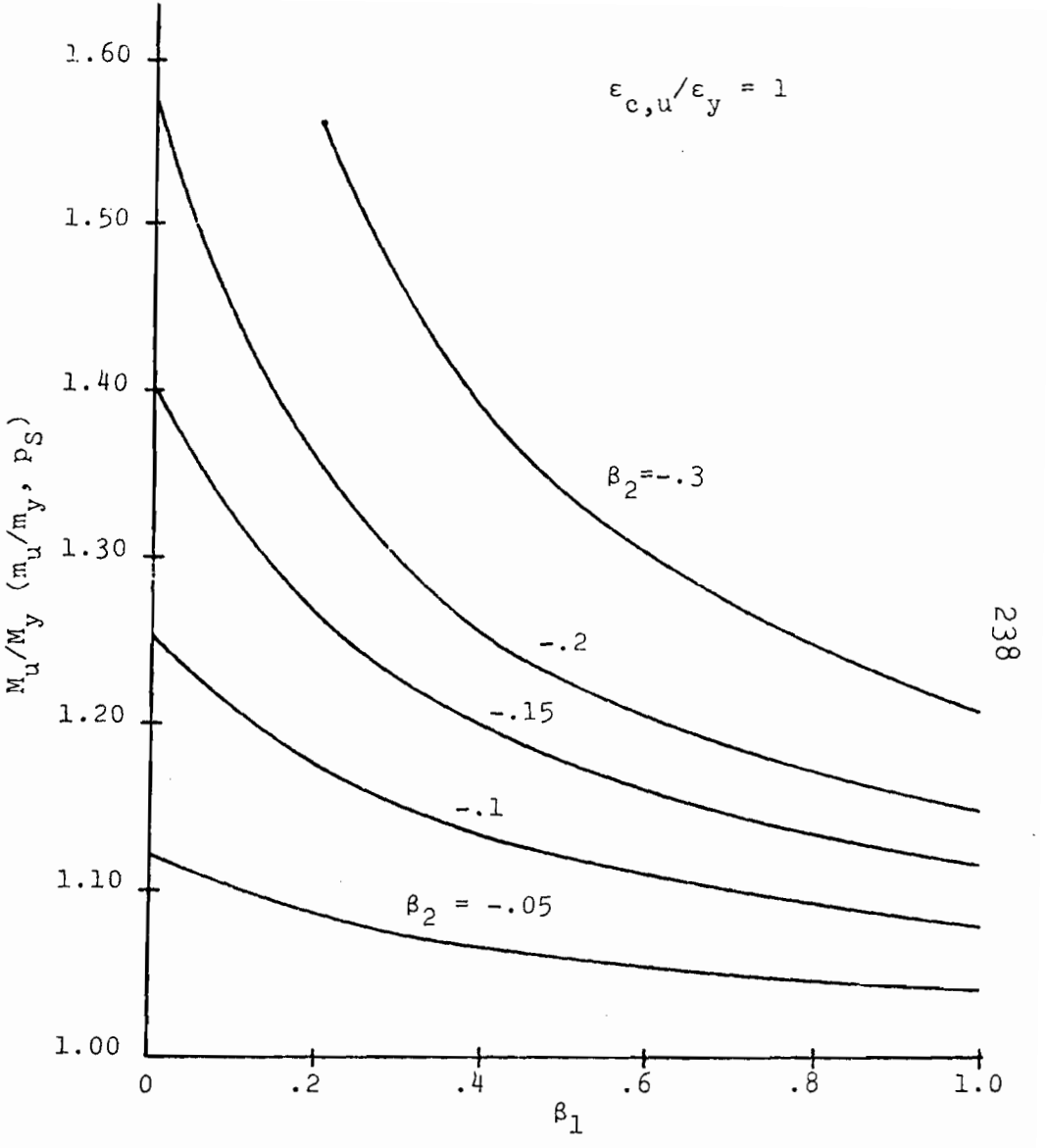

Fig. 3.5 INELASTIC RESERVES OF RESISTANCE FOR MONOSYMMETRIC COLDFORMED SECTION FAILURE CRITERION $\varepsilon_{c,u}/\varepsilon_y$ = 1

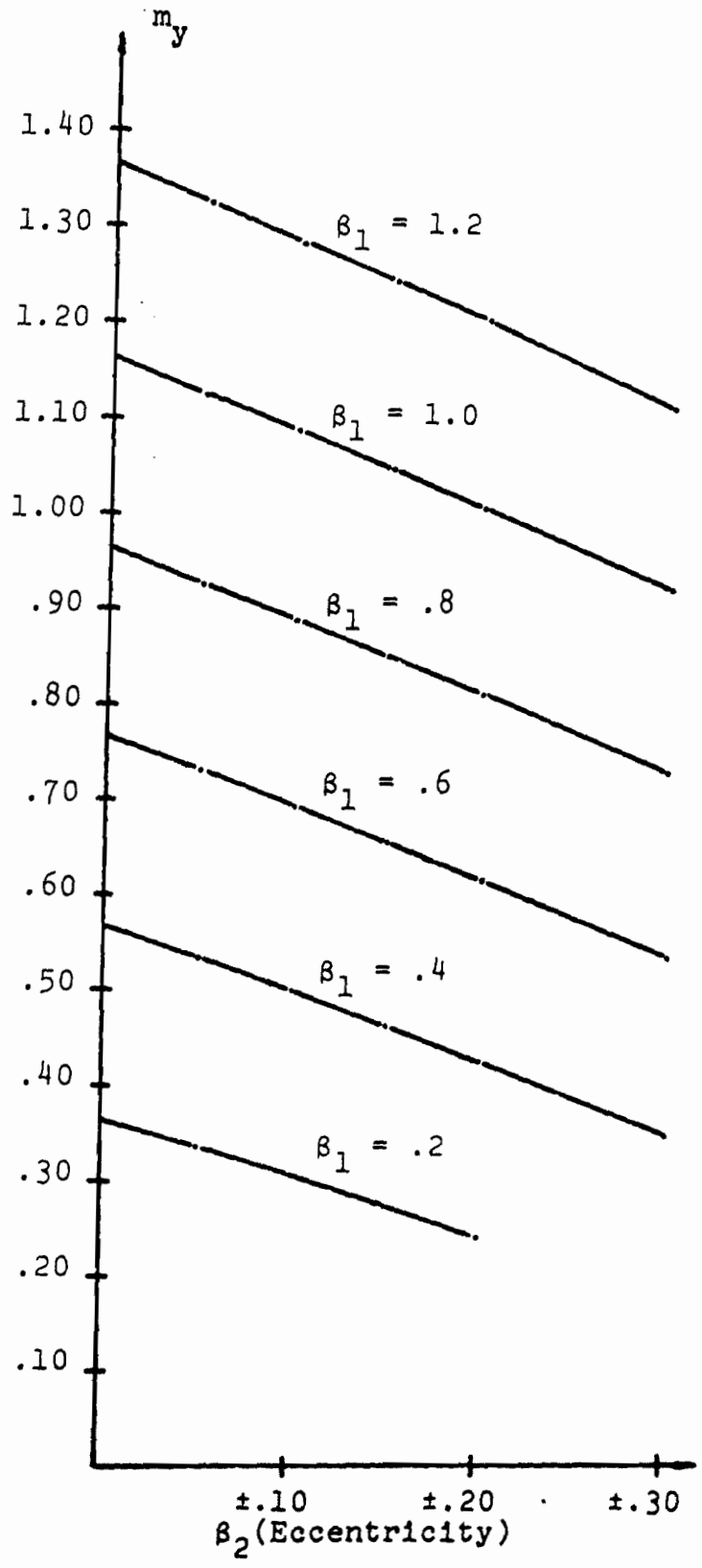

Fig. 3.6 DESIGN GRAPHS FOR NORMALIZED YIELD MOMENT $m_y = M_y/(\sigma_y t d^2)$

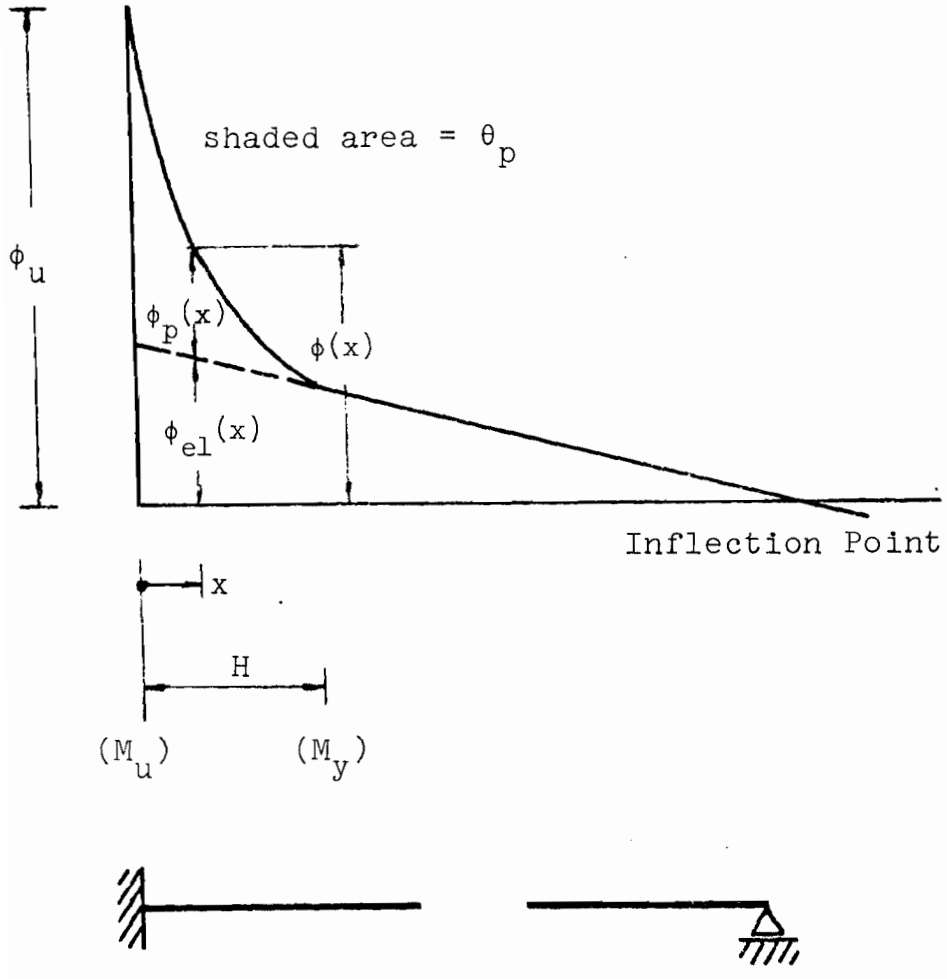

Fig. 4.1

CURVATURE DIAGRAM WITH PARTIAL HINGE AT SUPPORT

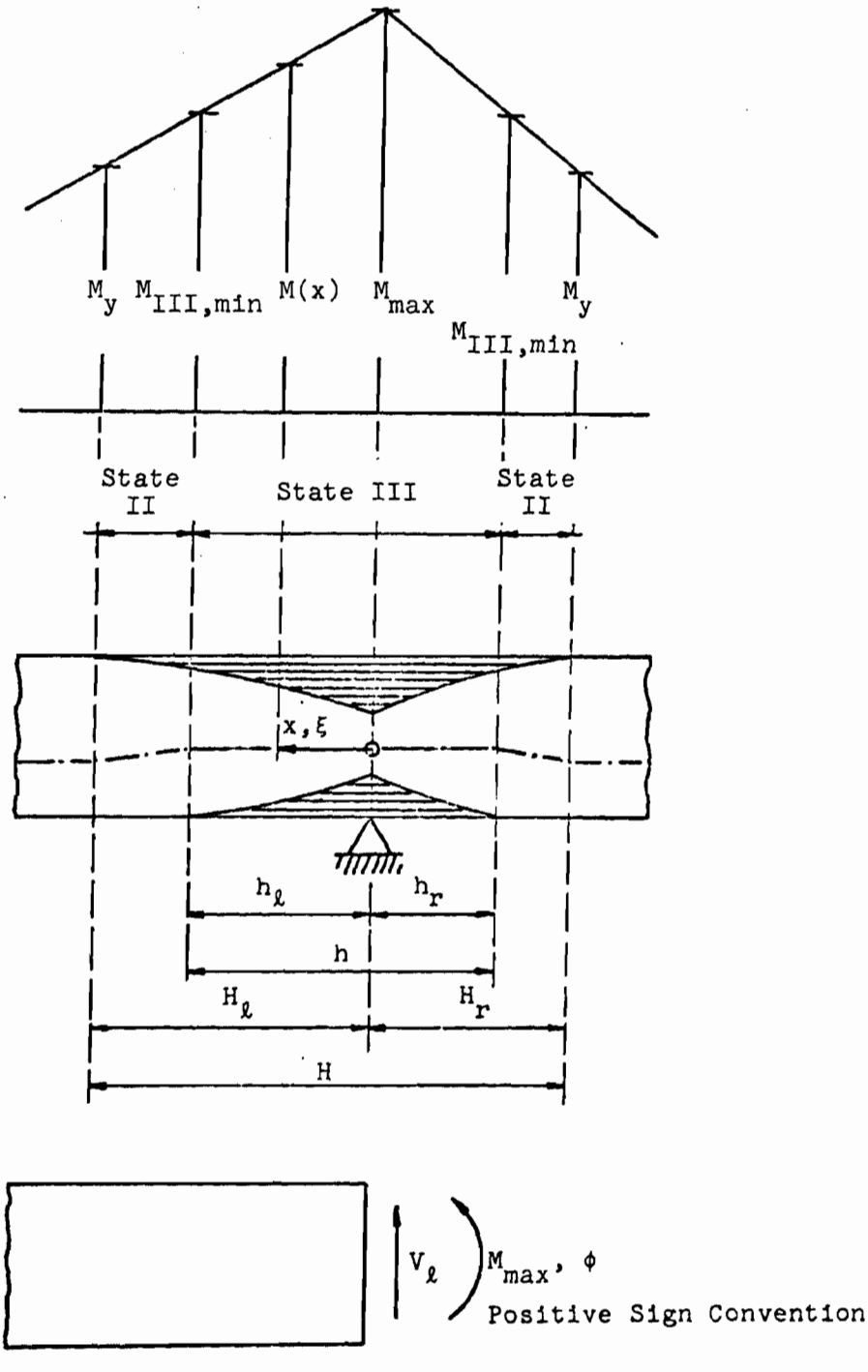

Fig. 4.2 NOTATIONS FOR PARTIAL HINGES

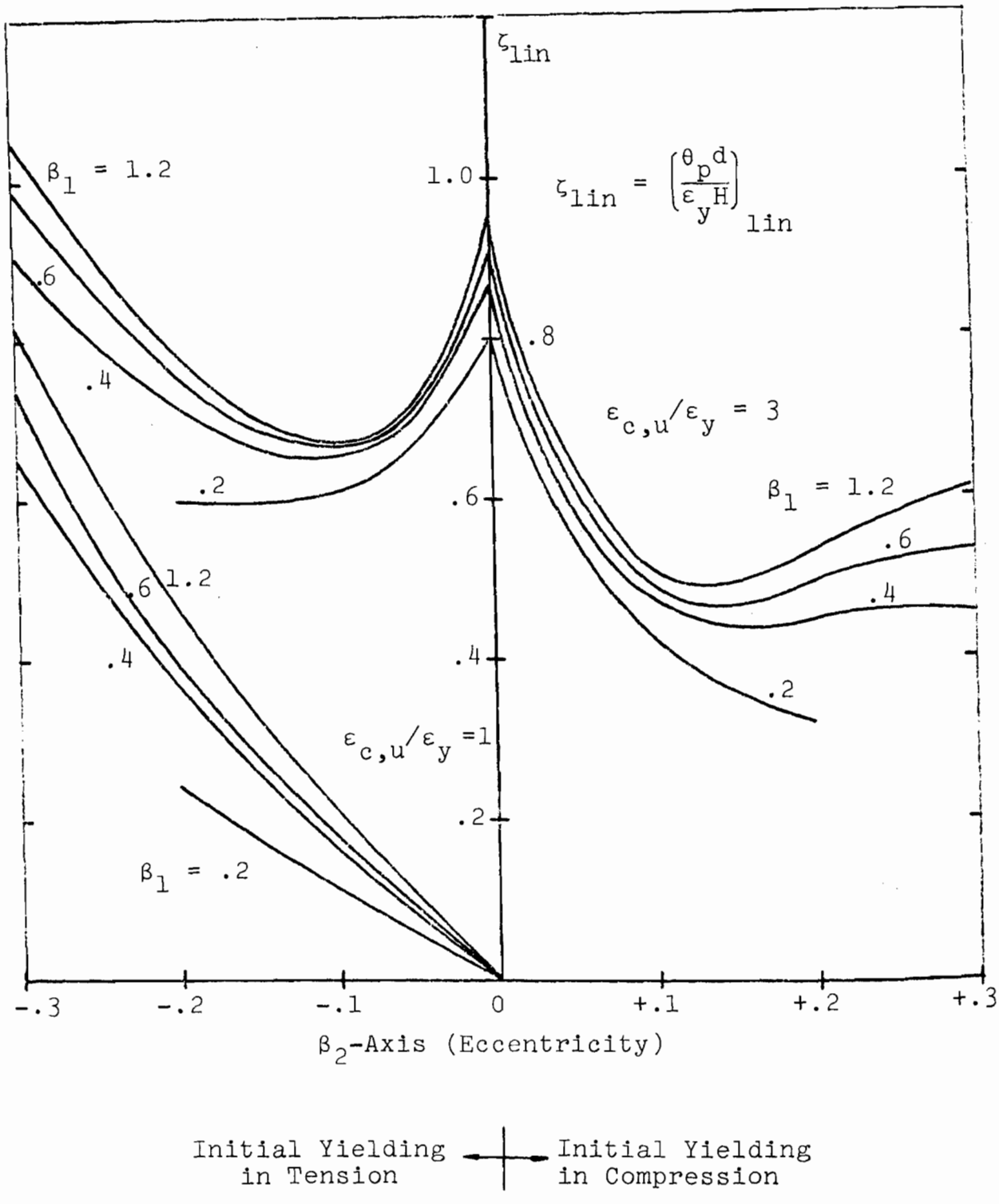

Fig. 4.3 NUMERICAL EVALUATION OF THE ROTATION INTEGRAL FOR LINEAR MOMENT-DISTRIBUTION (ROTATION CAPACITY)

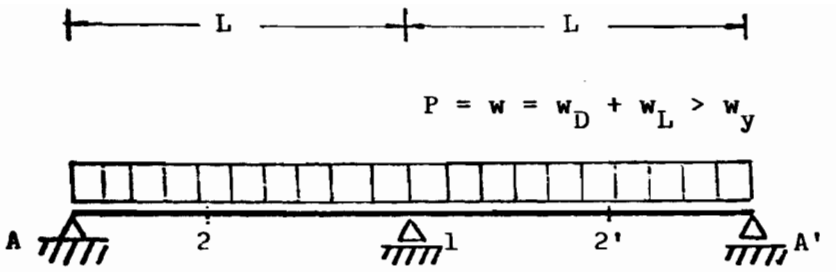

Fig. 5.1 EXAMPLE SYSTEM FOR PARTIAL MOMENT REDISTRIBUTION

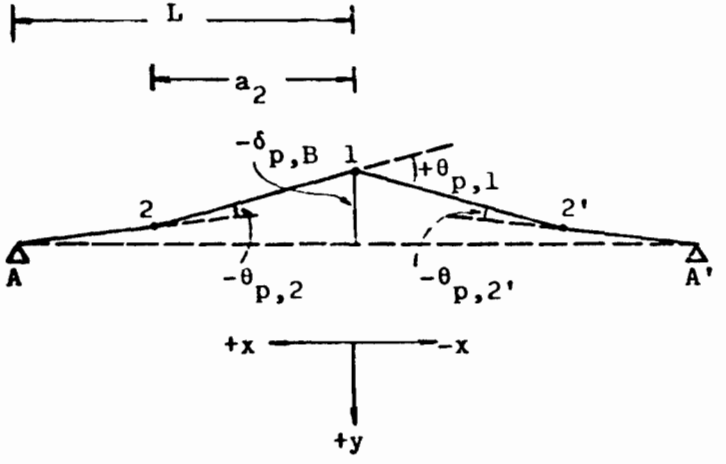

Fig. 5.2 RESIDUAL DEFORMATIONS ON THE STATICALLY DETERMINATE EXAMPLE SYSTEM AFTER UNLOADING

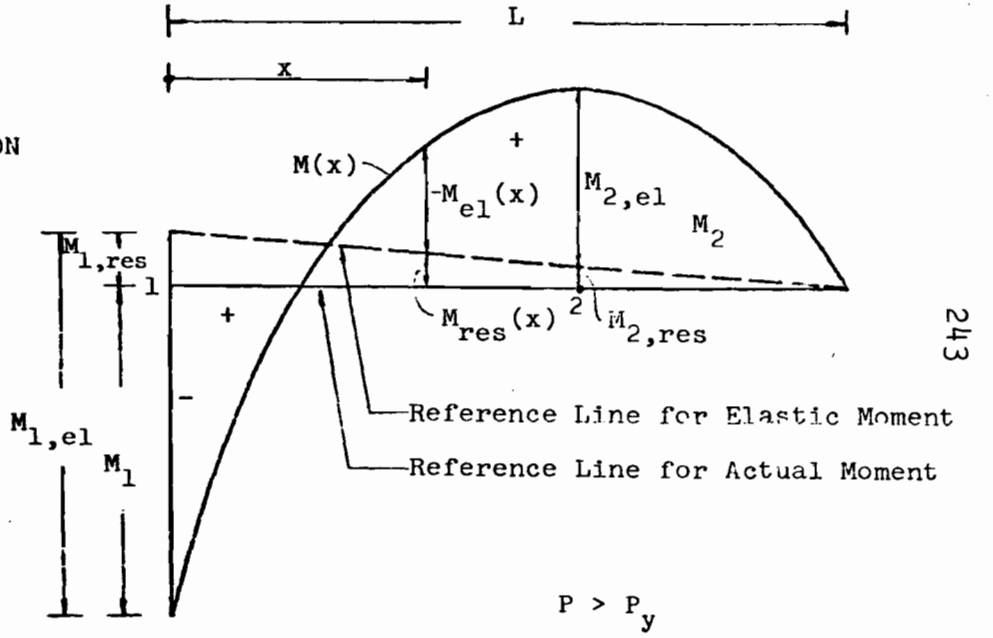

Fig. 5.3

COMPONENTS OF THE INELASTIC MOMENT DISTRIBUTION FOR THE EXAMPLE SYSTEM

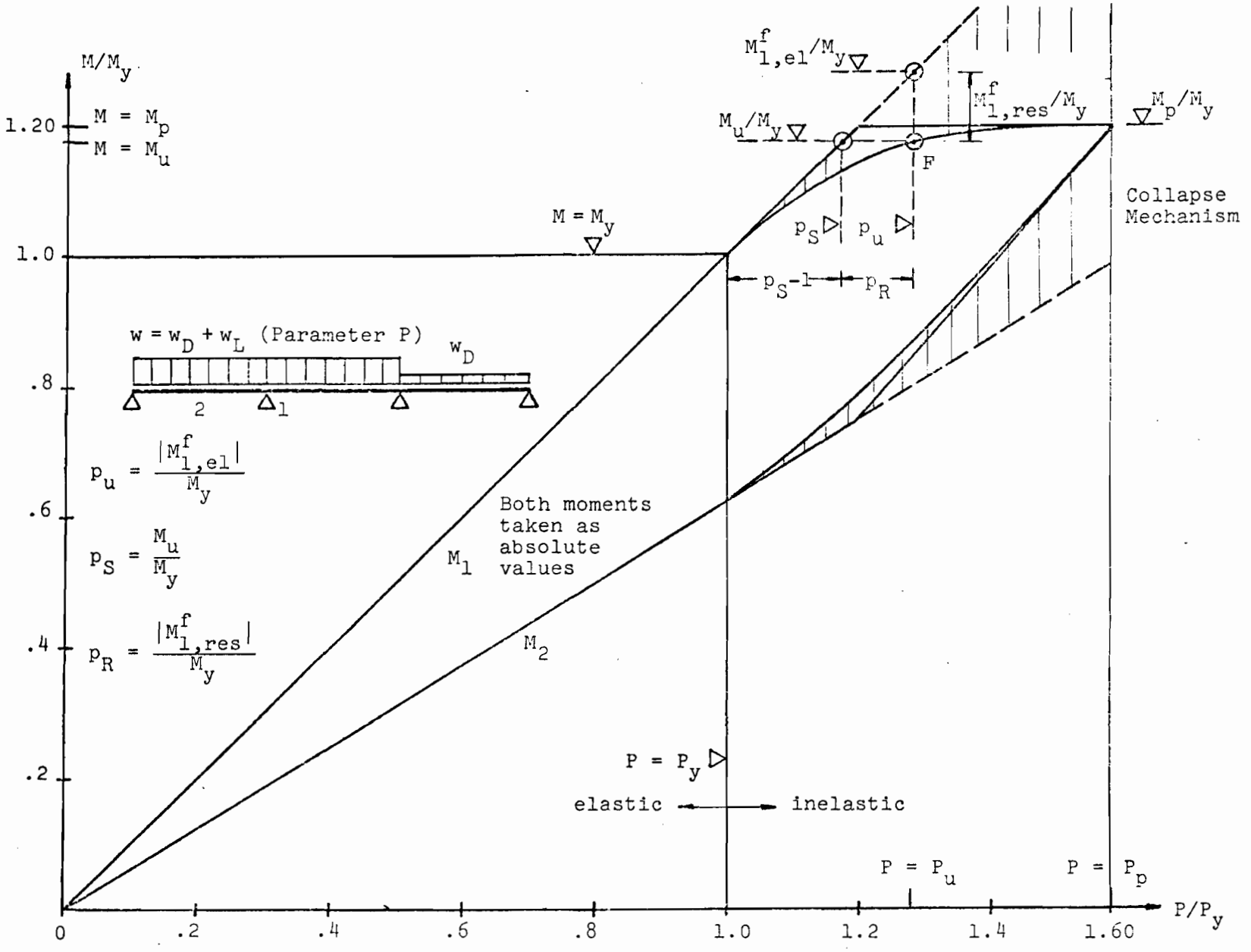

Fig. 5.4 MOMENT-LOAD DIAGRAM THROUGHOUT INELASTIC LOAD HISTORY

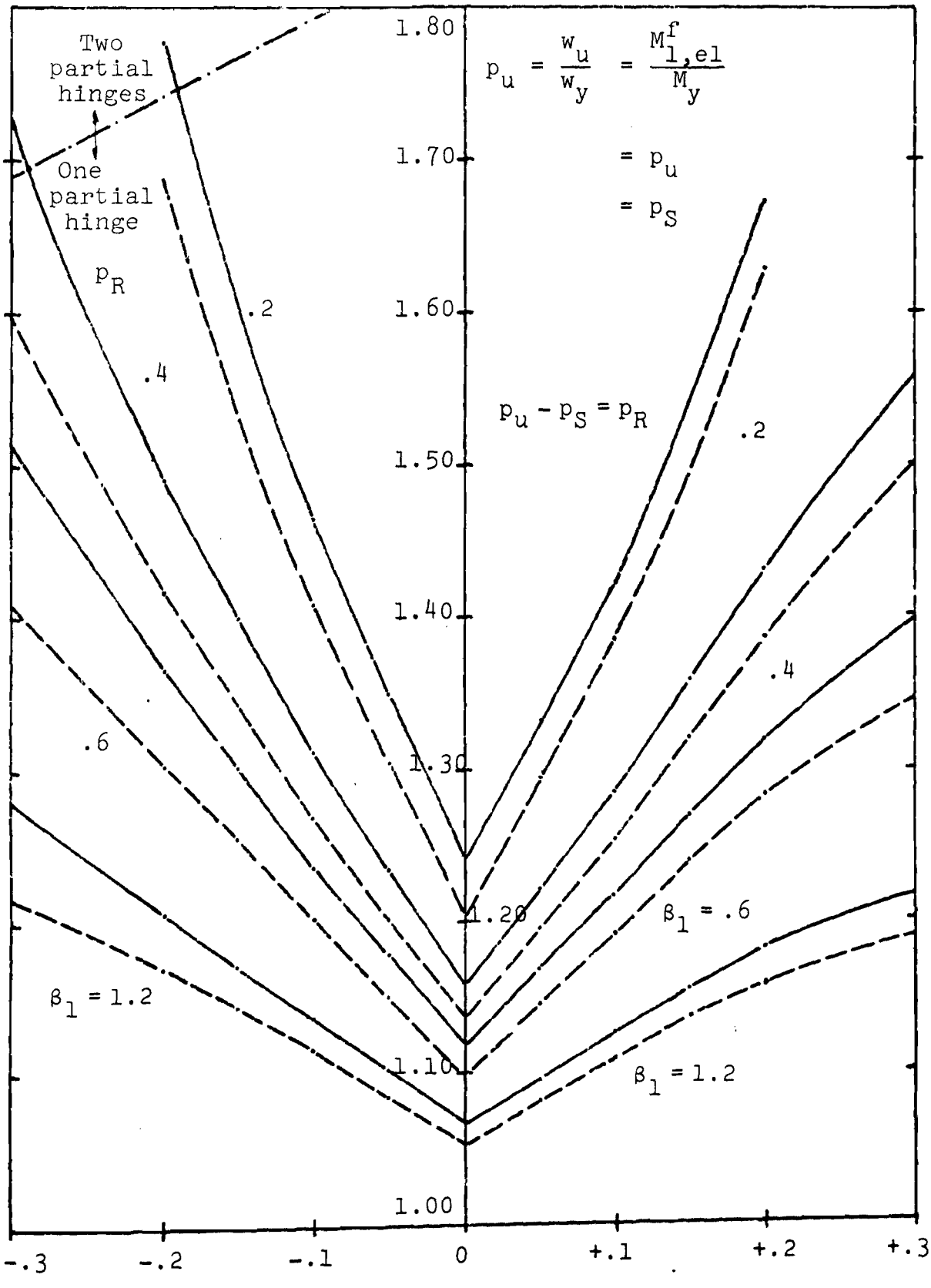

Fig. 5.5a INELASTIC LOAD FACTORS FOR SYSTEM OF Fig. 5.1
FAILURE CRITERION $\varepsilon_{c,u}/\varepsilon_y = 3$

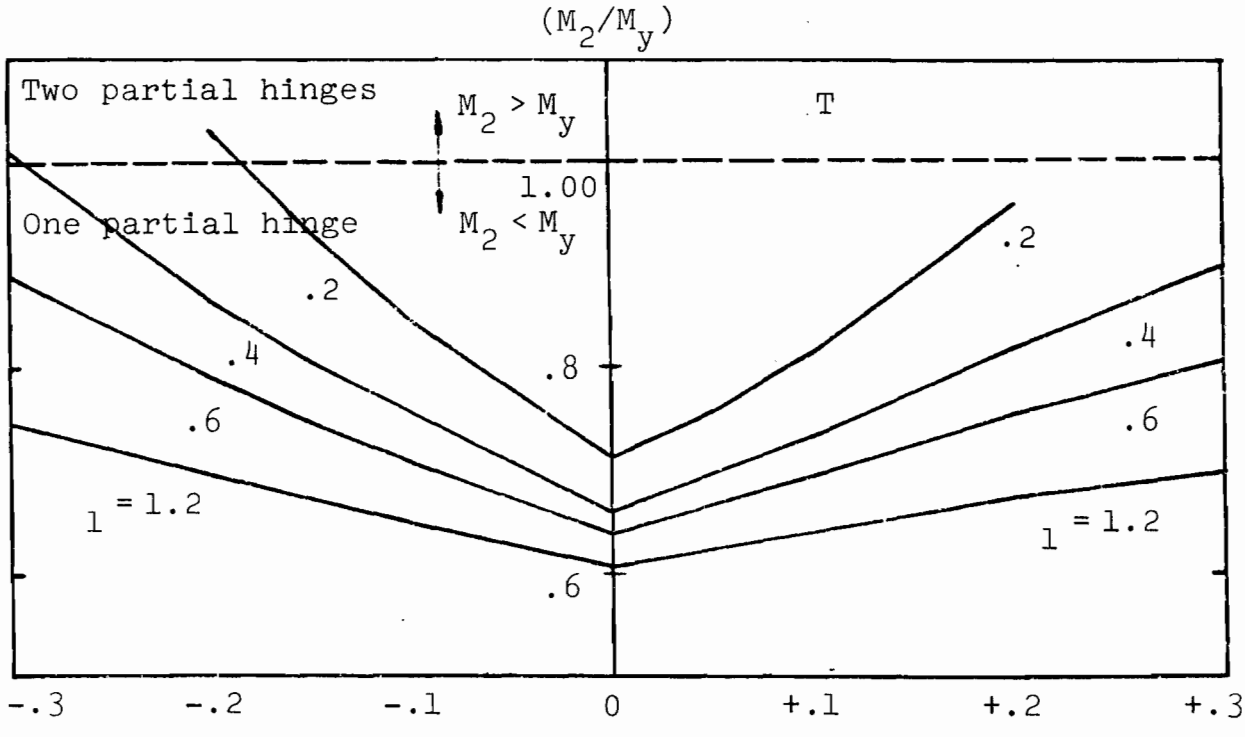

Fig. 5.5b MOMENT RATIO IN SPAN CORRESPONDING TO FAILURE AT SUPPORT

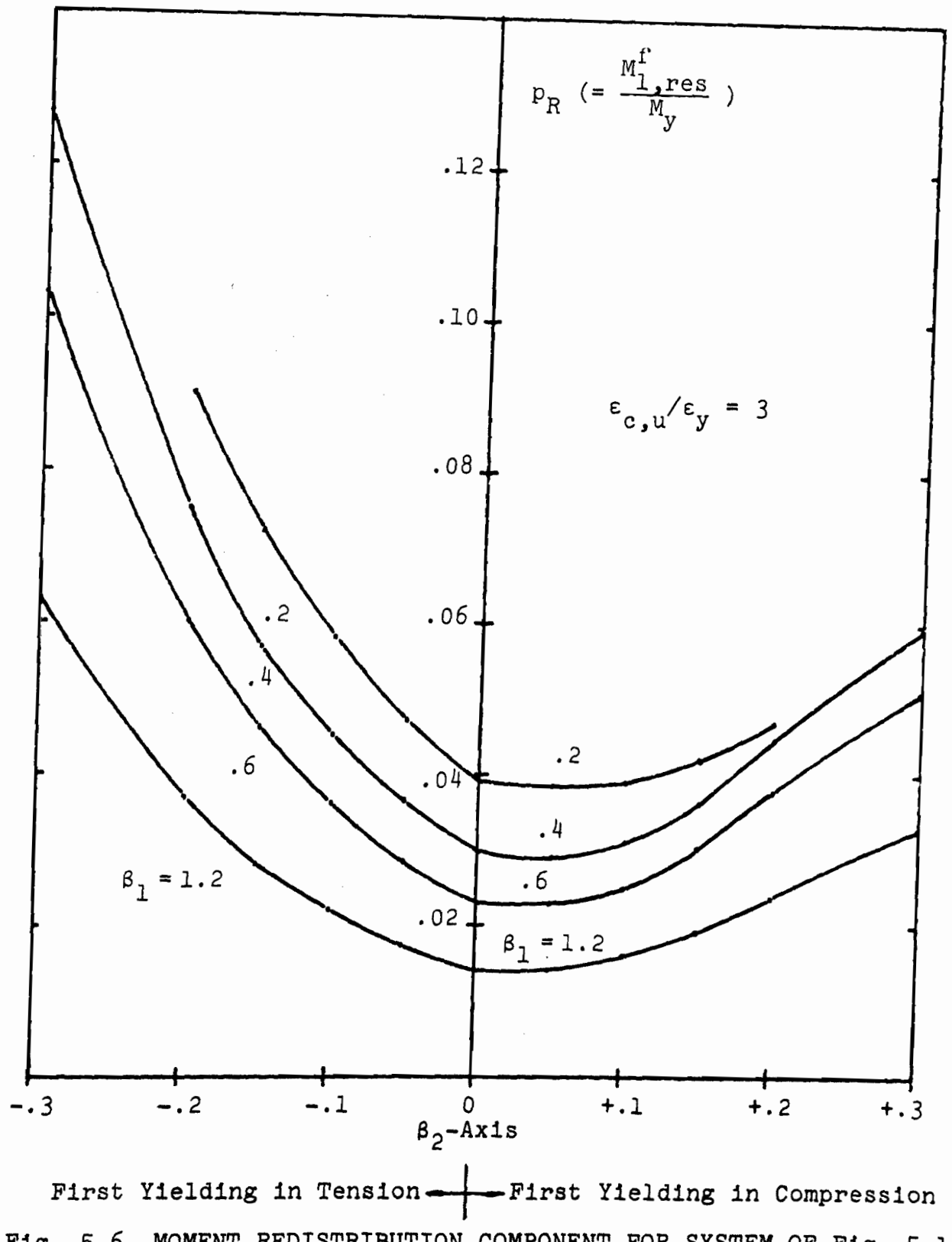

Fig. 5.6 MOMENT REDISTRIBUTION COMPONENT FOR SYSTEM OF Fig. 5.1
ALSO: DESIGN GRAPH FOR RESTRICTED MOMENT REDISTRIBUTION DESIGN

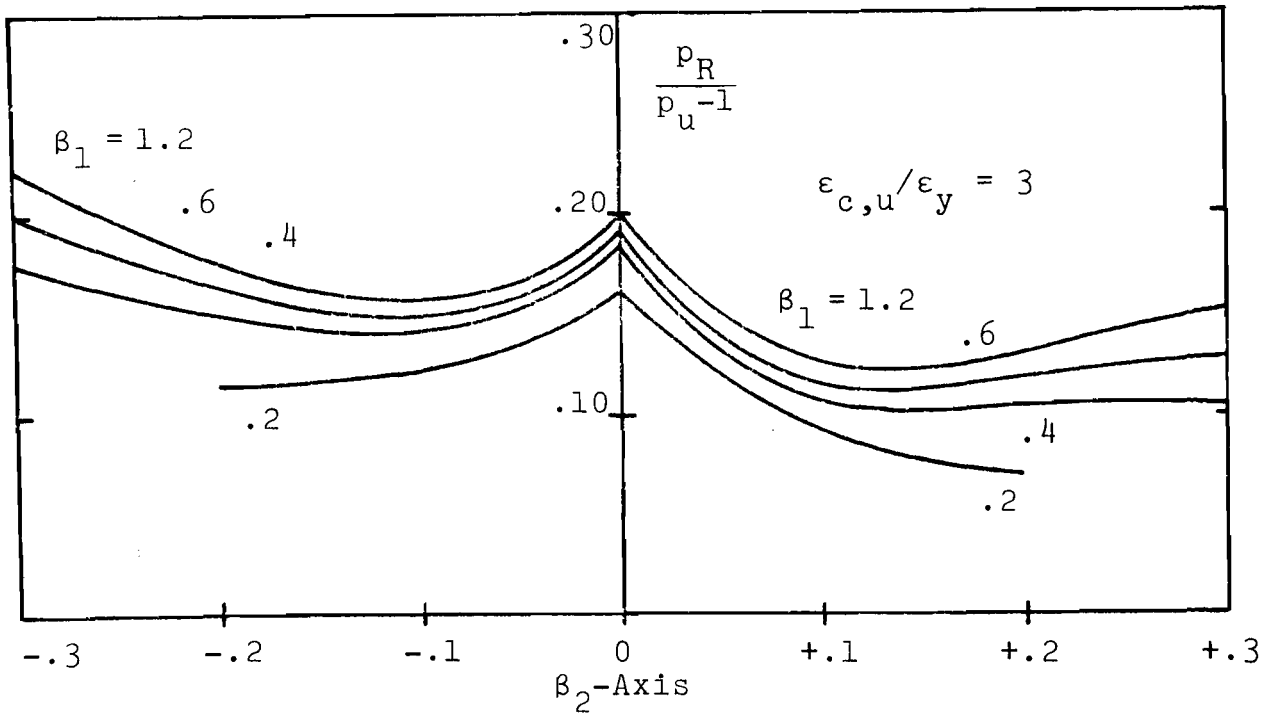

Fig. 5.7 MOMENT REDISTRIBUTION COMPONENT p_R AS PART OF THE TOTAL INELASTIC RESERVE
FAILURE CONDITION $\varepsilon_{c,u}/\varepsilon_y = 3$

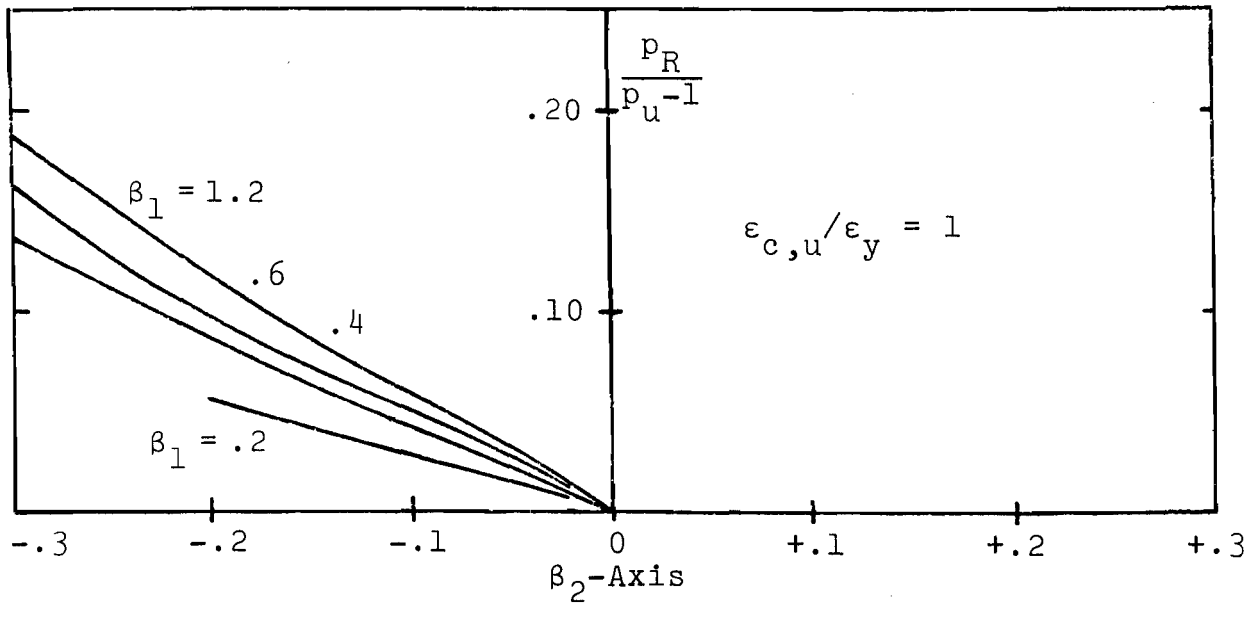

Fig. 5.8 MOMENT REDISTRICUTION COMPONENT p_R AS PART OF THE TOTAL INELASTIC RESERVE
FAILURE CONDITION $\varepsilon_{c,u}/\varepsilon_y = 1$

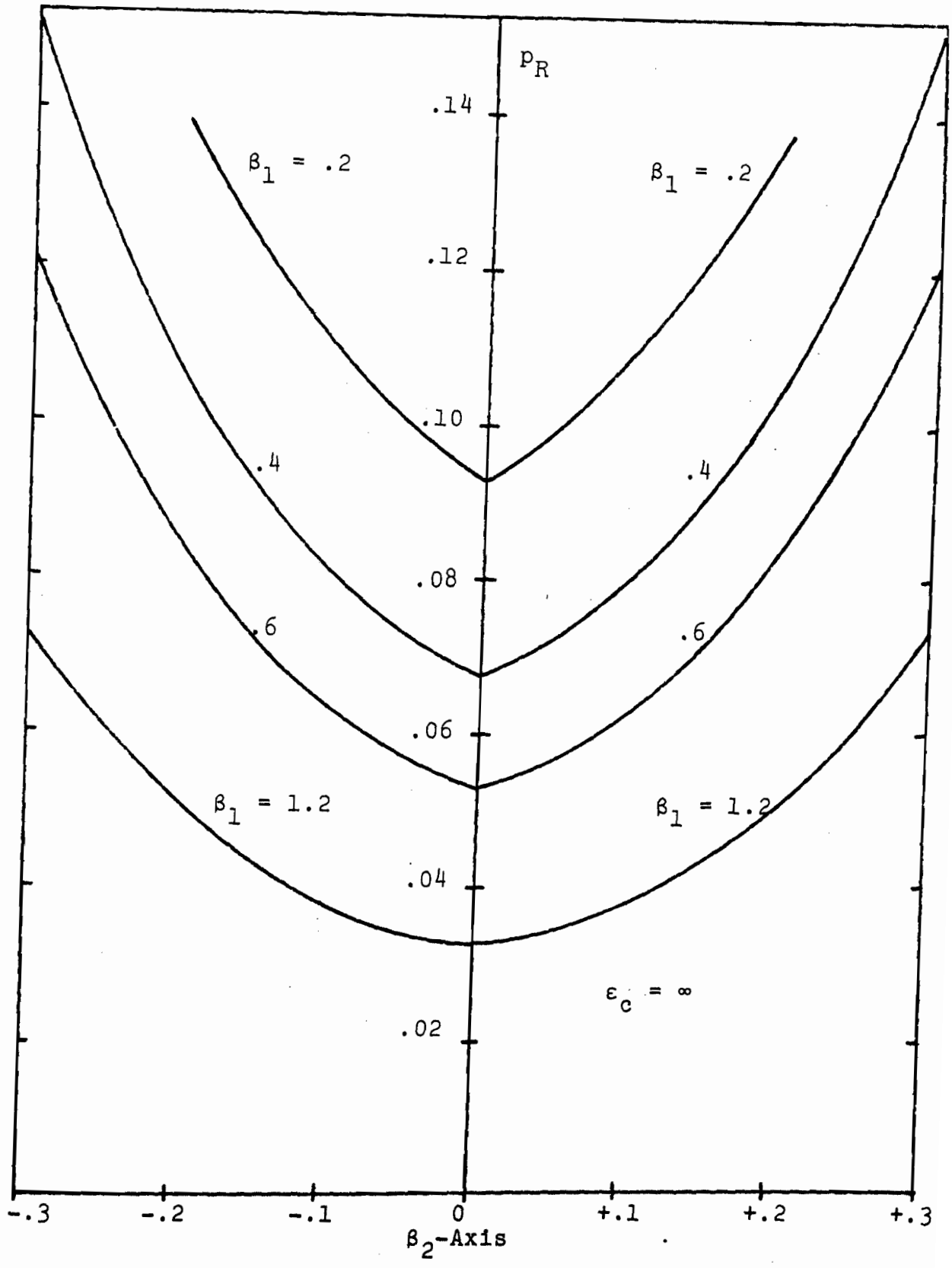

Fig. 5.9 MOMENT REDISTRIBUTION COMPONENT p_R FOR SAMPLE SYSTEM OF Fig. 5.1
SECTION FULLY PLASTIFIED AS $\varepsilon_c \to \infty$

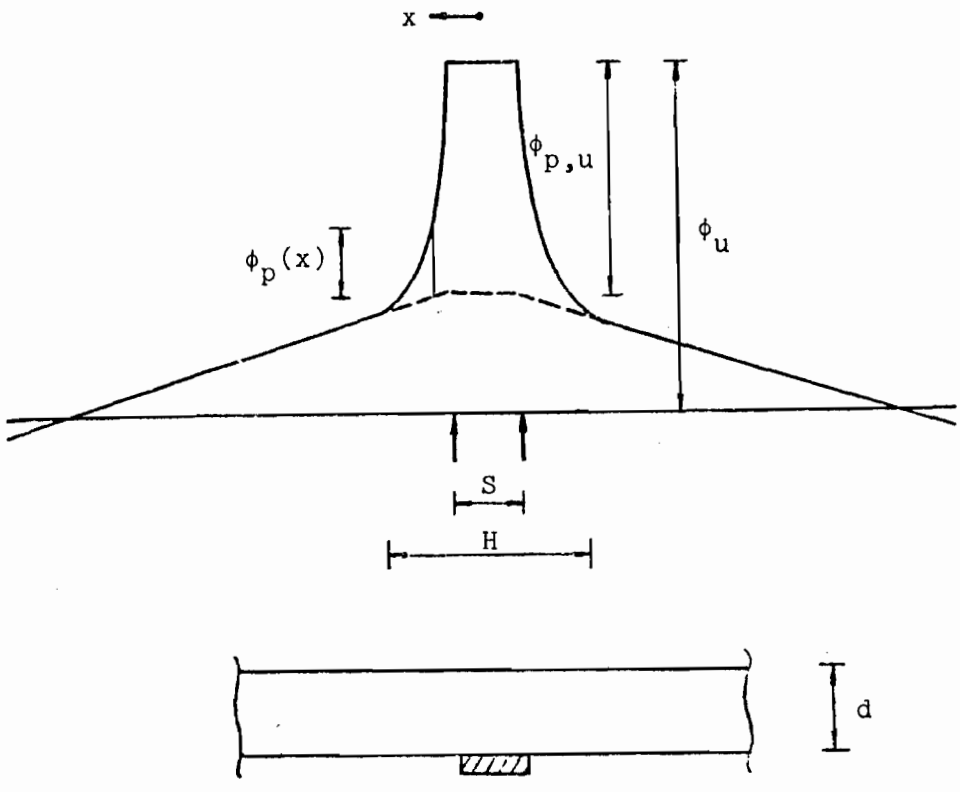

Fig. 5.10 CURVATURE DIAGRAM AT INTERIOR SUPPORT WITH BEARING PLATE (PROPOSED APPROXIMATION)